KAUNAS UNIVERSITY OF TECHNOLOGY

ULIANA TSIKO

SYNTHESIS AND PROPERTIES OF ORGANIC LIGHT-EMITTING COMPOUNDS BASED ON BENZANTHRONE AND PYRIMIDINE-5-CARBONITRILE MOIETIES

Doctoral dissertation
Technological Sciences, Chemical Engineering (T 005)

2022, Kaunas

This doctoral dissertation was prepared at Kaunas University of Technology, Faculty of Chemical Technology, Department of Polymer Chemistry and Technology during the period of 2018–2022. The studies were supported by the Research Council of Lithuania.

Scientific Supervisor:
Prof. Dr. Habil. Juozas Vidas GRAŽULEVIČIUS (Kaunas University of Technology, Technological Sciences, Materials Engineering T 008).

Scientific Advisor:
Dr. Rasa KERUCKIENĖ (Kaunas University of Technology, Technological Sciences, Materials Engineering, T 008).

Edited by: English language editor Dr. Armandas Rumšas (Publishing House *Technologija*), Lithuanian language editor Rozita Znamenskaitė (Publishing House *Technologija*)

The official defense of the dissertation will be held at 10 a.m. on 13 September, 2022 at the public meeting of the Dissertation Defense Board of Chemical Engineering Science Field in the Meeting Room at Santaka Valley of Kaunas University of Technology.

Address: Baršausko 59–A228, Kaunas, LT-51423, Lithuania.
Phone (+370) 37 300 042; email doktorantura@ktu.lt

The doctoral dissertation was sent out on the 12th of August, 2022.

The doctoral dissertation is available on the internet at http://ktu.edu and at the library of Kaunas University of Technology (Donelaičio 20, Kaunas, LT-44239, Lithuania).

KAUNO TECHNOLOGIJOS UNIVERSITETAS

ULIANA TSIKO

BENZANTRONO IR PIRIMIDINO-5-KARBONITRILO DARINIŲ KAIP ORGANINIŲ SPINDUOLIŲ SINTEZĖ IR SAVYBĖS

Daktaro disertacija
Technologniai mokslai, chemijos inžinerija (T 005)

2022, Kaunas

Disertacija rengta 2018–2022 metais Kauno technologijos universiteto Cheminės technologijos fakultete, Polimerų chemijos ir technologijos katedroje. Mokslinius tyrimus rėmė Lietuvos mokslo taryba.

Mokslinis vadovas:
Prof. habil. dr. Juozas Vidas GRAŽULEVIČIUS (Kauno technologijos universitetas, technologiniai mokslai, medžiagų inžinerija, T 008).

Mokslinis konsultantas:
Dr. Rasa KERUCKIENĖ (Kauno technologijos universitetas, technologijos mokslai, medžiagų inžinerija, T 008).

Redagavo: anglų kalbos redaktorius dr. Armandas Rumšas (leidykla „*Technologija*“), lietuvių kalbos redaktorė Rozita Znamenskaitė (leidykla „*Technologija*“).

Chemijos inžinerijos mokslo krypties disertacijos gynimo taryba:
Prof. Dr. Rimantas VENSKUTONIS (Kauno technologijos universitetas, technologijos mokslai, chemijos inžinerija, T 005) – **pirmininkas**;
Prof. Dr. Rasa PAULIUKAITĖ (Fizinių ir technologiniai mokslų centras, gamtos mokslai, fizika, N 002);
Prof. Dr. Ramunė RUTKAITĖ (Kauno technologijos universitetas, technologiniai mokslai, chemijos inžinerija, T 005);
Prof. Dr. Virgilijus VALEIKA (Kauno technologijos universitetas, technologiniai mokslai, chemijos inžinerija, T 005);
Prof. Dr. Valeriy YASHCHUK (Taraso Ševčenkos nacionalinis Kijevo universitetas, Ukraina, gamtos mokslai, fizika, N 002).

Disertacija bus ginama viešame Chemijos inžinerijos mokslo krypties disertacijos gynimo tarybos posėdyje 2022 m. rugsėjo 13 d. 10 val. Kauno technologijos universiteto „Santakos“ slėnyje, Posėdžių kambaryje.

Adresas: K. Baršausko g. 59-A228, LT-51423 Kaunas, Lietuva.
Tel. (370) 37 30 00 42; el. paštas doktorantura@ktu.lt

Disertacija išsiųsta 2022 m. rugpjūčio 12 d.
Su disertacija galima susipažinti interneto svetainėje http://ktu.edu ir Kauno technologijos universiteto bibliotekoje (K. Donelaičio g. 20, Kaunas LT-44239).

LIST OF ABBREVIATIONS

AIEE	Aggregation-induced emission enhancement
Al	Aluminum
BZA	Benzanthrone
CE	Current efficiency
CELIV	Charge extraction by linearly increasing voltage technique
CIE	Commission Internationale de l'Éclairage
CT	Charge transfer
CV	Cyclic voltammetry
DCM	Dichloromethane
DF	Delayed fluorescence
DSC	Differential scanning calorimetry
D	Thicknesses of the layers
E_{opt}	Optical gap
EA^{CV}	Electron affinity measured by CV
EA^{UPS}	Electron affinity measured by ultraviolet photoelectron spectroscopy
EL	Electroluminescence
EML	Emitting layer
EQE	External quantum efficiency
FWHM	Full width at half maxima
HAT-CN	Dipyrazino[2,3-f:2',3'-h]quinoxaline-2,3,6,7,10,11-hexacarbonitrile
HLCT	Hybridized local and charge transfer excited state
HOMO	Highest occupied molecular orbital
IC	Internal conversion
ICT	Intramolecular charge transfer
IQE	Internal quantum efficiency
IP^{CV}	Ionization potential measured by CV
IP^{UPS}	Ionization potential measured by ultraviolet photoelectron spectroscopy
ITO	Indium-tin oxide
K_{SV}	Stern-Volmer constant
LEAB	Low energy absorption band
LUMO	Lowest unoccupied molecular orbital
MeCN	Acetonitrile
mCBP	3,3′-Di(9*H*-carbazol-9-yl)-1,1′-biphenyl
mCP	1,3-Bis(*N*-carbazolyl)benzene
MLC	Mechanochromic luminescence

NIR	Near-infrared
NBPhen	2,9-bis(naphthalen-2-yl)-4,7-diphenyl-1,10-phenanthroline
NPB	*N*,*N*'-Di(1-naphthyl)-*N*,*N*'-diphenyl-(1,1'-biphenyl)-4,4'-diamine
OLED	Organic light emitting diode
PE	Power efficiency
PL	Photoluminescence/photoluminescent
R_1/R_2	contribution ratio of τ_1/τ_2
PXRD	Powder X-ray diffraction analysis
rISC	Reverse intersystem crossing
RTP	Room temperature phosphorescence
S_1	First singlet energy level
T_1	First triplet energy level
TADF	Thermally activated delayed fluorescence
TCTA	Tris(4-carbazoyl-9-ylphenyl)amine
TGA	Thermogravimetric analysis
T_g	Temperatures of glass transition
T_d	Temperature of 5% weight loss
T_m	Temperatures of melting point
THF	Tetrahydrofuran
TOF	Time-of-flight
t_{tr}	Transit times
TREL	Transient electroluminescence
TPBi	2,2',2''-(1,3,5-Benzinetriyl)-tris(1-phenyl-1*H*-benzimidazole)
TSPO1	Diphenyl-4-triphenylsilylphenylphosphine oxide
TTA	Triplet-triplet annihilation
UPS	Ultraviolet photoelectron spectroscopy
UV	Ultraviolet
U	Applied voltage thicknesses of the layers (d)
ΔE_{ST}	Difference between the first excited singlet and triplet states
f_w	Water fraction
λ	Wavelength
μ	Drift mobility of charge carriers
τ	Emission lifetime
χ^2	Weighted sum of squares of deviations of calculated points of multiexponential fitting of a photoluminescence decay curve
Φ	Photoluminescence quantum yield

TABLE OF CONTENTS

1. INTRODUCTION

The evolution of light-emitting organic compounds is a prerequisite for the development of highly efficient optoelectronic devices. Although a great deal of research efforts have been devoted to find easily synthesizable and efficient organic electroactive compounds, the preparation of most of them still involves complex synthesis pathways that are technologically complicated to implement[1,2]. Their synthetic processes are usually lengthy, multi-step, time-consuming and cost-ineffective. Therefore, one of the most significant ways to ensure the possibility of the commercialization of organic electroactive materials and the devices of organic electronics is the preparation of organic semiconductors and emitters by cost-effective single-step synthesis and simple methods of their purification.

Organic semiconductors as materials for optoelectronic devices have been investigated for over a century[3]. The first efforts to study the optical and electronic properties of organic semiconductors were done on a specimen of anthracene derivatives in 1910[4]. Nevertheless, only during the latest 30 years, researchers have been paying attention to the development of organic electroactive materials for the application in electronic devices. This has led to the considerable progress in this area. The main fields of the application of organic semiconductors are organic light-emitting diodes (OLEDs)[5–14], optical oxygen sensors[15–17], organic field-effect transinstors[18,19], vertical organic transistors[20,21], solar cells[22–24], etc. Among these devices, OLEDs have attracted a huge interest of the scientific and industrial communities due to their applications in displays and lighting devices[25]. Major progress has been achieved in the field of electroluminescent materials and devices since the time when the first OLED was fabricated by Tang and Van Slyke in 1987[26].

For the design of light-emitting or host materials, chemical structures containing donor and acceptor moieties have been recently applied[6,7,27,28]. A combination of donor and acceptor moieties allows obtaining highly emissive materials with bipolar charge-transporting properties. Carbazole[27,29–31], triphenylamine[32–34], phenothiazine[33,35], and phenoxazine[36,37] moieties have been used as electron-donating and hole-transporting units. As electron-withdrawing units and also as electron-transporting units, such moieties as pyridine[38,39], pyrimidine[28,30,40], triazine[41,42], benzophenone[27,43], oxadiazole[32,44], etc. have been used. At the time of the beginning of this work, benzanthrone and pyrimidine-5-carbonitrile were not being widely used as acceptor moieties in the design of emitters with the donor-acceptor structure. Benzanthrone (benzo[*de*]anthracen-7-one) is a polycyclic aromatic compound belonging to the class of ketones. Mainly, it was being used as an intermediate for the synthesis of various pigments[45,46]. Pyrimidine-5-carbonitrile is an aromatic nitrogen-containing a hetero-cycle substituted by a cyano (-CN) group. This compound was used in the fabrication of OLEDs[40,47] and as an anticancer agent[48,49].

Light-emitting materials with the donor-acceptor-donor structure can exhibit various phenomena of interest, such as room temperature phosphorescence (RTP)[50,51], triplet-triplet annihilation (TTA)[52,53], or thermally activated delayed fluorescence (TADF)[29,41,54]. Their emission can occur due to the hybridized local

and charge transfer (HLCT)[10,11] excited-state and hot-exciton mechanism[13,14,55]. Due to these phenomena, the conversion of the formed triplet excitons into the light under electrical excitation is possible[10,13,41,52]. They allow to overcome the theoretical limits of internal quantum efficiency (IQE) and external quantum efficiency (EQE) of 25% and 5%, correspondingly, for OLEDs fabricated by using fluorescent emitters[56,57]. The utilization of the above-mentioned phenomena leads to an increase of the efficiency of OLEDs, the purity of emission colors, and device stability.

Recently, significant efforts have been made to develop efficient emitters with the donor-acceptor structure exhibiting TADF, and up to 38% of EQE for modern TADF OLEDs has been obtained[58,59]. The materials exhibiting TADF can upconvert triplets to the first excited singlet states due to the mechanism of the reverse intersystem crossing (rISC); therefore, an IQE of 100% can theoretically be reached[29]. For efficient rISC, the difference between the first excited singlet and triplet states (ΔE_{ST}) should be as low as possible (ideally, $\Delta E_{ST} < 0.1$ eV)[1]. For an efficient TADF, a minimum overlapping of the highest occupied molecular orbital (HOMO) and the lowest unoccupied molecular orbital (LUMO) is needed[60,61]. The separation of HOMO and LUMO can be achieved by the twisted geometry of a molecule[62]. Thus, the development of materials with the donor-acceptor or the donor-acceptor-donor structure is the most favorable strategy to obtain compounds with the TADF properties. Since, in most cases, the donor-acceptor type molecules are characterized by twisted geometries[63], and they feature an increased dihedral angle between the donor and acceptor moieties, ΔE_{ST} is reduced.

The efficiency, durability and cost-efficiency are the most significant factors which have to be taken into account in the course of the development of OLEDs for displays and lighting devices[8]. The wider application of OLEDs is apparently limited by the insufficient performance of blue emitters. Blue TADF OLEDs suffer from low durability and decreasing efficiency roll-off at high luminance[8]. However, the participation of triplet excitons in emission allows increasing the IQE and obtaining highly efficient devices[58,59,64]. Meanwhile, the lifetimes of blue TADF devices are less than 500 h at an initial luminance of 1000 cd/m^{-2}; [65]. The reason is that, for blue emitters, high excitation energy is needed[8]. At such high energy, the stability of organic molecules decreases, and, as a result, blue OLEDs degrade within a short period of time. For this reason, the development of chemically and thermally stable organic electroactive materials is the main way to accelerate the implementation of blue TADF OLEDs in the industry. The blue emitters exhibiting singlet emission are denoted by two significant advantages, such as stability and cost-effective fabrication, whereas the main disadvantage is the low efficiency of devices limited by 5%. In order to increase the EQE of blue fluorescent devices up to 12%, it is possible by design and develop materials with additional phenomena, such as HLCT[10,11], or hot exciton mechanism[13,14].

TADF materials with the donor-acceptor structure offer a great potential to be used not only in OLEDs, but also for the preparation of active layers (indicators) in optical oxygen sensors[66–69]. Usually, phosphorescent emitters based on heavy metals (platinum, palladium, iridium, etc.) are applied as indicators. They are

environmentally unfriendly and expensive[15]. Various fullerenes and metal complexes characterized by delayed emission in the near-infrared region (NIR) demonstrated efficient oxygen sensing properties[16,17,70]. Purely organic NIR TADF emitters with the donor-acceptor structure demonstrating long-lived emission can also be used for oxygen probes as an alternative[71,72]. For the design of NIR TADF compounds, an acceptor with a rigid molecular structure has to be used[72]. NIR emission and NIR OLEDs are also applied in various types of devices used in bioimaging[73,74], detection of viruses[75], communication[76], etc.

Light-emitting materials with the donor-acceptor structure can change the color of emission under the influence of various external stimuli[77]. Mechanochromism, thermochromism, photochromism and acidochromism can be distinguished as the main phenomena which induce the color-changing ability of organic electronically active materials[78]. Mechanochromic luminescence (MLC) is characterized as reversible change of emission under mechanical stimuli[77]. MLC materials can be potentially used in mechanical sensors, data encryption devices and memory chips[79–81]. Various molecular packings and intermolecular interactions exert influence on mechanically-induced fluorescence, and, as a consequence, the shift of fluorescence in the blue or red region can be detected[82]. In addition, polymorphism can cause the MLC if the material consists of various crystals which are characterized by the different molecular packings[83–85]. MLC is mainly studied by using such stimuli as grinding, fuming and melting[82–85]. However, the emission of only a few materials can self-recover from that of the ground state to the initial one without any additional forces that is called self-recovering mechanochromism[86–88].

The development of new organic light-emitting materials with the donor-acceptor structure is one of the main means to overcome any issues related to the durability, efficiency, and cost-efficiency of OLEDs. In order to obtain materials with special properties, the careful selection of the donor and acceptor units has to be done. The chemical structure and the thermal stability of the selected molecular moieties have a decisive effect on the applicability of the organic semiconductor in electroluminescent devices. The combination of purposively selected donors and acceptors allows synthesizing novel organic light emitting semiconductors and predicting the mechanism of the emission or charge-transporting properties. The design, synthesis and investigation of the properties of the newly developed emitters is the main way to increase the efficiency of OLEDs and also to find new possible applications for the developed organic materials.

The aim of the present work is the synthesis and investigation of the properties of new donor-acceptor derivatives containing benzanthrone or pyrimidine-5-carbonitrile moieties for the application in OLEDs and oxygen sensors.

In order to achieve the aim of the work, the following tasks were outlined:

- Synthesis of new derivatives of benzanthrone with the donor-acceptor and the donor-acceptor-donor structures.

- Study of the thermal, photophysical and photoelectrical properties of benzanthrone-based materials.
- Investigation of the mechanochromic properties of the derivatives of benzanthrone and carbazole and their potential application in security probes.
- Study of the deep red/near-infrared TADF properties of phenothiazine or phenoxazine-substituted benzanthrones as promising candidates for oxygen sensing probes.
- Synthesis of new compounds with the symmetrical donor-acceptor-donor structure containing pyrimidine-5-carbonitrile and differently substituted carbazole or triphenylamine moieties.
- Investigation of the thermal, photophysical, photoelectrical and electroluminescent properties of pyrimidine-5-carbonitrile derivatives.
- Study of the derivatives of pyrimidine-5-carbonitrile and differently substituted carbazole as the emitters for sky-blue TADF OLEDs and oxygen sensing probes.
- Investigation of the triplet harvest abilities of triphenylamino or 9-phenyl carbazolyl substituted pyrimidine-5-carbonitriles and their application as bipolar emitters and hosts.

Novelty of the work:

- For a material containing benzanthrone and carbazole moieties, self-reversible mechanochromism has been detected; the concept of the potential application of its self-recovering properties for damage-resistive information recording and security probes has been developed.
- A new NIR TADF emitter based on benzanthrone and phenoxazine has been synthesized, and its applicability as an oxygen sensing probe has been demonstrated.
- New TADF emitters containing pyrimidine-5-carbonitrile moiety as the acceptor and carbazolyl and *tret*-butyl carbazolyl groups as donors have been developed; their applicability for the fabrication of efficient sky-blue OLEDs and oxygen sensors has been demonstrated.
- Triphenylamino or 9-phenyl carbazolyl substituted pyrimidine-5-carbonitriles have been synthesized for the first time and utilized as emitters for blue and green fluorescent OLEDs and as hosts for efficient orange-red TADF OLEDs with EQE exceeding 20%.

Contribution of the author:

The author has designed, synthesized and purified four series of the organic materials described in Chapters 2.1–2.4. The author has performed and analyzed the results of ultra-violet absorption measurements, the investigation of photoluminescence properties including quantum yield and lifetime exited measurements. Also, the author has investigated and analyzed mechanochromic

luminescence, as well as the thermal and oxygen-sensing properties of the materials. Dr. Galyna Sych (Université Grenoble Alpes, CNRS) advised and assisted with synthesis, and investigated the mechanochromic properties of the derivatives. Dr. Dmytro Volyniuk performed the ionization potential measurements and investigated the hole-transporting properties of the compounds. Fabrication and characterization of OLEDs was done by Dr. Oleksandr Bezvikonnyi and Mr. Karolis Leitonas. Also, Dr. Oleksandr Bezvikonnyi studied the oxygen properties of the materials. Dr. Viktorija Andrulevičienė has performed DFT calculations and analyzed the obtained data. Dr. Rasa Keruckienė and Dr. Monika Čekavičiūtė measured the thermal properties of the compounds, and the author analyzed the obtained results. Dr. Jūratė Simokaitienė advised regarding the description of the glass forming/thermal properties of the materials. Dr. Jonas Keruckas performed the characterization of the devices. Dr. Eglė Jatautienė and Dr. Asta Dabulienė advised with the synthesis of new materials. Dr. Audrius Bučinskas performed crystal X-ray analysis. Dr. Xiaofeng Tan advised with the photoluminescence measurements; all of them represent the Department of Polymer Chemistry and Technology, KTU. Dr. Pavlo Stakhira (Department of Electronic Devices, Lviv Polytechnic National University) advised in terms of the device structures for OLEDs. Dr. Algirdas Lazauskas (Institute of Materials Science, KTU) performed powder X-ray diffraction analysis, and the author analyzed the obtained results. Dr. Boris F. Minaev (Department of Chemistry and Nanomaterials Science, Bohdan Khmelnytsky National University) performed DFT calculations. Dr. Iryna Danyliv and Yan Danyliv (Department of Electronic Devices, Lviv Polytechnic National University) assisted with cyclic voltammetry measurements, and the data was analyzed by the author. Dr. Vidmantas Jasinskas and Dr. Vidmantas Gulbinas (Center for Physical Sciences and Technology, Vilnius) performed transient differential absorption measurements and analyzed the data. Prof. dr. Habil. Juozas Vidas Gražulevičius advised with the design of new light-emitting materials and the preparation of the manuscripts.

List of scientific publications on the topic of the dissertation

1. Tsiko Uliana; Sych Galyna; Volyniuk Dmytro; Bezvikonnyi Oleksandr; Keruckiene Rasa; Lazauskas Algirdas; Grazulevicius Juozas Vidas. Self-recovering mechanochromic luminescence of the derivatives of benzanthrone and carbazole: towards damage-resistive information recording and security probes // Dyes and pigments. ISSN 0143-7208. 2022, vol. 199, art. No. 110082, p. 1–8. (Web of Science). DOI: 10.1016/j.dyepig.2022.110082. [IF: 5.122; Q1].

2. Tsiko Uliana; Bezvikonnyi Oleksandr; Volyniuk Dmytro; Minaev Boris F.; Keruckas Jonas; Cekaviciute Monika; Jatautiene Egle; Andruleviciene Viktorija; Dabuliene Asta; Grazulevicius Juozas Vidas. TADF quenching properties of phenothiazine or phenoxazine-substituted benzanthrones emitting in deep red/near-infrared region towards oxygen sensing // Dyes and pigments. ISSN 0143-7208. 2022, vol. 197, art. No. 109952, p. 1–9. (Web of Science). DOI: 10.1016/j.dyepig.2021.109952. [IF: 5.122; Q1].

3. Tsiko Uliana; Bezvikonnyi Oleksandr; Sych Galyna; Keruckiene Rasa; Volyniuk Dmytro; Simokaitiene Jurate; Danyliv Iryna; Danyliv Yan; Bucinskas Audrius; Tan Xiaofeng; Grazulevicius Jouzas Vidas. Multifunctional derivatives of pyrimidine-5-carbonitrile and differently substituted carbazoles for doping-free sky-blue OLEDs and luminescent sensors of oxygen // Journal of Advanced Research. ISSN 2090-1232. 2021, vol. 33, p. 41–51. (Web of Science). DOI: 10.1016/j.jare.2021.01.014. [IF: 12.822; Q1].

4. Tsiko Uliana; Volyniuk Dmytro; Andruleviciene Viktorija; Leitonas Karolis; Sych Galyna; Bezvikonnyi Oleksandr; Jasinskas Vidmantas; Gulbinas Vidmantas; Stakhira Pavlo; Grazulevicius Juozas Vidas. Triphenylamino or 9-phenyl carbazolyl-substituted pyrimidine-5-carbonitriles as bipolar emitters and hosts with triplet harvesting abilities // Materials Today Chemistry, 2022, vol. 25, art. No. 100955, p. 1–13. (Web of Science). DOI: 10.1016/j.mtchem.2022.100955. [IF: 7.613; Q1].

2. REVIEW OF PUBLISHED ARTICLES

The *Review of Published Articles* Chapter contains the information from the articles of the author (see *7. List of Publications on the Subject of the Thesis*). [89–92]

2.1 Self-recovering mechanochromic luminescence of the derivatives of benzanthrone and carbazole: Towards damage-resistive information recording and security probes (Scientific publication No. 1, Q1)

This chapter is based on the article published in *Dyes and Pigments*, **2022**, *199*, 110082, p. 1–8[89]. The rapid development of optoelectronics is based on the many efforts of scientists directed towards finding new organic materials with unique properties. In this work, the novel synthesized material demonstrated self-recovering mechanochromic luminescence. For the design of the materials demonstrating MLC benzanthrone as a new acceptor with a rigid planar structure, carbazole and di-*tert* butyl carbazole as donors were used. The synthetic way of the synthesis of compounds 3-(9*H*-carbazol-9-yl)-7*H*-benzo[*de*]anthracen-7-one (**1**) and 3-(3,6-di-*tert*-butyl-9*H*-carbazol-9-yl)-7*H*-benzo[*de*]anthracen-7-one (**2**) is presented in Scheme 2.1. To obtain the target derivatives with the required donor-acceptor structure, Buchwald-Hartwig cross coupling reactions were performed. The chemical structures of compounds **1,2** were confirmed by using ^{1}H and ^{13}C NMR spectroscopies, mass spectrometry, and elemental analysis.

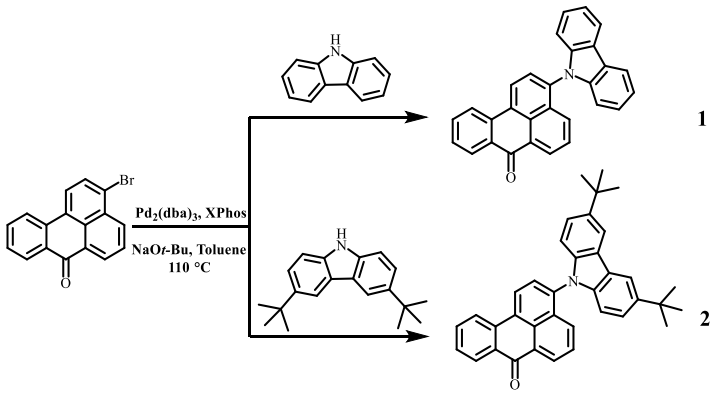

Scheme 2.1 Synthetic pathway and molecular structure of compounds **1** and **2**.

The thermal stability and the morphological transitions of derivatives **1** and **2** were studied by using thermogravimetric analysis (TGA) and differential scanning calorimetry (DSC) (Fig. 2.1a) measurements, correspondingly. All the data is summarized in Table 2.1. Both compounds showed high thermal stability, and they experienced sublimation, as confirmed by TGA analysis. The temperatures of glass transition (T_g) for compound **1** were found to be 93 °C, whereas, for compound **2**, 124 °C was determined. These values were recorded in the second heating scan. The two temperatures of the melting point (T_m) were detected in the first heating scan for both derivatives (Table 2.1, Fig. 2.1a). However, after the cooling and the second heating, only one melting point was observed for compounds **1** and **2**[93]. This observation was additionally investigated by doing DSC scans of a few crystals of

compound **1** in order to confirm the presence two polymorphs. The influence of different polymorphs on the MLC properties of the obtained materials was also studied.

Table 2.1. Thermal and photophysical properties of **1** and **2**.

Comp.	T_d [a], °C	T_m, °C	T_g [c], °C	T_{cr} [c], °C	λ_{PL} [tol/film], nm	Φ [tol/film], %	τ [tol], ns	τ_1/τ_2 [film], ns
1	344	259[b]/276[b,c]	93	140	501/560	34/22	4.30	1.32/5.36
2	359	264[b]/296[b,c]	124	197	530/590	53/22	8.72	1.61/6.38

[a] – determined from TGA; DSC: [b] – first heating scan, [c] – second heating scan; T_d – the temperature of 5% weight loss; T_g – the temperature of glass transition; T_m – the temperature of melting point; T_{cr} – crystallization; λ_{PL} is the wavelength of PL maximum; Φ is the photoluminescence quantum yield; τ_1, τ_2 are photoluminescence lifetimes of neat films of compounds.

The photophysical properties, such as absorption and photoluminescence (PL), of the obtained compounds **1** and **2** were studied and presented in Table 2.1 and Fig. 2.1b. Two absorptions bands at ca. 295 and 320–335 nm indicate π-π* transitions of the carbazole moiety[94] (Fig. 2.1b). The next band at ca. 380 nm can be attributed to the π-π* transitions on the whole molecule. Also, the last low-energy band at ca. 430 nm can apparently be characterized by the intramolecular charge transfer (ICT) between carbazole and BZA moieties[46]. The PL emission of the toluene solution and the neat film of compound **1** was investigated and characterized by two different fluorescence maximums centered at 501 nm (toluene solution) and 560 nm (neat film) (Table 2.1). Meanwhile, the toluene solution of compound **2** demonstrated emission with the maximum at 530 nm and the neat film at 590 nm. In the solid state, both compounds **1** and **2** showed a photoluminescent quantum yield (Φ) exceeding 22% (Table 2.1). The PL decay curves of the toluene solution of compounds **1** and **2** were measured in the range of ns that confirmed the fluorescence nature of the emission (Table 2.1).

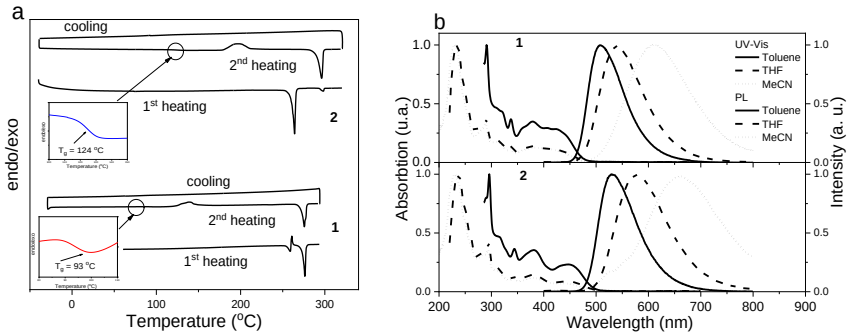

Fig 2.1. DSC (a) curves of powders of **1** and **2.** UV-Vis absorption and PL spectra (b) of solutions of compounds **1** and **2** (λ_{exc} = 330 nm).

The synthesized derivatives **1** and **2** demonstrated multi-colour mechanochromic properties. The color of emission can be changed by applying the additional stimuli, such as grinding, fuming or melting. All the data for as-prepared (initial), ground, fumed in case of compound **1** and self-recovered in the case of

compound **2** samples is listed in Table 2.2 and presented in Fig. 2.2. Compound **1** showed the changing of emission from green colour (538 nm, initial state) to yellow (574 nm, melted state), whereas, for compound **2**, the as-prepared sample showed green-yellowish emission (550 nm), and the melted sample gave orange emission (594 nm) (Table 2.2, Fig. 2.2a,b). Φ and emission lifetimes for each state are collected in Table 2.2.

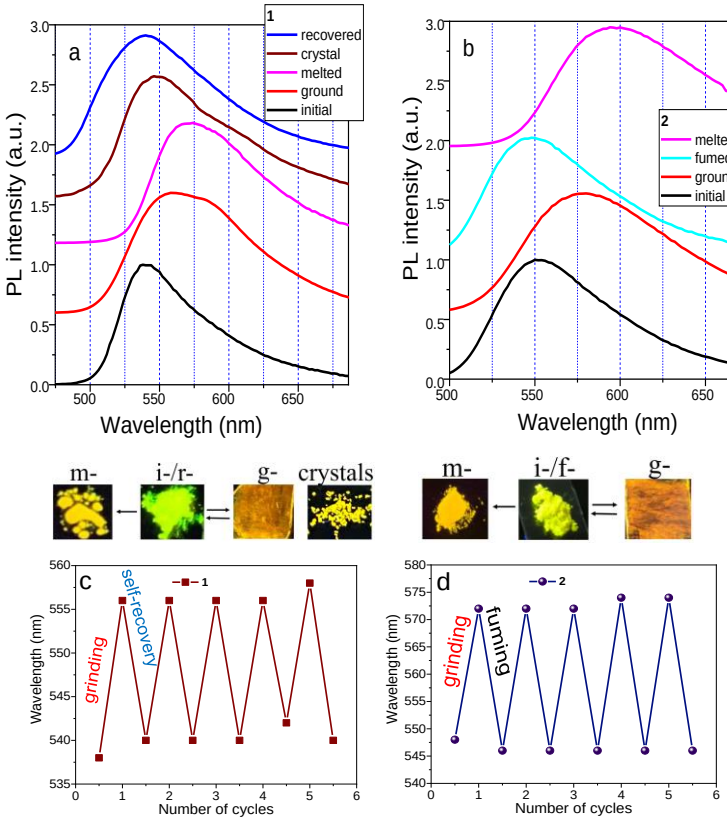

Fig. 2.2. Normalized PL spectra (a, b) of different states of compounds **1** and **2**. PL reversibility of compound **1** (c) and compound **2** (d) (λ_{exc}=350 nm).

Compound **1** containing carbazole exhibited self-reversible MCL at room temperature (Fig. 2.2a). After grinding, the sample can recover to the initial state without any additional stimuli within 20 min. This process is reversible up to 5 cycles of grinding/self-recovery (20 min), which is shown in Fig. 2.2c. The ground sample of compound **2** did not experience self-reversible MCL (one month of observations). However, it is still possible to recover the ground form of **2** to the initial form by using fuming in DCM vapors within 5 min (Fig. 2.2b). As it was in the case of **1**, compound **2** also demonstrated stable PL reversibility up to 5 cycles of grinding/fuming (5 min) (Fig. 2.2d).

In order to understand the MCL properties of compounds **1** and **2**, single crystal X-ray analysis (Fig. 2.3a,b), PL measurements for amorphous solid-state solutions (Fig. 2.3c,d), and powder X-ray diffraction (PXRD) analysis (Fig. 2. 3e,f)

were performed. The proper crystal for single crystal X-ray analysis was obtained only for compound **1** by slow evaporation of its methanol solution (Fig. 2.3a). The single crystal of **1** was characterized by several types of interactions: C-H···O (2.429 and 2.570 Å), C-H···H (2.367 Å), and C-H···π (2.751 Å).

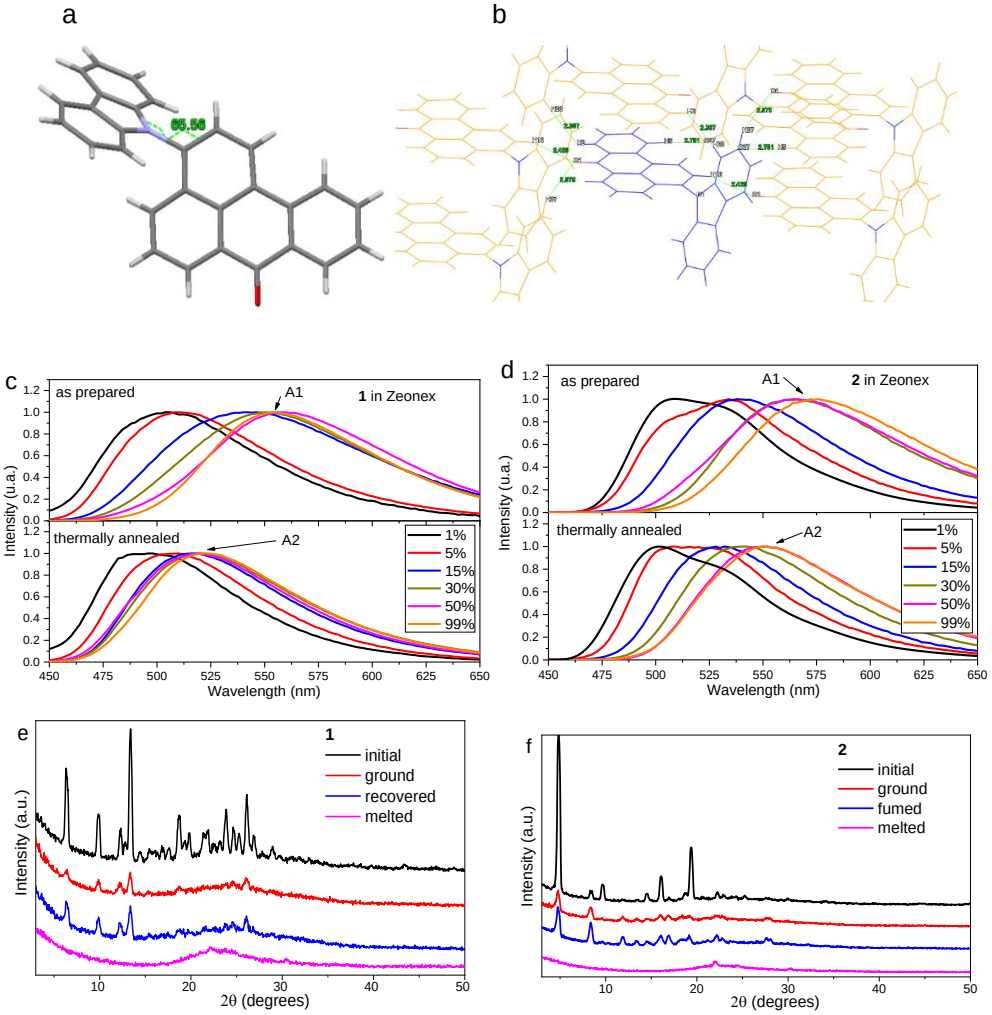

Fig. 2.3. Single crystal X-ray structure (a) and the packing mode (b) of compound **1** (CCDC number 2046803); PL spectra of solid mixtures of compound **1** (c) and **2** (d) with Zeonex as prepared (above), and after thermal annealing (below); PXRD patterns (e, f) of the different states of derivatives **1** and **2**.

The amorphous mixture of **1** and **2** doped in the rigid polymer matrix Zeonex was studied to confirm the possibility of formations of different amorphous aggregates (Fig. 2.3c,d). The red-shifts of PL were observed while increasing the concentration of the materials in the guest-host systems of the material Zeonex. It corresponds not only to solid solvatochromism, but also to the formation of amorphous aggregates (marked as A1, Fig. 2.3c,d). For compound **1**, the amorphous

aggregate A1 is described by PL spectra centered at 555nm, and, for compound **2**, this type of aggregate is located at 568 nm. After the thermal annealing of the samples at 150°C, it was decreased in terms of the aggregation degree of A1aggregates (red-shifted emission). Yet, at the same time, it led to the formation of the second type of aggregates (marked as A2, Fig. 2.3c,d) with the blue-shifted PL emission. These aggregates A2 are characterized by their PL spectra peaking at 521 and 550 nm for compounds **1** and **2**, respectively. The presence of both crystalline polymorphs (according to DSC measurements) and amorphous aggregates has influence on the total emission of the different states of materials **1** and **2** (Fig. 2.2).

Table 2.2. PL characteristics of MLC and morphological properties of compounds **1** and **2**.

State / Parameter	**1**					**2**			
	i-	g-	r-	m-	cr-	i-	g-	f-	m-
λ_{PL}, nm	538	560	540	574	546	550	580	548	594
Φ_{PL}, %	15	17	15	9	-	27	31	23	3
τ_1, ns	1.13	2.04	2.01	1.97	1.49	2.67	3.91	2.69	3.09
R_1, %	43	30	31	24	34	20	23	17	22
τ_2, ns	5.28	6.93	7.13	6.60	9.41	6.09	9.62	6.04	8.97
R_2, %	57	70	69	76	66	80	77	83	78
crystallinity* %	63.8	29.3	39.5	0	100	66.4	42.1	49.8	3.3

(i-) – initial, (g-) – ground, (r-) – recovered, (m-) – melted, (cr-) – crystal; λ_{PL} is the PL maxima (λ_{exc}=350 nm); Φ_{PL} is the photoluminescence quantum yield; τ_1, τ_2 are the PL lifetimes (well-fitted with the χ^2 values of 1.021–1.206), R_1,R_2 are the contribution ratio of τ_1/τ_2; *obtained from PXRD measurements.

The PXDR patterns shown in Fig. 2.3e,f confirmed the crystalline nature of powders compounds **1** and **2**. The degree of crystallinity for derivatives **1** and **2** was 63.8% and 66.4% in the initial state, respectively (Table 2.2). After melting, the degree of crystallinity was determined as 0% (compound **1**) and 3% (compound **2**), which confirmed the change of the state from crystalline to amorphous (Table 2.2). After the intense grinding of as-prepared powders, the degrees of crystallinity were decreased because the dihedral angle between carbazole/di-*tert*-butyl carbazole and BZA fragments most likely changed, and the crystalline packing of the as-prepared forms was partially destroyed and converted into the amorphous state. Regardless the full recovering of the PL emission, the self-recovered sample of **1** and the fumed form of **2** experienced only partial restoration of the crystallinity with the degrees of crystallinity of 39.5% and 49.8%, respectively (Table 2.3).

Taking into account, the above described experimental results for the obtained derivatives **1** and **2**, we presented the formation of two types of amorphous aggregates named A1 and A2 (Fig. 2.3c,d). Due to the high rigidity of Zeonex, the presence of crystalline aggregates in the molecular dispersions in this polymer is highly improbable[95,96]. Red-shifted PL emission was shown by the first type of aggregates A1 (as-prepared samples), and blue-shifted PL emission was demonstrated by the second type of polymorphs A2 (thermally-annealed samples) (Fig 2.3c,d). Also, according to the PXRD, photophysical and DSC measurements

we detected two types of crystalline polymorphs. One type of polymorph showed red-shifted PL emission (Fig. 2.2a). The other type of polymorph definitely exhibited blue-shifted emission similarly to the emission of the as-prepared powder. The formation of the second type of polymorph is evident due to the high degree of crystallinity (63.8% for **1** and 66.4% for **2**) of the as-prepared powders (Fig. 2.3e,f, Table 2.2). The single crystal X-ray structure and the PL emission spectrum were not measured for the second polymorph because of the difficulties of separation of the extremely small sizes of crystals for this type of polymorph. Fortunately, self-recovering mechanochromic luminescence is possible apparently because of the extremely small size of the second type of polymorph of compound **1**. As a result, we observed the red-shifted emission for the first type of amorphous aggregates and for one type of polymorph. Also, we observed blue-shifted emission for the second type of amorphous aggregates and for another type of polymorph. Thus, in comparison with the huge number of other reported MCL materials, we can conclude that the multi-color mechanochromic luminescence of compounds **1** and **2** was caused by the presence of different crystalline polymorphs and amorphous aggregates.

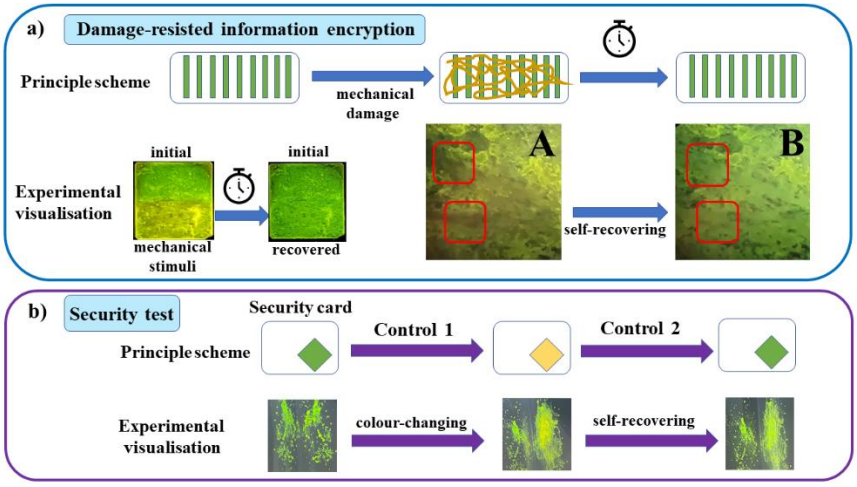

Fig. 2.4. Demonstration of possible application of self-recovering material **1** in data/code writing (a) or security probes (b) with the ability to recover after mechanical damage.

The self-recovering properties of compound **1** can potentially be applied for damage-resistive information encryption or for security check. The schematic schemes and experimental visualizations of the potential applications are shown in Fig. 2.4. In the test of the damage-resistive information encryption, the dark mechanically damaged areas marked by red rectangles in photo A, Fig. 2.4a become bright again after the recovery time (see the same rectangles in photo B, Fig. 2.4a. The unique properties of compound **1** can also be used for the multistep control of protected objects. The first step (control 1) is the change of the emission color from

bright green to yellow, whereas the second step (control 2) is the change of the emission color from yellow back to bright green (Fig. 2.4b).

2.2 TADF quenching properties of phenothiazine or phenoxazine-substituted benzanthrones emitting in deep-red/near-infrared region towards oxygen sensing (Scientific publication No. 2, Q1, 2 quotations)

This chapter is based on the article published in *Dyes and Pigments*, **2022**, *197*, 109952, p. 1–9[90]. The donors with stronger electron-donating abilities were used for the design of new benzanthrone-based materials for the investigation of their influence on light-emitting properties in comparison with carbazole-based materials. The manuscript introduces the study on the synthesis and investigations of light-emitting and oxygen sensing properties of new derivatives of BZA. For the development of new materials demonstrating emission in the deep-red/NIR region and TADF, BZA as a new acceptor characterized by a rigid molecular structure was chosen. The combination of planar moieties with strong electron-donating abilities (phenothiazine or phenoxazine) and a rigid moiety with the electron-accepting ability (BZA) allowed us to obtain four new NIR TADF emitters. For the synthesis of compounds 3-(10*H*-phenothiazin-10-yl)-7*H*-benzo[*de*]anthracen-7-one (**3**), 3,9-di(10*H*-phenothiazin-10-yl)-7*H*-benzo[*de*]anthracen-7-one (**4**), 3-(10*H*-phenoxazin-10-yl)-7*H*-benzo[*de*]anthracen-7-one (**5**), and 3,9-di(10*H*-phenoxazin-10-yl)-7*H*-benzo[*de*]anthracen-7-one (**6**) with the donor-acceptor and donor-acceptor-donor structures, Buchwald-Hartwig cross coupling reactions were used (Scheme 2.2). ^{1}H, ^{13}C NMR, IR, mass spectroscopies and elemental analysis were performed for the identification of derivatives **3–6**.

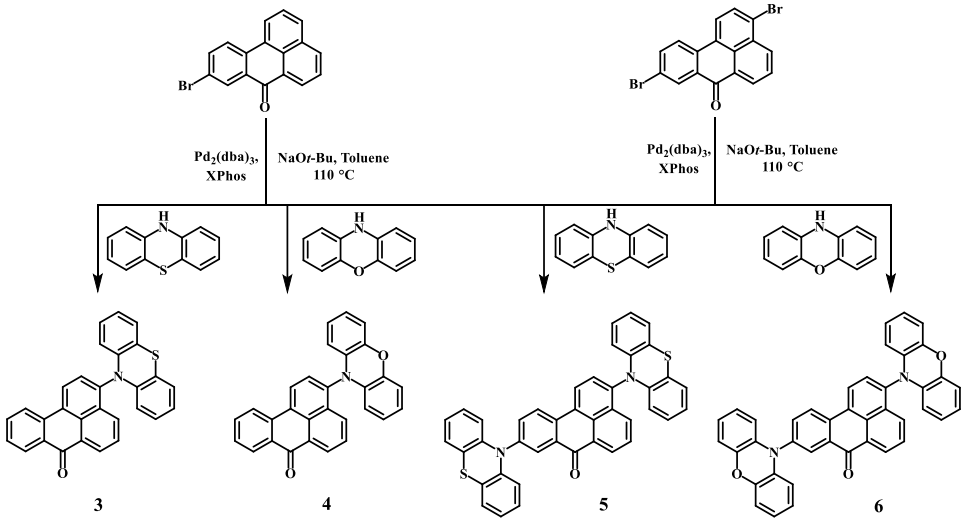

Scheme 2.2 Synthetic pathways of derivatives **3–6**.

The TGA and DSC curves were recorded to study the thermal properties of **3–6**. They demonstrated relatively high thermal stability. Compounds **3** and **4** with the D-A structure showed lower thermal stability (T_d exceeded 300 °C) in comparison

with compounds **5** and **6** with the donor-acceptor-donor structure (T_d exceeded 400 °C). During the second heating scan on the DSC curves, T_g values higher than 100 °C were observed for all derivatives (Table 2.3). For compounds **3** and **6**, the melting points were recorded in the first heating scan, and, for them, no crystallization was observed during the cooling scans. Two other compounds **4** and **6** did not demonstrate any the crystallization or melting peaks on the DSC curves (Table 2.3).

Table 2.3. Thermal and photoelectrical properties of compounds **3–6**.

Compounds	T_m, °C	T_{cr}, °C	T_g**, °C	IP^{UPS}, eV	μ^{holes}, $cm^2/V \cdot s$	$\mu^{electrons}$, $cm^2/V \cdot s$
3	286*, **	172**	111	5.68	9.8×10^{-6}	1.5×10^{-4}
4	-	-	114	-	-	-
5	-	-	174	-	-	-
6	391*,**	213**	170	5.49	7.4×10^{-8}	1.1×10^{-4}

* first heating scan; ** second heating scan. $\boldsymbol{\mu^{holes}}$ and $\boldsymbol{\mu^{electrons}}$ values taken at 3.6×10^5 V/cm.

Ultraviolet photoelectron spectroscopy (UPS) was used to record the photoelectron emission spectra of the vacuum-deposited layers of compounds **3–6** for the estimation of the ionization potential IP^{UPS} in the solid-state (Fig. 2.5a). The IP^{UPS} values were recorded only for compounds **3** and **6**, and their values were found to be below 6.0 eV (Fig. 2.5a, Table 2.3). For the two other compounds, the IP^{UPS} values were not obtained, apparently, due to the reason that the thermal properties of the compounds for which ionization potentials were measured are different from compounds **4** and **5**. According to Table 2.3 with the data on thermal properties, for compounds **3** and **6,** T_m was observed, while, for compounds **4** and **5**, it was not. Probably, it had influence on the film-forming properties of compounds **4** and **5**, and, during the vacuum-deposition of the layers of materials at a high temperature, the suitable samples were not obtained for UPS.

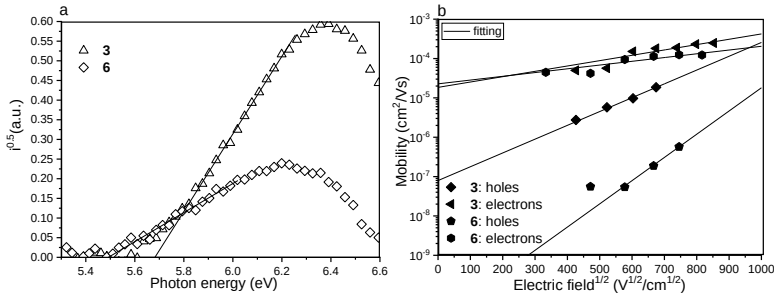

Fig. 2.5. Photoelectron emission spectra (a) and hole/electron drift mobilities versus electric field (b) for compounds **3** and **6**.

The time of flight (TOF) technique was applied to investigate the charge-transporting properties of compounds **3** and **6**. The samples of compounds **4** and **5** were not suitable for the TOF method because of their inferior film forming properties. Hole and electron mobilities were calculated according to the equation $\mu = d^2/(U \times t_{tr})$ taking transit times t_{tr} from the photocurrent transients at the applied voltage (U), and the thicknesses of the layers (d) were measured by the charge

extraction by linearly increasing the voltage (CELIV) technique assuming dielectric constant ε = 3 for the studied compounds.

In order to calculate hole and electron mobilities, the transit times at different applied voltages were used. The obtained materials **3** and **6** were characterized by the close values of electron mobility of 1.5×10^{-4}-1.1×10^{-4} $cm^2/V\cdot s$ at an electric field of $3.6\cdot10^5$ V/cm (Fig. 2.4b). This can be explained by the presence of the same electron-accepting unit, benzanthrone, in the structures of both molecules. Contrasting hole mobility values of 7.4×10^{-8} and 9.8×10^{-6} cm^2/Vs were obtained for compounds **3** and **6**, correspondingly (Table 2.3). It can be caused by different electron-donating moieties present in the molecular structures of the obtained materials.

The absorption and PL spectra of neat films and dilute toluene solutions of **3–6** recorded at 300 K are presented in Fig. 2.6a. The position of the absorption bands in the ultraviolet (UV) spectral region was independent of the type of donors attached to the BZA moiety, except for the location of the lowest energy absorption band (LEAB). The absorption spectra of toluene solutions of phenoxazine-based compounds **4** and **6** showed prominent LEAB at 500 nm. In the case of the toluene solutions of the derivatives containing phenothiazine units **3** and **5**, LEAB was hypsochromically shifted with a high-energy edge at 520 nm. The absorption bands of the films were slightly red-shifted and broader than the respective bands of the solutions, thus highlighting more efficient intramolecular interaction in the solid state.

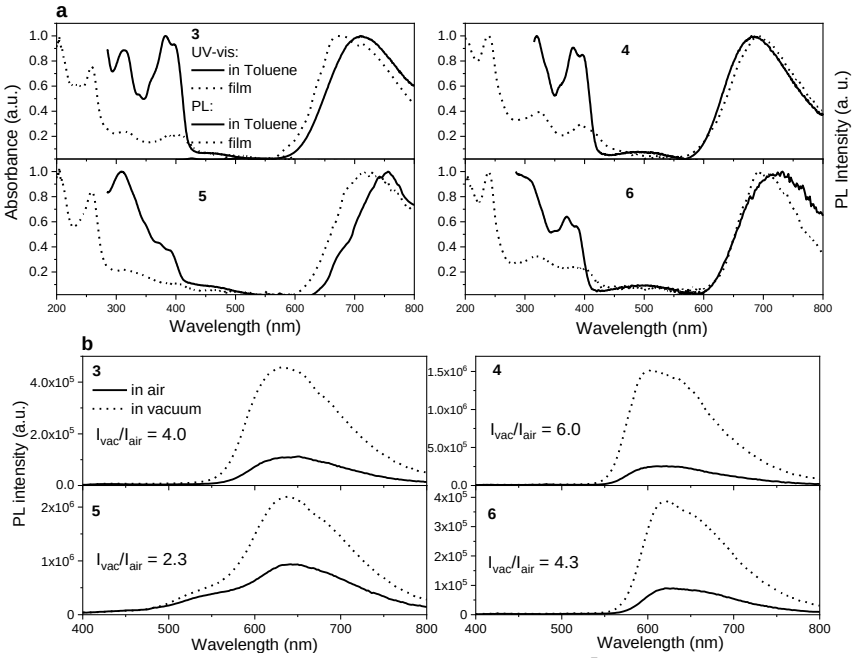

Fig. 2.6. Absorption and PL spectra of dilute 10^{-5} M toluene solutions and films of derivatives **3–6** (a). PL spectra of 1 wt% solid mixtures of derivatives in Zeonex recorded at different conditions (air and vacuum) (b).

The toluene solutions and films of the compounds **3–6** emitted in the red/NIR region (Fig. 2.6a). The extension of conjugation by the attachment of the second donor led to the red-shift of emission wavelengths. The PL quantum yields of the films and dilute toluene solutions were found to be ca. 0.01 for all the studied compounds (Table 2.4).

Zeonex is a polymer matrix used to study the photophysical properties of compounds in a condition of suppressed intermolecular interactions[17]. The solid molecular mixtures of **3–6** in Zeonex were prepared, and their PL spectra were measured under air and under vacuum (Fig. 2.6b). Due to the change of polarity, the blue-shift of PL of up to 75 nm for solid mixtures in Zeonex in comparison with the PL spectra on neat films was observed. The PL quantum yields of the solid solutions of **3–6** in Zeonex in air were found to be of 0.02, 0.03, 0.03 and 0.04, respectively (Table 2.4).

Table 2.4. Photophysical characteristics of derivatives **3–6**.

Compounds	Stokes shift^{tol}, nm	Stokes shift^{film}, nm	Φ^{tol}_{PL}, %	Φ^{film}_{PL}, %	Φ^{film}_{PL}, 1wt% in Zeonex, %	$\Phi^{film}_{PL}{}^{vac}$, 1wt% in Zeonex, %
3	316	275	1	1	2	8
4	308	273	1	1	3	7
5	193	188	1	1	3	18
6	196	225	1	1	4	17

Φ^{tol}_{PL}, Φ^{film}_{PL} values were recorded at air conditions and room temperature. $\Phi^{film}_{PL}{}^{vac}$ values at vacuum conditions were evaluated by using data of Φ^{film}_{PL} values and Fig. 2.6b.

For the confirmation of the TADF properties of materials, the PL decay curves were recorded at different temperatures (Fig. 2.7). The values of the TADF lifetimes of donor-acceptor compounds **3** and **5** were found to be of 788 and 1198 μs at room temperature, respectively, and, for compounds **4** and **6** – 291 and 368 μs, correspondingly.

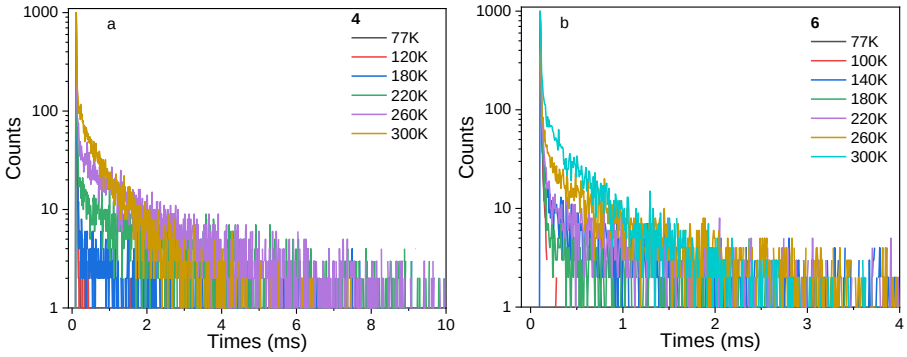

Fig. 2.7. Fig. 4. PL decay curves recorded at different temperatures under N2 atmosphere for 1 wt% solid solution of **5** (a) and **6** (b) in Zeonex.

Material **4** was chosen for the study of oxygen sensitivity because this compound demonstrated the most prominent increase of PL intensity upon the removal of air (Fig. 2.6b). The PL spectra and decay curves of the sample of a solid molecular mixture of **4** in Zeonex (1 wt%) placed in the atmosphere with the different oxygen/nitrogen ratios are presented in Fig. 2.8a. The data shows how

sensitive is the PL of the electronic excitation energy by collisional interactions with oxygen across a wide range of oxygen concentrations. For example, the TADF lifetime decreased to 245 μs for the sample under 8109 ppm of oxygen concentration (Fig. 2.8b). The ratio of intensity of TADF taken in vacuum and the prompt fluorescence taken under oxygen purge was found to be of 15.2. This value is comparable to the highest values reported for TADF-based optical oxygen sensors[67,97].

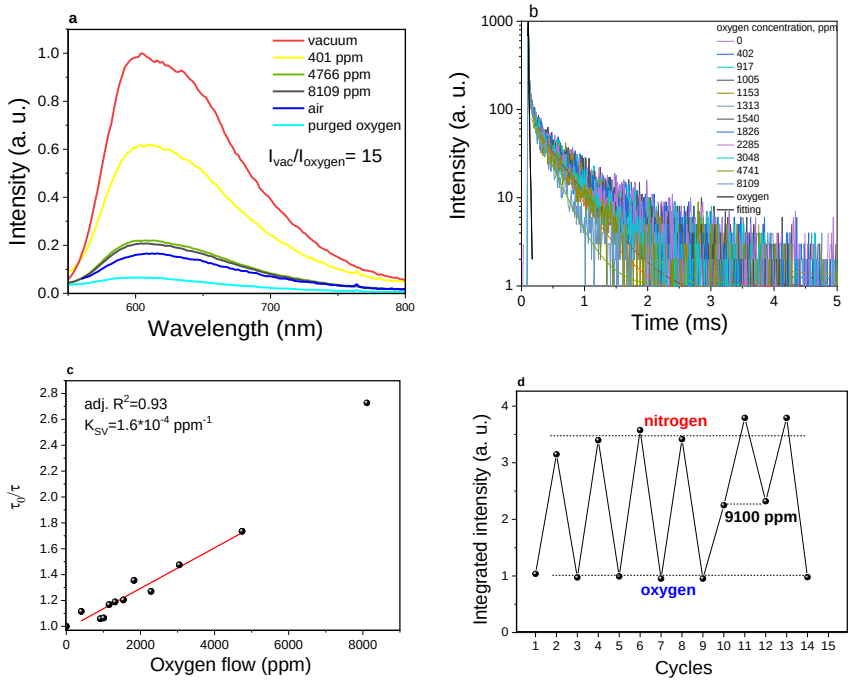

Fig. 2.8. PL spectra in media with different oxygen concentrations (a); PL decay curves (b), the Stern-Volmer plot (c) and oxygen response (d) for 1 wt% solid solution of **4** in Zeonex.

The Stern-Volmer plot (Fig. 2.8c) was built based on the equation $\tau_0/\tau - 1 = K_{SV}[O_2]$, where τ_0, and τ, are the lifetimes of TADF in the absence and in the presence of oxygen, respectively, and $K_{SV}[O_2]$ is the so-called Stern-Volmer constant. The plot showed linear dependence in the range of oxygen concentration up to 5×10^3 ppm with a $K_{SV}[O_2]$ of $1.6\cdot10^{-4}$ ppm^{-1}. The reversibility of the oxygen sensitivity after the removal of the quencher, i.e., oxygen, was also estimated. The PL decay curves of the sample were measured after its purging with oxygen, with nitrogen and 9100 ppm of oxygen flow within cycles with the duration of 7 min for each cycle (Fig. 2.8d). The value of integrated intensity of the solid mixture under oxygen atmosphere represents the instrument response of the microsecond lamp and the intensity of prompt fluorescence. It remains stable repeatedly after the following deoxygenation and oxygenation, which shows that the delayed fluorescence is totally suppressed after oxygenation. The integrated intensity under nitrogen continuously increased over time. Apparently, the diffusion of oxygen and the film is minimized after continuous nitrogen purge. Therefore, oxygen is more efficiently

removed from the sample with the additional cycles. The above mentioned diffusion does not have any impact on the integrated intensity under purged oxygen as the interaction of the film with oxygen is maximal in this case. The sample also showed the definitive response to the exact value of the oxygen flow manifested by the intensity level correlated to 9,100 ppm (Fig. 2.8d).

2.3. Multifunctional derivatives of pyrimidine-5-carbonitrile and differently substituted carbazoles for doping-free sky-blue OLEDs and luminescent sensors of oxygen (Scientific publication No. 3, Q1, 9 quotations)

This chapter is based on the article published in *Journal of Advanced Research*, **2021**, *33*, p. 41–51[91]. While aiming to achieve efficient bipolar charge transport, high Φ in the solid-state and triplet harvesting abilities (TADF) of organic semiconductors, symmetrical donor-acceptor-donor compounds were designed by selecting pyrimidine-5-carbonitrile as the acceptor and differently substituted carbazole as the donor moieties. The newly synthesized derivatives were applied for both efficient non-doped sky-blue OLEDs and optical sensors of oxygen with sustainable oxygen sensitivity. All the materials were obtained by one-step synthesis *via* nucleophilic substitution reactions from commercially available reagents. The synthetic route for the target compounds 4,6-di(9*H*-carbazol-9-yl)pyrimidine-5-carbonitrile (**7**), 4,6-bis(3,6-di-*tert*-butyl-9*H*-carbazol-9-yl)pyrimidine-5-carbonitrile (**8**) and 4,6-bis(3,6-dimethoxy-9*H*-carbazol-9-yl)pyrimidine-5-carbonitrile (**9**) is presented (Scheme 2.3). The chemical structures of the compounds were confirmed by ^{1}H and ^{13}C NMR spectroscopies, mass spectrometry, and elemental analysis.

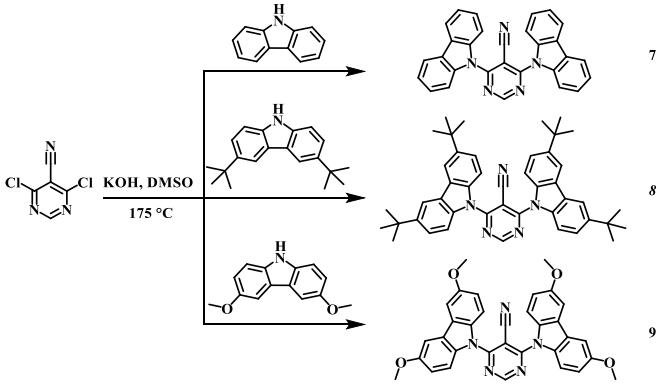

Scheme 2.3. Synthetic pathway to compounds **7–9**.

TGA and DSC were used to investigate the thermal properties of materials **7–9**. The results of the measurements are collected in Table 2.5. All the compounds demonstrated high thermal stability, and their values of 5% weight loss temperatures (T_d) significantly exceeded 300 °C. In comparison to compound **7** with T_d of 338 °C, compounds **8** and **9** exhibited higher T_d values of 396 °C and 383 °C, correspondingly (Table 2.5). Apparently, the presence of *tert*-butyl and methoxy groups in the molecular structures of compounds **8** and **9** led to the enhancement of intermolecular interaction in the solid state. All the compounds were obtained as

crystalline substances after synthesis and showed two melting points in the first DSC scans (Table 2.5). It can be assumed that two crystal forms of the synthesized compounds were obtained[93]. In the second heating scan of compound **7,** glass transition was observed at 112 °C. T_g of 177 °C was detected for compound **8** in the repeated heating scan, while compound **9** did not show any capability of glass formation (Table 2.5).

Table 2.5. Thermal, electrochemical and photoelectrical characteristics of **7**–**9**.

Comp.	T_d,[a] °C	T_g, °C	T_m, °C	E_{ox}^{onset}, V	E_{red}^{onset}, V	IP^{CV}, eV	EA^{CV}, eV	IP^{UPS}, eV	EA^{UPS}, eV
7	338	112[d]	273[b,d]/287[b]	1.02	- 1.90	5.82	2.90	6.30	3.91
8	396	177[d]	297[b]/326[b]	1.07	- 2.00	5.87	2.80	6.10	3.63
9	383	–	281[b,d]/298[b,d]	0.76	- 1.20	5.56	3.60	5.86	3.43

[a] estimated from TGA; DSC: [b] first heating scan, [c] first cooling scan, [d] second heating scan; E_{ox}^{onset} and E_{red}^{onset} are onset oxidation and reduction potentials determined from CV scans of dilute DCM solutions of pyrimidine derivatives; IP^{CV}, IP^{UPS} – ionization potential and EA^{CV}, EA^{UPS} – electron affinity determined from CV and UV photoelectron spectroscopy, respectively.

Cyclic voltammetry measurements (CV) were performed for dichloromethane (DCM) solutions of **7**–**9** with tetra-*n*-butylammonium hexafluorophosphate ($TBAPF_6$) as the supporting electrolyte (Fig. 2.9a). The potentials of oxidation (E_{ox}^{onset}) and reduction (E_{red}^{onset}) half-waves and with respect to ferrocene are collected in Table 2.5. The close values of IP^{CV} and EA^{CV} were observed for **7** and **8** (5.82, 5.87/2.9, 2.8 eV, respectively) due to the similar electron-donating/electron-accepting abilities of the building moieties. The lower IP^{CV} value of **9** is attributed to the stronger electron-donating ability of methoxy-substituted carbazole.

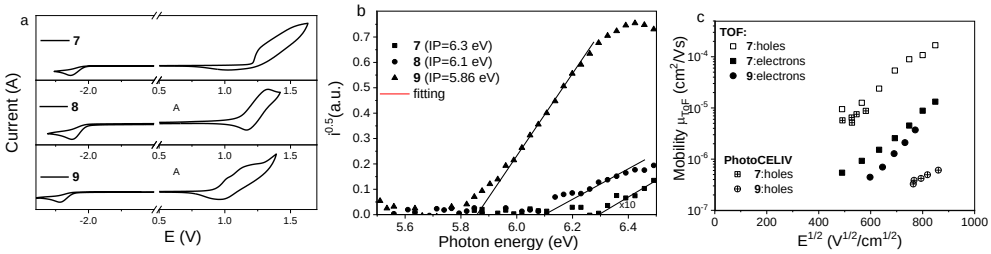

Fig. 2.9. CV (a) and photoelectron emission spectra (b) of compounds **7**–**9**. Hole/electron drift mobilities versus electric field (*E*) for the layers of compounds **7** and **9**.

Since IP^{CV} and EA^{CV} energies cannot be referred to the HOMO and LUMO of the studied materials[98], UPS was further used for getting IP^{UPS} and EA^{UPS} for their solid-state samples (Fig. 2.9b). IP^{UPS} and EA^{UPS} values can be referred to the HOMO and LUMO energies of derivatives **7**–**9** which are required for the design of the appropriate structures of optoelectronic devices, OLEDs in particularly (Table 2.5). By using the TOF technique, the charge mobilities were calculated for **7** (for holes and electrons) and for **9** (for electrons) (Fig. 2.9c). A hole mobility (μ_h) of 1.6×10^{-4} $cm^2/V\cdot s$ was observed for **7** at an electric field (E) of 7.2×10^5 V/cm, which is close to that of many other typical carbazole-containing emitters[27] (Fig. 2.9c). An electron mobility (μ_e) of 1.37×10^{-5} $cm^2/V\cdot s$ was detected for **7** at the same electric field.

Also, the CELIV technique was applied to obtain complete charge-transporting data for the studied compounds. CELIV hole mobility of **7** was in good agreement with the corresponding TOF hole mobility (Fig. 2.9c).

The absorption and PL spectra of the dilute solutions and solid films of **7–9** are shown in Fig. 2.10a. All the photophysical data is summarized in Table 2.6. The absorption of neat films and dilute toluene solutions of the compounds in the spectral region below 330 nm corresponds to a great extent to the π–π* transition of carbazole[94] (Fig. 2.10a). The attachment of *tert*-butyl groups to carbazole units in **8** resulted in the red-shift of LEB compared to that of **7**. The presence of methoxy groups in the structure of **9** caused a bigger bathochromic shift in comparison with compounds **7** and **8**. These observations can be explained by the prolonged π-conjugation of the *tert*-butyl or methoxy substituted carbazole moieties[40]. The PL spectra of solutions of **7–9** contain a single narrow peak in the sky-blue/green region (Fig. 2.10a). The bathochromic shift of the PL spectral peak with an increase of polarity of solvents (Fig. 2.10a) is a clear evidence of the ICT state of emission. The non-doped films of compounds containing carbazole (**7**) and *tert*-butyl carbazole (**8**) demonstrated emission with the maximum at 488 nm; however, the neat film of compound **9** substituted by methoxy carbazole showed green emission with the maximum at 542 nm. The Φ values of the films are higher than those of the solutions, which is a manifestation of the aggregation-induced emission enhancement (AIEE) effect (Table 2.6). The only exclusion is the Φ values observed for **9** which were found to be similar (of ca. 2%) for the solid samples and dilute solutions.

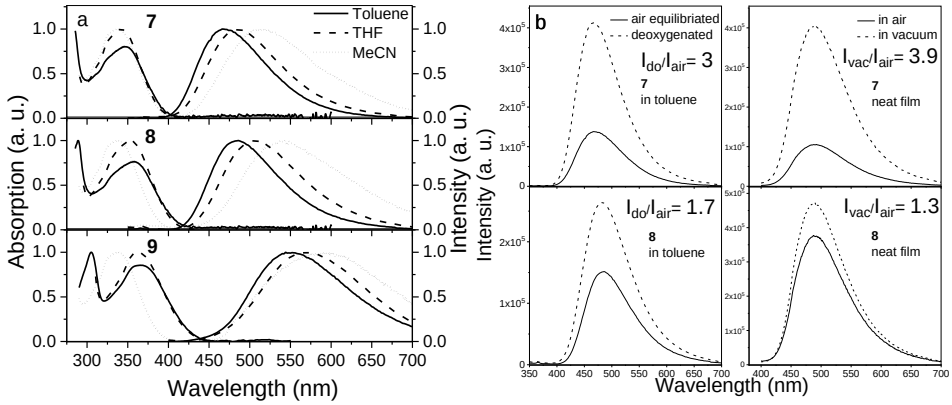

Fig. 2.10. Absorption spectra and normalized PL spectra of dilute 10^{-5} M toluene, THF and MeCN solutions of **7–9** (a). PL spectra of air equilibrated and deoxygenated dilute 10^{-5} M toluene solutions and neat films recorded in air and in vacuum of **7** and **8**.

The intensity of PL of toluene solutions and neat films of the compounds was found to be considerably higher in the absence of oxygen compared to that of air equilibrated samples (Fig. 2.10b). For **7**, the increase was substantially higher, and it reached the factor of 3–3.85. The increase of the emission intensity after deoxygenation is ascribed to delayed fluorescence (DF)[6]. After the removal of

oxygen, the spectral shape remained the same. This observation shows that the excitons utilized in DF are recombined radiatively from the same energy levels as for prompt fluorescence (PF), thus pointing to the triplet up-conversion via rISC.

Table 2.6. Photophysical characteristics of pyrimidine-carbonitrile derivatives.

Compounds/ Parameters	**7**	**8**	**9**
Φ^{touene} (%)	2 (6*)	12 (21*)	3
Φ^{THF} (%)	15	12	1
$\Phi^{\#}$ (%)	33 (53*)	20 (25*)	2
$\chi^{2\ \#}$	1.111	1.109	1.016
$E_{S1,\ THF}$ (eV)	3.17	3.02	2.89
$E_{T1,\ THF}$ (eV)	3.03	2.93	2.88
$\Delta E_{ST,\ THF}$ (eV)	0.14	0.09	0.01
$E_{S1,\ mCP}$ (eV)	2.99	2.93	2.74
$E_{T1,\ mCP}$ (eV)	2.91	2.86	2.71
$\Delta E_{ST,\ mCP}$ (eV)	0.08	0.07	0.03

Estimated by the measurements: #of neat films; *upon removing oxygen. χ^2 is a weighted sum of squares of deviations of calculated points of multiexponential fitting of a PL decay curve. The empirical formula E_{ph} [eV] = 1239.84/ λ [nm] was used to estimate energy levels of E_{S1} and E_{T1}, where λ is the wavelength of the onset of fluorescence and phosphorescence spectral bands.

The values of ΔE_{ST} were obtained from the fluorescence and phosphorescence spectra of the solutions of the compounds recorded at the liquid nitrogen temperature (Table 2.6). The doping of **7** and **8** into the 1,3-bis(N-carbazolyl)benzene (mCP) matrix resulted in the reduction of ΔE_{ST} (Table 2.6). The PL spectra and decay curves of the films of the molecular mixtures were recorded at different temperatures. The PL spectra of the film of **8** remained steady over heating when the sample was degassed (Fig. 2.11a). The PL decay curves for compound **8** are presented in Fig. 2.11b. As it is evident from the PL decay curves, the intensity of the phosphorescent component was quenched over heating due to the rapidly enhanced interactions with oxygen. Simultaneously, the thermal activation of DF resulted in the essential increase of the TADF intensity at temperatures exceeding 180 K (Fig. 2.12b).

The dispersions of **7** and **8** in THF/water mixtures were prepared for the investigation of the AIEE effect. The dependencies of the PL intensities on the water fraction are presented in Fig. 2.11c,d. As it can be seen from the graphs and photos (Fig. 2.11c,d), at low water fractions (f_w), the dispersions of both compounds are poorly emissive. A decrease of the PL intensity in the range f_w below 40% is ascribed to the emission quenching due to the exhaustion of the electronic excitation energy by intramolecular rotations. The bathochromic shift by nearly 50 nm with the increase of the water fraction from 0% to 40% is caused by the increase of concentration of highly polar water influencing strong intramolecular CT processes in the emitters, which is an additional reason of PL quenching. At high f_w, both compounds emit blue light with the intensity maxima at ca. 480 nm as the molecules which are insoluble in the water form are aggregating. Consequently, there is a rapid increase of intensity at f_w>70% for the dispersions of **7** and for **8** in the range of f_w from 40% to 60% due to AIEE since the rotation motions of moieties of the

compounds are restricted in the solid state. The following decrease of the PL intensity at f_w exceeding 70% observed for the dispersion of **8** is explained by the formation of precipitates of a significant size.

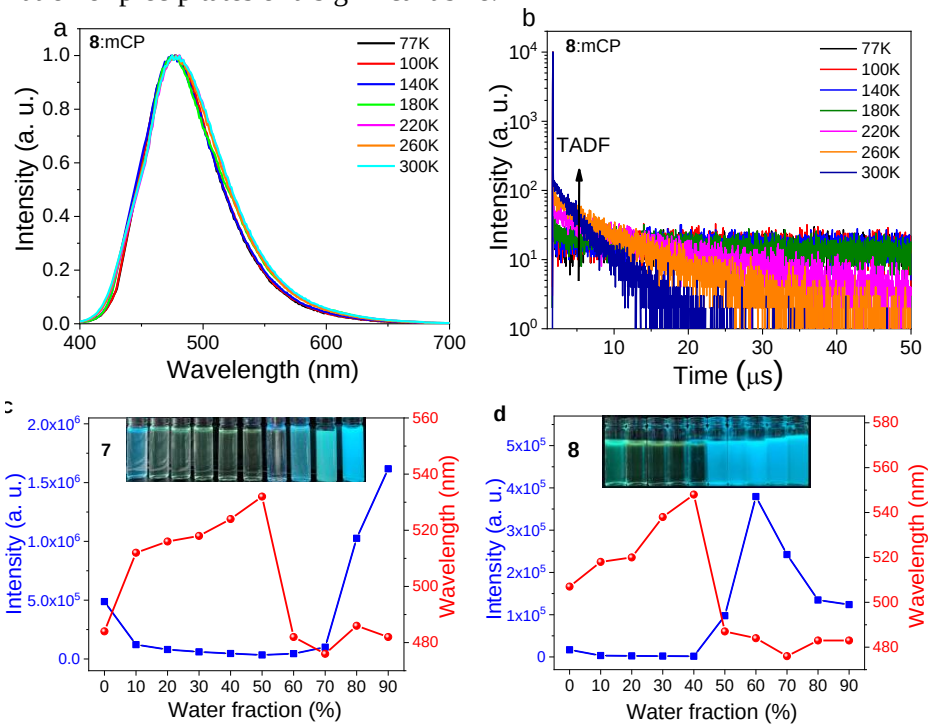

Fig. 2.11. Normalized PL spectra (a) and PL decay curves (b) recorded at different temperatures under N_2 atmosphere for 10 wt% solid solution of **8** in mCP. Plots of PL intensities and peak wavelengths *versus* water fraction of the dispersions of **7** (c) and **8** (d) in THF/water mixtures.

Interactions with oxygen are mostly responsible for the non-radiative deactivation of excitations through the energy losses. Due to the AIEE properties and the high values of Φ in the solid-state, compounds **7** and **8** were selected for the investigation of the optical oxygen sensitivity. The 10 wt% solid solutions of the compounds in a rigid matrix were prepared so that to detect the collisional quenching of a luminophore. Zeonex was selected as a matrix because of its well-studied ability of suppressing intermolecular interactions[35,99]. The samples were put into inert atmosphere of nitrogen. Upon increasing the oxygen concentration, the PL intensity continuously dropped (Fig. 2.12a,b). No significant difference in the intensity under the same conditions over time was detected, thus showing a great immediate response to the molecules of oxygen and a great stability of the emission. The PL decay curves of the solid solutions of **7** and **8** in Zeonex were recorded under nitrogen and oxygen conditions to study the impact of collisional quenching on emissive characteristics of the systems (Fig. 2.12c). The long-lived component of the emission was dramatically reduced in the presence of oxygen, especially for the solid solutions of **7** in Zeonex.

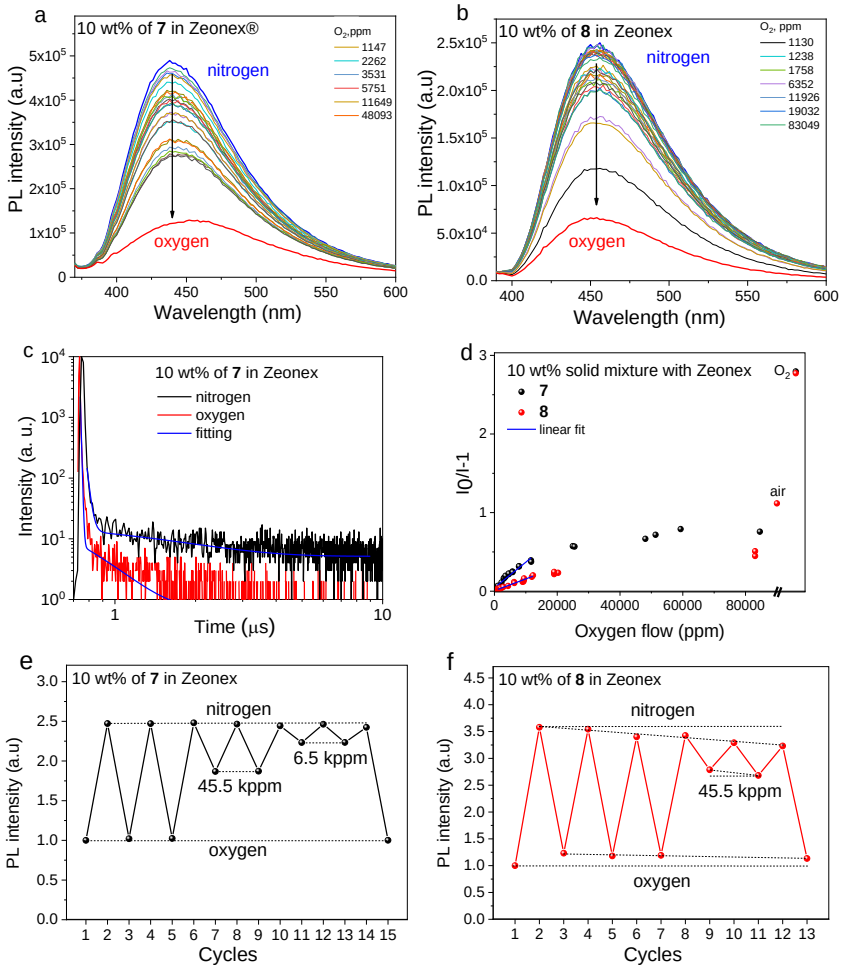

Fig. 2.12. PL spectra (a, b) and PL decays (c) of 10 wt% solid solutions **7** (a, c) or **8** (b) in Zeonex recorded in different atmospheres at room temperature; d) Stern-Volmer plots and oxygen response (e, f) of the films of 10 wt% solid solutions of **8** (e) and **9** (f) in Zeonex.

The Stern-Volmer relation of $\frac{I_0}{I} - 1$ and oxygen flow (Fig. 2.12d) demonstrated oxygen sensitivity in a wide range of the oxygen flow corresponding to the oxygen partial pressure[100]. Since fluorophore quenching by oxygen is a dynamic process, the correlation is linear. However, as expected for dye:matrix systems, downward curvature[101] takes place at the oxygen flow exceeding 20,000 ppm. According to the Stern-Volmer equation, the well-known characteristic of optical sensors Stern-Volmer constant $K_{SV} = \frac{I_0}{I} - 1$ was estimated from the slope of the linear fit, as shown in Fig. 2.12d (adjusted R^2 values are 0.94 and 0.97 for the samples containing **7** and **8**, respectively)[101]. K_{SV} was calculated to be $3.24 \cdot 10^{-5}$ and $1.49 \cdot 10^{-5}$ ppm^{-1} for the solid dispersions of **7** and **8** in Zeonex, correspondingly. These values are comparable with that of TADF oxygen probes[66]. They are slightly

lower than the K_{SV} values earlier observed for phosphorescent oxygen probes with long-lived emission (>1 ms)[102,103]. The synthesized compounds offer a great potential for the application as optical oxygen sensors reaching the necessary requirements: a) fast response to the oxygen postulated from the stability of PL quenching over time; b) sustainable oxygen sensitivity; c) good quality of the films of solid dispersions in Zeonex; d) appropriate thermal stability and photophysical properties, as described above[101].

Upon considering the TADF and AIEE capabilities of the synthesized compounds, they can be used as promising emitters for doping-free devices. The series of OLEDs N1-N3 with the structure of ITO / HAT-CN (10 nm) / TCTA (30 nm) / mCP (7 nm) / EML (25 nm) / TSPO1 (3 nm) / TPBi (30 nm) / LiF (0.4 nm) / Al were fabricated in order to test the layers of **7–9** as non-doped light-emitting layers, respectively (Fig. 2.13a). The key electroluminescent data is collected in Table 2.7. Dipyrazino[2,3-f:2',3'-h]quinoxaline-2,3,6,7,10,11-hexacarbonitrile (HAT-CN) and lithium fluoride (LiF) were employed for the injection of charge carriers. The layers of tris(4-carbazoyl-9-ylphenyl)amine (TCTA) and 2,2′,2"-(1,3,5-benzinetriyl)-tris(1-phenyl-1-H-benzimidazole) (TPBi) were utilized as the hole and electron transporting layers, respectively. Also, mCP and diphenyl[4-(triphenylsilyl)phenyl]phosphine oxide (TSPO1) were employed for the blocking of electrons and holes, respectively. The electrodes were indium-tin oxide (ITO) and aluminum (Al).

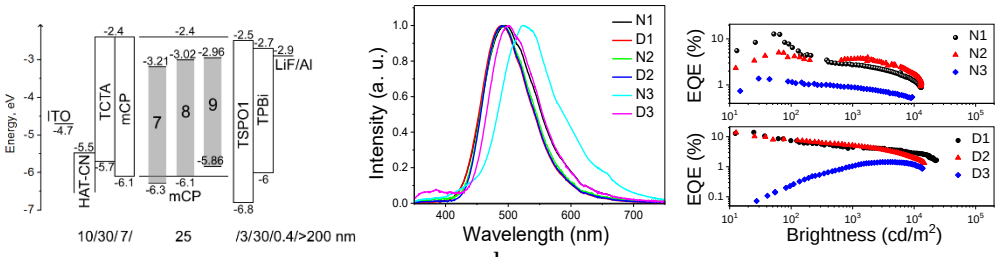

a b c

Fig. 2.13. OLEDs N1-N3 and D1-D3: a) Equilibrium energy diagram and structure; b) normalized EL spectra recorded at 8V; c) EQE.

Table 2.7. Summary of OLED parameters.

OLED	EML	L_{max}, 10^3 cd/m^2	CE, cd/A	PE, lm/W	λ_{EL} nm	EQE, %	CIE 1931
N1	**7**	13.1	32.4 (17.5)	18.8 (9.2)	494	12.8 (6.9)	(0.20, 0.36)
D1	**7**:mCP	23.1	33.3 (17.6)	20.2 (9.1)	489	14 (7.4)	(0.18, 0.33)
N2	**8**	13.2	12.3 (9.9)	4.6 (3.6)	490	5.1 (4.1)	(0.19, 0.35)
D2	**8**:mCP	14.8	33.7 (19.4)	18 (8.7)	490	13.7 (7.9)	(0.18, 0.35)
N3	**9**	9.3	4.0 (3.4)	2.1 (1.6)	524	1.4 (1.2)	(0.30, 0.49)
D3	**9**:mCP	13.7	3.8 (0.6)	1.2 (0.3)	500	1.4 (0.2)	(0.21, 0.43)

L_{max} – maximum brightness. CE and PE – maximum current and power efficiency, respectively. λ_{EL} – wavelength of the EL spectral peak at 8V. Efficiency values at L of 100 cd/m^2 are shown in parentheses.

OLEDs containing emitting layers (EML) of **7** and **8** demonstrated electroluminescence (EL) in the near sky-blue range, while **9** is a totally green emitter (Table 2.7., Fig. 2.13b). The obtained maximum values of EQE of the devices (Table 2.7, Fig. 2.13c) correlate with the values of Φ of the neat films of compounds **7–9** (Table 2.6). This observation is an indication of the excellent charge balance in EML. Device N1 exhibited a maximum EQE value of 12.8%, which is practically the same as for the corresponding doped device D1 which shall be discussed below. A much lower maximum EQE of 5.1% was obtained for the non-doped device N2 based on compound **8** (Table 2.7).

OLEDs were additionally modified by the insertion of the guest:host system instead of the neat EML. The series of devices D1-D3 were fabricated, where the guest:host systems (10 wt% of **7–9** doped into mCP) were used. As mentioned above, device D1 showed a slight improvement of efficiency compared to device N1. Meanwhile, the efficiency of OLED D2 was significantly higher than that of N2 (EQE of 5.1 and 13.7%) (Table 2.7). This observation can apparently be attributed to the better hole-electron balance in the doped light-emitting layer of device D2 compared to that of the non-doped device N2. A high efficiency OLED based on the EML of **8** doped in mCP can be additionally explained by the suppression of non-radiative ways of relaxation of the excited states. Analogous improvement was not achieved for the device based on the emitter with methoxy groups (**9**) since this derivative exhibited a low Φ value (Table 2.6). The efficiency roll-off evident from the rapid decline of efficiency at 100 cd/m^2 of *L* is bigger for device D3 than for N3 despite the exhibition of the same maximum EQE of 1.4%.

2.4. Triphenylamino or 9-phenyl carbazolyl-substituted pyrimidine-5-carbonitriles as bipolar emitters and hosts with triplet harvesting abilities (Scientific publication No. 4, Q1).

This chapter is based on the article published in *Materials Today Chemistry*[92]. This study is a continuation of the previous work about the development of new pyrimidine-5-carbonitrile-based emitters or hosts suitable for the fabrication of OLEDs. The manuscript introduces a study on new pyrimidine-5-carbonitriles substituted by two triphenylamino or 9-phenyl carbazolyl moieties which were used as emitters and hosts in OLEDs. The derivatives showed nanosecond-lived emission with absolute quantum yields reaching 98% and with hole mobility exciding 10^{-3} cm^2/V×s. The developed materials demonstrated ability to harvest high-lying triplet excitons and to convert them into singlet excitons due to the upper-level triplet-singlet intersystem crossing. The target compounds 4,6-bis(4-(diphenylamino)phenyl)pyrimidine-5-carbonitrile (**10**) and 4,6-bis(4-(9H-carbazol-9-yl)phenyl)pyrimidine-5-carbonitrile (**11**) were obtained by Suzuki-Miyaura cross-coupling reactions as outlined in Scheme 2.4. The chemical structures of the compounds were confirmed by ^{1}H and ^{13}C NMR analysis, mass spectrometry, and elemental analysis.

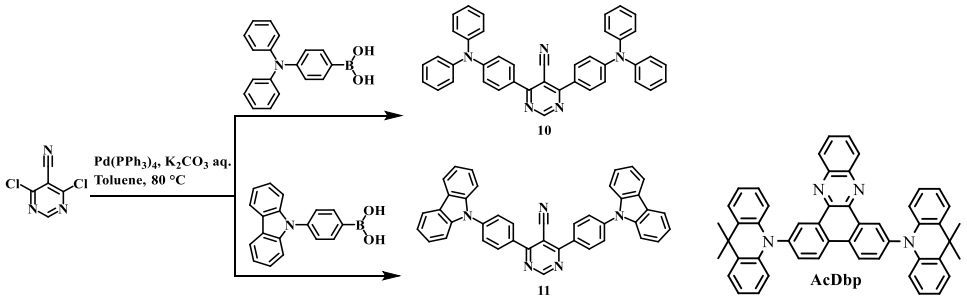

Scheme 2.4. Synthetic pathway to compounds **10** and **11** and the chemical structure of emitter **AcDbp**.

The thermal properties of **10** and **11** were studied by TGA and DSC measurements. Both compounds exhibited high thermal stability. Their T_d values were found to be of 375 °C and 423 °C, respectively (Table 2.8). During DSC measurements, for compounds **10** and **11**, glass formation was detected in the second heating. The carbazolyl-containing compound demonstrated a higher value of T_g of 135 °C (Table 2.8) relative to the compound containing triphenylamino moieties (102 °C). This observation can be explained by the enhanced rigidity of the carbazole unit. According to these T_g values, both compounds are expected demonstrate stable work in OLEDs under Joule heating across a wide temperature range. Also, the T_m and T_{cr} values for materials **10** and **11** are collected in Table 2.8.

The transport levels of **10** and **11**, thus IP^{UPS} and EA^{UPS} of the solid films of the compounds, were investigated by the combination of UPS in air and absorption spectroscopy (Fig. 2.15a). The lower IP^{UPS} value of 5.61 eV was obtained for compound **10** in comparison to 5.98 eV observed for **11** (Fig. 2.14a, Table 2.8). It can be explained by the presence of triphenylamine substituents with stronger electron-donating abilities in **10**. The slightly different optical gap (E_{opt}) values of 2.75 and 2.94 eV, respectively, were obtained for compounds **10** and **11** because of the different formation of the charge transfer (CT) states. The close EA^{UPS} values of 2.86 and 2.92 eV were estimated for **10** and **11**, correspondingly (Table 2.8).

Table 2.8. Thermal, photoelectrical and charge-transporting properties of compounds **10** and **11**.

Compounds	T_d, °C	T_g, °C	T_m, °C	T_{cr}, °C	IP^{UPS}, eV	E_{opt}, eV	EA^{UPS}, eV	$\mu^{holes,*}$ $cm^2/V\times s$	$\mu^{electrons,*}$ $cm^2/V\times s$
10	375	102[b]	243[a,b]	167[b]	5.61	2.75	2.86	7.3×10^{-3}	4.4×10^{-4}
11	423	135[b]	305[a]/270[b]	206[b]	5.98	2.94	2.92	2.1×10^{-3}	0.4×10^{-4}

a – first heating, b – second heating, E_{opt} – the optical gap. * - values taken at 3.6×10^5 V/cm.

Charge mobilities versus the electric field are plotted in Fig. 2.14b. In contrast to organic semiconductors typically used in OLEDs[104], both compounds showed high values of hole mobilities exceeding 10^{-3} $cm^2/V\times s$ and by ca. one order of magnitude lower electron mobilities exceeding 10^{-4} $cm^2/V\times s$ (Fig. 2.14b). The compound containing triphenylamine moiety (**10**) showed higher both hole and electron mobilities at the same electric fields than the compound containing

carbazole moiety (**11)** (Table 2.8). This observation can be attributed to the flexible structure of the triphenylamino moiety in contrast to the rigid structure of the carbazole moiety leading to the more compact molecular packing in the films of **10**. As a result, more appropriate HOMO/HOMO and LUMO/LUMO overlapping is realized for the hopping of free holes or electrons between the neighboring molecules of **10**. Nevertheless, according to the results of the charge transport measurements, both **10** and **11** offer great potential for application in OLEDs at least as the host materials.

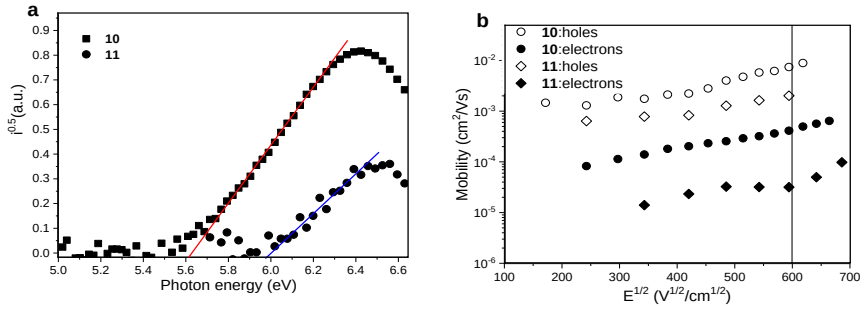

Fig. 2.14. Photoelectron emission spectra (a), hole/electron drift mobilities (b) for the films of **10** and **11**.

The absorption bands observed in the high-energy region (286, 298 nm for the films of **10** and 283, 318, 334 nm for the solid samples of **11**) (Fig. 2.15a) are attributed to the localized aromatic π-π* or n–π* transitions of triphenylamino or 9-phenylcarbazolyl moieties[105]. Also, the absorption spectra of both compounds show high intensity low-energy absorption bands (Fig. 2.15a). According to the theoretical results, these bands can be attributed to the electronic transition $S_0 \rightarrow S_1$ which is dominated by ICT between the electron-donating phenyl-carbazolyl fragment in **11** or the triphenylamino fragment in **10** and electron-accepting pyrimidine-5-carbonitrile moieties.

The toluene solutions of compounds **10** and **11** demonstrated blue emission with the maximum intensities at 486 nm and 458 nm, correspondingly (Table 2.9). The neat films of both derivatives showed green emission with the maximum centered at 506 nm (Fig. 2.15a). The fluorescence of toluene solutions of the synthesized compounds is highly efficient. The values of Φ reached 90% for the solution of **10** and 98% for the solution of **11**. For the neat films of **10** and **11** the values of Φ were found to be lower and exceeded 45% and 30%, respectively (Table 2.9). For the analysis of the excited state properties of **10** and **11** in more detail, their solvatochromic effects were investigated by using the Lippert–Mataga solvatochromic model (Fig. 2.15b). For this purpose, the absorption and PL spectra of ten dilute solutions of **10** and **11** were recorded. The positions of the PL spectral peaks are mostly predetermined by the polarity of the solvents . The Lippert-Mataga dependences[106–108] of the Stokes shifts $\Delta\tilde{\nu}$ versus the orientation polarizability of the solvent Δf value are plotted in Fig. 2.15b.

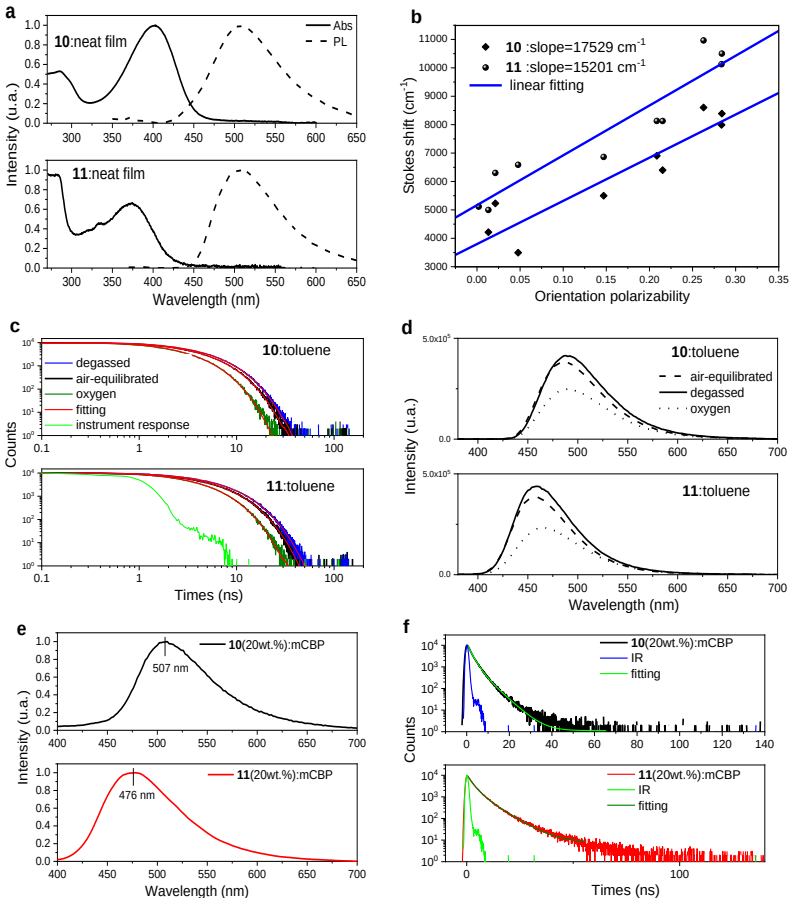

Fig. 2.15. Absorption and PL spectra of neat films (a) and Lippert-Mataga plots (b) of compounds **10** and **11**. PL decay curves (c) and PL spectra (d) of toluene solutions of **10** and **11** under different conditions. PL spectra (e) and PL decay curves (f) of guest-host systems.

Table 2.9. Photophysical parameters of toluene solutions and non-doped films of derivatives **10** and **11** and guest-host solid solutions.

Compounds	λ_{PL}, nm	Φ, %	τ_1/τ_2, ns	R_1/R_2, %	χ^2
10^{tol}	486	90*	3.75	100	1.084
11^{tol}	458	98*	5.17	100	1.027
10^{film}	506	45	2.86/8.49	62.64/37.56	1.222
11^{film}	508	30	3.88/9.63	37.65/62.35	1.228
10 in mCBP	506	21	2.02/4.87	67.36/32.64	1.224
11 in mCBP	476	18	2.44/7.04	49.71/50.29	1.218

guest-host solid solutions: 20 wt% of emitters in hosts; * – degassed conditions; τ_1/τ_2 – the lifetimes of prompt and delayed fluorescence; χ^2 – the weighted sum of the squares of deviations of the calculated points of multiexponential fitting of a PL decay curve.

The approach is based on the Onsager interpretation of the non-specific electrostatic interactions between the molecules of the material and the solvent in a solution[109]. The relation, which the plot is based on, is $\Delta\tilde{\nu} = \frac{2\Delta f}{4\pi\varepsilon_0\hbar c a^3}(\mu_e - \mu_g)^2 + \Delta\tilde{\nu}^0$. Here, $\Delta\tilde{\nu}^0$ is the Stokes shift in a condition of the absence of the impact of solvation, while a is denoted as the Onsager cavity radius. The slope of the Lippert-Mataga plot corresponds directly to the difference of the dipole moments of a molecule in the excited and ground states. The values of slopes for **10** and **11** were found to be of 15,201 and 17,529 cm^{-1}, correspondingly.

The PL decay curves of the toluene solutions of **10** and **11** were found in the nanosecond range, thereby confirming the prompt fluorescence nature of emission without any sign of delayed fluorescence, e.g., TADF or TTA (Fig. 2.15c, Table 2.9). This observation is not expected if taking into account the results of the investigation of the PL intensity of the toluene solutions of **10** and **11** under different conditions (air equilibrated, degassed, and oxygen equilibrated) (Fig. 2.15d). After deoxygenation, the PL intensity of the toluene solutions of **10** and **11** slightly increased, but, after purging with oxygen, their PL intensity significantly dropped down. This observation confirms that triplet excitons participate in the emission processes of derivatives **10** and **11**. It is known that triplet excitons are highly sensitive to the presence of oxygen[110,111]. The PL decay curves of the toluene solutions of **10** and **11** were recorded under different conditions (Fig. 2.15c**)**. The lifetimes of excited states in the oxygen atmosphere were found to be considerably shorter than in air, which additionally confirms the participation of triplet excitons in emission, which is not usual for purely fluorescent materials. Several mechanisms[7,10,13,14,112] could be responsible for the emissive triplet harvesting of **10** and **11.**

- One of them is RTP[50,51]. Since additional bands or shoulders were not observed after deoxygenation, room-temperature phosphorescence is highly unlikely (Fig. 2.15d).
- Another possible mechanism might be TADF. However, it is not the case for **10** and **11** since no delayed fluorescence was observed due to relatively high singlet-triplet splitting (Fig. 2.15c).
- TTA is also unlikely for **10** and **11** since the linear fits of their integrated PL intensities versus excitation intensities revealed the slopes lower than unity, thus displaying no contribution of TTA emission[52].
- HLCT can partly be the case for **10** and **11** due to the closely situated several excited states predicted by theoretical calculations (see discussion below, Fig. 2.16).
- We suppose that the mechanism of emissive triplet harvesting is the upper level triplet-singlet intersystem crossing[13,14]. This mechanism may be partly in combination with the contribution of TADF and/or TTA, although their evidence is very limited/non-observed.

When taking into account the results of the theoretical study and the device properties described below, it can be stated that the most probable mechanism of emissive triplet harvesting is the upper level triplet-singlet intersystem crossing[13,14]. The theoretical study revealed a relatively large ΔE_{ST} between the first singlet (S_1)

and triplet (T_1) energy levels of 0.52 eV and 0.26 eV for **10** and **11**, respectively (Fig. 2.16). It complicates the transfer of triplet excitons from T_1 to S_1 through rISC, which is typical for TADF materials. However, a very small ΔE_{ST} between high energy levels (ΔE_{S1T3} = 0.02 eV, ΔE_{S2T4} = 0.02 eV for **10** and ΔE_{S3T3} = 0.05 eV and ΔE_{S3T4} = 0.02 eV for **11**) suggests that rISC along the high-lying triplet states and singlet states can compete with the internal conversion (IC) process between the triplet excited states (ΔE_{T2T3} = 0.34 eV for **10** and ΔE_{T2T3} = 0.29 eV for **11**). This kind of rISC channels results in the formation of 'hot excitons' in **10** and **11**. Theoretically, 100% exciton utilization can be reached in materials containing 'hot excitons' materials, thus enhancing the efficiency of OLEDs[113].

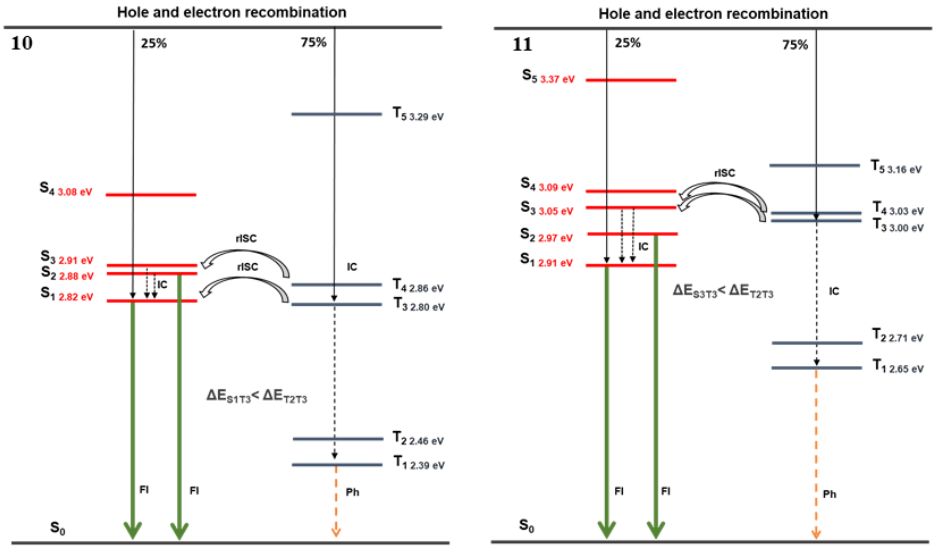

Fig. 2.16. Energy diagram of the singlet and triplet excited states of **10** and **11** calculated by using TD-B3LYP 6-31G(d,p):CPCM (DMSO).

At 77 K, the photoluminescence and phosphorescence spectra of frozen THF solutions of the compounds were measured. The wavelengths of PL and PH spectra at maximum intensities of the emission were used for the estimation of the values of the S_1 and T_1 energy levels of **10** and **11**. Compound **10** demonstrated a low triplet energy of 2.31 eV, while **11** showed a significantly higher triplet energy of 2.54 eV. Compound **10** showed ΔE_{ST} of 0.32 eV, while compound **11** exhibited ΔE_{ST} of 0.34 eV. As a result, TADF properties were not detected for **10** and **11**, as mentioned above.

When aiming to study the emitting and hosting properties of compounds **10** and **11**, the layers of the guest-host systems **10**:mCBP/**11**:mCBP and AcDbp:**10**/AcDbp:**11** were used as light-emitting layers in OLEDs with the structure ITO/HAT-CN[5]/NPB[40 nm]/TCTA[10 nm]/mCBP[10 nm]/ light-emitting layer [50 nm]/NBPhen[30 nm]/LiF[2 nm]/Al. In devices **E-10** and **E-11**, compounds **10** and **11** were used as the emitters, while in devices **H-10** and **H-11**, they were used as the hosts (Fig. 2.17a, Table 2.10). The reference device **H**-mCBP was also

fabricated for the comparison of the hosting properties of **10** and **11** with those of the commercial host mCBP. 2,7-bis(9,9-dimethylacridin-10(9H)-yl)dibenzo[a,c]phenazine (AcDbp) emitter was recently used for the fabrication of highly efficient OLEDs[114]. By briefly introducing AcDbp (Scheme 2.4), it should be mentioned that this compound additionally to the combination of TADF/TTA triplet-harvesting properties is characterized by the singlet energy of 2.55 eV and the triplet energy of 2.35 eV, the ionization potential of 5.5eV, and the electron affinity of 2.77 eV. It shows good performance in OLED as the emitter (with the maximum EQE of 19.4%)[114]. Also, this TADF/TTA emitter AcDbp was used in the reference device **H**-mCBP.

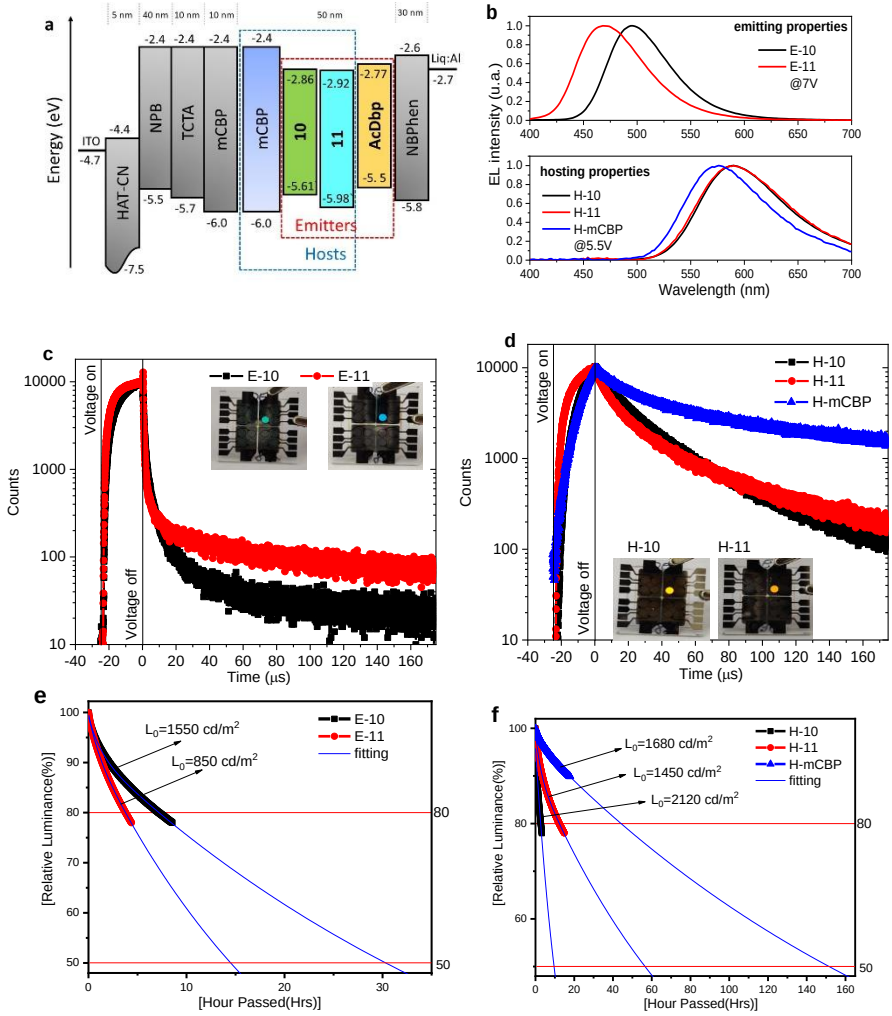

Fig. 2.17. Equilibrium energy diagram (a) and electroluminescence spectra at constant voltage (b). TREL curves of devices **E-10** and **E-11** (c) and devices **H-10, H-11** and **H**-mCBP (d) (Insets show photos of OLEDs). Device lifetimes (e, f) for the fabricated devices.

The multi-layer device structure contained the layers of commercial materials, such as the hole-injecting layer of HAT-CN, the hole-transporting layers of di(1-naphthyl)-N,N′-diphenyl (NPB), TCTA and mCBP, the electron-transporting layer of 2,9-bis(naphthalen-2-yl)-4,7-diphenyl-1,10-phenanthroline (NBPhen), and the electron-injecting layer of LiF (Fig. 2.17a). Such a device structure ensures the recombination of charges and the generation of excitons within the light-emitting layers. Devices **E-10** and **E-11** were characterized by bluish green and blue EL (Fig. 2.17b) with the CIE color coordinates of (0.174, 0.454) and (0.149, 0.203), respectively. The EL spectra of devices **E-10** and **E-11** were very similar to the PL spectra of the corresponding films of the host-guest mixtures **10**:mCBP and **11**:mCBP used as the light-emitting layers (Fig. 2.15e).

When compounds **10** and **11** were used as the hosts for the orange emitter AcDbp, orange EL was observed for devices **H-10** and **H-11** without any evidence of the emissions of the hosts in their EL spectra (Fig. 2.17b). The EL spectra of devices **H-10** and **H-11** were found to be slightly red-shifted in comparison to the EL spectra of the reference device **H**-mCBP (Fig. 2.17b and Table 2.10) and the previously published EL spectra of AcDbp-based devices[114]. It could be explained by the strong sensitivity of TADF/TTA emission of the emitter AcDbp to the dipole moments of the surrounding molecules which are higher for bipolar compounds **10** and **11** than that of mCBP. Since compounds **10** and **11** are characterized by prompt fluorescence, and by a narrower full width at the half maxima (FWHM), thus purer emission colors were observed for devices **E-10** and **E-11** than for TADF OLEDs **H-10**, **H-11** and **H**-mCBP (Table 2.10).

Transient electroluminescence (TREL) signals help to prove the considerable participation of triplet excitons in the electroluminescence of the devices (Fig. 2.17c,d). In contrast to the PL decay curves of emitters **10** and **11** (Fig. 2.15f), the TREL signals of devices **E-10** and **E-11** demonstrated hundreds of microseconds lived emission related to the triplet harvesting abilities of compounds **10** and **11**. Since the intensity of the long-lived EL of device **E-11** is stronger than that of device **E-10**, emitter **11** is characterized by more efficient triplet harvesting than emitter **10.** When compound AcDbp was used as an emitter, the shapes of the TREL signals of OLEDs **H-10**, **H-11** and **H**-mCBP were very similar to the previously published TREL signals of devices based on a TADF/TTA emitter[115]. Considerably faster EL kinetics were observed for devices **H-10** and **H-11** than for **H**-mCBP. This observation could be related to the process of the upper level triplet singlet intersystem crossing of **10** and **11** hosts, which is not observed for the conventional host mCBP. When taking into account the big differences of the shapes of the TREL signals of devices **E-10**/**E-11** and AcDbp-based devices (Fig. 2.18c,d), the triplet harvesting of emitters **10** and **11** is rather attributed to the upper level rISC, but not to TADF or TTA, as it was in the case of emitter AcDbp[114]. This observation additionally confirms the above outlined considerations.

When compounds **10** and **11** were being used as the emitters for OLED, devices with high maximum EQEs of 6% and 7% were fabricated (Table 2.10). Since the theoretical limit of EQE for prompt fluorescence-based OLEDs is that of 5%, this result additionally confirms the ability of triplet harvesting by compounds

10 and **11**, as it was discussed above. In addition, this observation shows the considerable participation of triplet excitons in electroluminescence. When compounds **11** and **11** were being used as the hosts for OLED, the high maximum EQEs of 20.7% and 13.7% were obtained for devices **H-10** and **H-11**, respectively. The EQE of **H-10** slightly exceeded the EQE of the reference device **H**-mCBP which was found to be of 20.2% (Table 2.10). The EQE differences of devices **H-10** and **H-11** can be explained by the different charge mobilities of hosts **10** and **11** (Fig. 2.14b).

The EL intensities versus applied voltages are plotted in Fig. 2.17e,f. Since the different initial luminance (marked by the arrows) was selected for the devices, the direct comparison of device lifetimes is not possible. Therefore, the formula $LT(L_1) = LT(L_0) \times (L_0/L_1)^n$ was used for the prediction of the device lifetimes (LT80 and LT50) at 80% and 50% EL intensity, the initial luminance of 100 and 1000 cd/m^2, while assuming the escalation factor n=1.75. The experimental values of the escalation factor for OLEDs are typically in the range of 1.65–1.95[116,117] (Table 2.10). In this formula, $LT(L_0)$ is the experimental value of LT80 at the EL intensity of 80% of chosen luminance L_0, $LT(L_1)$ is the predicted lifetime at luminance L_1. To get LT50, experimental data was analyzed by using the formula $L/L0=a\times\exp^{-\alpha t}+ b\times\exp^{-\beta t}$, where the first-exponential term is related to the rapid initial decay, the second one is related to the long-term degradation, a, b, α, β are fitting parameters which are related to the functional materials in use and device processing[118].

Table 2.10. Device output parameters.

Motif of EL test	Emitting property test		Hosting property test		
Device structure	ITO/HAT-CN/NPB/TCTA/mCBP/emitting layer/nBPhen/LiF/Al				
Device name	**E-10**	**E-11**	**H-10**	**H-11**	H-mCBP
Emitting layer	**10**:mCBP	**11**:mCBP	AcDbp:**10**	AcDbp:**11**	AcDbp:mCBP
V_{ON} (V) @ 10 cd/m^2	4.3	4.4	3.0	4.5	3.85
EQE_{max}, EQE_{100}, EQE_{1000} (%)	**6.0, 4.7, 4.2**	**7.0, 4.7, 3.9**	**20.7, 12.0, 7.9**	**13.7, 6.1, 4.7**	**20.2, 12.4, 5.3**
Peak (nm) @ 1000 cd/m^2	494	468	590	590	576
CIE (x,y) @ 1000 cd/m^2	(0.174, 0.454)	(0.149, 0.203)	(0.546, 0.449)	(0.54, 0.455)	(0.5, 0.49)
LT50,* hour @ 100 cd/m^2	3896	648	2063	6481	22336

V_{ON} - turn-on voltage * device lifetimes calculated by formula $LT(L_1) = LT(L_0) \times (L_0/L_1)^n$ using experimental data from Fig. 2.18e and 2.18f and assuming n=1.75, where L_1 is luminescence at 100 cd/m^2.

Approximately, five times higher device lifetimes were obtained for OLEDs **E-10** in comparison to those of device **E-11** (Fig. 2.17e and Table 2.10). When compounds **10** and **11** were being used as hosts for the same emitter AcDbp, the opposite device lifetimes were observed. Device **H-11** was characterized by higher stability in comparison to the stability of device **H-10** (Fig. 2.17f). Thus, high triplet excitons of **11** practically did not affect the device stability. Apparently, the molecular stability plays the main role in this case. In particular, the fused carbazole

unit provided higher device stability than flexible triphenylamine moieties. The reference device (**H**-mCBP) showed the highest stability with the predicted LT50 of 22,336 hours at the initial luminance of 100 cd/m^2 (Table 2.10). To summarize, the device investigations demonstrate the high potential of the developed compounds **10** and **11** as the emitters and hosts with rare triplet-harvesting ability.

CONCLUSIONS

1. New derivatives of benzanthrone and carbazole exhibiting mechanochromic luminescence were synthesized and investigated. It has been determined that:

1.1. The change of the emission color from green to orange was observed for the synthesized derivatives after the application of external stimuli such as grinding, fuming and melting.

1.2. Mechanochromic luminescence of the derivatives was caused mainly by the presence of different crystalline polymorphs and amorphous aggregates.

1.3. The compound containing benzanthrone and carbazole moieties showed self-reversible mechanochromism and the property of self-recovering.

1.4. The carbazolyl-containing compound demonstrated intensive green emission peaking at 537 nm in the initial state, and weak yellowish green emission peaking at 557 nm after mechanical treatment which self-recovered back to intensive green emission with the intensity maximum at 539 nm. These processes are fully reversible. They include the following set of states: highly emissive state → damaged weak-emissive state → self-recovering → recovered highly emissive state.

2. Four compounds with the donor-acceptor and donor-acceptor-donor structures containing benzanthrone as the acceptor moiety and phenothiazine or phenoxazine as donor moieties have been designed and synthesized as fully organic near-infrared thermally activated delayed fluorescence probes of oxygen with long-lived emission. It has been determined that:

2.1. The maximum intensity of photoluminescence of the solid samples of the compounds was observed at 700 nm.

2.2. The values of emission lifetimes of the films of the derivatives at room temperature were found to be of in the range of 291–1198 μs.

2.3. The ratio of the intensity of the emission of the film of the molecular mixture of the phenoxazine-based compound in an inert polymer recorded in air and the intensity of the emission taken under oxygen was found to be of 15.2.

2.4. The oxygen sensitivity of the film of a phenoxazine-containing material was estimated by the Stern-Volmer constant and was found to be of 1.6×10^{-4} ppm^{-1}, thus demonstrating good reversibility.

3. New derivatives of pyrimidine-5-carbonitrile and differently substituted carbazoles have been synthesized and used as emitters for the fabrication of thermally activated delayed fluorescence organic light-emitting diodes and as sensitive oxygen probes. It has been determined that:

3.1. The obtained compounds demonstrated efficient thermally activated delayed fluorescence properties.

3.2. Bipolar charge-transporting properties were detected for a carbazole-based compound with the hole mobility of 1.6×10^{-4} $cm^2/V\cdot s$ and the electron mobility of 1.37×10^{-5} $cm^2/V\cdot s$ at the electric field of 7.2×10^5 V/cm.

3.3. Aggregation induced emission enhancement was characterized for the compounds containing carbazole and *tert*-butyl carbazole moieties allowing to reach photoluminescence quantum yields up to 50% in the solid state.

3.4. A non-doped sky-blue organic light-emitting diode with external quantum efficiency of 12.8% has been fabricated by using a compound based on carbazole and pyrimidine-5-carbonitrile with the best set of charge-transporting and thermally activated delayed fluorescence properties.

3.5. The oxygen sensing ability of the compounds was investigated; it was demonstrated that they can be used as active oxygen probes with fast response, high sensitivity, and good stability. The Stern-Volmer constants were found to be 3.24×10^{-5} and 1.49×10^{-5} ppm^{-1} for the solution dispersions of carbazole- and *tert*-butyl carbazole-based derivatives in the Zeonex matrix, respectively.

4. Two new compounds with the donor-acceptor-donor structures containing pyrimidine-5-carbonitrile as the acceptor moiety and 9*H*-phenylcarbazole and triphenylamine as the donor moieties have been developed and characterized by the ability to harvest high-lying triplets. It has been determined that:

4.1. The compounds were characterized as highly emissive emitters with the absolute photoluminescence quantum yields of their solutions reaching 98%.

4.2. The developed materials showed bipolar charge-transporting properties with the hole mobility exceeding 10^{-3} $cm^2/V\times s$ at an electric field of 3.6×10^5 V/cm, which makes them suitable for the application in organic light-emitting diodes as the host materials.

4.3. Triplet-harvesting via the upper level triplet-singlet intersystem crossing was proven by the different methods including theoretical calculations and time-resolved electroluminescence spectroscopy.

4.4. A pure blue fluorescent organic light-emitting diode with an EQE of 7% based on the 9*H*-phenyl carbazolyl-containing emitter has been fabricated, which proves the considerable participation of triplet excitons in electroluminescence.

4.5. Excellent charge-transporting properties of the compounds allowed to use them as highly efficient bipolar hosts for orange-red organic light-emitting diodes. The device based on one developed host containing a carbazole moiety exhibited the maximum external quantum efficiency exceeding 20%.

4. SANTRAUKA

4.1. ĮVADAS

Elektroaktyviųjų organinių junginių evoliucija yra būtina sąlyga didelio efektyvumo optoelektroninių prietaisų kūrimui. Nepaisant didelių pastangų atrasti lengvai susintetinamus elektroaktyviuosius junginius, daugumos jų gavimas vis dar yra sudėtingas tiek cheminiu, tiek technologiniu požiūriu.[1,2] Vienas iš pagrindinių kelių siekiant komercializuoti organines elektroaktyviąsias medžiagas ir organinės elektronikos prietaisus yra rentabili vienos pakopos organinių puslaidininkių sintezė ir paprasti jų gryninimo metodai.

Pagrindinė organinių puslaidininkių taikymo sritis yra organiniai šviesą skleidžiantys diodai (OLED)[5–14]. Pastaruoju metu šviesą skleidžiančios medžiagos arba jų matricos kuriamos jungiant elektronų donorinius ir akceptorinius fragmentus [6,7,27,28]. Naudojant tokius derinius, galima gauti efektyvius spinduolius, pasižyminčius bipoline elektros krūvininkų pernaša. Šio darbo pradžioje benzantronas ir pirimidin-5-karbonitrilas nebuvo plačiai naudojami kaip akceptoriniai fragmentai kuriant „donoro–akceptoriaus“ tipo šviesos emiterius. „Donoro–akceptoriaus–donoro“ struktūros emiteriai gali pasižymėti skirtingais reiškiniais, tokiais kaip fosforescencija kambario temperatūroje (RTP)[50,51], tripletų anihiliacija (TTA)[52,53], termiškai aktyvinama uždelstoji fluorescencija (TADF)[29,41,54]. Dėl šių reiškinių susidarę tripletiniai eksitonai gali būti paverčiami šviesa esant elektriniam sužadinimui[10,13,41,52]. Tai leidžia peržengti teorines vidinio (IQE) ir išorinio (EQE) kvantinio efektyvumo ribas, siekiančias atitinkamai 25 % ir 5 %, būdingas įprastiems OLED su fluorescenciniais emiteriais[56]. Išvardintų reiškinių pritaikymas padidina OLED efektyvumą, spalvos grynumą ir veikimo stabilumą.

Pastaruoju metu dedamos didelės pastangos sukurti efektyvius „donoro–akceptoriaus“ struktūros emiterius, kurie pasižymėtų TADF, o juos panaudojus buvo sukurti modernūs OLED, kurių EQE siekia iki 38 %[58,59]. „Donoro–akceptoriaus“ struktūros TADF medžiagos turi daug potencialo būti taikomos ne tik OLED, bet ir optinių deguonies jutiklių aktyviuosiuose sluoksniuose[66–69]. Paprastai tokiems tikslams naudojami fosforescenciniai sunkiųjų metalų (platinos, paladžio, iridžio ir t. t.) kompleksai, kurie yra brangūs ir kenksmingi aplinkai[15]. Organiniai artimosios infraraudonosios (NIR) spinduliuotės TADF emiteriai, pasižymintys ilgos trukmės emisija, taip pat gali būti naudojami deguonies jutikliams[71,72].

Šviesą skleidžiančios „donoro–akceptoriaus“ struktūros medžiagos gali keisti emisijos spalvą, kuri priklauso nuo išorinių veiksnių[77]. Mechanochrominė liuminescencija (MCL) yra apibūdinama kaip grįžtamas emisijos spalvos pokytis dėl mechaninio poveikio[77]. MCL medžiagos potencialiai gali būti naudojamos mechaniniams sensoriams, duomenų kodavimo prietaisams ir atminties lustams[79–81]. MCL daugiausia yra tyrinėjama, kai poveikis sukuriamas trinant, garinant arba lydant[82–85]. Tačiau tik nedaugelio medžiagų emisija gali atsistatyti be jokio papildomo poveikio, t. y. pasižymėti savaime atsistatančiu mechanochromizmu[86–88].

Naujų organinių „donoro–akceptoriaus“ struktūros šviesos emiterių, pasižyminčių konkrečiomis savybėmis, sukūrimas yra vienas iš pagrindinių būdų išspręsti OLED ilgaamžiškumo, efektyvumo ir rentabilumo problemą. Siekiant

sukurti tam tikrų savybių medžiagas, būtina kruopščiai parinkti donorinius ir akceptorinius fragmentus. Pasirinktų fragmentų cheminė struktūra ir terminis stabilumas turi lemiamą poveikį organinių puslaidininkių pritaikomumui elektroliuminescenciniuose prietaisuose. Tikslingai parinktų donorinių ir akceptorinių fragmentų derinys įgalina susintetinti naujus šviesą skleidžiančius organinius puslaidininkius ir numatyti jų emisijos mechanizmus arba krūvininkų pernašos savybes. Naujų emiterių struktūrų projektavimas, sintezė ir savybių tyrimas yra pagrindinis būdas padidinti OLED efektyvumą, taip pat atrasti naujas sukurtų organinių medžiagų taikymo sritis.

Šio **darbo tikslas** – naujų „donoro–akceptoriaus“ struktūros darinių, turinčių benzantrono arba pirimidin-5-karbonitrilo fragmentus, sintezė ir savybių tyrimai siekiant juos pritaikyti OLED, deguonies jutikliams ir apsaugos zondams.

Siekiant užsibrėžto tikslo, būtina įgyvendinti **tokius uždavinius:**

- susintetinti naujus „donoro–akceptoriaus“ ir „donoro–akceptoriaus–donoro“ struktūros benzantrono darinius;
- ištirti benzantrono darinių termines, fotofizikines ir fotoelektrines savybes;
- ištirti mechanochromines benzantrono ir karbazolo darinių savybes ir įvertinti jų pritaikymo saugos zondams potencialą;
- ištirti sodriai raudona–infraraudonąja emisija pasižyminčių fentiazino arba fenoksazino pakaitus turinčių benzantrono darinių, kaip potencialių kandidatų deguonies jutikliams, TADF savybes;
- susintetinti naujus simetrinės „donoro–akceptoriaus–donoro“ struktūros junginius su pirimidin-5-karbonitrilo ir skirtingo pakeitimo karbazolo arba trifenilamino fragmentais;
- ištirti pirimidin-5-karbonitrilo darinių termines, fotofizikines, fotoelektrines ir elektroliuminescencines savybes;
- ištirti pirimidin-5-karbonitrilo darinius su skirtingo pakeitimo karbazolo fragmentais, tokius kaip žydros spalvos TADF OLED emiteriai ir deguonies jutimo zondai;
- ištirti trifenilamino arba 9-fenilkarbazolo pakaitus turinčių pirimidin-5-karbonitrilo darinių gebėjimą spinduliuoti dalyvaujant tripletiniams eksitonams ir įvertinti jų kaip bipolinių emiterių arba matricų pritaikymo galimybes.

Darbo naujumas:

- Benzantrono ir karbazolo fragmentus turintis darinys pasižymi atsistatančiu mechanochromizmu. Šios savybės gali būti pritaikytos pažeidimams atspariam informacijos perkodavimui ir saugos zondams.
- Susintetintas naujas benzantrono ir fenoksazino NIR TADF emiteris ir pademonstruotas jo pritaikomumas deguonies jutikliams.
- Sukurti nauji TADF emiteriai, turintys pirimidin-5-karbonitrilo akceptorinius ir *tret*-butilkarbazolo donorinius fragmentus; pademonstruotas jų pritaikomumas efektyviems žydros šviesos OLED ir deguonies jutikliams.

- Pirmą kartą susintetinti pirimidin-5-karbonitrilo dariniai, turintys trifenilamino arba 9-fenilkarbazolo fragmentus, kurie panaudoti kaip žydros ir žalios šviesos emiteriai fluorescenciniuose OLED ir kaip matricos efektyviuose oranžiniuose–raudonuose TADF OLED, kurių EQE viršija 20 %.

4.2. PASKELBTŲ PUBLIKACIJŲ APŽVALGA

4.2.1. Savaime atsistatančia mechanochromine liuminescencija pasižymintys benzantrono ir karbazolo dariniai pažeidimams atspariam informacijos perkodavimui ir saugos zondams

Kuriant MCL reiškiniu pasižyminčias medžiagas buvo panaudotas naujas standžios plokščios struktūros benzantrono fragmentas kaip akceptorius ir karbazolas bei di-*tret*-butil-pakeistas jo analogas kaip donorai. Junginių **1** ir **2** sintezės kelias pavaizduotas 4.1 schemoje. Tiksliniai „donoro–akceptoriaus“ struktūros junginiai buvo gauti atliekant Buchwald-Hartwig kryžminio jungimo reakciją. Junginių **1** ir **2** cheminė sandara buvo patvirtinta ^{1}H ir ^{13}C BMR spektroskopijos, masių spektrometrijos ir elementinės analizės metodais.

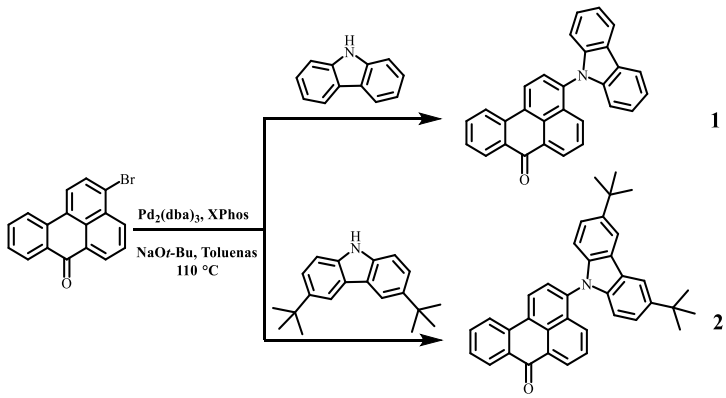

4.1 schema. Junginių **1** ir **2** sintezės schema

Darinių **1** ir **2** terminis stabilumas bei morfologiniai virsmai buvo tiriami atitinkamai termogravimetrinės analizės (TGA) ir diferencinės skenuojamosios kalorimetrijos (DSC) metodais (4.1a pav.). Tyrimų duomenys apibendrinti 4.1 lentelėje. Junginiui **1** būdinga 93 °C stiklėjimo temperatūra (T_{st}), o junginiui **2** – 124 °C. Abiem junginiams būdingos dvi lydymosi temperatūros (T_{lyd}), užfiksuotos pirmojo šildymo skenavimo metu (4.1 lentelė, 2.1a pav.). Šitas reiškinys buvo papildomai tiriamas atliekant skirtingų junginio **1** kristalų DSC skenavimus, siekiant patvirtinti dviejų skirtingų kristalinių atmainų buvimą. Šių kristalinių atmainų įtaka MCL savybėms taip pat buvo ištirta.

Ištirtos gautų junginių **1** ir **2** fotofizikinės savybės, tokios kaip absorbcija ir fotoliuminescencija (PL), kurios pateiktos 4.1 lentelėje ir 4.1b pav. Dvi absorbcijos juostos ties 295 ir 320–335 nm yra būdingos karbazolo fragmento π-π* šuoliams[94] (4.1b pav.). Abiejų junginių tolueno tirpalai pasižymėjo žalios šviesos emisija, tačiau grynų medžiagų sluoksniai švietė geltonai (4.1b pav., 4.1 lentelė). Junginių **1**

ir **2** tolueno tirpalų fotoliuminescencijos gesimo kreivės, išsidėsčiusios ns srityje, parodė fluorescencinę spinduliuotės prigimtį (4.1 lentelė).

4.1 lentelė. Junginių **1** ir **2** terminės ir fotofizikinės savybės

Jungi-nys	T_d [a], °C	T_{lyd}, °C	T_{st} [c], °C	λ_{PL} tol/sluoksnis, nm	Φ tol/sluoksnis, %	τ tol, ns	τ_1/τ_2 sluoksnis, ns
1	344	259[b]/276[b,c]	93	501/560	34/22	4,30	1,32/5,36
2	359	264[b]/296[b,c]	124	530/590	53/22	8,72	1,61/6,38

[a] – Nustatyta TGA metodu; DSC metodu: [b] – pirmasis šildymo skenavimas, [c] – antrasis šildymo skenavimas; T_d – masės 5 % nuostolio temperatūra, T_{lyd} – lydymosi temperatūra, T_{st} – stiklėjimo temperatūra; λ_{PL} – fotoliuminescencijos spektro maksimumas; Φ – fotoliuminescencijos kvantinis našumas; τ_1, τ_2 – fotoliuminescencijos gyvavimo trukmės.

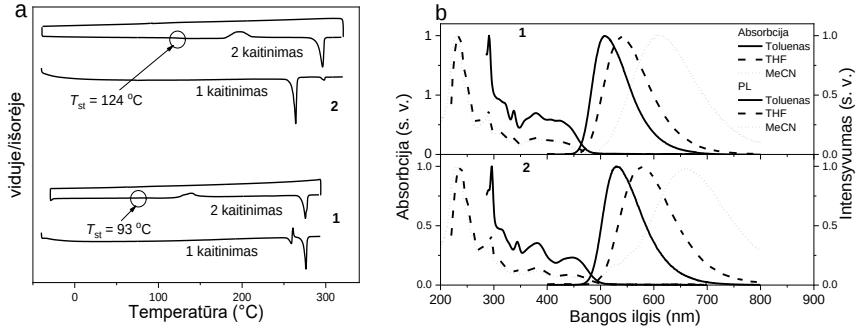

4.1 pav. (a) Junginių **1** ir **2** DSK kreivės; (b) junginių **1** ir **2** praskiestų tirpalų absorbcijos ir PL (λ_{eks} = 330 nm) spektrai

Susintetinti dariniai **1** ir **2** pasižymėjo mechanochrominėmis savybėmis. Jų emisijos spalva gali būti keičiama taikant papildomą poveikį, tokį kaip malimas, garinimas arba lydymas. Šių tyrimų duomenys apibendrinti 4.2 lentelėje ir 4.2 pav. Junginio **1** šviežiai paruoštas bandinys šviečia žaliai (538 nm), o išlydytas – geltonai (574 nm). Analogiški junginio **2** bandiniai skleidžia atitinkamai gelsvai žalią (550 nm) ir oranžinę šviesą (594 nm) (4.2 lentelė, 4.2(a, b) pav.).

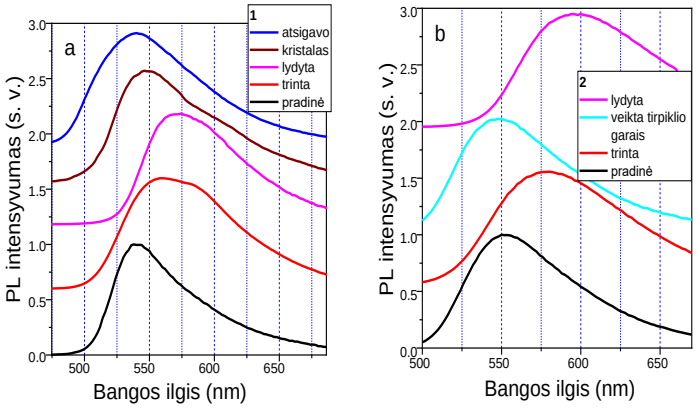

4.2 pav. Įvairių būsenų normalizuoti PL spektrai (λ_{eks} = 350 nm)

Karbazolo fragmentą turintis junginys **1** pasižymėjo kambario temperatūroje savaime atsistatančia MCL (4.2a pav.). Po sutrynimo bandinys grįžta į pradinę būseną be jokio papildomo išorinio poveikio per 20 min. Šis procesas yra grįžtamas iki 5 sutrynimo / atsistatymo (per 20 min) ciklų. Sutrinto junginio **2** bandinio emisija negrįžo į pradinę net ir po mėnesio.

4.2 lentelė. **1** ir **2** junginių PL parametrai ir morfologinės savybės.

Būsena / Parametras	**1**					**2**			
	p-	t-	a-	l-	cr-	p-	t-	ap-	l-
λ_{PL}, nm	538	560	540	574	546	550	580	548	594
Φ_{PL}, %	15	17	15	9	–	27	31	23	3
τ_1, ns	1,13	2,04	2,01	1,97	1,49	2,67	3,91	2,69	3,09
τ_2, ns	5,28	6,93	7,13	6,60	9,41	6,09	9,62	6,04	8,97
kristališkumas*, %	63,8	29,3	39,5	0	100	66,4	42,1	49,8	3,3

(p-) – pradinės, (t-) – trintos, (a-) – atsigavo, (l-) – lydytos, (k-) – kristalas, (a-) – apdorota tirpalo garais; λ_{PL} – PL maksimumas (λ_{eks} = 350 nm); * – gautas iš PXRD matavimų

Siekiant patvirtinti skirtingų amorfinių agregatų susidarymą, buvo ištirti **1** ir **2** amorfiniai mišiniai standžioje polimerinėje „Zeonex“ matricoje (2.3(a, b) pav.). Didinant medžiagų koncentraciją „šeimininko–svečio“ sistemose „matrica–medžiaga“ buvo pastebėtas raudonasis PL poslinkis. Tai patvirtina ne tik kietos būsenos solvatochromizmą, bet ir amorfinių agregatų susidarymą (pažymėta A1, 4.3(a,b) pav.). Junginio **1** amorfinio agregato A1 PL spektro viršūnė yra ties 555 nm, o junginio **2** agregato – ties 568 nm. Po bandinių terminio apdorojimo 150 °C temperatūroje A1 agregacijos laipsnis sumažėjo (raudonasis emisijos poslinkis), tačiau kartu susidarė kitokio tipo agregatai A2 (4.3(a, b) pav.) su jiems būdingu mėlynuoju emisijos poslinkiu. Šių A2 agregatų PL spektrų viršūnės yra ties 521 ir 550 nm (atitinkamai junginio **1** ir **2**). Tiek abiejų kristalinių atmainų (pagal DSC duomenis), tiek amorfinių agregatų buvimas nulemia bendrą šių medžiagų skirtingų pavidalų (šviežio, išlydyto arba užgarinto bandinio) emisijos spektrą (4.2 pav.).

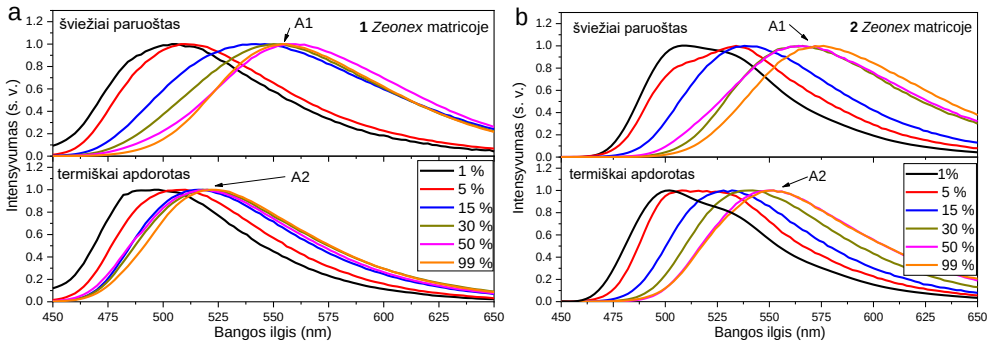

4.3 pav. Junginių **1** (a) ir **2** (b) kietosios būsenos PL spektrai „Zeonex“ matricoje prieš (viršuje) ir po terminio apdorojimo (apačioje)

Junginio **1** savaime atsistatančios savybės turi potencialo būti pritaikytos atspariam pažeidimams informacijos šifravimui arba saugos patikrinimui. Unikalios junginio **1** savybės taip pat gali būti panaudotos daugiapakopei apsaugotų objektų kontrolei. Pirmoji pakopa yra emisijos spalvos pasikeitimas iš ryškios žalios į geltoną, o antroji – spalvos grįžimas iš geltonos atgal į žalią.

4.2.2. Fentiazino ir fenoksazino pakaitus turinčio benzantrono, emituojančio sodriai raudonoje / artimojoje infraraudonojoje srityje, TADF slopinimo savybės deguonies jutikliams

„Donoro–akceptoriaus“ ir „donoro–akceptoriaus–donoro“ struktūros junginiams **3–6** gauti buvo panaudotos Buchwald-Hartwig kryžminio jungimo reakcijos (4.2 schema). Darinių **3–6** cheminė sandara buvo patvirtinta ^{1}H, ^{13}C BMR, IR, masių spektrometrijos ir elementinės analizės metodais.

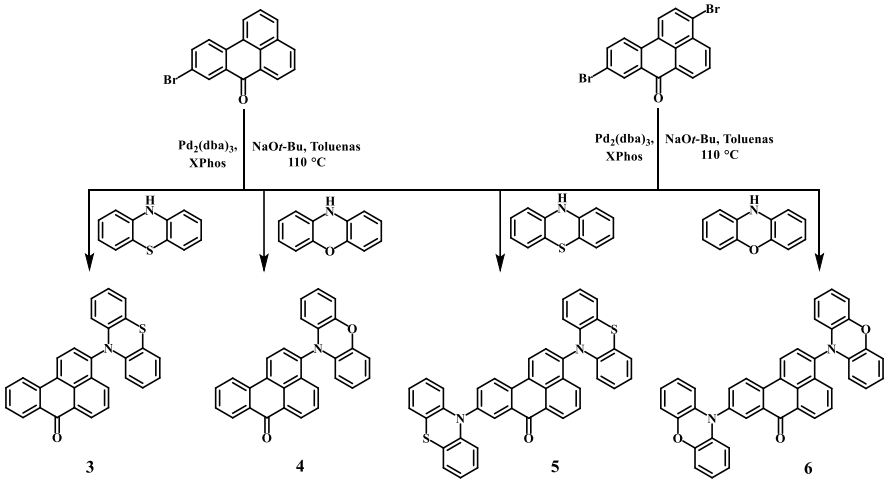

4.2 schema. Junginių **3–6** sintezės schema

TGA ir DSC kreivės buvo užrašytos siekiant ištirti medžiagų **3–6** termines savybes. Tyrimai atskleidė sąlygiškai didelį terminį stabilumą. D-A struktūros junginiams **3** ir **4** būdingas mažesnis terminis stabilumas (T_d viršijo 300 °C) lyginant su „donoro–akceptoriaus–donoro“ struktūros junginiais **5** ir **6** (T_d viršijo 400 °C). Iš DSC antrojo šildymo kreivių matoma, kad visiems junginiams būdinga 100 °C viršijanti T_{st} (4.3 lentelė).

4.3 lentelė. Terminės ir fotoelektrinės charakteristikos

Junginys	T_{lyd}, °C	T_{st}^{**}, °C	IP^{UPS}, eV	$\mu^{skylės}$, cm^2/V·s	$\mu^{elektronai}$, cm^2/V·s
3	286*,**	111	5,68	$9{,}8\times10^{-6}$	$1{,}5\times10^{-4}$
4	–	114	–	–	–
5	–	174	–	–	–
6	391*,**	170	5,49	$7{,}4\times10^{-8}$	$1{,}1\times10^{-4}$

* pirmasis šildymo skenavimas; ** antrasis šildymo skenavimas; $\boldsymbol{\mu}^{skylės}$ ir $\boldsymbol{\mu}^{elektronai}$ vertės paimtos $3{,}6\times10^{5}$ V/cm

Vakuume užgarintų junginių **3–6** sluoksnių fotoelektronų emisijos spektrai buvo užrašyti ultravioletinės fotoelektronų spektroskopijos (UPS) metodu siekiant nustatyti jų kietosios būsenos jonizacijos potencialą (IP^{UPS}). IP^{UPS} vertes pavyko nustatyti tik junginiams **3** ir **6**, kurios buvo mažesnės už 6,0 eV (4.3 lentelė). Junginių **3** ir **6** krūvio pernašos savybės buvo tiriamos lėkio trukmės (TOF) metodu. Junginių **4** ir **5** bandiniai nebuvo tinkami TOF matavimams dėl jų prastesnių plėvėdaros savybių. Gautiesiems junginiams **3** ir **6** būdingos artimos elektronų judrumo vertės, kurios atitinkamai yra $1{,}5\times10^{-4}$-$1{,}1\times10^{-4}$ $cm^2/V\cdot s$ ($3{,}6\cdot10^5$ V/cm stiprio elektriniame lauke). To paties stiprio elektriniame lauke buvo užfiksuotas pastebimai mažesnis skylių judrumas, kurio vertės yra $7{,}4\times10^{-8}$ ir $9{,}8\times10^{-6}$ cm^2/Vs atitinkamai junginio **3** ir **6** atveju (4.3 lentelė).

Grynų medžiagų kietų sluoksnių ir tolueno tirpalų absorbcijos ir PL spektrai, užrašyti 300 K temperatūroje, pateikti 4.4a pav. Tiek tirpalai, tiek grynos medžiagos emituoja raudonojoje / artimoje infraraudonojoje srityje (4.4a pav.). Visų tirtų junginių PL kvantinės išeigos (tiek grynų medžiagų, tiek tirpalų) yra apie 0,01 (4.4 lentelė). „Zeonex“ yra polimerinė matrica, naudojama tirti junginių fotofizikinėms savybėms esant susilpnintoms tarpmolekulinėms sąveikoms[17] (autorė dėkoja „Zeon Europe GmbH“ (Diuseldorfas, Vokietija) už neatlygintinai padovanotą 1 kg šio polimero moksliniams tyrimams). Junginių **3–6** kietųjų 1 % tirpalų „Zeonex“ matricoje fotofizikinės savybės buvo tiriamos oro ir azoto aplinkoje (2.5b pav.). Oro aplinkoje nustatytos šių sistemų PL kvantinės išeigos yra 0,02, 0,03, 0,03 ir 0,04 atitinkamai junginių **3–6** atveju (4.4 lentelė).

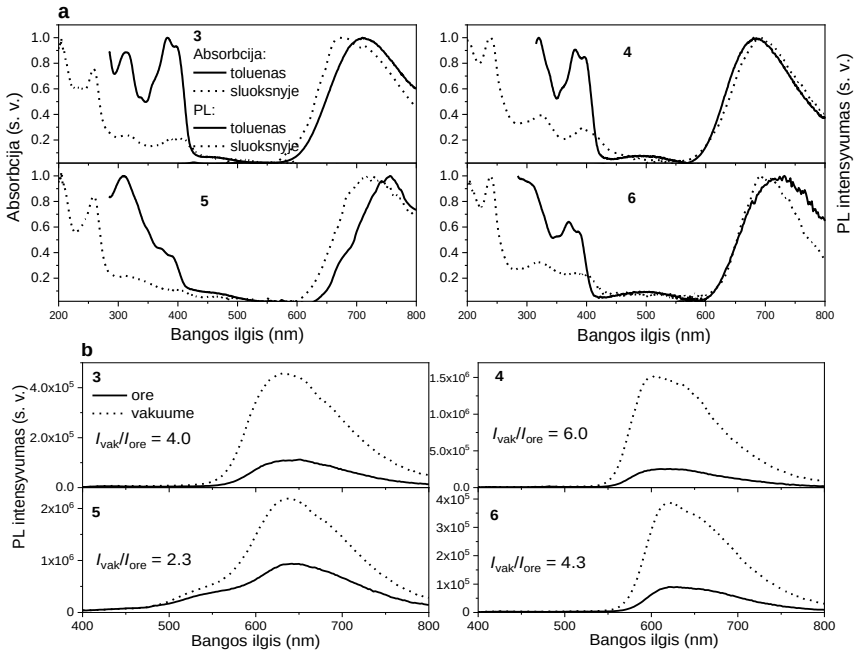

4.4 pav. (a) Junginių **3–6** praskiestų tolueno tirpalų (10^{-5} M) ir sluoksnių absorbcijos ir PL spektrai; (b) kietųjų 1 % tirpalų „Zeonex“ matricoje PL spektrai, užrašyti oro aplinkoje ir vakuume

Nustatyta „donoro–akceptoriaus“ tipo junginių **3** ir **5** TADF gyvavimo trukmė kambario temepratūroje yra atitinkamai 788 ir 1198 µs, o junginių **4** ir **6** – atitinkamai 291 ir 368 µs. Kadangi junginys **4** pasižymėjo didžiausiu PL intensyvumo sustiprėjimu pašalinus orą (4.4b pav.), jis buvo pasirinktas tirti deguonies jutimo savybėms. Junginio **4** kietojo 1 % tirpalo „Zeonex“ matricoje, patalpinto aplinkoje su skirtingu deguonies / azoto santykiu, PL spektrai pateikti 4.5a pav. Vakuume išmatuoto TADF ir deguonies sraute išmatuoto momentinės fluorescencijos intensyvumo santykis buvo 15,2. Ši vertė yra artima didžiausioms žinomoms tarp TADF medžiagų, naudojamų optiniams TADF deguonies jutikliams[67,97].

4.4 lentelė. Junginių **3–6** fotofizikinės charakteristikos

Junginys	Stokso poslinkis^{tol}, nm	Stokso poslinkis $_{sluoksnis}$, nm	$\Phi^{tol}{}_{PL}$, %	$\Phi_{sluoksnis\ PL}$, %	$\Phi_{sluoksnis\ PL}$, 1m %: „Zeonex“, %	$\Phi_{sluoksnis\ PL}{}^{vak}$, 1m %: „Zeonex“, %
3	316	275	1	1	2	8
4	308	273	1	1	3	7
5	193	188	1	1	3	18
6	196	225	1	1	4	17

Stern-Volmer diagrama (4.5b pav.) buvo sudaryta pagal lygtį $\tau_0/\tau - 1 = K_{SV}[O_2]$; čia τ_0 ir τ yra TADF gyvavimo trukmės atitinkamai bedeguonėje ir deguonies turinčioje aplinkoje, o $K_{SV}[O_2]$ yra vadinamoji Stern-Volmer konstanta. Iš diagramos galima pastebėti, kad tiesinė priklausomybė galioja esant deguonies koncentracijai iki 5×10^3 ppm, o $K_{SV}[O_2]$ vertė yra $1{,}6\cdot10^{-4}$ ppm^{-1}. Taip pat buvo įvertintas jautrumo deguoniui grįžtamumas pašalinus PL slopikilį, t. y. deguonį. Bandinio PL gesimo kreivės buvo užrašytos po prapūtimo deguonimi, azotu ir 9100 ppm deguonies srautu 7 min trukmės ciklais (4.5c pav.).

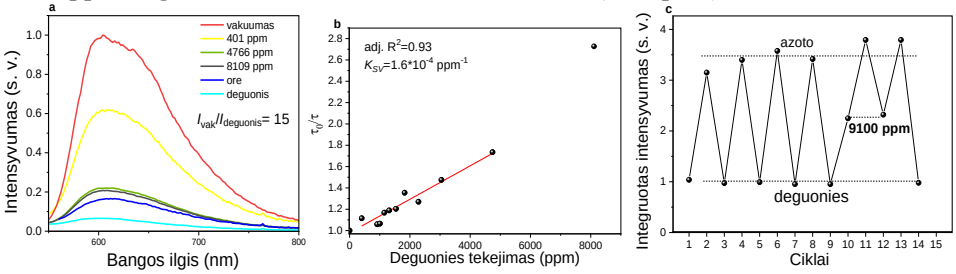

4.5 pav. Junginio **4** kietojo 1 % tirpalo „Zeonex“ matricoje PL spektrai esant skirtingai deguonies koncentracijai aplinkoje (a), Stern-Volmer diagrama (b) ir atsakas į deguonies poveikį (c)

4.2.3. Multifunkciniai pirimidin-5-karbonitrilo ir skirtingo pakeitimo karbazolo dariniai nelegiruotiems žydros spalvos OLED ir liuminescenciniams deguonies jutikliams

Simetriniai „donoro–akceptoriaus–donoro“ junginiai buvo suprojektuoti pasirinkus pirimidin-5-karbonitrilo akceptorių ir skirtingo pakeitimo donorinius karbazolo fragmentus. Visos šios medžiagos buvo gautos vienos pakopos

nukleofilinės substitucijos reakcija iš komercinių reagentų. Junginių **7–9** sintezės kelias pavaizduotas 4.3 schemoje. Junginių cheminė sandara buvo patvirtinta ^{1}H ir ^{13}C BMR spektroskopijos, masių spektrometrijos ir elementinės analizės metodais.

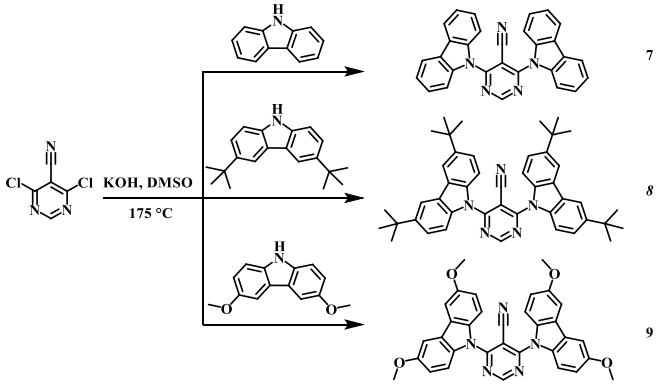

4.3 schema. Junginių **7–9** sintezės schema

TGA ir DSC metodais buvo ištirtos terminės medžiagų **7–9** savybės. Matavimų rezultatai apibendrinti 4.5 lentelėje. Visi junginiai pasižymėjo dideliu terminiu stabilumu: jų 5 % masės nuostolių temperatūros vertės (T_d) gerokai viršijo 300 °C. Visi junginiai po sintezės buvo išskirti kaip kristalinės medžiagos. Junginio **7** antrojo DSC šildymo metu užfiksuota 112 °C stiklėjimo temperatūra. Junginio **8** pakartotinio šildymo metu nustatyta T_{st} vertė yra 177 °C, o junginys **9** stiklo nesudaro.

4.5 lentelė. Terminės, elektrocheminės ir fotoelektrinės charakteristikos

Junginys	T_d,[a] °C	T_{st}, °C	T_{lyd}, °C
7	338	112[d]	273[b,d]/287[b]
8	396	177[d]	297[b]/326[b]
9	383	–	281[b,d]/298[b,d]

[a] – Nustatyta TGA metodu; DSC metodu: [b] – pirmasis šildymo skenavimas, [c] – aušinimo skenavimas, [d] – antrasis šildymo skenavimas

Pagal TOF duomenis buvo apskaičiuotos junginio **7** skylių bei elektronų ir junginio **9** elektronų judrumo vertės. Junginio **7** skylių judrumas siekia $1{,}6\times10^{-4}$ $cm^2/V\cdot s$ $7{,}2\times10^5$ V/cm stiprio elektriniame lauke (E). Panaši skylių judrumo vertė yra būdinga daugeliui kitų karbazolo fragmentą turinčių emiterių[27]. Junginio **7** elektronų judrumas siekė $1{,}37\times10^{-5}$ $cm^2/V\cdot s$ to paties stiprio elektriniame lauke.

Junginių **7–9** praskiestų tirpalų ir grynų (kietosios būsenos) medžiagų absorbcijos ir PL spektrai pateikti 4.6a pav., o visi fotofizikos duomenys apibendrinti 4.6 lentelėje. Junginių **7–9** tirpalų PL spektrams būdinga viena siaura emisijos juosta žydros / žalios spalvos srityje (4.6a pav.). Fotoliuminescencijos kvantinės išeigos (Φ) yra didesnės grynų medžiagų lyginant su tirpalais; tai rodo junginiams būdingą agregacijos indukuoto emisijos sustiprėjimo (AIEE) efektą (4.6 lentelė).

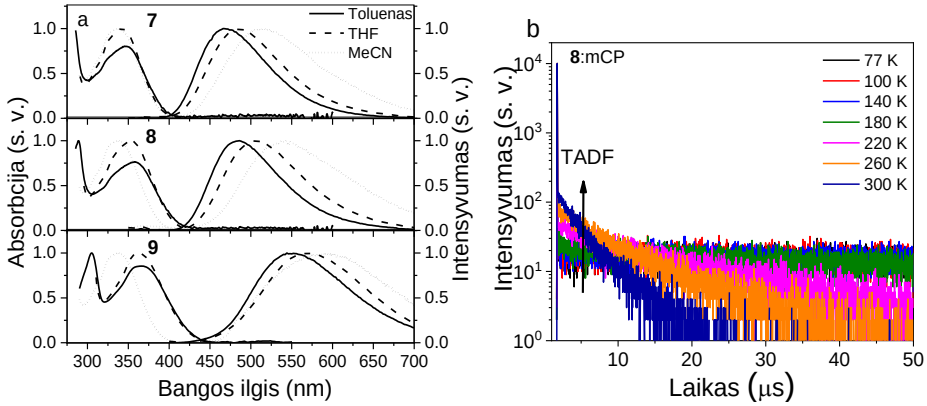

4.6 pav. (a) Junginių **7**–**9**, praskiestų toluenu, THF ir MeCN tirpalais (10^{-5} M) absorbcijos ir PL spektrai; (b) junginio **8** 10 % kietojo tirpalo mCP sluoksnio PL gesimo kreivės įvairiose temperatūrose

Grynų medžiagų sluoksnių PL gesimo kreivių daugiaeksponentė aproksimacija atskleidė PF, kurios gyvavimo trukmė (τ_{PF}) apie 12 ns, ir DF, kurios gyvavimo trukmė (τ_{DF}) yra μs eilės (4.6 lentelė, 4.6b pav.). ΔE_{ST} vertės buvo apskaičiuotos iš junginių tirpalų fluorescencijos ir fosforescencijos spektrų, užrašytų skysto azoto temperatūroje (4.6 lentelė).

4.6 lentelė. Pirimidinkarbonitrilo darinių fotofizinės charakteristikos

Junginiai / Parametrai	**7**	**8**	**9**
Φ^{tolueno} (%)	2 (6*)	12 (21*)	3
Φ^{THF} (%)	15	12	1
$\Phi^{\#}$ (%)	33 (53*)	20 (25*)	2
$\tau_{PF}{}^{\#}$ (ns)	12,9	12,2	11,4
$\tau_{DF}{}^{\#}$ (μs)	2,1	2,3	1
$E_{S1,\,THF}$ (eV)	3,17	3,02	2,89
$E_{T1,\,THF}$ (eV)	3,03	2,93	2,88
$\Delta E_{ST,\,THF}$ (eV)	0,14	0,09	0,01
$E_{S1,\,mCP}$ (eV)	2,99	2,93	2,74

$^{\#}$ – grynų medžiagų sluoksnių; * – pašalinus deguonį. Pagal empirinę formulę E_{ph} [eV] = 1239,84/λ [nm] buvo apskaičiuoti E_{S1} ir E_{T1} energetiniai lygmenys; čia λ yra bangos ilgis ties fluorescencijos ir fosforescencijos spektrų pradžia.

ΔE_{ST} sumažėjo junginius **7** ir **8** įterpus į 1,3-bis(9-karbazolil)benzeno (mCP) matricą (4.6 lentelė). Tokių kietųjų molekulinių mišinių (su mCP) PL spektrai ir gesimo kreivės buvo registruojamos esant skirtingai temperatūrai. Junginio **8** PL gesimo kreivės pateiktos 4.6b pav. Iš jų akivaizdu, kad fosforescencijos dedamoji buvo nuslopinta keliant temperatūrą dėl staigiai stiprėjančios sąveikos su deguonimi. Tuo pat metu šiluminė DF aktyvacija nulėmė esminį TADF intensyvumo padidėjimą temperatūroje, didesnėje nei 180 K (4.6b pav.).

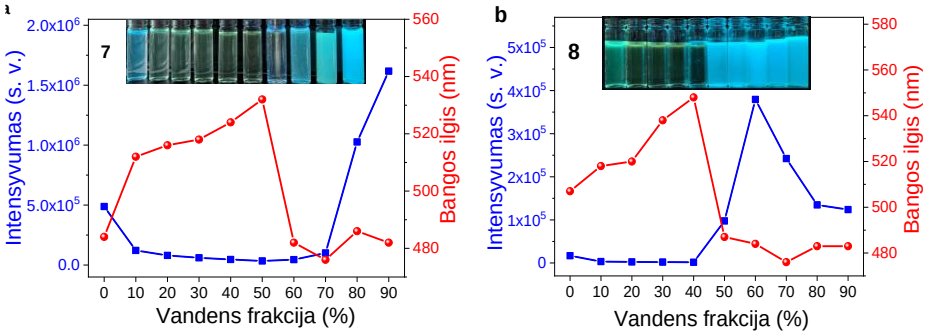

4.7 pav. PL intensyvumo ir spektrų viršūnių bangos ilgio priklausomybė nuo vandens dalies junginių **7** (a) ir **8** (b) dispersijose THF / vandens mišiniuose

AIEE efekto tyrimams buvo pagamintos junginių **7** ir **8** dispersijos THF / vandens mišiniuose. PL intensyvumo priklausomybė nuo vandens dalies šiuose mišiniuose pavaizduota 4.7(a, b) pav. Esant mažai daliai (f_w) vandens, abiejų junginių dispersijos šviečia silpnai. Esant didelei f_w, abu junginiai skleidžia mėlyną šviesą, kurios bangos ilgis ties didžiausiu intensyvumu yra apie 480 nm, kadangi šios molekulės, būdamos netirpios vandenyje, sudaro agregatus.

Dėl AIEE savybių ir didelių kietosios būsenos Φ junginiai **7** ir **8** buvo pasirinkti optinio jautrumo deguoniui tyrimams. Bandiniai buvo patalpinti inertinėje azoto aplinkoje. Didinant deguonies koncentraciją, PL intensyvumas atitinkamai mažėjo. Stern-Volmer sąsaja tarp $I_0/I - 1$ ir deguonies srauto (4.8 pav.) atskleidė jautrumą deguoniui plačiose deguonies srauto ribose esant skirtingam deguonies parcialiniam slėgiui[100].

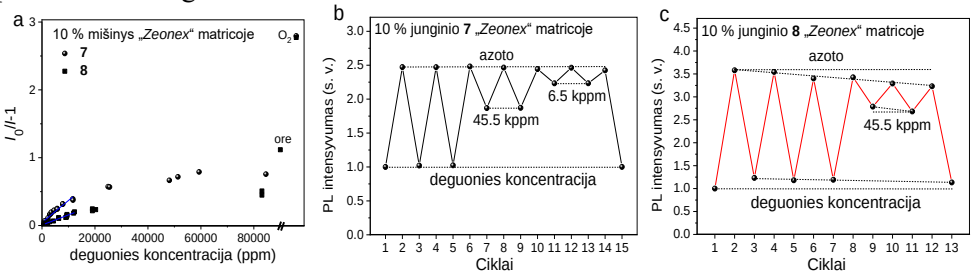

4.8 pav. Junginių **8** ir **9** kietųjų 10 % molekulinių mišinių „Zeonex“ matricoje Stern-Volmer diagramos (a) ir atsakas į deguonies poveikį (b, c)

Apskaičiuotos junginių **7** ir **8** molekulinių mišinių „Zeonex“ matricoje K_{SV} vertės yra atitinkamai $3{,}24 \cdot 10^{-5}$ ir $1{,}49 \cdot 10^{-5}$ ppm^{-1}. Tokios vertės yra panašios į TADF deguonies zondų[66]. Susintetinti junginiai turi daug potencialo būti pritaikyti optiniuose deguonies jutikliuose, kadangi atitinka būtinus reikalavimus: a) greitas atsakas į deguonies koncentracijos pokyčius, kuris pasireiškia atitinkamu ir stabiliu PL pokyčiu per pakankamai ilgą laiką; b) tvarus jautrumas deguoniui; c) gera kietų sluoksnių „Zeonex“ matricoje kokybė; d) tinkamas terminis stabilumas ir fotofizikinės savybės (aptartos prieš tai)[101].

4.7 lentelė. Elektroliuminescencinių parametrų santrauka

Prietaisas	EML	L_{max}, 10^3 cd/m^2	η_c, cd/A	η_p, lm/W	λ_{EL} nm	EQE, %	CIE 1931
N1	**7**	13,1	32,4 (17,5)	18,8 (9,2)	494	12,8 (6,9)	(0,20, 0,36)
D1	**7**:mCP	23,1	33,3 (17,6)	20,2 (9,1)	489	14 (7,4)	(0,18, 0,33)
N2	**8**	13,2	12,3 (9,9)	4,6 (3,6)	490	5,1 (4,1)	(0,19, 0,35)
D2	**8**:mCP	14,8	33,7 (19,4)	18 (8,7)	490	13,7 (7,9)	(0,18, 0,35)
N3	**9**	9,3	4,0 (3,4)	2,1 (1,6)	524	1,4 (1,2)	(0,30, 0,49)
D3	**9**:mCP	13,7	3,8 (0,6)	1,2 (0,3)	500	1,4 (0,2)	(0,21, 0,43)

L_{max} – maksimalus skaistis; η_c ir η_p – maksimalus srovės ir galios efektyvumas; λ_{EL} – EL spektro maksimumo bangos ilgis ties 8V; EQE – maksimalus išorinis kvantinis efektyvumas; CIE 1931 – spalvotumo koordinatės. Skliaustuose pateiktos efektyvumo vertės esant 100 cd/m^2 ryškiui.

Įvertinus susintetintų junginių TADF ir AIEE potencialą, jie gali būti panaudoti kaip šviesos emiteriai nelegiruotuose prietaisuose. Siekiant įvertinti grynų junginių **7–9** šviesos emisijos sluoksnius, buvo pagaminta serija OLED (prietaisai N1–N3), kurių sandara yra tokia: ITO / HAT-CN (10 nm) / TCTA (30 nm) / mCP (7 nm) / šviesos emisijos sluoksnis (25 nm) / TSPO1 (3 nm) / TPBi (30 nm) / LiF (0,4 nm) / Al. Svarbiausi OLED elektroliuminescenciniai parametrai pateikti 4.7 lentelėje. Šie OLED taip pat buvo modifikuoti įterpiant „matricos–emiterio“ sistemą vietoj gryno emiterio sluoksnio: buvo pagaminta D1–D3 prietaisų serija, kurių šviesos emisijos sluoksnius sudarė junginių **7–9** 10 % mCP matricoje mišiniai.

OLED su šviesos emisijos sluoksniais iš junginių **7** ir **8** pasižymėjo artima žydrai elektroliuminescencija, o štai junginys **9** yra visiškai žalias emiteris (4.7 lentelė). N1 prietaiso EQE siekė 12,8 %, kuris yra beveik toks pat kaip ir atitinkamo legiruoto prietaiso D1. Daug mažesniu EQE (5,1 %) pasižymėjo nelegiruotas prietaisas N2 su junginiu **8** (4.7 lentelė).

4.2.4. Trifenilamino arba 9-fenilkarbazolo pakaitus turintys pirimidin-5-karbonitrilo dariniai: bipoliniai emiteriai ir matricos, šviesos emisijai pritaikančios tripletines būsenas

Tiksliniai junginiai buvo gauti Suzuki-Miyauros kryžminio jungimo reakcijomis, kaip pavaizduota 4.4 schemoje. Junginių cheminė sandara buvo patvirtinta ^{1}H ir ^{13}C BMR analize, masių spektrometrija ir elementine analize.

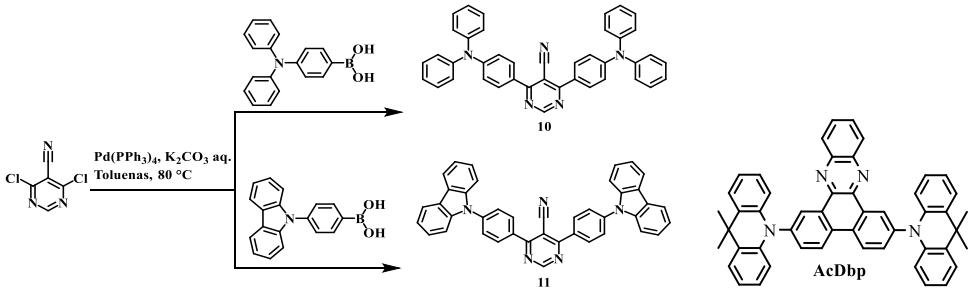

4.4 schema. Junginių **10** ir **11** sintezės schema ir emiterio **AcDbp** cheminė struktūra

Terminės junginių **10** ir **11** savybės buvo ištirtos atliekant TGA ir DSC matavimus. Abu junginiai pasižymėjo dideliu terminiu stabilumu. Jų 5 % masės nuostolių temperatūros (T_d) vertės yra atitinkamai 375 °C ir 423 °C (4.8 lentelė). DSC antrojo šildymo metu buvo užfiksuotas šių junginių gebėjimas sudaryti stiklus.

4.8 lentelė. Terminės ir fotoelektrinės savybės

Junginys	T_d, °C	T_{st}, °C	T_{lyd}, °C	IP^{UPS}, eV	E_{opt}, eV	EA^{UPS}, eV	$\mu_{s,*}$ $cm^2/V\times s$	$\mu_{e,*}$ $cm^2/V\times s$
10	375	102[c]	243[a,b]	5,61	2,75	2,86	$7,3\times10^{-3}$	$4,4\times10^{-4}$
11	423	135[c]	305[a]/270[b]	5,98	2,94	2,92	$2,1\times10^{-3}$	$0,4\times10^{-4}$

a – pirmasis šildymo, b – antrasis šildymo, IP_{UPS} – jonizacijos potencialas, gautas iš elektronų fotoemisijos metodu; EA_{UPS} – gimininguma elektronui, nustatytas ultravioletinės fotoelektronų emisijos metodu; E_{opt} – optinis tarpas; μ_{sk} ir μ_e – skylių ir elektronų judris; * – ties $3,6\times10^5$ V/cm.

Junginių **10** ir **11** pernašos lygmenys, taigi kietų sluoksnių IP^{UPS} ir EA^{UPS} buvo tiriami ultravioletinės fotoelektronų emisijos (UPS) ore ir absorbcinės spektroskopijos deriniu (4.9a pav.). Gimininguma elektronui vertės buvo apskaičiuotos pagal formulę $EA_{UPS} = IP^{UPS} - E_{opt}$; čia E_{opt} yra optinis tarpas, paimtas iš absorbcijos spektro. Mažesne IP^{UPS} verte (5,61 eV) pasižymėjo junginys **10** lyginant su junginiu **11**, kuriam būdingas 5,98 eV IP^{UPS} dydis (4.9a pav., 4.8 lentelė). Krūvininkų judrumo priklausomybė nuo elektros lauko stiprio pavaizduota 4.9b pav. Junginiui su trifenilamino fragmentais (**10**) būdingas didesnis tiek skylių, tiek elektronų judrumas tame pačiame elektros lauke lyginant su junginiu, turinčiu karbazolo pakaitus (**11**) (4.8 lentelė). Jie abu turi daug potencialo būti pritaikyti OLED bent jau kaip emiterių matricos.

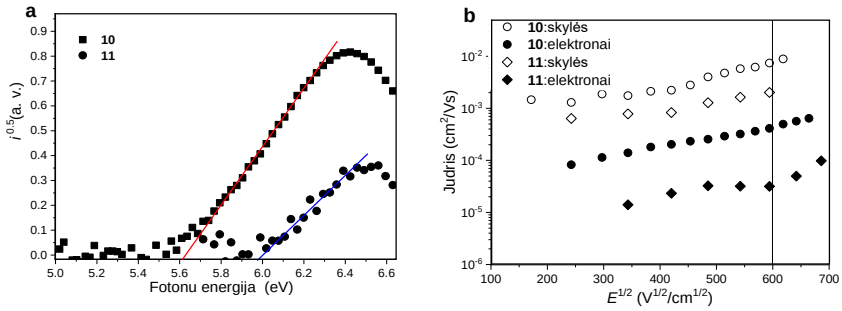

4.9 pav. Elektronų dreifinio judrumo priklausomybės nuo elektros lauko stiprio

Junginių **10** ir **11** tolueno tirpalai pasižymėjo mėlyna emisija (4.9 lentelė), o grynų junginių sluoksniams yra būdinga žalia emisija, kurios spektro viršūnė yra ties 506 nm. Susintetintų junginių tolueno tirpalų fluorescencija yra labai efektyvi (4.9 lentelė).

Junginių **10** ir **11** tolueno tirpalų PL gesimo kreivės išsidėsčiusios ns srityje – tai rodo, kad jų emisija yra momentinės fluorescencijos prigimties be jokių uždelstosios fluorescencijos požymių, pvz., TADF arba TTA (4.10a pav., 4.9 lentelė).

Toks pastebėjimas yra netikėtas įvertinus **10** ir **11** tolueno tirpalų PL intensyvumo tyrimų skirtingomis sąlygomis (oro arba deguonies prisotintų ir

degazuotų tirpalų) rezultatus (4.10b pav.). Abiejų junginių tolueno tirpalų PL intensyvumas po degazavimo šiek tiek padidėjo, tačiau po prisotinimo deguonimi jų PL intensyvumas žymiai sumažėjo. Tai patvirtina, kad tripletiniai eksitonai dalyvauja abiejų darinių **10** ir **11** šviesos emisijos procese. Yra žinoma, kad tripletiniai eksitonai yra labai jautrūs deguoniui.[110,111] Junginių **10** ir **11** tolueno tirpalų PL gesimo kreivės buvo užrašytos esant skirtingoms sąlygoms (4.10a pav.).

4.9 lentelė. Junginių **10** ir **11** tolueno tirpalų, grynų medžiagų sluoksnių ir kietųjų 20 % tirpalų matricoje fotofizikiniai parametrai

Junginys	λ_{PL}, nm	Φ, %	τ_1/τ_2, ns	Rel_1/Rel_2, %	χ^2
10^{tol}	486	90*	3,75	100	1,084
11^{tol}	458	98*	5,17	100	1,027
10 ^{sluoksnis}	506	45	2,86/8,49	62,64/37,56	1,222
11 ^{sluoksnis}	508	30	3,88/9,63	37,65/62,35	1,228
10 mCBP	506	21	2,02/4,87	67,36/32,64	1,224
11 mCBP	476	18	2,44/7,04	49,71/50,29	1,218

λ_{PL} – fotoliuminescencijos spektro maksimumas; Φ_{PL} – fotoliuminescencijos kvantinis našumas, * – degazuotos sąlygos; τ_1/τ_2 – PL gyvavimo trukmės; Rel_1/Rel_2 – įnašo santykis τ_1/τ_2

Junginių užšaldytų THF tirpalų PL ir fosforescencijos (PH) spektrai buvo užrašyti 77 K temperatūroje. Pagal PL ir PH spektrų viršūnių (didžiausio spinduliuotės intensyvumo) bangos ilgį buvo įvertintos junginių **10** ir **11** pirmųjų singletinių (S_1) ir tripletinių (T_1) energijos lygmenų vertės. Junginiui **10** būdinga maža 2,31 eV tripletinė energija, o štai junginio **11** tripletinė energija yra žymiai didesnė – 2,54 eV. Junginio **10** apskaičiuota ΔE_{ST} yra 0,32 eV, o junginio **11** – 0,34 eV. Šie rezultatai rodo, kad junginiams **10** ir **11** nėra būdingas TADF reiškinys, kaip jau buvo minėta anksčiau.

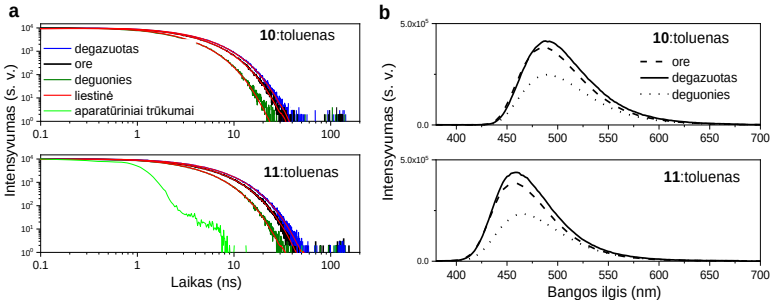

4.10 pav. Junginių **10** ir **11** tolueno tirpalų PL gesimo kreivės (a) ir PL spektrai (b) esant skirtingoms sąlygoms

Teoriniai tyrimai taip pat parodė didelius skirtumus (ΔE_{ST}) tarp junginių **10** ir **11** singletinės (S_1) ir tripletinės (T_1) energijos lygmenų, kurie yra atitinkamai 0,52 eV ir 0,26 eV (4.11 pav.). Tai apsunkina tripletinių eksitonų perėjimą iš T_1 į S_1 lygmenį atvirkštinės interkombinacinės konversijos (rISC) keliu, kuris yra būdingas TADF medžiagoms. Tačiau labai mažas ΔE_{ST} tarp didelės energijos lygmenų (junginio **10** ΔE_{S1T3} = 0,02 eV, ΔE_{S2T4} = 0,02 eV ir junginio **11** ΔE_{S3T3} = 0,05 eV, ΔE_{S3T4} = 0,02 eV) suponuoja, kad rISC tarp didesnės energijos tripletinių ir singletinių polygmenių gali konkuruoti su vidinės konversijos (IC) procesu tarp

sužadintųjų tripletinių lygmenų (junginio **10** ΔE_{T2T3} = 0,34 eV ir junginio **11** ΔE_{T2T3} = 0,29 eV) (4.11 pav.). Esant tokiems rISC keliams junginiuose **10** ir **11** susidaro vadinamieji „karštieji“ eksitonai. Teoriškai medžiagose, kuriose susidaro „karštieji“ eksitonai, galima pasiekti 100 % eksitonų utilizaciją taip padidinant OLED efektyvumą[113].

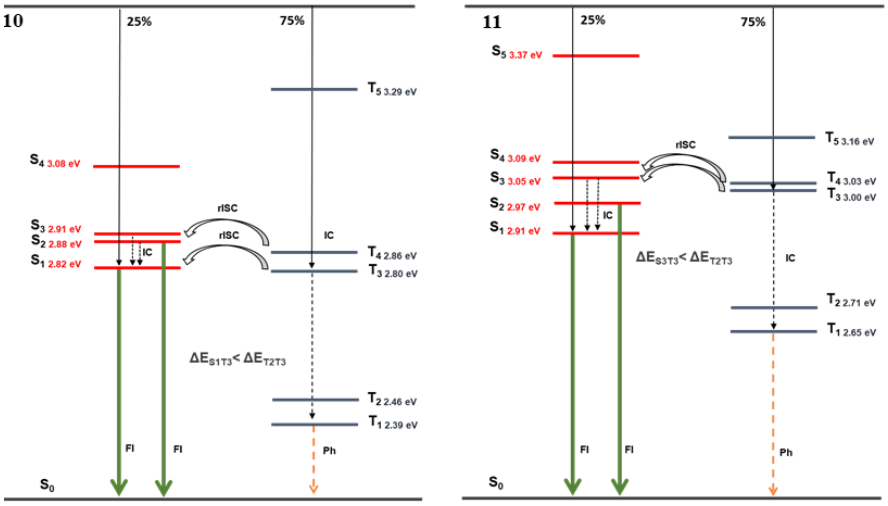

4.11 pav. Junginių **10** ir **11** singletinių ir tripletinių sužadintųjų būsenų, apskaičiuotų TD-B3LYP 6-31G(d,p) metodu, energijos diagrama

Siekiant ištirti junginių **10** ir **11** šviesos emisijos ir energijos perdavimo gebą, buvo pagaminti OLED su šviesos emisiniais sluoksniais iš **10** arba **11** emiterių mCBP matricoje ir AcDbp emiterio **10** arba **11** matricoje. Daugiasluoksnių OLED sandara parinkta tokia: ITO/HAT-CN[5]/NPB[40 nm]/TCTA[10 nm]/mCBP[10 nm]/ šviesos emisinis sluoksnis [50 nm]/NBPhen[30 nm]/Liq[2 nm]/Al. Prietaisuose E-10 ir E-11 atitinkamai junginiai **10** ir **11** buvo panaudoti kaip šviesos emiteriai, o štai prietaisuose H-10 ir H-11 – kaip matricos (4.10 lentelė). Palyginamasis prietaisas H-mCBP buvo pagamintas siekiant palyginti **10** ir **11** matricų efektyvumą su komercine mCBP. 2,7-bis(9,9-dimetilakridin-10(9H)-il)dibenz[a,c]fenazino (AcDbp) emiteris neseniai buvo panaudotas gaminant labai efektyvius OLED[114] (4.4 schema).

Junginius **10** ir **11** panaudojus kaip OLED emiterius, buvo pasiekti dideli, 6 ir 7 % siekiantys, EQE (4.10 lentelė). Kadangi momentine fluorescencija paremtų OLED teorinė EQE riba yra 5 %, rezultatai patvirtina, kad junginių **10** ir **11** elektroliuminescencijoje dalyvauja ir tripletiniai eksitonai. Junginius **10** ir **11** panaudojus kaip OLED matricas, buvo pasiekti dideli EQE – atitinkamai 20,7 ir 13,7 % prietaisuose H-10 ir H-11. Prietaiso H-10 efektyvumas šiek tiek viršijo palyginamojo prietaiso H-mCBP efektyvumą, kuris siekė 20,2 % (4.10 lentelė). Skirtumus tarp prietaisų H-10 ir H-11 efektyvumo galima paaiškinti skirtingu krūvio judrumu **10** ir **11** matricose (4.12b pav.).

Prietaisų E-10 veikimo trukmė buvo apytiksliai penkiskart ilgesnė negu E-11 (4.10 lentelė). Junginius **10** ir **11** naudojant kaip matricas AcDbp emiteriui, prietaisų veikimo trukmė buvo priešinga: prietaisas H-11 pasižymėjo didesniu veikimo stabilumu lyginant su H-10 (4.10 lentelė). Apibendrinant prietaisų veikimo tyrimą galima pasakyti, kad sukurti junginiai **10** ir **11** turi didelį potencialą kaip šviesos emiteriai ir energijos perdavimo matricos, kadangi pasižymi reta tripletinių eksitonų išnaudojimo geba.

4.10 lentelė. OLED elektroliuminescenciniai parametrai

Bandymo pobūdis	Emisijos savybių tyrimas		Matricos savybių tyrimas		
Prietaiso sandara	ITO/HAT-CN/NPB/TCTA/mCBP/emisinis sluoksnis/nBPhen/LiF/Al				
Prietaiso pavadinimas	E-10	E-11	H-10	H-11	H-mCBP
Šviesos emisijos sluoksnis	**10**:mCBP	**11**:mCBP	AcDbp:**10**	AcDbp:**11**	AcDbp:mCBP
V_{ON} (V) @ 10 cd/m^2	4,3	4,4	3,0	4,5	3,85
EQE_{max}, EQE_{100}, EQE_{1000} (%)	6,0, 4,7, 4,2	7,0, 4,7, 3,9	20,7, 12,0, 7,9	13,7, 6,1, 4,7	20,2, 12,4, 5,3
EL spektro viršūnė (nm) @ 1000 cd/m^2	494	468	590	590	576
CIE (x,y) @ 1000 cd/m^2	(0,174, 0,454)	(0,149, 0,203)	(0,546, 0,449)	(0,54, 0,455)	(0,5, 0,49)
LT50,* val. @ 100 cd/m^2	3896	648	2063	6481	22336

$V_{ON.}$ – atitinkamai įsijungimo įtampa; * – prietaisų gyvavimo trukmė, apskaičiuota pagal formulę $LT(L_1) = LT(L_0) \times (L_0/L_1)^n$, darant prielaidą, kad $n = 1,75$; čia L_1 – liuminescencija esant 100 cd/m^2

4.3. IŠVADOS

1. Susintetinti ir ištirti nauji mechanochromine liuminescencija pasižymintys benzantrono ir karbazolo dariniai. Nustatyta, kad:

1.1. Susintetintiems junginiams yra būdingas išorinio mechaninio poveikio (malimo, garinimo, lydymo) sukeltas emisijos spalvos pasikeitimas iš geltonos į oranžinę.

1.2. Darinių mechanochrominę liuminescenciją iš esmės nulemia dviejų kristalinių atmainų ir amorfinių agregatų susidarymas.

1.3. Junginys, sudarytas iš benzantrono ir karbazolo fragmentų, pasižymi savaime grįžtamu mechanochromizmu ir savaiminio atsistatymo savybėmis.

1.4. Karbazolo fragmentą turintis junginys pasižymi intensyvia žalios šviesos emisija (537 nm) pradinėje būsenoje ir silpna gelsvai žalia emisija (557 nm) po mechaninio poveikio, kuri savaime atsistato atgal į intensyvią žalią emisiją (539 nm). Šie procesai yra visiškai grįžtami. Jie apima tokias pakopas: intensyvios emisijos → pažeistos silpnos emisijos → atsistatymo → atgautos intensyvios emisijos.

2. Suprojektuoti ir susintetinti keturi „donoro–akceptoriaus“ ir „donoro–akceptoriaus–donoro“ struktūros junginiai su benzantrono akceptoriumi ir fentiazino arba fenoksazino donoriniais pakaitais, kurie yra organiniai TADF deguonies zondai, pasižymintys ilgai gyvuojančia emisija. Nustatyta, kad:

2.1. Kietosios būsenos junginių fotoliuminescencijos intensyvumo maksimumas yra ties 700 nm.

2.2. Darinių kietųjų sluoksnių emisijos gyvavimo trukmė kambario temperatūroje išsidėsto 291–1198 μs ribose.

2.3. Fenoksazino darinio molekulinio mišinio su inertiniu polimeru sluoksnio emisijos intensyvumo ore ir deguonyje santykis yra 15,2.

2.4. Fenoksazino darinio sluoksnio jautrumas deguoniui, pasižymintis geru grįžtamumu, įvertintas Stern-Volmer konstanta, kurios nustatyta vertė yra $1{,}6 \times 10^{-4}$ ppm^{-1}.

3. Susintetinti nauji pirimidin-5-karbonitrilo ir skirtingo pakeitimo karbazolo dariniai, kurie panaudoti kaip TADF OLED emiteriai ir jautrūs deguonies zondai. Nustatyta, kad:

3.1. Gautieji junginiai pasižymi efektyviomis TADF savybėmis, jų atvirkštinės interkombinacinės konversijos greitis viršija 10^6 s^{-1}.

3.2. Karbazolo pakaitą turintis junginys pasižymi bipoline krūvininkų pernaša: jam būdingas $1{,}6 \times 10^{-4}$ $cm^2/V{\cdot}s$ skylių ir $1{,}37 \times 10^{-5}$ $cm^2/V{\cdot}s$ elektronų judris $7{,}2 \times 10^5$ V/cm stiprio elektriniame lauke.

3.3. Karbazolo ir *tret*-butilkarbazolo fragmentus turintiems junginiams būdingas agregacijos sukeltas emisijos sustiprėjimas: jų fotoliuminescencijos kvantinė išeiga kietoje būsenoje siekia iki 50 %.

3.4. Panaudojus karbazolo ir pirimidin-5-karbonitrilo darinį, pasižymintį geriausiu krūvio pernašos ir TADF savybių deriniu, suformuotas nelegiruotas žydros šviesos OLED, kurio išorinis kvantinis efektyvumas siekė 12,8 %.

3.5. Ištirtas junginių jautrumas deguoniui; jie gali būti naudojami kaip aktyvūs deguonies zondai, pasižymintys greitu atsaku, dideliu jautrumu ir stabilumu.

4. Sukurti du nauji „donoro–akceptoriaus–donoro“ tipo struktūros junginiai, sudaryti iš pirimidin-5-karbonitrilo akceptoriaus ir trifenilamino arba 9-fenilkarbazolo donorų ir galintys šviesos emisijai išnaudoti didesnės energijos tripletinius polygmenius. Nustatyta, kad:

4.1. Junginiai yra intensyviai spinduliuojantys emiteriai, o jų tirpalų absoliučioji fotoliuminescencijos kvantinė išeiga siekia 98 %.

4.2. Sukurtos medžiagos pasižymi bipolinėmis krūvio pernašos savybėmis, o skylių judris jose viršija 10^{-3} $cm^2/V \times s$ $3{,}6 \times 10^5$ V/cm stiprio elektriniame lauke. Tokios medžiagos gali būti efektyvios OLED emiterių matricos.

4.3. Tripletinių būsenų dalyvavimas šviesos emisijoje interkombinacinės konversijos keliu patvirtintas skirtingais metodais, įskaitant teorinius skaičiavimus ir laiko skyros elektroliuminescencinę spektroskopiją.

4.4. Grynos mėlynos spalvos fluorescencinis OLED, kurio EQE siekia 7 %, suformuotas panaudojus 9-fenilkarbazolo fragmentą turintį emiterį. Tai įrodo tripletinių eksitonų dalyvavimą elektroliuminescencijoje.

4.5. Dėl puikių krūvininkų pernašos savybių šie junginiai gali būti labai efektyvios bipolinės oranžinių–raudonų OLED matricos. Prietaiso su karbazolo fragmentą turinčiu dariniu didžiausias išorinis kvantinis efektyvumas viršijo 20 %.

5. LIST OF REFERENCES

1. ZHANG, Q., *et al*. Efficient Blue Organic Light-Emitting Diodes Employing Thermally Activated Delayed Fluorescence. *Nature Photonics* [interactive]. 2014, vol. 8(4), 326–332. Access via the Internet: <https://doi.org/10.1038/nphoton.2014.12>.

2. LEE, D. R., *et al*. Ideal Molecular Design of Blue Thermally Activated Delayed Fluorescent Emitter for High Efficiency, Small Singlet-Triplet Energy Splitting, Low Efficiency Roll-off, and Long Lifetime. *ACS Applied Materials and Interfaces* [interactive]. 2016, vol. 8(35), 23190–23196. Access via the Internet: <https://doi.org/10.1021/acsami.6b05877>.

3. KÖHLER, A. and BÄSSLER, H. *Electronic Processes in Organic Semiconductors: An Introduction;* [interactive]. 2015. Access via the Internet: <https://doi.org/10.1002/9783527685172>.

4. POPE, M. and SWENBERG, C. E. *Electronic Processes in Organic Crystals and Polymers*. 1999.

5. SAVAGE, N. Tomorrow's Industries: From OLEDs to Nanomaterials. *Nature* [interactive]. 2019, 20–22. Access via the Internet: <https://doi.org/10.1038/d41586-019-03764-1>.

6. ADACHI, C. Third-Generation Organic Electroluminescence Materials. *Japanese Journal of Applied Physics* [interactive]. 2014, 060101. Access via the Internet: <https://doi.org/10.7567/JJAP.53.060101>.

7. WEI, Q., *et al*. Small-Molecule Emitters with High Quantum Efficiency: Mechanisms, Structures, and Applications in OLED Devices. *Advanced Optical Materials* [interactive]. 2018, 1800512. Access via the Internet: <https://doi.org/10.1002/adom.201800512>.

8. XU, Z., *et al*. Recent Advances in High Performance Blue Organic Light-Emitting Diodes Based on Fluorescence Emitters. *Journal of Materials Chemistry C* [interactive]. 2020, 2614–2642. Access via the Internet: <https://doi.org/10.1039/c9tc06441a>.

9. LIU, Y., *et al*. All-Organic Thermally Activated Delayed Fluorescence Materials for Organic Light-Emitting Diodes. *Nature Reviews Materials* [interactive]. 2018, 18020. Access via the Internet: <https://doi.org/10.1038/natrevmats.2018.20>.

10. USTA, H., *et al*. Hybridized Local and Charge Transfer Excited State for Solution-Processed Non-Doped Green Electroluminescence Based on Oligo(: P -

Phenyleneethynylene). *Journal of Materials Chemistry C* [interactive]. 2020, vol. 8(24), 8047–8060. Access via the Internet: <https://doi.org/10.1039/d0tc01266a>.

11. LV, X., *et al*. Highly Efficient Non-Doped Blue Fluorescent OLEDs with Low Efficiency Roll-off Based on Hybridized Local and Charge Transfer Excited State Emitters. *Chemical Science* [interactive]. 2020, vol. 11(19), 5058–5065. Access via the Internet: <https://doi.org/10.1039/d0sc01341b>.

12. WANG, X., *et al*. An Energetics Perspective on Why There Are so Few Triplet-Triplet Annihilation Emitters. *Journal of Materials Chemistry C* [interactive]. 2020, vol. 8(31), 10816–10824. Access via the Internet: <https://doi.org/10.1039/d0tc00044b>.

13. LV, X., *et al*. High External Quantum Efficiency and Low Efficiency Roll-off Achieved Simultaneously in Nondoped Pure-Blue Organic Light-Emitting Diodes Based on a Hot-Exciton Fluorescent Material. *Chemical Engineering Journal* [interactive]. 2021, vol. 408, 127333. Access via the Internet: <https://doi.org/10.1016/j.cej.2020.127333>.

14. XU, Y., *et al*. Highly Efficient Blue Fluorescent OLEDs Based on Upper Level Triplet–Singlet Intersystem Crossing. *Advanced Materials* [interactive]. 2019, vol. 31(12), 1807388. Access via the Internet: <https://doi.org/10.1002/adma.201807388>.

15. QUARANTA, M., *et al*. Indicators for Optical Oxygen Sensors. *Bioanalytical Reviews* [interactive]. 2012, vol. 4(2–4), 115–157. Access via the Internet: <https://doi.org/10.1007/s12566-012-0032-y>.

16. KOCHMANN, S., *et al*. Sensing and Imaging of Oxygen with Parts per Billion Limits of Detection and Based on the Quenching of the Delayed Fluorescence of 13C 70 Fullerene in Polymer Hosts. *Analytical Chemistry* [interactive]. 2013, vol. 85(3), 1300–1304. Access via the Internet: <https://doi.org/10.1021/ac303486f>.

17. ZIEGER, S. E., *et al*. TADF-Emitting Zn(II)-Benzoporphyrin: An Indicator for Simultaneous Sensing of Oxygen and Temperature. *ACS Sensors* [interactive]. 2020, vol. 5(4). Access via the Internet: <https://doi.org/10.1021/acssensors.9b02512>.

18. ZHANG, H., *et al*. Crystalline Organic Pigment-Based Field-Effect Transistors. *ACS Applied Materials and Interfaces* [interactive]. 2017, vol. 9(26), 21891–21899. Access via the Internet: <https://doi.org/10.1021/acsami.7b03170>.

19. SURYA, S. G., *et al*. Organic Field Effect Transistors (OFETs) in Environmental Sensing and Health Monitoring: A Review. TrAC - Trends Anal.

Analytical Chemistry [interactive]. 2019, vol. 111, 27–36. Access via the Internet: <https://doi.org/10.1016/j.trac.2018.11.027>.

20. KLEEMANN, H., *et al*. Review of Vertical Organic Transistors. *Advanced Functional Materials* [interactive]. 2020, vol. 30(20), 1907113. Access via the Internet: <https://doi.org/10.1002/adfm.201907113>.

21. KWON, H., *et al*. Toward High-Output Organic Vertical Field Effect Transistors: Key Design Parameters. *Advanced Functional Materials* [interactive]. 2016, vol. 26(38), 6888–6895. Access via the Internet: <https://doi.org/10.1002/adfm.201601956>.

22. KIM, J. Y., *et al*. High-Efficiency Perovskite Solar Cells. *Chemical Reviews* [interactive]. 2020, vol. 120(15), 7867–7918. Access via the Internet: <https://doi.org/10.1021/acs.chemrev.0c00107>.

23. FUKUDA, K., *et al*. The Future of Flexible Organic Solar Cells. *Advanced Energy Materials* [interactive]. 2020, vol. 10(25), 2000765. Access via the Internet: <https://doi.org/10.1002/aenm.202000765>.

24. HU, Z., *et al*. A Critical Review on Semitransparent Organic Solar Cells. *Nano Energy* [interactive]. 2020, vol. 78, 105376. Access via the Internet: <https://doi.org/10.1016/j.nanoen.2020.105376>.

25. ZOU, S. J., *et al*. Recent Advances in Organic Light-Emitting Diodes: Toward Smart Lighting and Displays. *Materials Chemistry Frontiers* [interactive]. 2020, vol. 4(3), 788–820. Access via the Internet: <https://doi.org/10.1039/c9qm00716d>.

26. TANG, C. W. and VANSLYKE, S. A. Organic Electroluminescent Diodes. *Applied Physical. Letters* [interactive]. 1987, vol. 51(12), 913–915. Access via the Internet: <https://doi.org/10.1063/1.98799>.

27. WEX, B. and KAAFARANI, B. R. Perspective on Carbazole-Based Organic Compounds as Emitters and Hosts in TADF Applications. *Journal of Materials Chemistry C* [interactive]. 2017, 8622–8653. Access via the Internet: <https://doi.org/10.1039/c7tc02156a>.

28. LI, S. W., *et al*. Cyanopyrimidine-Carbazole Hybrid Host Materials for High-Efficiency and Low-Efficiency Roll-Off TADF OLEDs. *ACS Applied Materials and Interfaces* [interactive]. 2018, vol. 10(15), 12930–12936. Access via the Internet: <https://doi.org/10.1021/acsami.8b02766>.

29. UOYAMA, H., *et al*. Highly Efficient Organic Light-Emitting Diodes from Delayed Fluorescence. *Nature* [interactive]. 2012, vol. 492(7428), 234–238. Access via the Internet: <https://doi.org/10.1038/nature11687>.

30. YOON, J., *et al*. Pyrimidine-Based Bipolar Host Materials for High Efficiency Solution Processed Green Thermally Activated Delayed Fluorescence OLEDs. *Journal of Materials Chemistry C* [interactive]. 2020, vol. 8(6), 2196–2204. Access via the Internet: <https://doi.org/10.1039/c9tc05727g>.

31 SEREVIČIUS, T., *et al*. Optimization of the Carbazole-Pyrimidine Linking Pattern for Achieving Efficient TADF. *Journal of Materials Chemistry C* [interactive]. 2020, vol. 8(32), 11192–11200. Access via the Internet: <https://doi.org/10.1039/d0tc02194f>.

32. TAO, Y., *et al*. Multifunctional Bipolar Triphenylamine/Oxadiazole Derivatives: Highly Efficient Blue Fluorescence, Red Phosphorescence Host and Two-Color Based White OLEDs. *Chemical Communications* [interactive]. 2009, vol. 1, 77–79. Access via the Internet: <https://doi.org/10.1039/b816264f>.

33. SHEN, Y., *et al*. Effects of Electron Donor on Luminescence and Mechanochromism of D-π-A Benzothiazole Derivatives. *Dyes and Pigments* [interactive]. 2018, vol. 150, 354–362. Access via the Internet: <https://doi.org/10.1016/j.dyepig.2017.12.034>.

34. CHATTERJEE, T., *et al*. Carbazole-Bridged Triphenylamine-Bipyridine Bipolar Hosts for High-Efficiency Low Roll-off Multi-Color PhOLEDs. *Organic Electronics* [interactive]. 2017, vol. 50, 204–212. Access via the Internet: <https://doi.org/10.1016/j.orgel.2017.07.036>.

35. WARD, J. S., *et al*. The Interplay of Thermally Activated Delayed Fluorescence (TADF) and Room Temperature Organic Phosphorescence in Sterically-Constrained Donor-Acceptor Charge-Transfer Molecules. *Chemical Communication* [interactive]. 2016, vol. 52(12), 2612–2615. Access via the Internet: <https://doi.org/10.1039/c5cc09645f>.

36. PAN, Y., *et al*. Multiple "Hot Exciton" Channel Molecular Design in Organic Electroluminescence Materials: A Theoretical Investigation. *Materials Advances* [interactive]. 2021, vol. 2(4), 1351–1357. Access via the Internet: <https://doi.org/10.1039/d0ma00927j>.

37. YANG, W., *et al*. AIE-Active Multicolor Tunable Luminogens: Simultaneous Mechanochromism and Acidochromism with High Contrast beyond 100 Nm. *Materials Chemistry Frontiers* [interactive]. 2020. Access via the Internet: <https://doi.org/10.1039/d0qm00247j>.

38. YE, S. H., *et al*. Pyridine Linked Fluorene Hybrid Bipolar Host for Blue, Green, and Orange Phosphorescent Organic Light-Emitting Diodes toward Solution Processing. *Journal of Materials Chemistry C* [interactive]. 2017, vol. 5(45), 11937–11946. Access via the Internet: <https://doi.org/10.1039/c7tc04339b>.

39. LEE, D. R., *et al*. Above 30% External Quantum Efficiency in Green Delayed Fluorescent Organic Light-Emitting Diodes. *ACS Applied Materials and Interfaces* [interactive]. 2015, vol. 7(18), 9625–9629. Access via the Internet: <https://doi.org/10.1021/acsami.5b01220>.

40. JANG, J. S., *et al*. Electrostatic Potential Dispersing Pyrimidine-5-Carbonitrile Acceptor for High Efficiency and Long Lifetime Thermally Activated Delayed Fluorescence Organic Light-Emitting Diodes. *Journal of Materials Chemistry C* [interactive]. 2019, vol. 7(40), 12695–12703. Access via the Internet: <https://doi.org/10.1039/c9tc04304g>.

41. KAJI, H., *et al*. Purely Organic Electroluminescent Material Realizing 100% Conversion from Electricity to Light. *Nature Communication* [interactive]. 2015, vol. 6(1), 1–8. Access via the Internet: <https://doi.org/10.1038/ncomms9476>.

42. BAO, L., *et al*. New Carbazole-Based Bipolar Hosts for Efficient Green Phosphorescent Organic Light-Emitting Diodes. *Organic Electronics* [interactive]. 2020, vol. 83, 105672. Access via the Internet: <https://doi.org/10.1016/j.orgel.2020.105672>.

43. LEE, S. Y., *et al*. Luminous Butterflies: Efficient Exciton Harvesting by Benzophenone Derivatives for Full-Color Delayed Fluorescence OLEDs. *Angewandte Chemie - Intarnational Edition* [interactive]. 2014, vol. 53(25), 6402–6406. Access via the Internet: <https://doi.org/10.1002/anie.201402992>.

44. LI, W., *et al*. High-Performance near-Infrared (NIR) Polymer Light-Emitting Diodes (PLEDs) Based on Bipolar Ir(III)-Complex-Grafted Polymers. *Journal of Materials Chemistry C* [interactive]. 2021, vol. 9(1), 173–180. Access via the Internet: <https://doi.org/10.1039/d0tc04377j>.

45. CARLINI, F. M., *et al*. New Daylight Fluorescent Pigments. *Dyes and Pigments* [interactive]. 1982, vol. 3(1), 59–69. Access via the Internet: <https://doi.org/10.1016/0143-7208(82)80013-2>.

46. GONTA, S., *et al*. Fluorescent Substituted Amidines of Benzanthrone: Synthesis, Spectroscopy and Quantum Chemical Calculations. *Spectrochimica Acta - Part A: Molecular and Biomolecular Spectroscopy* [interactive]. 2013, vol. 101, 325–334. Access via the Internet: <https://doi.org/10.1016/j.saa.2012.09.104>.

47. JANG, J. S., *et al*. Pyrimidine-5-Carbonitrile Acceptor Combined with Anortho-Linked Donor for Long Lifetime through Facilitated Reverse Intersystem Crossing in Thermally Activated Delayed Fluorescence Emitters. *Journal of Materials Chemistry C* [interactive]. 2021, vol. 9(7), 2408–2415. Access via the Internet: <https://doi.org/10.1039/d0tc04564k>.

48. NASSER, A. A., *et al*. Discovery of New Pyrimidine-5-Carbonitrile Derivatives as Anticancer Agents Targeting EGFRWTand EGFRT790M. *Organic and Biomolecular Chemistry* [interactive]. 2020, vol. 18(38), 7608–7634. Access via the Internet: <https://doi.org/10.1039/d0ob01557a>.

49. AKHTAR, W., *et al*. Synthesis, COX-2 Inhibition and Metabolic Stability Studies of 6-(4-Fluorophenyl)-Pyrimidine-5-Carbonitrile Derivatives as Anticancer and Anti-Inflammatory Agents. *Journal of Fluorine Chemistry* [interactive]. 2020, vol. 236, 109579. Access via the Internet: <https://doi.org/10.1016/j.jfluchem.2020.109579>.

50. DATA, P., *et al*. Thermally Activated Delayed Fluorescence: Vs. Room Temperature Phosphorescence by Conformation Control of Organic Single Molecules. *Journal of Materials Chemistry C* [interactive]. 2019, vol. 7(22), 6616–6621. Access via the Internet: <https://doi.org/10.1039/c9tc00909d>.

51. WU, H., *et al*. Multidimensional Structure Conformation of Persulfurated Benzene for Highly Efficient Phosphorescence. *ACS Applied Materials and Interfaces* [interactive]. 2021, vol. 13(1), 1314–1322. Access via the Internet: <https://doi.org/10.1021/acsami.0c16338>.

52. QIAO, X. and MA, D. Nonlinear Optoelectronic Processes in Organic Optoelectronic Devices: Triplet-Triplet Annihilation and Singlet Fission. *Materials Science and Engineering R: Reports* [interactive]. 2020, vol. 139, 100519. Access via the Internet: <https://doi.org/10.1016/j.mser.2019.100519>.

53. LIU, W., *et al*. Nondoped Blue Fluorescent Organic Light-Emitting Diodes Based on Benzonitrile-Anthracene Derivative with 10.06% External Quantum Efficiency and Low Efficiency Roll-Off. *Journal of Materials Chemistry C* [interactive]. 2019, vol. 7(4), 1014–1021. Access via the Internet: <https://doi.org/10.1039/c8tc05707a>.

54. HOSOKAI, T., *et al*. Evidence and Mechanism of Efficient Thermally Activated Delayed Fluorescence Promoted by Delocalized Excited States. *Science Advances* [interactive]. 2017, vol. 3(5), e160328. Access via the Internet: <https://doi.org/10.1126/sciadv.1603282>.

55. YAO, L., *et al*. Progress in Next-Generation Organic Electroluminescent Materials: Material Design beyond Exciton Statistics. *Science China Chemistry* [interactive]. 2014, vol. 57(3), 335–345. Access via the Internet: <https://doi.org/10.1007/s11426-013-5046-y>.

56. TSUTSUI, T. Progress in Electroluminescent Devices Using Molecular Thin Films. *MRS Bulletin* [interactive]. 1997, vol. 22(6), 39–45. Access via the Internet: <https://doi.org/10.1557/S0883769400033613>.

57. BARMAN, D., *et al*. Recent Developments on Multi-Functional Metal-Free Mechanochromic Luminescence and Thermally Activated Delayed Fluorescence Organic Materials. *Frontiers in Chemistry* [interactive]. 2020, vol. 8, 483. Access via the Internet: <https://doi.org/10.3389/fchem.2020.00483>.

58. BRAVEENTH, R., *et al*. Achieving Narrow FWHM and High EQE Over 38% in Blue OLEDs Using Rigid Heteroatom-Based Deep Blue TADF Sensitized Host. Advanced Functional Materials [interactive]. 2021, vol. 31(47), 2105805. Access via the Internet: <https://doi.org/10.1002/adfm.202105805>.

59. WU, T. L., *et al*. Diboron Compound-Based Organic Light-Emitting Diodes with High Efficiency and Reduced Efficiency Roll-Off. *Nature Photonics* [interactive]. 2018, vol. 12(4), 235–240. Access via the Internet: <https://doi.org/10.1038/s41566-018-0112-9>.

60. WONG, M. Y. and ZYSMAN-COLMAN, E. Purely Organic Thermally Activated Delayed Fluorescence Materials for Organic Light-Emitting Diodes. *Advanced Materials* [interactive]. 2017. Access via the Internet: <https://doi.org/10.1002/adma.201605444>.

61. DIAS, F. B., *et al*. Photophysics of Thermally Activated Delayed Fluorescence Molecules. *Methods and Applications in Fluorescence* [interactive]. 2017. Access via the Internet: <https://doi.org/10.1088/2050-6120/aa537e>.

62. LIN, T. A., *et al*. Sky-Blue Organic Light Emitting Diode with 37% External Quantum Efficiency Using Thermally Activated Delayed Fluorescence from Spiroacridine-Triazine Hybrid. *Advanced Materials* [interactive]. 2016, vol. 28(32), 6976–6983. Access via the Internet: <https://doi.org/10.1002/adma.201601675>.

63. GODUMALA, M., *et al*. Recent Breakthroughs in Thermally Activated Delayed Fluorescence Organic Light Emitting Diodes Containing Non-Doped Emitting Layers. *Journal of Materials Chemistry C* [interactive]. 2019, vol. 7(8), 2172–2198. Access via the Internet: <https://doi.org/10.1039/c8tc06293e>.

64. LI, W., *et al*. Tri-Spiral Donor for High Efficiency and Versatile Blue Thermally Activated Delayed Fluorescence Materials. *Angewandte Chemie - Intarnational Edition* [interactive]. 2019, vol. 58(33), 11301–11305. Access via the Internet: <https://doi.org/10.1002/anie.201904272>.

65. XU, Z., *et al*. Recent Advances in High Performance Blue Organic Light-Emitting Diodes Based on Fluorescence Emitters. *Journal of Materials Chemistry C* [interactive]. 2020, vol. 8(8), 2614–2642. Access via the Internet: <https://doi.org/10.1039/c9tc06441a>.

66. STEINEGGER, A., *et al*. Purely Organic Dyes with Thermally Activated Delayed Fluorescence—A Versatile Class of Indicators for Optical Temperature Sensing. *Advanced Optical Materials* [interactive]. 2017, vol. 5(18). Access via the Internet: <https://doi.org/10.1002/adom.201700372>.

67. PAISLEY, N. R., *et al*. Stimuli-Responsive Thermally Activated Delayed Fluorescence in Polymer Nanoparticles and Thin Films: Applications in Chemical Sensing and Imaging. *Frontiers in Chemistry* [interactive]. 2020. Access via the Internet: <https://doi.org/10.3389/fchem.2020.00229>.

68. NI, F., *et al*. Organic Thermally Activated Delayed Fluorescence Materials for Time-Resolved Luminescence Imaging and Sensing. *Advanced Optical Materials* [interactive]. 2020, vol. 8(14), 1902187. Access via the Internet: <https://doi.org/10.1002/adom.201902187>.

69. NGUYEN, V. N., *et al*. Recent Advances in Biomedical Applications of Organic Fluorescence Materials with Reduced Singlet–Triplet Energy Gaps. Coord. *Chemical Reviews* [interactive]. 2020, vol. 425, 213545. Access via the Internet: <https://doi.org/10.1016/j.ccr.2020.213545>.

70. STEINEGGER, A. and BORISOV, S. M. Zn(II) Schiff Bases: Bright TADF Emitters for Self-Referenced Decay Time-Based Optical Temperature Sensing. *ACS Omega* [interactive]. 2020, vol. 5(13), 7729–7737. Access via the Internet: <https://doi.org/10.1021/acsomega.0c01062>.

71. TUONG LY, K., *et al*. Near-Infrared Organic Light-Emitting Diodes with Very High External Quantum Efficiency and Radiance. *Nature Photonics* [interactive]. 2017, vol. 11(1), 63–68. Access via the Internet: <https://doi.org/10.1038/nphoton.2016.230>.

72. LENG, C., *et al*. Unraveling the Mechanism of Near-Infrared Thermally Activated Delayed Fluorescence of TPA-Based Molecules: Effect of Hydrogen Bond Steric Hindrance. *Journal of Physical Chemistry A* [interactive]. 2021, vol. 125(14), 2905–2912. Access via the Internet: <https://doi.org/10.1021/acs.jpca.1c00739>.

73. SHAFIKOV, M. Z., *et al*. Extended Ligand Conjugation and Dinuclearity as a Route to Efficient Platinum-Based near-Infrared (NIR) Triplet Emitters and Solution-Processed NIR-OLEDs. *Journal of Materials Chemistry C* [interactive]. 2021, vol. 9(1), 127–135. Access via the Internet: <https://doi.org/10.1039/d0tc04881j>.

74. SHI, L., *et al*. Transmission in Near-Infrared Optical Windows for Deep Brain Imaging. *Journal of Biophotonics* [interactive]. 2016, vol. 9(1–2), 38–43. Access via the Internet: <https://doi.org/10.1002/jbio.201500192>.

75. KIM, J., *et al*. Rapid and Background-Free Detection of Avian Influenza Virus in Opaque Sample Using NIR-to-NIR Upconversion Nanoparticle-Based Lateral Flow Immunoassay Platform. *Biosensors and Bioelectronics* [interactive]. 2018, vol. 112, 209–215. Access via the Internet: <https://doi.org/10.1016/j.bios.2018.04.047>.

76. MINOTTO, A., *et al*. Visible Light Communication with Efficient Far-Red/near-Infrared Polymer Light-Emitting Diodes. *Light: Science and Applications* [interactive]. 2020, vol. 9(1), 2047–7538. Access via the Internet: <https://doi.org/10.1038/s41377-020-0314-z>.

77. XIE, Y. and LI, Z. The Development of Mechanoluminescence from Organic Compounds: Breakthrough and Deep Insight. *Materials Chemistry Frontiers* [interactive]. 2020, vol. 4(2), 317–331. Access via the Internet: <https://doi.org/10.1039/c9qm00580c>.

78. HUANG, G., *et al*. Multiple Anti-Counterfeiting Guarantees from a Simple Tetraphenylethylene Derivative – High-Contrasted and Multi-State Mechanochromism and Photochromism. *Angewandte Chemie - Intarnational Edition* [interactive]. 2019, 17814–17819. Access via the Internet: <https://doi.org/10.1002/anie.201910530>.

79. WANG, Y., *et al*. Dynamic Behavior of Molecular Switches in Crystal under Pressure and Its Reflection on Tactile Sensing. *Journal of American Chemical Society* [interactive]. 2015, vol. 137(2), 931–939. Access via the Internet: <https://doi.org/10.1021/ja511499p>.

80. HU, J., *et al*. Strategy for Optical Data Encryption and Decryption Using a D-A Type Stimuli-Responsive AIE Material. *Spectrochimica Acta - Part A: Molecular and Biomolecular Spectroscopy* [interactive]. 2020, vol. 239. Access via the Internet: <https://doi.org/10.1016/j.saa.2020.118486>.

81. PARK, S. K., *et al*. Stimuli-Responsive Reversible Fluorescence Switching in a Crystalline Donor-Acceptor Mixture Film: Mixed Stack Charge-Transfer Emission versus Segregated Stack Monomer Emission. *Angewandte Chemie - Intarnational Edition* [interactive]. 2016, vol. 55(1), 203–207. Access via the Internet: <https://doi.org/10.1002/anie.201508210>.

82. YU, H. X., *et al*. Donor-Acceptor Type Aggregation-Induced Emission Luminophores Based on the 1,1-Dicyanomethylene-3-Indanone Unit for Bridge-Dependent Reversible Mechanochromism and Light-up Biosensing of Hypochlorites. *Journal of Materials Chemistry C* [interactive]. 2019, vol. 7(29), 8888–8897. Access via the Internet: <https://doi.org/10.1039/c9tc01772k>.

83. YANG, W., *et al*. AIE-Active Smart Cyanostyrene Luminogens: Polymorphism-Dependent Multicolor Mechanochromism. *Journal of Materials Chemistry C* [interactive]. 2018, vol. 6(2), 290–298. Access via the Internet: <https://doi.org/10.1039/c7tc04773h>.

84. LEI, Y., *et al*. Polymorphism and Mechanochromism of N -Alkylated 1,4-Dihydropyridine Derivatives Containing Different Electron-Withdrawing End Groups. *Journal of Materials Chemistry C* [interactive]. 2017, vol. 5(21), 5183–5192. Access via the Internet: <https://doi.org/10.1039/c7tc00362e>.

85. XIONG, Y., *et al*. High-Contrast Luminescence Dependent on Polymorphism and Mechanochromism of AIE-Active (4-(Phenothiazin-10-Yl)Phenyl)(Pyren-1-Yl)Methanone. *Journal of Materials Chemistry C* [interactive]. 2020, vol. 8(7), 2460–2466. Access via the Internet: <https://doi.org/10.1039/c9tc05064g>.

86. XU, P., *et al*. Halogenated Tetraphenylethene with Enhanced Aggregation-Induced Emission: An Anomalous Anti-Heavy-Atom Effect and Self-Reversible Mechanochromism. *Chemical Communication* [interactive]. 2019, vol. 55(99), 14938–14941. Access via the Internet: <https://doi.org/10.1039/c9cc07045a>.

87. HARIHARAN, P. S., *et al*. Self-Reversible Mechanochromism and Thermochromism of a Triphenylamine-Based Molecule: Tunable Fluorescence and Nanofabrication Studies. *Journal of Physical Chemistry C* [interactive]. 2015, vol. 119(17), 9460–9469. Access via the Internet: <https://doi.org/10.1021/acs.jpcc.5b00310>.

88. WU, H., *et al*. Molecular Stacking Dependent Phosphorescence-Fluorescence Dual Emission in a Single Luminophore for Self-Recoverable Mechanoconversion of Multicolor Luminescence. *Chemical Communication*. [interactive]. 2017, vol. 53(18), 2661–2664. Access via the Internet: <https://doi.org/10.1039/c6cc04901j>.

89. TSIKO, U., *et al*. Self-Recovering Mechanochromic Luminescence of the Derivatives of Benzanthrone and Carbazole: Towards Damage-Resistive Information Recording and Security Probes. *Dyes and Pigments* [interactive]. 2022, vol. 199, 110082. Access via the Internet: <https://doi.org/10.1016/j.dyepig.2022.110082>.

90. TSIKO, U., *et al*. TADF Quenching Properties of Phenothiazine or Phenoxazine-Substituted Benzanthrones Emitting in Deep-Red/near-Infrared Region towards Oxygen Sensing. *Dyes and Pigments* [interactive]. 2022, vol. 197, 109952. Access via the Internet: <https://doi.org/10.1016/j.dyepig.2021.109952>.

91. TSIKO, U., *et al*. Multifunctional Derivatives of Pyrimidine-5-Carbonitrile and Differently Substituted Carbazoles for Doping-Free Sky-Blue OLEDs and Luminescent Sensors of Oxygen. *Journal of Advanced Research* [interactive]. 2021, vol. 33, 41–51. Access via the Internet: <https://doi.org/10.1016/j.jare.2021.01.014>.

92. TSIKO, U., *et al*. Triphenylamino or 9-Phenyl Carbazolyl-Substituted Pyrimidine-5-Carbonitriles as Bipolar Emitters and Hosts with Triplet Harvesting Abilities. *Materials Today Chemistry* [interactive]. 2022, vol. 25, 100955. Access via the Internet: <https://doi.org/10.1016/j.mtchem.2022.100955>.

93. GALER, P., *et al*. Crystal Structures and Emission Properties of the BF2 Complex 1-Phenyl-3-(3,5-Dimethoxyphenyl)-Propane-1,3-Dione: Multiple Chromisms, Aggregation- or Crystallization-Induced Emission, and the Self-Assembly Effect. *Journal of American Chemistry Society* [interactive]. 2014, vol. 136(20), 7383–7394. Access via the Internet: <https://doi.org/10.1021/ja501977a>.

94. SIRAJ, N., *et al*. Enhanced S2 Emission in Carbazole-Based Ionic Liquids. *RSC Advances* [interactive]. 2015, vol. 5(13), 9939–9945. Access via the Internet: <https://doi.org/10.1039/c4ra12362j>.

95. KERUCKIENE, R., *et al*. Dual Emission Fluorescence/Room-Temperature Phosphorescence of Phenothiazine and Benzotrifluoride Derivatives and Its Application for Optical Sensing of Oxygen. *Sensors and Actuators, B Chemistry* [interactive]. 2020, 321. Access via the Internet: <https://doi.org/10.1016/j.snb.2020.128533>.

96. YAMAZAKI, M. Industrialization and Application Development of Cyclo-Olefin Polymer. *Journal of Molecular Catalysis A: Chemical* [interactive]. 2004, vol. 213(1), 81–87. Access via the Internet: <https://doi.org/10.1016/J.MOLCATA.2003.10.058>.

97. TONGE, C. M., *et al*. Color-Tunable Thermally Activated Delayed Fluorescence in Oxadiazole-Based Acrylic Copolymers: Photophysical Properties and Applications in Ratiometric Oxygen Sensing. *ACS Applied Materials and Interfaces* [interactive]. 2020, vol. 12(5). Access via the Internet: <https://doi.org/10.1021/acsami.9b22464>.

98. BREDAS, J. L. Mind the Gap! *Materials Horizons* [interactive]. 2014, vol. 1(1), 17–19. Access via the Internet: <https://doi.org/10.1039/c3mh00098b>.

99. KABE, R. and ADACHI, C. Organic Long Persistent Luminescence. *Nature* [interactive]. 2017, vol. 550(7676). Access via the Internet: <https://doi.org/10.1038/nature24010>.

100. NARAYANASWAMY, R. and WOLFBEIS, O. S. *Optical Sensors: Industrial Environmental and Diagnostic Applications*; 2004; Vol.1. Access via the Internet: <https://doi.org/10.1007/978-3-662-09111-1>.

101. SANTOS, P. L., *et al*. Engineering the Singlet-Triplet Energy Splitting in a TADF Molecule. *Journal of Materials Chemistry C* [interactive]. 2016, vol. 4(17), 3815–3824. Access via the Internet: <https://doi.org/10.1039/c5tc03849a>.

102. YOSHIHARA, T., *et al*. Ratiometric Molecular Sensor for Monitoring Oxygen Levels in Living Cells. *Angewandte Chemie - Intarnational Edition* [interactive]. 2012, vol. 51(17), 4148–4151. Access via the Internet: <https://doi.org/10.1002/anie.201107557>.

103. ZACH, P. W., *et al*. Electron-Deficient Near-Infrared Pt(II) and Pd(II) Benzoporphyrins with Dual Phosphorescence and Unusually Efficient Thermally Activated Delayed Fluorescence: First Demonstration of Simultaneous Oxygen and Temperature Sensing with a Single Emitter. *ACS Applied Materials and Interfaces* [interactive]. 2017, vol. 9(43), 38008–38023. Access via the Internet: <https://doi.org/10.1021/acsami.7b10669>.

104. CHULKIN, P., *et al*. Impedance Spectroscopy of OLEDs as a Tool for Estimating Mobility and the Concentration of Charge Carriers in Transport Layers. *Journal of Materials Chemistry C* [interactive]. 2018, vol. 6(5), 1008–1014. Access via the Internet: <https://doi.org/10.1039/c7tc04599a>.

105. BAGNICH, S. A., *et al*. Excimer Formation by Steric Twisting in Carbazole and Triphenylamine-Based Host Materials. *Journal of Physical Chemistry C* [interactive]. 2015, vol. 119(5), 2380–2387. Access via the Internet: <https://doi.org/10.1021/jp512772j>.

106. MATAGA, N., *et al*. Solvent Effects upon Fluorescence Spectra and the Dipolemoments of Excited Molecules. *Bulletin of the Chemical Society of Japan* [interactive]. 1956, vol. 29(4), 465–470. Access via the Internet: <https://doi.org/10.1246/bcsj.29.465>.

107. SUMALEKSHMY, S. and GOPIDAS, K. R. Photoinduced Intramolecular Charge Transfer in Donor-Acceptor Substituted Tetrahydropyrenes. *Journal of Physical Chemistry B* [interactive]. 2004, vol. 108(12), 3705–3712. Access via the Internet: <https://doi.org/10.1021/jp022549l>.

108. LIPPERT, E. Dipolmoment Und Elektronenstruktur von Angeregten Molekülen. *Zeitschrift für Naturforschung A.* [interactive]. 1955, vol. 10(7), 541–545. Access via the Internet: <https://doi.org/10.1515/zna-1955-0707>.

109. ONSAGBR, L. Electric Moments of Molecules in Liquids. *Journal of American Chemistry Society* [interactive]. 1936, vol. 58(8), 1486–1493. Access via the Internet: <https://doi.org/10.1021/ja01299a050>.

110. MINAEV, B. F. Ab Initio Study of the Ground State Properties of Molecular Oxygen. *Spectrochimica Acta - Part A: Molecular and Biomolecular Spectroscopy* [interactive]. 2004, vol. 60(5), 1027–1041. Access via the Internet: <https://doi.org/10.1016/S1386-1425(03)00334-2>.

111. BREGNHØJ, M., *et al*. Singlet Oxygen Photophysics in Liquid Solvents: Converging on a Unified Picture. *Accounts of Chemical Research* [interactive]. 2017, vol. 50(8), 1920–1927. Access via the Internet: <https://doi.org/10.1021/acs.accounts.7b00169>.

112. ZHOU, C., *et al*. Modulation of Excited State Property Based on Benzo[a, c]Phenazine Acceptor: Three Typical Excited States and Electroluminescence Performance. *Frontiers in Chemistry* [interactive]. 2019, vol. 7, 141. Access via the Internet: <https://doi.org/10.3389/fchem.2019.00141>.

113. XU, Y., *et al*. Recent Progress in Hot Exciton Materials for Organic Light-Emitting Diodes. *Chemical Society Reviews* [interactive]. 2021, vol. 50(2), 1030–1069. Access via the Internet: <https://doi.org/10.1039/d0cs00391c>.

114. ANDRULEVICIENE, V., *et al*. TADF versus TTA Emission Mechanisms in Acridan and Carbazole-Substituted Dibenzo[a,c]Phenazines: Towards Triplet Harvesting Emitters and Hosts. *Chemical Engineering Journal* [interactive]. 2021, vol. 417, 127902. Access via the Internet: <https://doi.org/10.1016/j.cej.2020.127902>.

115. GRÜNE, J., *et al*. Kinetic Modeling of Transient Electroluminescence Reveals TTA as an Efficiency-Limiting Process in Exciplex-Based TADF OLEDs. *Journal of Physical Chemistry C* [interactive]. 2020, vol. 124(47), 25667–25674. Access via the Internet: <https://doi.org/10.1021/ACS.JPCC.0C06528>.

116. CUI, L. S., *et al*. Fast Spin-Flip Enables Efficient and Stable Organic Electroluminescence from Charge-Transfer States. *Nature Photonics* [interactive]. 2020, vol. 14(10), 636–642. Access via the Internet:< https://doi.org/10.1038/s41566-020-0668-z>.

117. ZHU, Z. Q., *et al*. Efficient Cyclometalated Platinum(II) Complex with Superior Operational Stability. *Advanced Matererials* [interactive]. 2017, vol. 29(6), 1605002. Access via the Internet: <https://doi.org/10.1002/adma.201605002>.

118. Fry, C., *et al*. Physical Mechanism Responsible for the Stretched Exponential Decay Behavior of Aging Organic Light-Emitting Diodes. *Applied*

Physics Letters [interactive]. 2005, vol. 87(21), 1–3. Access via the Internet: <https://doi.org/10.1063/1.2133922>.

6. CURRICULUM VITAE

Name: Uliana

Surname: Tsiko

Date of the birth: 03 May 1995

Email: ulyana.ziko@gmail.com

Education:

2018 – 2022	**PhD studies in Chemical Engineering** Kaunas University of technology, Lithuania
2016 – 2018	**Chemistry, Master's degree** Ivan Franko National University of Lviv, Ukraine
2012 – 2016	**Chemistry, Bachelor's degree** Ivan Franko National University of Lviv, Ukraine

Work experience:

14 May 2020 – 20 December 2021	**Project junior researcher** Project *Vertical organic light-emitting transistors based on thermally-activated-delayed-fluorescence emitters* (Smartlight) No. 01.2.2-LMT-K-718-01-0015. It was funded by the European Regional Development Fund. Department of Polymer Chemistry and Technology, Kaunas University of Technology, Lithuania.

Internships:

20 December 2020 – 10 January 2021	Department of Electronic Devices, Lviv Polytechnic National University, Ukraine. Project *Development of highly efficient white light-emitting diodes utilizing organic emitters exciplex and thermally-assisted fluorescence for lighting application*, No. P-LU-20-42 funded by intergovernmental programme administrated by the Research Council of Lithuania: Lithuania–Ukraine.

Secondments:

01 June 2021 – 27 November 2021	CreaPhys, Dresden, Germany. The international project Horizon 2020 *Heavy metal free emitters for new-generation light sources* (MEGA). This research project was funded by H2020-MSCA-RISE-2018 Marie Sklodowska-Curie.

7. LIST OF ARTICLES AND PRESENTATIONS AT SCIENTIFIC CONFERENCES

List of publications on the subject of the thesis:

1. Tsiko Uliana; Sych Galyna; Volyniuk Dmytro; Bezvikonnyi Oleksandr; Keruckiene Rasa; Lazauskas Algirdas; Grazulevicius Juozas Vidas. Self-recovering mechanochromic luminescence of the derivatives of benzanthrone and carbazole: towards damage-resistive information recording and security probes // Dyes and Pigments. 2022, vol. 199, art. No. 110082, p. 1–8.
2. Tsiko Uliana; Bezvikonnyi Oleksandr; Volyniuk Dmytro; Minaev Boris F.; Keruckas Jonas; Cekaviciute Monika; Jatautiene Egle; Andruleviciene Viktorija; Dabuliene Asta; Grazulevicius Juozas Vidas. TADF quenching properties of phenothiazine or phenoxazine-substituted benzanthrones emitting in deep-red/near-infrared region towards oxygen sensing // Dyes and Pigments. 2022, vol. 197, art. No. 109952, p. 1–9.
3. Tsiko Uliana; Bezvikonnyi Oleksandr; Sych Galyna; Keruckiene Rasa; Volyniuk Dmytro; Simokaitiene Jurate; Danyliv Iryna; Danyliv Yan; Bucinskas Audrius; Tan Xiaofeng; Grazulevicius Jouzas Vidas. Multifunctional derivatives of pyrimidine-5-carbonitrile and differently substituted carbazoles for doping-free sky-blue OLEDs and luminescent sensors of oxygen // Journal of Advanced Research. 2021, vol. 33, p. 41–51.
4. Tsiko Uliana; Volyniuk Dmytro; Andruleviciene Viktorija; Leitonas Karolis; Sych Galyna; Bezvikonnyi Oleksandr; Jasinskas Vidmantas; Gulbinas Vidmantas; Stakhira Pavlo; Grazulevicius Juozas Vidas. Triphenylamino or 9-phenyl carbazolyl substituted pyrimidine-5-carbonitriles as bipolar emitters and hosts with triplet harvesting abilities // Materials Today Chemistry, 2022, vol. 25, art. No. 100955, p. 1–13.

List of presentations delivered at conferences:

1. Tsiko, Uliana; Bezvikonnyi, Oleksandr; Volyniuk, Dmytro; Andruleviciene, Viktorija; Dabuliene, Asta; Grazulevicius, Juozas Vidas. TADF properties of derivatives of phenothiazine or phenoxazinesubstituted benzanthrones emitting in deep-red/near-infrared region // 10th international conference on molecular electronics, November 29 – December 2, 2021, ENS de Lyon, France: book of abstracts. 2021, p.126.
2. Tsiko, Uliana; Pakštys, Saimonas; Volyniuk, Dmytro; Keruckas, Jonas; Bernard, Ronit Sebastine; Andrulevičienė, Viktorija; Grazulevicius, Juozas Vidas. New organic materials exhibiting thermally activated delayed fluorescence and their application in organic light-emitting diodes // 15th international scientific conference "The vital nature sign", May 20-21, 2021, Kaunas, Lithuania: abstract book. 2021, p. 86.
3. Tsiko, Uliana; Sych, Galyna; Danyliv, Yan; Hladka, Iryna; Grazulevicius, Juozas Vidas. Triphenylamine- and carbazole-based compounds exhibiting delayed

fluorescence // Open readings 2020: 63rd international conference for students of physics and natural sciences, March 17-20, Vilnius, Lithuania: abstract book. 2020, p. 248.

4. Tsiko, Ulians; Sych, Galyna; Bezvikonnyi, Oleksander; Simokaitiene, Jurate; Volynuik, Dmytro; Grazulevicius, Juozas Vidas; Non-doped organic light-emitting diodes based on compounds exhibiting aggregation induced emission enhancment. Poster presentation // Baltic polymer symposium 2019, Vilnius, Lithuania, September 18-20, 2019: programme and proceedings. 2019, p. 62.

5. Tsiko, Uliana; Sych, Galyna; Danyliv, Yan; Hladka, Iryna; Grazulevicius, Juozas V. New multifunctional pyrimidine-based compounds exhibiting delayed fluorescence and aggregation induced emission enhancement // 24th international Krutyń summer school 2019, 01-07 September 2019, Krutyń, Poland: abstract book. 2019, p. 70.

8. ACKNOWLEDGEMENTS

Professor Habil. Dr. Juozas Vidas Grazulevicius (Department of Polymer Chemistry and Technology, KTU) is thanked for the great opportunity to be part of his team, supervision, valuable advice and outstanding support during my study.

Dr. Dmytro Volyniuk (Department of Polymer Chemistry and Technology) is thanked for scientific advice and valuable discussions, measurement of the charge-transporting properties of the materials I was researching, for the friendship and co-operation.

Dr. Galyna Sych (Université Grenoble Alpes, CNRS, France) is kindly thanked for her support in the development and synthesis of the materials I was researching, for the friendship, and moral support.

Dr. Oleksandr Bezvikonnyi (Department of Polymer Chemistry and Technology, KTU) is thanked for the fabrication of OLEDs and the contribution to the photophysical measurements.

Dr. Viktorija Andrulevičienė (Department of Polymer Chemistry and Technology, KTU) is thanked for helping with the theoretical calculations which played an important role in my investigations.

Dr. Jūratė Simokaitienė (Department of Polymer Chemistry and Technology, KTU) is thanked for the measurement of the thermal properties of the compounds I was investigating and for the support regarding the organisation of my study.

All the colleagues of the research group are sincerely thanked for their help and friendly working atmosphere.

Finally, I am thankful to my family and my best friend for incredible moral support.

9. COPIES OF PUBLICATIONS

Dyes and Pigments 199 (2022) 110082

Contents lists available at ScienceDirect

Dyes and Pigments

journal homepage: www.elsevier.com/locate/dyepig

Self-recovering mechanochromic luminescence of the derivatives of benzanthrone and carbazole: Towards damage-resistive information recording and security probes

Uliana Tsiko [a], Galyna Sych [a,b], Dmytro Volyniuk [a], Oleksandr Bezvikonnyi [a], Rasa Keruckiene [a], Algirdas Lazauskas [c], Juozas Vidas Grazulevicius [a,*]

[a] Department of Polymer Chemistry and Technology, Kaunas University of Technology, K. Barsausko 59, LT, 51423, Kaunas, Lithuania
[b] Univ. Grenoble Alpes, Univ. Savoie Mont Blanc, CNRS, Grenoble INP, LEPMI, 30000, Grenoble, France
[c] Institute of Materials Science, Kaunas University of Technology, K. Barsausko 59, LT, 51423, Kaunas, Lithuania

ARTICLE INFO

Keywords:
Self-recovering
Self-reversible mechanochromism
Benzanthrone
Carbazole
Information encryption
Security check

ABSTRACT

Discovery of organic luminophores with unique properties typically leads to new applications of such emitters in the field of organic optoelectronics. The example is demonstrated in this study. One of the newly synthesized mechanochromic derivatives of benzanthrone and carbazole demonstrates ability of self-regulation of its solid-state structure and related light-emitting properties. This compound shows intensive green emission peaking at 537 nm in the initial state, weak yellowish green emission peaking at 557 nm after mechanical treatment which self-recovers back to intensive green emission with the intensity maximum at 539 nm. The processes are completely reversible. They include the following set of states: highly emissive state → damaged weak-emissive state → self-recovering → recovered highly emissive state. The developed compound is a very rare example of materials which can be used for security probes or data/code writing with recovering ability after mechanical damage. Variety of experimental studies including spectroscopy of thermally annealed samples and single crystal and powder diffraction X-ray analysis revealed the ability of the developed derivatives of benzanthrone and carbazole to form different polymorphs and aggregates in solid-state responsible for their multicolour mechanochromic emission.

1. Introduction

Smart materials demonstrating colour-changing ability are divided into the different groups in accordance to the type of external stimulus. According to the general classification, a change of colour can be caused by the different phenomena such as mechanochromism, thermochromism, electrochromism, photochromism, acidochromism, etc [1]. A great attention is paid to organic mechanochromic luminescent (MCL) materials that exhibit reversible colour or emission changing under external mechanical force [2]. MCL materials depending on their emission properties and chemical structures can exhibit mechanically-induced fluorescence, phosphorescence or room temperature phosphorescence [3]. Molecular conformations, different types of architecture of molecular packing and intermolecular interactions have an impact on MCL of organic compounds and as a result, blue- or red-shift of luminescence is observed [4]. Due to high stimuli response, reversibility and switching emission, MCL materials have potential applications in mechanosensors [5–7], optical recording [8,9] and memory chips [10].

Currently, a number of MCL materials demonstrating aggregation induced emission (AIE) were reported [2,11,12]. The presence of different molecular packings of crystalline forms (polymorphism) can also induce the mechanochromic properties [13–16]. It was recently reported that almost identical polymorphic crystalline structures of the material demonstrated high-contrast emission due to the small difference in intermolecular interactions and the significant influence on intramolecular charge transfer (ICT) [17]. Although many MCL materials demonstrating polymorphism, AIE and another phenomena were reported, only few of them can recover after grinding to the initial state without any additional stimulus and demonstrate self-reversible mechanochromism [14,18–26]. Huge number of donor-acceptor (D-A) materials exhibiting MCL were reported but small number of them demonstrating self-recovering light-emitting properties were introduced

* Corresponding author.
E-mail address: juozas.grazulevicius@ktu.lt (J.V. Grazulevicius).

https://doi.org/10.1016/j.dyepig.2022.110082
Received 16 August 2021; Received in revised form 22 December 2021; Accepted 4 January 2022
Available online 6 January 2022

[14,20,21,25,27–29].

Herein, we report on two new derivatives of benzanthrone (benzo[de]anthracen-7-one, BZA) and carbazole or di-*tert* butyl carbazole as MCL materials. The rigid electron-accepting and electron-donating moieties with relatively high molecular weights were selected and flexibly linked. As it was expected exploiting such approach, both compounds showed mechanochromic properties. Carbazolyl-containing compound showed self-reversible mechanochromism. In order to understand mechanochromic nature of the obtained materials the relationships between their structure and photophysical properties, aggregation phenomena, polymorphism and self-recovering effect were studied. In most cases, the shift of emission under external stimuli of MCL material with D-A structure is explained by the change of dihedral angles between donor and acceptor units when the structure of a compound is changed from crystalline to amorphous [3,30,31]. In contrast to many other studies that mainly show effect of crystallization of organic materials on self-reversible mechanochromism [20–26], we demonstrate that mechanochromic luminescence of organic semiconductor is caused by combination of both polymorphs and amorphous aggregates. The unique potential applications of self-recovering mechanochromic luminescence of the developed compound such as damage-resistive information recording and security probes are also demonstrated. Despite of well-known donor-acceptor structure of the synthesized compounds, BZA, to our knowledge, was used only once in the design of organic emitters [32].

2. Results and discussions

2.1. Synthesis

Buchwald-Hartwig cross coupling reactions were performed to obtain 3-(9*H*-carbazol-9-yl)-7*H*-benzo[*de*]anthracen-7-one (**BZACz**) and 3-(3,6-di-*tert*-butyl-9*H*-carbazol-9-yl)-7*H*-benzo[*de*]anthracen-7-one (**BZAtCz**). The synthetic pathway for the target compounds is presented in Scheme 1. ^{1}H and ^{13}C NMR spectroscopies, mass spectrometry and elemental analysis were done for the identification of the chemical structures of compounds (SI).

2.2. Thermal, photoelectrical and photophysical properties

Compounds **BZACz** and **BZAtCz** demonstrated a high thermal stability that was confirmed by thermogravimetric analysis (TGA) (Fig. 1a, Table 1). The value of the temperature of 5% weight loss (T_d) of 359 °C observed for compound **BZAtCz** was slightly higher than that of **BZACz** (344 °C). The complete weigh loss shows that during TGA experiments the compounds experienced sublimation.

Differential scanning calorimetry (DSC) measurements were performed for investigation of the morphological transitions of the compounds. The temperatures of glass transition (T_g) were detected in the second heating scan for both the compounds (Fig. 1b, Table 1). Their values were found to be of 93 °C and 124 °C for **BZACz** and **BZAtCz**, respectively. In the first heating scan both the derivatives showed two melting signals. This observation can be explained by the presence of two different polymorphs in the samples of the compounds. However, in the repeated heating scan after crystallization only one type of crystal was obtained and single melting signals were observed for **BZACz** and **BZAtCz** [33]. The possible effects of existence of polymorphs of **BZACz** and **BZAtCz** on their MCL properties will be discussed below in more details.

We performed the additional DSC measurements for **BZACz**. Notably, the DSC scan was performed for few crystals of **BZACz** (Fig. S1). In addition, such type of crystals (the first type of polymorph) was also used for recording of PL spectrum and PL decay curve (Fig. 2) as well as for recording of single crystal X-ray structure (Fig. 3a). The sizes of the crystals were big enough. Unfortunately, the sizes of another type of crystals (the second type of polymorph) was too small for the recording of DSC curves, PL spectrum, PL decay curve and for single crystal X-ray analysis of the separate crystal(s). Nevertheless, the formation of the second type of polymorph is evident due to the PXRD patterns and emission behaviour of as-prepared powder of **BZACz** (initial stage). This observation is described below in more details. DSC measurements for as-prepared powder of **BZACz** also demonstrated melting signal that was identified as formation of the second type of polymorph (Fig. 1b). However, the melting signals observed for the second type of polymorph of **BZACz** were not so clear as that observed for **BZAtCz**. This observation apparently can be explained by the small size of the second type of polymorph which leads to simultaneous recrystallization of the second type of polymorph to the first type of polymorph (Fig. 1b). In the case of the first type of polymorph of **BZACz**, DSC curve demonstrated one melting signal at 278 °C (Fig. S1).

Ionization potentials (IP^{UPS}) of the layers of compounds were investigated by ultraviolet photoelectron spectroscopy (UPS) (Fig. 1c). For **BZACz** and **BZAtCz** the values of IP^{UPS} were found to be of 6.04 and 5.85 eV, respectively. Electron affinities (EA^{UPS}) were estimated by the formula $EA^{UPS} = IP^{UPS} - E_{opt}$, where E_{opt} is the optical gap taken from the absorption spectra. The values of EA^{UPS} of 3.42 and 3.36 eV were estimated for **BZACz** and **BZAtCz**, respectively The lower IP^{UPS} and EA^{UPS} values obtained for compound **BZAtCz** can be attributed to the stronger electron-donating property of di-*tert* butyl carbazole moiety relative to that of carbazole unit.

The photophysical properties of compounds **BZACz** and **BZAtCz** were investigated and the results are demonstrated in Fig. 1d–f, S2 and

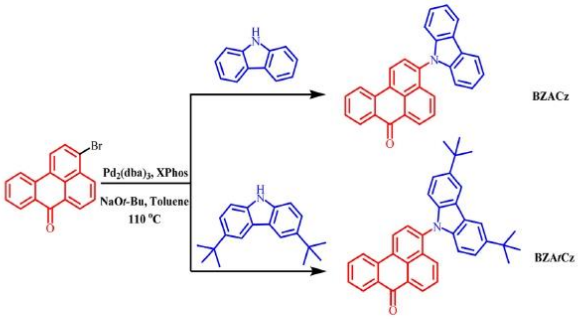

Scheme 1. Synthesis of **BZACz** and **BZAtCz**.

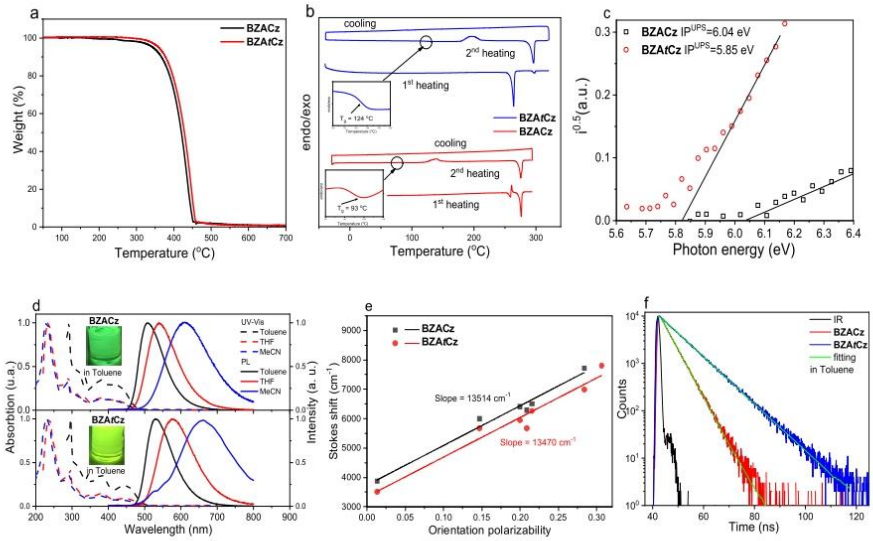

Fig. 1. TGA (a), DSC (b) curves of powders and photoelectron emission spectra of the layers (c) of compounds **BZACz** and **BZAtCz**. Absorption and PL spectra (d) of dilute 10^{-5} M toluene, THF and MeCN solutions of **BZACz** and **BZAtCz** (λ_{ex} = 330 nm). Lippert-Mataga plots (e) for **BZACz** and **BZAtCz**. PL decays curves (f) of toluene solutions.

Table 1
Thermal, photoelectrical and photophysical characteristics of the compounds.

Compounds	T_d [a], °C	T_m, °C	T_g [c], °C	T_{cr} [c], °C	IP^{UPS}, eV	EA^{UPS}, eV	$\lambda_{PL}^{tol/film}$, nm	$\Phi^{tol/film}$, %	τ^{tol}, ns	τ_1/τ_2^{film}, ns
BZACz	344	259[b]/276[b,c]	93	140	6.04	3.42	501/560	34/22	4.30	1.32 (40%)/5.36(52%)
BZAtCz	359	264[b]/296[b,c]	124	197	5.05	3.36	530/590	53/22	8.72	1.61(32%)/6.30(60%)

[a] – determined from TGA; DSC.
[b] – first heating scan.
[c] – second heating scan; T_d – the temperature of 5% weight loss; T_g – the temperature of glass transition; T_m – the temperature of melting point; T_{cr} – crystallization; λ_{PL} is the wavelength of PL maximum; Φ is the photoluminescence quantum yield; τ_1, τ_2 are photoluminescence lifetimes of neat films of compounds.

Table 1. The absorption bands observed at ca. 295 and 320–335 nm are characteristics of π-π* transitions of carbazole moiety [34]. The band observed at ca. 380 nm can be assigned to the π-π* transitions on the molecule as the whole while low-energy band at ca. 430 nm apparently originates from ICT between electron-donating carbazole unit and BZA moiety [35]. This assumption is confirmed by the hypsochromic shifts of the low-energy bands of the solutions of the compounds with increasing polarity of the solvents (Figs. 1d and S2). Attachment of *tert*-butyl substituents to carbazolyl groups caused slight bathochromic shifts in both absorption and emission spectra.

Absorption and photoluminescence (PL) spectra of the solutions of the compounds in solvents of the different polarities were recorded (Fig. S2). The Lippert-Mataga plot presented in Fig. 1e is based on the equation $\Delta\nu = \frac{2\Delta f}{4\pi\varepsilon_0 hca^3}(\mu_e - \mu_g)^2 + b$, where $\Delta\nu$ stands for the Stokes shift, Δf is the orientation polarizability, ε_0 corresponds to the permittivity of vacuum, h is a Planck constant, c stands for the speed of light in vacuum, a is a so called Onsager radius. The Lippert-Mataga approach [36–38] is based on the interpretation of Onsager [39] of non-specific electrostatic interactions between molecules and solvents. Slopes of the plots of 13.51×10^3 and 13.47×10^3 cm^{-1} reveal the square value of the difference/similarity in dipole moments of the excited and ground states, μ_e and μ_g, of **BZACz** and **BZAtCz**, respectively. The obtained values of linear fits additionally prove the apparent ICT character of transitions of the compounds.

The toluene solution of the compound containing carbazole moiety (**BZACz**) demonstrated green emission with fluorescence maximum centered at 501 nm (Fig. 1d, Table 1) while its neat film exhibited emission with the intensity maximum at 560 nm (Fig. S2, Table 1). Whereas the toluene solution and the film of compound with *tert*-butylcarbazole unit (**BZAtCz**) exhibited emission in green-orange region with maxima at 530 nm and 590 nm respectively. The toluene solutions of compounds **BZACz** and **BZAtCz** exhibited PLQY of 34% and 53% correspondingly, while the solid samples of both the compounds showed lower value of 22% (Table 1). PL decays of toluene solutions and films of the derivatives recorded in nanosecond range, confirmed that emission was prompt fluorescence (resulting from recombination of singlet ICT states) (Fig. 1f, S2, S3, Table 1.).

2.3. Mechanochromism and its self-recovering

The solid-state samples of benzanthrone-based D-A compounds **BZACz** and **BZAtCz** demonstrated high-contrast multi-color MCL. The

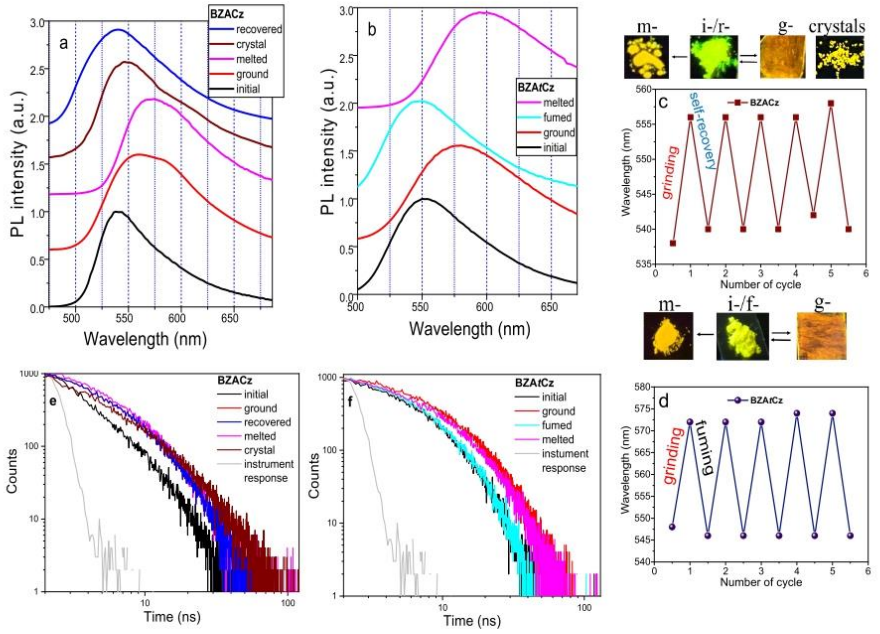

Fig. 2. Normalized fluorescence spectra (a, b) of initial (i-), ground (g-), self-recovered (r-)/fumed (f-) and melted (m-) states of compounds **BZACz** and **BZAtCz**; PL reversibility of compounds **BZACz** after five grinding/self-recovery (20 min) cycles (c). PL reversibility of compound **BZAtCz** after five grinding/DCM fuming cycles (λ_{exc} = 350 nm) (d). Photoluminescence decay curves of different states of compounds **BZACz** (e) and **BZAtCz** (f).

emission colour of the compounds was sensitive to the environment and could be altered by the application of variety of external stimuli (grinding, fuming, melting) (Fig. 2). The data for as-prepared (initial), ground, fumed with DCM vapors and self-reversible solids are collected in Table 2. The as-prepared powders of **BZACz** and **BZAtCz** emitted light with the wavelengths of maximum intensities of 538 and 550 nm, respectively. Melting of as-prepared solids resulted in the red-shifts of the PL, which peaked at 574 nm for **BZACz** and 594 nm for **BZAtCz**.

Upon grinding with spatula, the emission spectra of as-prepared powders of **BZACz** and **BZAtCz** bathochromically shifted towards yellow-orange region with peaks located at 560 and 580 nm respectively. Larger MCL spectral shift after transition from as-prepared to the melted form was observed for the **BZAtCz**. This observation can be explained by the presence of *tert*-butyl groups in **BZAtCz** causing the bigger intermolecular distances in as-prepared form which are disturbed by grinding or melting. The carbazolyl containing compound (**BZACz**) exhibited dynamical self-reversible MCL. The emission of the ground powder of **BZACz** self-recovered at room temperature within 20 min to the initial colour with the intensity maximum at 540 nm (Fig. 2a, videoclip X). The initial colour of the powders of **BZACz** could be recovered for up to five grinding – self-reversibility cycles within 20 min (Fig. 2c, S4). The ground form of **BZAtCz** did not exhibit room temperature self-recovery. The emission of ground form remained stable and did not change in time during one month of observations. Nevertheless, the stable orange emission (580 nm) of ground form of **BZAtCz** could be recovered to the initial green emission (548 nm) after fuming of ground powder in DCM vapors for 5 min (Fig. 2b). Similarly, to **BZACz**, the **BZAtCz** experienced stable PL reversibility of as-prepared powders during five grinding-fuming (with DCM) cycles (Fig. 2d, S4).

The PLQY values of as-prepared, ground and recovered forms of **BZACz** were found to be close (15–17%) (Table 2). The forms of **BZAtCz** exhibited considerably higher PLQY of 27–31%. This observation can be attributed to the presence of di-*tert* butyl groups in **BZAtCz** which increase the intermolecular distances, thus decreasing the π- π interactions. The PLQY values of amorphous melted forms of **BZACz** (9%) and **BZAtCz** (3%) were much lower than those of the initial powders due to extend π-π stacking of neighbouring aromatic rings. The PL decay curves of the different forms of the compounds had biexponential character. The emission lifetimes varied in the nanosecond range (1.13–9.62 ns) revealing the prompt fluorescence nature of the emission (Fig. 2e and f). Since PL decays of initial, ground, self-recovered and melted states of compound **BZACz** are visibly different from PL decay of its crystals (Fig. 2e), the total emission of the different states of compound **BZACz** apparently resulted from overlapping of emission of different crystal polymorphs and amorphous aggregates which will be discussed below.

To get deeper insights in MCL properties of compounds **BZACz** and **BZAtCz**, single crystal X-ray analysis (Fig. 3a and b), spectroscopic measurements for amorphous solid-state solutions (Fig. 3c and d) and powder X-ray diffraction (PXRD) analysis (Fig. 3e and f) were performed. The proper single crystal was obtained only for **BZACz**. It was obtained by slow evaporation of the methanol solution (Fig. 3a). In the crystalline lattice, **BZACz** experienced several types of interactions: C–H···O interactions between the adjacent BZA units with the distances

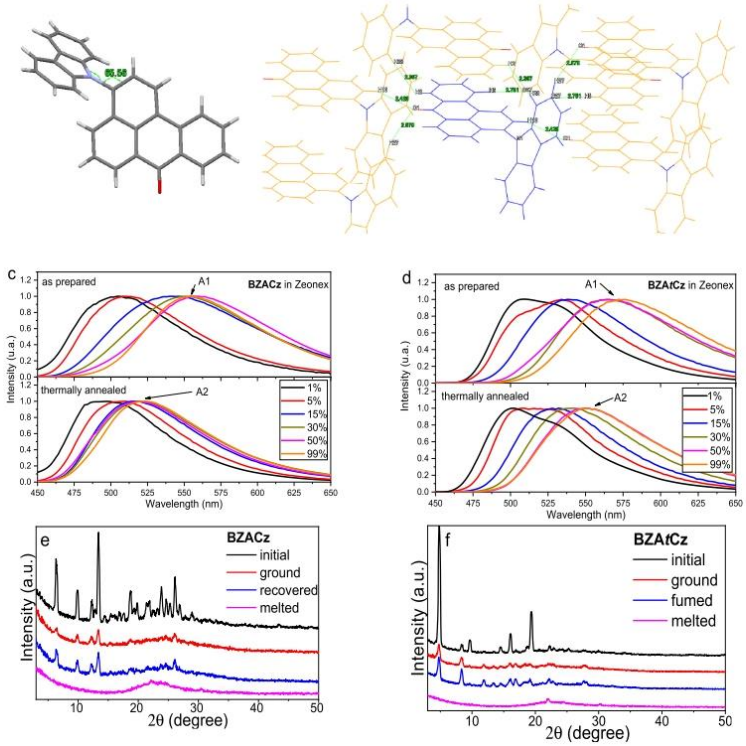

Fig. 3. Single crystal X-ray structure (a) and packing mode (b) of compound **BZACz** (CCDC number 2046803); PL spectra of solid mixtures of compound **BZACz** (c) and **BZAtCz** (d) with Zeonex as prepared (above) and after thermal annealing (below); and PXRD patterns (e, f) of the different states of compounds **BZACz** and **BZAtCz**.

Table 2
PL properties of MCL states (initial, ground, recovered, fumed, melted) and of single crystals of compounds **BZACz** and **BZAtCz**.

State / Parameter	BZACz					BZAtCz			
	initial	ground	recovered	melted	crystal	initial	ground	fumed	melted
λ_{PL}, nm	530	560	540	574	546	550	500	540	594
Φ_{PL}, %	15	17	15	9	–	27	31	23	3
τ_1, ns	1.13	2.04	2.01	1.97	1.49	2.67	3.91	2.69	3.09
R_1, %	43	30	31	24	34	20	23	17	22
τ_2, ns	5.28	6.93	7.13	6.60	9.41	6.09	9.62	6.04	0.97
R_2, %	57	70	69	76	66	80	77	83	78
*crystallinity** %	63.8	29.3	39.5	0	100	66.4	42.1	49.8	3.3

λ_{PL} is the PL maxima (λ_{exc} = 350 nm); Φ_{PL} is the photoluminescence quantum yield; τ_1, τ_2 are the PL lifetimes (well-fitted with the χ^2 values of 1.021–1.206), R_1,R_2 are the contribution ratio of τ_1/τ_2; *obtained from PXRD measurements.

of 2.429 and 2.570 Å; C–H···H interactions between H atoms of carbazole and BZA fragments with the distances of 2.367 Å and C–H•••π interactions (2.751 Å).

Interestingly, the emission of the single crystal with PL peak located at 546 nm was red-shifted in respect to those of as-prepared crystalline powder and of the recovered form. This observation can be attributed to the intermolecular interactions and molecular organization mediated fluorescence change in crystals and amorphous powder. On the other hand, it can be caused by formations of different amorphous aggregates. To prove this assumption, the amorphous mixtures of compounds **BZACz** and **BZAtCz** doped in rigid matrix Zeonex were investigated (Fig. 3c and d). It should be noted that red-shifts of PL observed with

increasing concentration of dopants of the spin-coated films of guest-host systems **BZACz**-Zeonex and **BZAtCz**-Zeonex are related not only to solid solvatochramism but also to formation of amorphous aggregates (marked as A1, Fig. 3c and d). Those amorphous aggregates are characterized by PL spectra peaked at 555 and 568 nm for compounds **BZACz** and **BZAtCz**, respectively. This conclusion is supported by the different red-shifts of PL spectra observed for the same films of molecularly doped polymer **BZACz**-Zeonex and **BZAtCz**-Zeonex after thermal annealing at 150 °C which increased thermodynamic stability of the guest-host mixtures. At concentrations of guest exceeding 15 wt%, polarity effect of Zeonex on emission properties of **BZACz** and **BZAtCz** is very low. Thus, formation of aggregates mainly affects the emission properties of **BZACz** and **BZAtCz**. The thermal annealing of the samples of compounds **BZACz** and **BZAtCz** allowed to reduce the aggregation degree of one type of aggregates (A1) with red-shifted PL spectra peaking at 555 and 568 nm and led to the formation of another type of aggregates (marked as A2, Fig. 3c and d) which were characterized by blue-shifted PL spectra peaking at 521 and 550 nm, correspondingly (Fig. 3c and d). These observations reveal impact of both crystalline polymorphs and amorphous aggregates on the total emission of different states of compounds **BZACz** and **BZAtCz** (Fig. 2). Quantitatively, the impact of the different treatment of the samples on their morphology can be estimated from the PXRD patterns given in Fig. 3 e,f.

The sharp and intense peaks in PXRD patterns of initial forms confirm the crystalline nature of the powders (Fig. 3e,f). After melting of initial powders, the samples were converted from crystalline to the amorphous state with the degrees of crystallinity of 0 and 3.3% observed for **BZACz** and **BZAtCz**, respectively. Tight packing leads to the stronger molecular π-π interactions in amorphous state which is the main reason of the red-shifted PL of the melted forms. After intense grinding of as-prepared powders, the dihedral angle between carbazole/di-*tert*-butyl carbazole and BZA fragments most likely changed and crystalline packing of the as-prepared forms were partially destroyed and converted into the amorphous state. Degrees of crystallinity of 29.3% and 42.1% were observed for **BZACz** and **BZAtCz**, respectively after grinding. Interestingly, despite the full restoration of the PL emission, the self-recovered sample of **BZACz** and fumed form of **BZAtCz** experienced only the partial restoration of the crystallinity with the degrees of crystallinity of 39.5 and 49.8%, respectively. The higher degree of crystallinity of the as-prepared powder in respect to that of the recovered form resulted in the higher half-width of the emission spectrum at maximum of the recovered state of **BZACz** relative to that of the initial one (Fig. 2a).

As was reported previously, the introduction of alkyl substitution can cause self-recovering properties of compounds [24]. Also, some MLC materials with low molecular mass demonstrated self-reversible mechanochromism due to the possibility of fast spontaneous recrystallization of the amorphous phase [21,23,25,26]. The synthesized compound **BZAtCz** containing *tert*-butyl groups showed stimuli-induced switching by using solvent vapors whereas carbazole-based compound **BZACz** demonstrated self-reversible mechanochromism. For material **BZACz** the meta-stable ground form experienced easier rearrangement and spontaneous crystallization of the amorphous samples due to lower molecular weight and the tighter packing. At the same time, the *tert*-butyl groups in molecular structure of **BZAtCz** increased its molecular weight and cause the steric hindrance and prevent self-recovering the intermolecular interaction and reorganization to the initial highly crystalline state.

Summarizing of above described experimental results for **BZACz** and **BZAtCz**, we demonstrated formation of two types of amorphous aggregates named as A1 and A2 (Fig. 3c and d). The formation of crystalline aggregates in the molecular dispersions in polymer ZEONEX is highly improbable. This presumption is supported by the considerable rigidity of ZEONEX [40,41]. Thus, only very limited movements of the molecules are expected similarly to those reported elsewhere [42]. The first type of aggregates A1 (of as prepared samples) demonstrated red-shifted emission spectra. The second type of aggregates A2 (of the thermally annealed samples) demonstrate blue-shifted emission spectra (Fig. 3c and d). In addition, in case of **BZACz** and **BZAtCz**, we detected formation of two types of polymorphs according to the PXRD, photophysical and DSC measurements. For instance, one type of polymorph exhibited red-shifted emission (Fig. 2a). Another type of polymorph definitely exhibited blue-shifted emission similarly to the emission of as-prepared powder. The formation of the second type of polymorph is evident due to the high degree of crystallinity (63.8% for **BZACz** and 66.4% for **BZAtCz**) of the as-prepared powders (Fig. 3e and f, Table 2). Unfortunately, we did not manage to obtain single crystal X-ray structure and emission spectrum of the second polymorph due to the difficulties of separation of the extremely small sizes of crystals of this type of polymorph. Fortunately, self-recovering mechanochromic luminescence is possible apparently because of the extremely small size of the second type of polymorph of **BZACz**. Thus, we observed the red-shifted emission for one type of amorphous aggregates and for one type of polymorph. We also observed blue-shifted emission for the second type of amorphous aggregates and for another type of polymorph. Therefore, in contrast to many other reports on MCL materials, we concluded that the multi-color mechanochromic luminescence of the compounds was caused by the presence of different crystalline polymorphs and amorphous aggregates. Thus, possibility of formation of both crystalline polymorphs and amorphous aggregates, have to be taken into account in the investigations of MCL materials.

Self-recovering properties of compound **BZACz** can potentially be employed for either damage-resistive information encryption or for security check. The schematic principles and experimental visualisations of the potential applications are presented in Fig. 4. In the test of the damage-resistive information encryption, the dark mechanically damaged areas marked by red rectangles in photo A, Fig. 4a become bright again after recovering time (see the same rectangles in photo B, Fig. 4a, videoclip Y). The unique properties of compound **BZACz** can also be utilized for multistep control of protected objects. Thus, the first step (control 1) is the change of emission colour from bright green to yellow and the second step (control 2) is the change of emission colour from yellow back to bright green (Fig. 4b).

3. Conclusions

New derivatives of benzanthrone and carbazoles were designed, synthesized and investigated. One of the compounds showed reversible mechanochromism and the property of recovering without external stimuli. After the application of variety of external stimuli such as grinding, fuming, melting the emission colour change from green to orange was observed for both the synthesized derivatives. The multi-color mechanochromic luminescence of the compounds was caused by the presence of different crystalline polymorphs and amorphous aggregates which were confirmed by experimental studies. The carbazolyl-containing compound demonstrated the ability of self-regulation of its solid-state structure and related light-emitting properties. The developed compound showed unique self-recovering properties which can be potentially applied in damage-resistive information recording or security check.

Author contribution statement

Uliana Tsiko designed and synthesized the materials, wrote draft of the manuscript. Galyna Sych advised and assisted with synthesis and identifications of materials. Dmytro Volyniuk performed ionization potential measurements, contributed to writing and revising of the manuscript. Oleksandr Bezvikonnyi performed photoluminescence measurements. Rasa Keruckiene investigated glass forming/thermal properties of new compounds and contributed to their interpretation. Algirdas Lazauskas performed powder X-ray diffraction (PXRD) analysis. Juozas Vidas Grazulevicius the team leader of the project, discussed

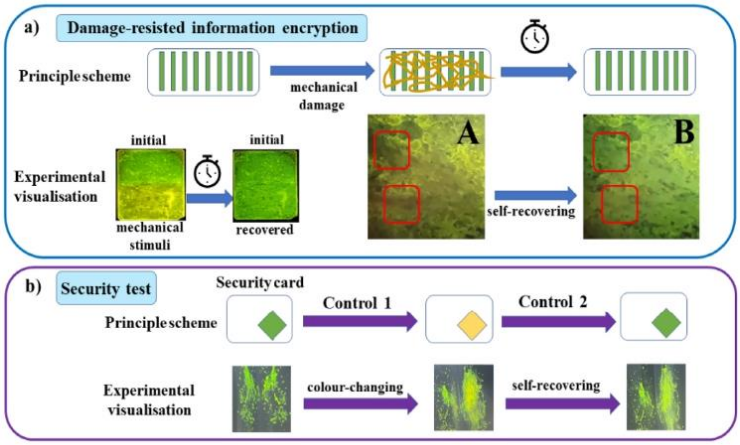

Fig. 4. Demonstration of possible application of self-recovering material **BZACz** in data/code writing (a) or security probes (b) with the ability to recover after mechanical damage.

the results obtained and reviewed the manuscript.

Declaration of competing interest

The authors declare that they have no known competing financial interests or personal relationships that could have appeared to influence the work reported in this paper.

Acknowledgements

This project has received funding from European Regional Development Fund (project No 01.2.2-LMT-K-718-01-0015) under grant agreement with the Research Council of Lithuania (LMTLT).

Appendix A. Supplementary data

Supplementary data to this article can be found online at https://doi.org/10.1016/j.dyepig.2022.110082.

References

[1] Huang G, Xia Q, Huang W, Tian J, He Z, Li BS, et al. Multiple anti-counterfeiting guarantees from a simple tetraphenylethylene derivative – high-contrasted and multi-state mechanochromism and photochromism. Angew Chem Int Ed 2019;58: 17014–9. https://doi.org/10.1002/anie.201910530.

[2] Yang W, Yang Y, Qiu Y, Cao X, Huang Z, Gong S, et al. AIE-active multicolor tunable luminogens: simultaneous mechanochromism and acidochromism with high contrast beyond 100 nm. Mater Chem Front 2020;4:2047–53. https://doi.org/10.1039/d0qm00247j.

[3] Xie Y, Li Z. The development of mechanoluminescence from organic compounds: breakthrough and deep insight. Mater Chem Front 2020;4:317–31. https://doi.org/10.1039/c9qm00500c.

[4] Yu HX, Zhi J, Shen T, Ding W, Zhang X, Wang JL. Donor-acceptor type aggregation-induced emission luminophores based on the 1,1-dicyanomethylene-3-indanone unit for bridge-dependent reversible mechanochromism and light-up biosensing of hypochlorites. J Mater Chem C 2019;7:8888–97. https://doi.org/10.1039/c9tc01772k.

[5] Wang Y, Tan X, Zhang YM, Zhu S, Zhang I, Yu B, et al. Dynamic behavior of molecular switches in crystal under pressure and its reflection on tactile sensing. J Am Chem Soc 2015;137:931–9. https://doi.org/10.1021/ja511499p.

[6] Ito H, Muromoto M, Kurenuma S, Ishizaka S, Kitamura N, Sato H, et al. Mechanical stimulation and solid seeding trigger single-crystal-to-single- crystal molecular domino transformations. Nat Commun 2013;4. https://doi.org/10.1038/ncomms3009.

[7] Hu J, Han T, Liu Y, Zhang X, Duan Y, Li Z, et al. Strategy for optical data encryption and decryption using a D-A type stimuli-responsive AIE material. Spectrochim Acta Part A Mol Biomol Spectrosc 2020;239. https://doi.org/10.1016/j.saa.2020.118406.

[8] Dong Y, Xu B, Zhang J, Tan X, Wang L, Chen J, et al. Piezochromic luminescence based on the molecular aggregation of 9,10-Bis[(E)-2-(pyrid-2-yl)vinyl]anthracene. Angew Chem Int Ed 2012;51:10782–5. https://doi.org/10.1002/anie.201204660.

[9] Yoon SJ, Chung JW, Gierschner J, Kim KS, Choi MG, Kim D, et al. Multistimuli two-color luminescence switching via different slip-stacking of highly fluorescent molecular sheets. J Am Chem Soc 2010;132:13675–83. https://doi.org/10.1021/ja1044665.

[10] Park SK, Cho I, Gierschner J, Kim JH, Kim JH, Kwon JE, et al. Stimuli-Responsive reversible fluorescence switching in a crystalline donor-acceptor mixture film: mixed stack charge-transfer emission versus segregated stack monomer emission. Angew Chem Int Ed 2016;55:203–7. https://doi.org/10.1002/anie.201508210.

[11] Yang X, Wang Q, Hu P, Xu C, Guo W, Wang Z, et al. Achieving remarkable and reversible mechanochromism from a bright ionic AIEgen with high specificity for mitochondrial imaging and secondary aggregation emission enhancement for long-term tracking of tumors. Mater Chem Front 2020;4:941–9. https://doi.org/10.1039/c9qm00744j.

[12] Ye F, Liu Y, Chen J, Liu SH, Zhao W, Yin J. Tetraphenylene-coated near-infrared benzoselenodiazole dye: AIE behavior, mechanochromism, and bioimaging. Org Lett 2019;21:7213–7. https://doi.org/10.1021/acs.orglett.9b02292.

[13] Yang W, Liu C, Lu S, Du J, Gao Q, Zhang R, et al. AIE-active smart cyanostyrene luminogens: polymorphism-dependent multicolor mechanochromism. J Mater Chem C 2018;6:290–8. https://doi.org/10.1039/c7tc04773h.

[14] Ekbote A, Mobin SM, Misra R. Stimuli-responsive phenothiazine-based donor-acceptor isomers: AIE, mechanochromism and polymorphism. J Mater Chem C 2020;8:3509–602. https://doi.org/10.1039/c9tc05192a.

[15] Lei Y, Zhou Y, Qian L, Wang Y, Liu M, Huang X, et al. Polymorphism and mechanochromism of N -alkylated 1,4-dihydropyridine derivatives containing different electron-withdrawing end groups. J Mater Chem C 2017;5:5103–92. https://doi.org/10.1039/c7tc00362e.

[16] Xiong Y, Huang J, Liu Y, Xiao B, Xu B, Zhao Z, et al. High-contrast luminescence dependent on polymorphism and mechanochromism of AIE-active (4-(phenothiazin-10-yl)phenyl)(pyren-1-yl)methanone. J Mater Chem C 2020;8: 2460–6. https://doi.org/10.1039/c9tc05064g.

[17] Wang K, Xie Y, Liu M, Tao W, Zhang H, Huang M, et al. High-contrast polymorphic luminogen formed through effect of tiny differences in intermolecular interactions on the intramolecular charge transfer process. Adv Opt Mater 2020;8. https://doi.org/10.1002/adom.202000436.

[18] Xu P, Qiu Q, Ye X, Wei M, Xi W, Feng H, et al. Halogenated tetraphenylethene with enhanced aggregation-induced emission: an anomalous anti-heavy-atom effect and self-reversible mechanochromism. Chem Commun 2019;55:14930–41. https://doi.org/10.1039/c9cc07045a.

[19] Hariharan PS, Venkataramanan NS, Moon D, Anthony SP. Self-reversible mechanochromism and thermochromism of a triphenylamine-based molecule:

tunable fluorescence and nanofabrication studies. J Phys Chem C 2015;119:9460–9. https://doi.org/10.1021/acs.jpcc.5b00310.
[20] Divya TT, Ramshad K, Saheer VC, Chakkumkumarath L. Self-reversible mechanochromism and aggregation induced emission in neutral triarylmethanes and their application in water sensing. New J Chem 2018;42:20227–30. https://doi.org/10.1039/c8nj04479a.
[21] Ito S, Taguchi T, Yamada T, Ubukata T, Yamaguchi Y, Asami M. Indolylbenzothiadiazoles with varying substituents on the indole ring: a systematic study on the self-recovering mechanochromic luminescence. RSC Adv 2017;7:16953–62. https://doi.org/10.1039/c7ra01006k.
[22] Wu H, Hang C, Li X, Yin L, Zhu M, Zhang J, et al. Molecular stacking dependent phosphorescence-fluorescence dual emission in a single luminophore for self-recoverable mechanoconversion of multicolor luminescence. Chem Commun 2017;53:2661–4. https://doi.org/10.1039/c6cc04901j.
[23] Alam P, Leung NLC, Cheng Y, Zhang H, Liu J, Wu W, et al. Spontaneous and fast molecular motion at room temperature in the solid state. Angew Chem 2019;131:4504–8. https://doi.org/10.1002/ange.201813554.
[24] Ikeya M, Katada G, Ito S. Tunable mechanochromic luminescence of 2-alkyl-4-(pyren-1-yl)thiophenes: controlling the self-recovering properties and the range of chromism. Chem Commun 2019;55:12296–9. https://doi.org/10.1039/c9cc06406k.
[25] Ito S, Yamada T, Taguchi T, Yamaguchi Y, Asami M. N-Boc-Indolylbenzothiadiazole derivatives: efficient full-color solid-state fluorescence and self-recovering mechanochromic luminescence. Chem Asian J 2016;11:1963–70. https://doi.org/10.1002/asia.201600526.
[26] Mizuguchi K, Kageyama H, Nakano H. Mechanochromic luminescence of 4-[bis(4-methylphenyl)amino]benzaldehyde. Mater Lett 2011;65:2650–61. https://doi.org/10.1016/j.matlet.2011.05.060.
[27] Josse P, Allain M, Calupitan JP, Jiang Y, Cabanetos C, Roncali J. Structural control of the molecular packing and dynamics of mechanofluorochromic materials based on small donor–acceptor systems with turn-on luminescence. Adv Opt Mater 2020;8:2000420. https://doi.org/10.1002/adom.202000420.
[28] Zhan Y, Wang Y. Donor-acceptor π-conjugated quinoxaline derivatives exhibiting multi-stimuli-responsive behaviors and polymorphism-dependent multicolor solid-state emission. Dyes Pigments 2020;173:107971. https://doi.org/10.1016/J.DYEPIG.2019.107971.
[29] Wang T, Zhang N, Zhang K, Dai J, Bai W, Bai R. Pyrene boronic acid cyclic ester: a new fast self-recovering mechanoluminescent material at room temperature. Chem Commun 2016;52:9679–82. https://doi.org/10.1039/C6CC03240F.
[30] Misra R, Jadhav T, Dhokale B, Mobin SM. Reversible mechanochromism and enhanced AIE in tetraphenylethene substituted phenanthroimidazoles. Chem Commun 2014;50:9076–8. https://doi.org/10.1039/c4cc02024d.
[31] Yang W, Yang Y, Qiu Y, Cao X, Huang Z, Gong S, et al. AIE-active multicolor tunable luminogens: simultaneous mechanochromism and acidochromism with high contrast beyond 100 nm. Mater Chem Front 2020. https://doi.org/10.1039/d0qm00247j.
[32] Yu MX, Chang LC, Lin CH, Duan JP, Wu FI, Chen IC, et al. Luminescence properties of aminobenzanthrones and their application as host emitters in organic light-emitting devices. Adv Funct Mater 2007;17:369–78. https://doi.org/10.1002/adfm.200600730.
[33] Galer P, Korošec RC, Vidmar M, Šket B. Crystal structures and emission properties of the BF2 complex 1-phenyl-3-(3,5-dimethoxyphenyl)-propane-1,3-dione: multiple chromisms, aggregation- or crystallization-induced emission, and the self-assembly effect. J Am Chem Soc 2014;136:7303–94. https://doi.org/10.1021/ja501977a.
[34] Siraj N, Das S, Hasan F, Lu C, Kiruri LW, Steege Gall KE, et al. Enhanced S2 emission in carbazole-based ionic liquids. RSC Adv 2015;5:9939–45. https://doi.org/10.1039/c4ra12362j.
[35] Gonta S, Utinans M, Kirilov G, Belyakov S, Ivanova I, Fleisher M, et al. Fluorescent substituted amidines of benzanthrone: synthesis, spectroscopy and quantum chemical calculations. Spectrochim Acta Part A Mol Biomol Spectrosc 2013;101:325–34. https://doi.org/10.1016/j.saa.2012.09.104.
[36] Mataga N, Kaifu Y, Koizumi M. Solvent effects upon fluorescence spectra and the dipolemoments of excited molecules. Bull Chem Soc Jpn 1956;29:465–70. https://doi.org/10.1246/bcsj.29.465.
[37] Sumalekshmy S, Gopidas KR. Photoinduced intramolecular charge transfer in donor-acceptor substituted tetrahydropyrenes. J Phys Chem B 2004;108:3705–12. https://doi.org/10.1021/jp022549l.
[38] Lippert E. Dipolmoment und Elektronenstruktur von angeregten Molekülen. Zeitschrift Fur Naturforsch - Sect A J Phys Sci 1955;10:541–5. https://doi.org/10.1515/zna-1955-0707.
[39] Onsagbr L. Electric moments of molecules in liquids. J Am Chem Soc 1936;58:1406–93. https://doi.org/10.1021/ja01299a050.
[40] Leitonas K, Tomkeviciene A, Baratte G, Dabuliene A, Punniyakoti SM, Volyniuk D, et al. Oxygen sensing properties of thianthrene and phenothiazine derivatives exhibiting room temperature phosphorescence: effect of substitution of phenothiazine moieties. Sensor Actuator B Chem 2021;345:130369. https://doi.org/10.1016/j.snb.2021.130369.
[41] Yamazaki M. Industrialization and application development of cyclo-olefin polymer. J Mol Catal Chem 2004;213:81–7. https://doi.org/10.1016/j.molcata.2003.10.050.
[42] Skuodis E, Bezvikonnyi O, Tomkeviciene A, Volyniuk D, Mimaite V, Lazauskas A, et al. Aggregation, thermal annealing, and hosting effects on performances of an acridan-based TADF emitter. Org Electron 2018;63:29–40. https://doi.org/10.1016/j.orgel.2018.09.002.

Dyes and Pigments 197 (2022) 109952

Contents lists available at ScienceDirect

Dyes and Pigments

journal homepage: www.elsevier.com/locate/dyepig

TADF quenching properties of phenothiazine or phenoxazine-substituted benzanthrones emitting in deep-red/near-infrared region towards oxygen sensing

Uliana Tsiko [a], Oleksandr Bezvikonnyi [a], Dmytro Volyniuk [a], Boris F. Minaev [b], Jonas Keruckas [a], Monika Cekaviciute [a], Egle Jatautiene [a], Viktorija Andruleviciene [a], Asta Dabuliene [a], Juozas Vidas Grazulevicius [a,*]

[a] Department of Polymer Chemistry and Technology, Kaunas University of Technology, Radvilenu pl. 19, LT-50254, Kaunas, Lithuania
[b] Department of Chemistry and Nanomaterials Science, Bohdan Khmelnytsky National University, 18031, Cherkasy, Ukraine

ARTICLE INFO

Keywords:
Phenoxazine
Benzanthrone
Thermally activated delayed fluorescence
Near-infrared emission
Optical oxygen sensor
Organic light-emitting diode

ABSTRACT

Aiming to develop new deep-red/near-infrared emitters, benzanthrone as a new acceptor moiety with a rigid molecular structure was used. For the design of target compounds phenothiazine and phenoxazine moieties with strong electron-donating ability were also used. Such combination allowed new materials demonstrating thermally activated delayed fluorescence (TADF) in the long wavelength region to be obtained. The maximum intensity of fluorescence of the solid samples of the synthesized compounds was observed at 700 nm. Electroluminescence was peaked at similar wavelength when the compounds were used as emitters for the fabrication of non-doped organic light-emitting diodes. Due to the different substitutions of benzanthrone moieties, the values of TADF lifetimes at room temperature were found to be of in the range of 291–1198 μs which are directory related to their different oxygen sensing properties. Due to high sensitivity to the presence of oxygen in the atmosphere one of the obtained compounds was used for radiometric oxygen sensing. The film of molecular dispersion of phenoxazine containing compound in inert polymer ZEONEX® showed the ratio of intensity of TADF taken in vacuum and of prompt fluorescence taken under oxygen purge of 15.2. The oxygen sensitivity of the film estimated by Stern-Volmer constant was found to be of 1.6×10^{-4} ppm^{-1} demonstrating good reversibility. The time dependent density functional theory (DFT) calculations were used for the interpretation of the experimental results related to the structure and photophysical properties of the compounds.

1. Introduction

The development of new materials demonstrating red and near-infrared (NIR) emission has attracted the attention of the researchers over the last two decades due to the number of possible applications in bioimaging, photodynamic therapy, sensors, information-secured displays, night vision devices and optical telecommunications [1–4]. Such a broad area of the possible applications of NIR emission in organic electronics stimulates the development of new devices exhibiting NIR electroluminescence (EL) [5]. In case of organic emitters, application in optical sensors, organic light-emitting diodes (OLEDs) and probes used for diagnostics of biological analytes, there are domains of the visible and infrared spectra, named optical transmission windows in which the radiation can be transmitted through water. These domains range approximately from 650 to 1200 nm [6]. Emission of this range can penetrate biological tissues such as skin and blood vessels more efficiently than visible light since the tissues scatter and absorb less light of the longer wavelengths [6].

The different types of materials such as colloidal inorganic quantum dots [7], phosphorescent organometallic complexes [8,9], and conjugated polymers [10,11] were investigated and used for fabrication of OLEDs emitting in near infrared region (NIR OLEDs). The external quantum efficiency (EQE) of the reported NIR OLEDs remains below 5% [7–11]. One of the ways to increase the EQE of OLEDs is to implement emitters exhibiting thermally activated delayed fluorescence (TADF). TADF materials [12] as emitters or hosts are successfully used in OLEDs reaching internal quantum efficiency up to 100% [13]. Blue [14], green [15] and red [16] TADF OLEDs were fabricated with EQE exceeding

* Corresponding author.
E-mail address: juozas.grazulevicius@ktu.lt (J.V. Grazulevicius).

https://doi.org/10.1016/j.dyepig.2021.109952
Received 27 September 2021; Received in revised form 14 November 2021; Accepted 14 November 2021
Available online 18 November 2021
0143-7208/

30%. Meanwhile, examples of organic donor-acceptor compounds exhibiting long-lived emission (preferably TADF) in the NIR region and bipolar charge transport is limited [9,17,18].

In addition to the above mentioned conventional applications of TADF emitters, they have also significant potential to be used as active indicators (luminescent probes) in optical oxygen sensors. They can be good an alternative of commonly used Pt-, Pd-, Os-, Ru-, Ir-based phosphorescent indicators which are not perfect at least due to environmental and cost efficiency reasons [19]. There are examples of TADF probes emissions of which commonly fall in the visible region [20–23]. Fullerenes and metal complexes emitting delayed fluorescence in near infrared region showed good oxygen sensing properties [24–26]. Meanwhile, non-fullerene infrared TADF probes of oxygen for optical sensors are not developed yet to the best of our knowledge. For reaching valid oxygen sensitivity, good candidates of infrared TADF oxygen probes should be characterized by long lifetimes of emission according the Stern-Volmer equations [27] the simplest of which is: $\tau_0/\tau = 1 + K_{sv}[O_2]$, where τ, τ_0 are emission lifetimes under the presence and absence of oxygen, respectively; K_{sv} is the Stern–Volmer constant. According to this equation, the concentration of oxygen can be estimated by emission decay measurements. Searching for fully organic infrared TADF probes of oxygen with long-lived emission was one of the main aims of this work.

High rigidity and a twist between donor and acceptor moieties are required for the design of efficient NIR TADF emitters [17]. We have predicted that combination of planar moieties with strong electron-donating and electron-accepting abilities can enable the design compounds with both NIR long-lived emission and bipolar charge transporting properties. Benzo[*de*]anthracen-7-one (BZA) electron accepting moiety is characterized by the planar rigid molecular structure and relatively strong electron-accepting ability [28,29]. Therefore, it is a good candidate for the design of bipolar organic semiconductors emitting in NIR and infrared region of electromagnetic spectrum. BZA is a polycyclic heteroaromatic compound. Its derivatives are used as daylight fluorescent pigments [28] and as fluorescent dyes for estimation of solvent polarity due to strong solvatochromism [29].

In this work, BZA moiety was used for the design of the NIR TADF emitters for the first time. Four new compounds with donor-acceptor and donor-acceptor-donor structures based on BZA and two different donor moieties, i.e., phenothiazine and phenoxazine were synthesized and investigated. The compounds demonstrated TADF in NIR region with the lifetimes of delayed fluorescence in the range of 2–10 ms. The EL properties of the synthesized materials were studied. Also, sensing properties of phenoxazine-based material to molecular oxygen were investigated for potential application in optical sensors operating in the NIR region. The mechanism of the TADF quenching by dioxygen is discussed in detail.

2. Results and discussion

2.1. Synthesis

3-(10*H*-Phenothiazin-10-yl)-7*H*-benzo[*de*]anthracen-7-one (***m*PTZ**), 3,9-di(10*H*-phenothiazin-10-yl)-7*H*-benzo[*de*]anthracen-7-one (***di*PTZ**), 3-(10*H*-phenoxazin-10-yl)-7*H*-benzo[*de*]anthracen-7-one (***m*PNZ**), and 3,9-di(10*H*-phenoxazin-10-yl)-7*H*-benzo[*de*]anthracen-7-one (***di*PNZ**) were synthesized by Buchwald-Hartwig cross coupling reactions. The pathways of synthesis are demonstrated in Scheme 1. The chemical structures of the derivatives were confirmed by ^{1}H, ^{13}C NMR, IR, mass spectrometries and elemental analysis (SI).

2.2. Thermal, photoelectrical and charge-transporting properties

Thermogravimetric analysis (TGA) and differential scanning calorimetry (DSC) were employed to investigate the thermal properties of the new compounds. They were characterized by relatively high thermal stability. Their temperature of 5% weight loss ($T_{d\text{-}5\%}$) exceed 300 °C and 400 °C for donor-acceptor (***m*PTZ** and ***m*PNZ**), and donor-acceptor-donor compounds (***di*PTZ** and ***di*PNZ**), respectively (Fig. 1a). The single-step full weight loss of ***m*PNZ** observed during TGA indicates that 336 °C is its sublimation temperature rather than the temperature of the onset of thermal degradation. Glass-transition temperatures (T_g) higher than 100 °C were recorded for all the compounds during the second heating scan (Table 1, Fig. S1) confirming that they form molecular glasses. The highest T_g value was observed for donor-acceptor-donor type compound ***di*PTZ** containing strongly-donating phenothiazine units. Compounds ***m*PTZ** and ***di*PNZ** showed melting signals in first heating scans, however they did not crystallize during the cooling scans (Fig. S1). In the following repeated heating scans the showed glass transitions at 111 °C and 170 °C respectively (Table 1). The further heating after glass transitions of these compounds revealed crystallization and melting signals. The samples of ***m*PNZ** and ***di*PTZ** did not show any the crystallization or melting peaks on DSC curves.

To estimate the ionization potentials (IP^{UPS}) of the compounds in the solid-state, photoelectron emission spectra of vacuum-deposited layers were recorded by ultraviolet photoelectron spectroscopy (UPS) (Fig. 1b). The samples for photoelectron emission measurements were fabricated under vacuum of $1–4 \times 10^{-6}$ Bar onto glass substrates with fluorine-doped tin oxide-based electrode. The IP^{UPS} values are collected in Table 1. For compounds ***m*PTZ** and ***di*PNZ** the IP^{UPS} were found to be

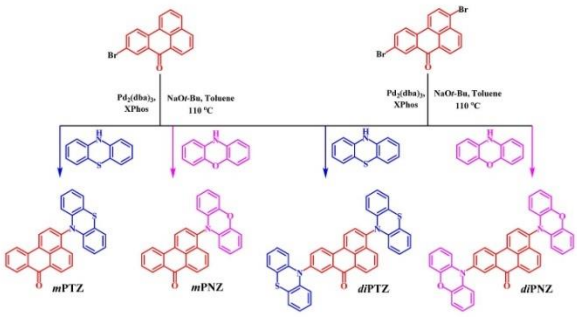

Scheme 1. Synthesis of the derivatives of benzo[de]anthracen-7-one.

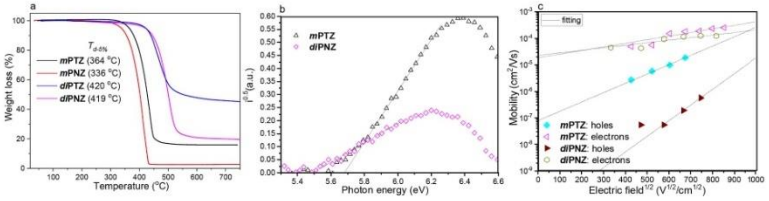

Fig. 1. TGA curves of the compounds (a), photoelectron emission spectra (b) and hole/electron drift mobilities versus electric field (c) for ***m*PTZ** and ***di*PNZ**.

Table 1
Thermal and photoelectrical characteristics of the derivatives of benzanthrone.

Compounds	T_m, °C	T_{cr}, °C	T_g[b], °C	*IP*, eV	μ^{holes}, cm²/V·s	$\mu^{electrons}$, cm²/V·s
***m*PTZ**	286[a,b]	172[b]	111	5.68	9.8×10^{-6}	1.5×10^{-4}
***m*PNZ**	–	–	114	–	–	–
***di*PTZ**	–	–	174	–	–	–
***di*PNZ**	391[a,b]	213[b]	170	5.49	7.4×10^{-8}	1.1×10^{-4}

T_m, T_{cr}, and T_g estimated from DSC curves at heating rate of 10 °C/min, N_2 atmosphere.
[a] First heating scan.
[b] Second heating scan. μ^{holes} and $\mu^{electrons}$ values taken at 3.6×10^5 V/cm.

below 6.0 eV meaning that holes can be injected from electrodes using appropriate device structures. The IP^{UPS} values for compounds ***m*PNZ** and ***di*PTZ** were not obtained by UPS measurements, apparently due to limitation of this method and due to the absorption of deep-UV light by oxygen present in air.

Charge-transporting properties of the layers of compounds ***m*PTZ** and ***di*PNZ** were investigated by the time of flight (TOF) technique. It was impossible to obtained appropriate TOF samples of compounds *m*PNZ and *di*PTZ due to their inferior film forming properties. To test ability of the compounds to transport holes and electrons, TOF transients under positive and negative polarity of applied electric fields were recorded for their layers (Fig. S2). When two different slopes (intercepts of which gave the transit times (t_{tr})) were obtained from the corresponding TOF transients built in log-log scales, hole and/or electron transport was proved for the samples. Hole and electron mobilities were calculated according to the equation $\mu = d^2/(U \times t_{tr})$ taking transit times t_{tr} from the photocurrent transients at applied voltage (U) and thicknesses of the layers (d) measured by the charge extraction by linearly increasing voltage (CELIV) technique assuming dielectric constant $\varepsilon = 3$ for the studied compounds.

Bipolar charge transport with relatively strong dispersity was observed for vacuum-deposited films of compounds ***m*PTZ** and ***di*PNZ** (Fig. 1c). Taking transit times at different applied voltages, hole and electron mobilities were calculated. The dependences on electric field were in a good agreement with the Poole–Frenkel type mobility predicted by the relationship $\mu = \mu_0 e^{\gamma E^{1/2}}$. At an electric field of $3.6 \cdot 10^5$ V/cm, close electron mobility values of 1.5×10^{-4} and 1.1×10^{-4} cm²/V·s were obtained for compounds ***m*PTZ** and ***di*PNZ**, apparently because of the same electron accepting moiety present in their molecular structures (Table 1). Slight differences in their electron mobilities may be attributed to the differences in molecular packing in their vacuum-deposited films. At the same electric field of $3.6 \cdot 10^5$ V/cm, very different hole mobility values of 7.4×10^{-8} and 9.8×10^{-6} cm²/V were obtained for compounds ***m*PTZ** and ***di*PNZ** respectively (Table 1). This difference can be explained by the different electron-donating units present in the molecular structures of the studied compounds.

2.3. Photophysical properties

Absorption and PL spectra of solid films and dilute toluene solutions of ***m*PTZ**, ***di*PTZ**, ***m*PNZ** and ***di*PNZ** recorded at 300 K are presented in Fig. 2a. The position of absorption bands in the UV spectral region was independent of type of donors attached to the benzanthrone moiety, except the location of the lowest energy absorption band (LEAB).

UV spectra of toluene solutions of phenoxazine-based compounds ***m*PNZ** and ***di*PNZ** showed prominent LEAB at 500 nm. The UV spectra of the toluene solutions of the derivatives containing phenothiazine units (***m*PTZ**, ***di*PTZ**) exhibited hypsochromically shifted LEAB with a high-energy edge at 520 nm. The difference may be assigned to the donor-acceptor interactions, which make possible the intramolecular charge transfer character of the LEAB. The absorption bands of the films were slightly redshifted and broader than the respective bands of the solutions highlighting more efficient intramolecular interaction in the solid state. The compounds emitted in the red/infrared region. The extension of conjugation by attachment of the second donor lead to the redshift of emission wavelengths. The PL quantum yields of the films and dilute toluene solutions were found to be ca. 0.01 for all the studied compounds (Table 2).

For the interpretation of photophysical properties of the studied molecules we have optimized their structures by density functional theory (DFT) with B3LYP functional and 6-31G(d,p) basis set. The time-dependent (TD) DFT calculations explain the absorption and PL spectra of the studied molecules (Table 3, Fig. S3-S7). In Fig. 3 the highest occupied molecular orbital (HOMO) and the lowest unoccupied molecular orbital (LUMO) of the ***m*PNZ** molecule are shown as typical examples. As follows from quantum chemical DFT calculations the absorption LEAB and PL emission are determined by the first excited singlet state S_1 of the HOMO-LUMO nature, which bears pure charge transfer (CT) character. The HOMO is mainly localized on the donor phenothiazine or phenoxazine moieties (Fig. 3a), while the LUMO wave function belongs entirely to the planar benzanthrone (acceptor) moiety (Fig. 3b).

The HOMO wave function has rather small contribution from the C–N link and the nearest carbon atom of the acceptor moiety. Such small penetration of the HOMO (donor orbital) into the frontier benzanthrone region provides finally some small non-zero "overlap" between two molecular orbitals and leads to very weak but nonzero intensity of the S_0–S_1 charge transfer transition. In the molecules of **mPNZ** and ***di*PNZ** the HOMO-LUMO donor-acceptor mixing is a little bit more efficient, which leads to more intense absorption band at 500 nm (Fig. 2a). A very small electric dipole transition moment (EDTM) of this CT band explains a low PL quantum yield. The calculated oscillator strength in the output of TD DFT method is less than 10^{-4}; thus, the S_0–S_1 transition is predicted as forbidden one in the electric dipole approximation at the printed output of the Gaussian 09 program. However, the calculated EDTM is of 0.02 ea_0, which corresponds to DFT predicted oscillator strength $f = 1.58 \times 10^{-5}$; the corresponding radiative lifetime (τ_R) for spontaneous PL is calculated to be 0.69 ms. The measured lifetime (τ_R =

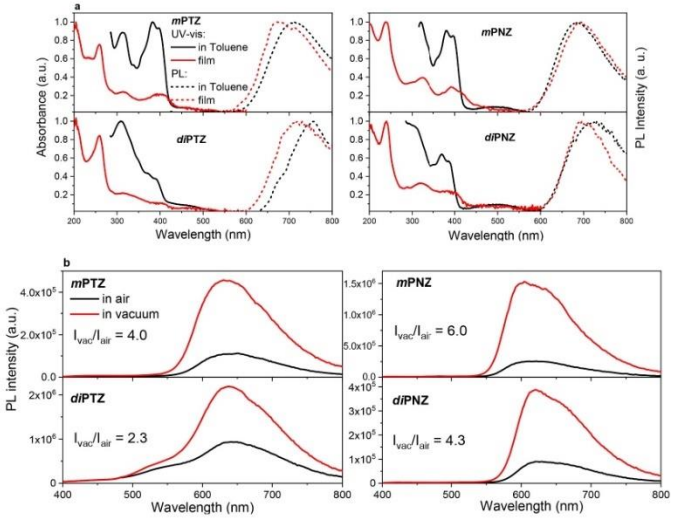

Fig. 2. Absorption and PL spectra of dilute 10^{-5} M toluene solutions and films of the derivatives of benzanthrone (a). PL spectra of 1 wt% solid solutions of ***m*PTZ**, ***m*PNZ**, ***di*PNZ** and ***di*PNZ** in ZEONEX® recorded in air and in vacuum (b).

Table 2
Photophysical data of ***m*PTZ**, ***di*PTZ**, ***m*PNZ** and ***di*PNZ**.

Compounds	Stokes shift^{tol}, nm	Stokes shift^{film}, nm	Φ^{tol}_{PL}, %	Φ^{film}_{PL}, %	Φ^{film}_{PL}, 1 wt % in Zeonex, %	$\Phi^{film}_{PL}{}^{vac}$, 1 wt % in Zeonex, %
***m*PTZ**	316	275	1	1	2	8
***di*PTZ**	308	273	1	1	3	7
***m*PNZ**	193	188	1	1	3	18
***di*PNZ**	196	225	1	1	4	17

Φ^{tol}_{PL}, Φ^{film}_{PL} values were recorded at air condition and room temperature. $\Phi^{film}_{PL}{}^{vac}$ values at vacuum condition were evaluated using data of Φ^{film}_{PL} values and Fig. 2b.

Table 3
Vertical absorption and emission spectra of ***m*PNZ** calculated by TD DFT.

C_s group	λ, nm (abs)	λ, nm (exp.)	λ, nm (emission)	Orbital assignment	f	A (s^{-1})
$1^1A''$	728	580	700	H→L (97.4%)	$6\ 10^{-5}$	$7.5\ 10^3$
$2^1A''$	402			H-3→L (91%)	0	
$3^1A''$	386			H-2→L+1	0.0001	
$2^1A'$	382.6	390		H-1→L	0.2934	
$6^1A''$	331	320		H→L+4	0.0204	
$8^1A''$	296.6	310		H→L+5	0.1225	
$7^1A'$	275.1	250		H-1→L+1	0.0838	

A – Einstein coefficient for spontaneous emission, f –oscillator strength.

1.2 ms) is of the same order of magnitude, which also indicates the TADF character of the observed emission. The Stokes shifts of all the compounds (Table 2) can be explained by a bigger geometry distortion in the excited states S_1 and T_1 in comparison with the S_0 ground state structure. Thus, geometry optimization in the S_1 state by TD DFT method predicts considerable changes in the bond lengths of the mPNZ molecule in vacuum approximation (Table 4) and also in toluene solution with the PCM approach including T_1 state (Figure S3-S5). The donor phenoxazine moiety exhibits large distortions upon excitation only in the central part for C–N and C–O bonds; the later two are shrinked by 0.03 and 0.018 Å, respectively. However many C–C bonds are prolongated (by not more than 0. 018 Å). Distortions in the acceptor moiety are much more pronounced (Table 4). They include considerable shortening of the C_4–C_7 bond by 0.058 Å and lengthening of the C_7–C_{19} and C_{20}–N_{26} links by 0.044 and 0.032 Å, respectively. The rest bond lengths are changed in the order of ±0.02 Å inside BZA moiety upon S_0–S_1 CT transition. These changes in BZA moiety occur mostly in the "opposite" direction to the carbonyl group (they are related to the distortion of the quasi-quinoid structure upon π-π*excitation in the acceptor BZA moiety).

The most intense absorption band at 390 nm is produced by transition 1^1 A′→2^1 A′ (HOMO-1 → LUMO), which corresponds to π→π* excitation in the acceptor (BZA) moiety including C=O group and increase of its antibonding character. Other UV absorption bands (Fig. 2) are well reproduced by the vertical TD DFT calculations (Table 3).

ZEONEX® is a polymer matrix used to study photophysical properties of compounds in a condition of suppressed intermolecular interactions [25]. The photophysical properties of solid molecular

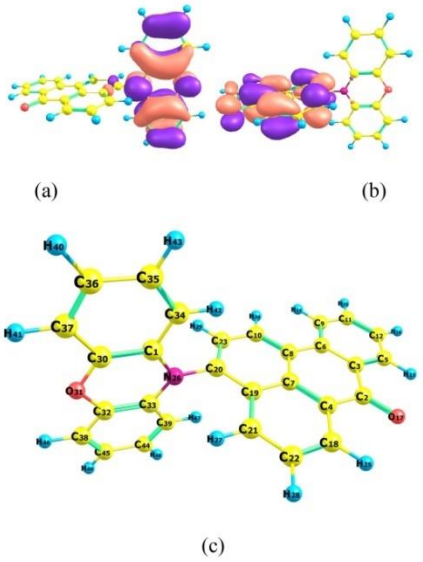

Fig. 3. HOMO (a) and LUMO (b) of the ***m*PNZ** molecule. Atomic numeration in the DFT optimized **mPNZ** molecule (D-A moieties are orthogonal) (c).

Table 4
Optimized bond lengths (Å) of the **mPNZ** molecule in the ground and excited singlet states.

Bond length	S_0 ground state	S_1 excited state
	Phenoxazine moiety	
C_1–N_{26}	**1.412**	1.382
C_1–C_{30}	1.407	1.419
C_1–C_{34}	1.399	1.411
C_{34}–C_{35}	1.398	1.382
C_{35}–C_{36}	1.391	1.409
C_{36}–C_{37}	1.398	1.387
C_{30}–C_{37}	1.387	1.393
C_{30}–O_{31}	**1.381**	1.363
Benzanthrone moiety		
C_2–C_3	1.485	1.470
C_2–C_4	**1.485**	1.464
C_2–O_{17}	1.230	**1.250**
C_5–C_3	1.402	1.409
C_6–C_3	1.414	1.424
C_4–C_7	**1.485**	1.427
C_4–C_{10}	1.386	**1.410**
C_6–C_5	**1.478**	1.456
C_6–C_9	1.408	1.418
C_7–C_8	1.433	1.437
C_7–C_{19}	1.433	**1.477**
C_8–C_{10}	1.389	**1.412**
C_9–C_{11}	1.390	1.380
C_{19}–C_{23}	**1.407**	1.386
C_{11}–C_{12}	1.400	1.408
C_{23}–C_{23}	1.379	1.394
C_{23}–O_{26}	1.431	**1.463**

mixtures of ***m*PTZ**, ***di*PTZ**, ***m*PNZ** and ***di*PNZ** and ZEONEX® (1 wt%) were investigated under air and under a nitrogen atmosphere (Fig. 2b). Dispersion of the molecules in the rigid polymer caused substantial blue-shift of PL of up to 75 nm, apparently mainly due to the change of polarity. Phenoxazine-based compounds doped in ZEONEX® exhibitted vibronic substructures in their PL spectra. Collisional interactions of compounds with oxygen molecules [30] are suppressed when the solid samples are located under a nitrogen atmosphere. Therefore, electronic excitation energy is not intercepted by oxygen and the radiative ways of deactivation of excited states, especially for triplet excitons, are not quenched. For this reason, PL quantum yields for the compounds in solid state and solutions are expected to be higher when interactions with oxygen are absent. PL spectrum of the solid solution of ***di*PTZ** in ZEONEX® contains a shoulder in the green spectral region which is assigned to locally excited (LE) state. Smaller increase of intensity of the LE band after removing oxygen was observed in comparison with the 2.3-fold increase of intensity of the CT emission peak of ***di*PTZ**. The solid solutions of the other compounds showed from 4 to 6 times higher increase of PL intensity indicating the role of triplet excitons in the emission and the absence of CT quenching by LE states. PL quantum yields of the solid solutions of ***m*PTZ**, ***di*PTZ**, ***m*PNZ** and ***di*PNZ** in ZEONEX® in air were found to be of 0.02, 0.03, 0.03 and 0.04, respectively (Table 2).

The thermal activation of delayed fluorescence (TADF) can be confirmed by the rise of the respective component of PL decay curves (Fig. 4, S8) upon heating thus manifesting the TADF character of emission. The values of TADF lifetimes of ***m*PTZ**, ***m*PNZ**, ***di*PTZ** and ***di*PNZ** at room temperature were found to be of 788, 1198, 291, and 368 μs, respectively (Fig. S9).

2.4. Electroluminescent properties

OLEDs with the layers of non-doped emitting compounds were fabricated and characterized. The EL characteristics are collected in Table 5, Fig. 5, S10, S11. The structure of the OLED was as follows: ITO/HAT-CN (15 nm)/NPB (50 nm)/mCBP (5 nm)/emitting layer (25 nm)/TSPO1 (5 nm)/TPBi (50 nm)/LiF (0.5 nm)/Al was utilized for this purpose (Fig. 5a). The layers of dipyrazino[2,3-*f*:2′,3′-*h*]quinoxaline-2,3,6,7,10,11-hexacarbonitrile (HAT-CN) and lithium fluoride (LiF) were employed as hole and electron injection layers, respectively. NPB N,N′-di(1-naphthyl)-N,N′-diphenyl-(1,1′-biphenyl)-4,4′-diamine) (NPB) and TPBi 2,2′,2″-(1,3,5-benzinetriyl)-tris(1-phenyl-1-*H*-benzimidazole) (TPBi) were used for the transport of holes end electrons, respectively, to recombination sites. Diphenyl[4-(triphenylsilyl)phenyl]phosphine oxide (TSPO1) was utilized as a hole blocking material. 3,3′-Di(9*H*-carbazol-9-yl)-1,1′-biphenyl (mCBP) was used for hole transport and electron blocking. OLEDs based on the emitters ***m*PTZ** and ***m*PNZ** having single phenoxazine or phenothiazine units exhibited single EL peak at 696 and 670 respectively, totally corresponding to the PL data. EL spectra of other OLEDs based on neat emitting layers, explicitly that of ***di*PTZ**, contained spectral contribution of emission of NPB [31] highlighting poor EL properties of the emitters (Fig. 5b). This is due to unbalanced mobilities of holes and electrons (Table 1).

The highest EQE was observed for OLED with the emitting layer of ***m*PNZ** doped (10 wt%) in mCBP (Fig. 5c). The structure of OLED remained the same except the different emitting layer. The absence of the spectral tail related to NPB or any other possible reason manifests efficient electronic excitation energy transfer from host to guest. The low turn-on voltage remained unchanged after doping of the emitter in mCBP. This observation indicates a favourable charge balance and compatibility of energy levels of the transporting and emitting layers. Similar to the PL spectra of the films of the molecular dispersions in ZEONEX® (Fig. 2b), the single EL band was found in green region. The hypsochromic shift and considerable increase of efficiency can be explained by specific dipole-dipole interactions induced by solid state solvation of ***m*PNZ** when doped in relatively low-polarity mCBP. Maximum EQE of 6.6% exceeded the theoretical limit for prompt

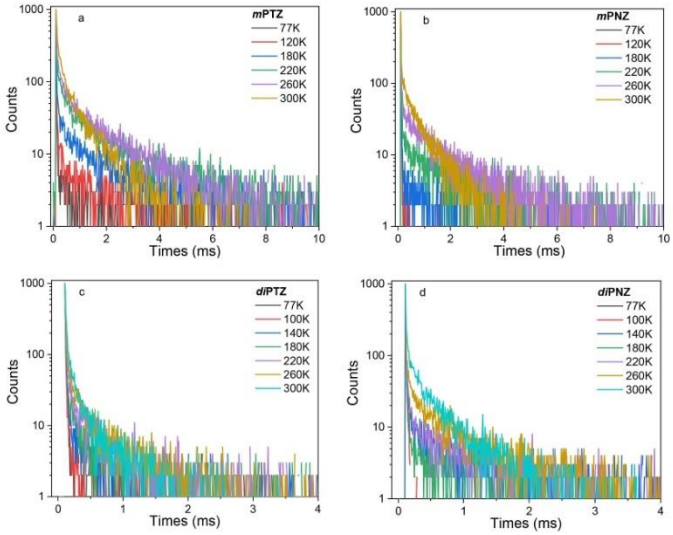

Fig. 4. PL decay curves recorded at the different temperatures under N_2 atmosphere for 1 wt% solid solution of ***m*PTZ** (a), ***m*PNZ** (b), ***di*PTZ** (c) and ***di*PNZ** (d) in ZEONEX®.

Table 5
EL characteristics of OLEDs.

Emitting layer	Turn-on voltage (V)	Maximum brightness (cd/m^2)	Current efficiency (cd/A)[a]	Power efficiency (lm/W)[a]	EQE (%)[a]	EL peak wavelength (nm)
***m*PTZ**	5.1	177	0.03/0.026	0.016/0.01	0.19/0.07	696
***m*PNZ**	4.4	296	0.19/0.08	0.13/0.02	0.37/0.15	670
***m*PNZ**:mCBP	4.4	4083	20.6/19.1	13.2/10.7	6.6/6.1	556

[a] Maximum value/value at 100 cd/m^2.

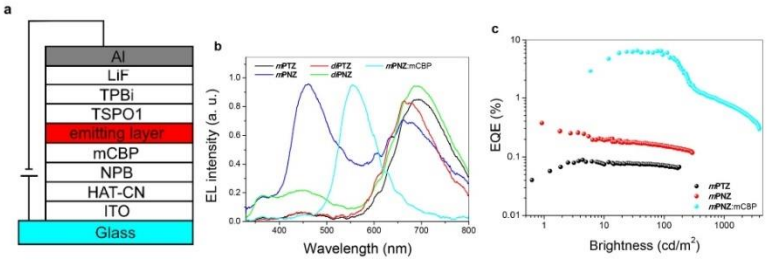

Fig. 5. Structure of OLEDs (a); normalized EL spectra (b), EQE vs brightness plots (c).

fluorescent OLEDs (Table 5) pointing to the clear TADF contribution to the efficiency of the device. It may be assumed that LE emission prevailed likewise in the PL spectrum of the molecular dispersion of ***di*PTZ** in ZEONEX®. Thus, ***m*PNZ** showed a great potential of tuning electroluminescent properties from NIR to green emission by managing the guest-host interaction.

2.5. Luminescent sensing of oxygen

Since ***m*PNZ** exhibited the biggest increase of PL intensity upon removal of air (Fig. 2b), it was selected for the investigation of oxygen sensing properties. PL spectra and decay curves of the sample of solid molecular mixture of ***m*PNZ** in ZEONEX® (1 wt%) placed in the atmosphere with the different oxygen/nitrogen ratio are presented in Fig. 6a. The data show how sensitive the PL of electronic excitation energy by collisional interactions with oxygen in the wide range of oxygen concentrations. For example, the TADF lifetime decreased to 245 μs for the sample under 8109 ppm of oxygen concentration (Fig. 6b). The ratio of intensity of TADF taken in vacuum and prompt fluorescence taken under oxygen purge was found to be of 15.2. This value is comparable to the highest values reported for TADF based optical oxygen sensors [21,32]. The Stern-Volmer plot (Fig. 6c) was built based on the equation $\tau_0/\tau - 1 = K_{SV}[O_2]$, where τ_0, are τ, are lifetimes of TADF in the absence and in the presence of oxygen respectively and $K_{SV}[O_2]$ is so-called Stern–Volmer constant. The plot showed linear dependence in the range of oxygen concentration up to 5×10^3 ppm with a $K_{SV}[O_2]$ of $1.6 \cdot 10^{-4}$ ppm^{-1}. The reversibility of the oxygen sensitivity after removal of quencher, *i. e.* oxygen, was also estimated. PL decay curves of the sample were measured after its purging with oxygen, with nitrogen and 9100 ppm of oxygen flow within cycles with the duration of 7 min for each cycle (Fig. S9e). The correlation of integrated intensity of the curves (Fig. S9e) and the medium is presented in Fig. 6d. The value of integrated intensity of the solid mixture under oxygen atmosphere represents the instrument response of the microsecond lamp and intensity of prompt fluorescence. It remains stable repeatedly after the following deoxygenation and oxygenation which shows that the delayed fluorescence is totally suppressed after oxygenation. The integrated intensity under nitrogen continuously increased over the time. Apparently, diffusion of oxygen and the film is minimized after continuous nitrogen purge. Therefore, oxygen is more efficiently removed from the sample with the additional cycles. The mentioned diffusion does not have any impact on the integrated intensity under purged oxygen as the interaction of the film with oxygen is maximal in this case. The sample also showed the definitive response to the exact value of oxygen flow manifested by the intensity level correlated to 9100 ppm (Fig. 6d).

2.6. Mechanism of the PL quenching by dioxygen

TADF quenching are determined by intermolecular electronic correlation and interaction between triplet ground state dioxygen $O_2(^3\Sigma_g^-)$ and the triplet T_1 excited organic dye ($^3M_1$*) during their collision. Depending on mutual spin orientation upon random collisions $^3O_2$ + $^3M_1$* the singlet, triplet and quintet total spin states can be realized in such temporary collision complex. Electronic correlation and configuration interaction (CI) in this open-shell system is rather complicated [33–35] but some general features can be taken into account. The singlet spin channel removes spin-forbidden character and provides effective energy transfer to the singlet $O_2(^1\Delta_g)$ dioxygen, which is the main mechanism of the TADF quenching

$$^1[^3O_2 + {}^3M_1^*] \rightarrow O_2(^1\Delta_g) + {}^1M_0 \quad (1)$$

Triplet spin orientation realized in other collisions can increase the reverse intersystem crossing (RISC) rate

$$^3[^3O_2 + {}^3M_1^*] \rightarrow O_2(^3\Sigma_g^-) + {}^1M_1^* \quad (2)$$

and partially competes with the TADF quenching. The PL from the singlet excited states of the organic dye ($^1M_1$*) in turn is quenched in the triplet collision complex

$$^3[^3O_2 + {}^1M_1^*] \rightarrow O_2(^3\Sigma_g^-) + {}^1M_0 \quad (3)$$

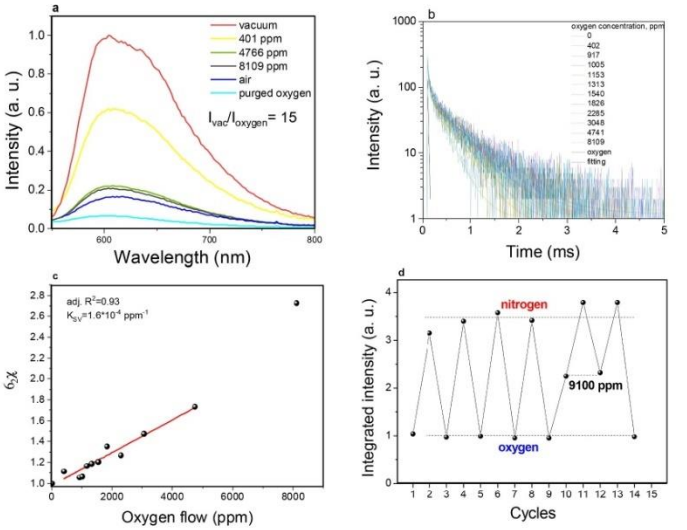

Fig. 6. PL spectra in media with different oxygen concentration (a); PL decay curves (b) and the Stern-Volmer plot (c) and oxygen response (d) for 1 wt% solid solution of ***m*PNZ** in ZEONEX®.

$$^3[^3O_2 + {}^1M_1{}^*] \rightarrow O_2(^3\Sigma_g^-) + {}^3M_1{}^* \quad (4)$$

Quantum chemical CI calculations have shown [33,34] that O_2 produces this important effect on the PL quenching, Eq. (3); in collision complex with organic dye dioxygen diminishes the radiative probability of the $S_1 - S_0$ transition in the dye, since this probability is borrowed for increase of the $T_1 - S_0$ transition. This quantum effect can be easily explained in terms of perturbation theory for intensity borrowing and is determined by exchange interaction between states of the same multiplicity, like those in Eq. (2) [35]. The quenching of radiative moment will also contribute to nonradiative relaxation by energy transfer mechanism of the type, Eq. (4) [33,35]. The most important stock of the excited singlet states is produced by the trivial mechanism of the intersystem crossing enhancement, Eq. (4), which is also spin allowed, but hindered by small statistical spin factor. Its contribution to the observed quenching of TADF in oxygen atmosphere depends also on RISC rate, Eq. (2). This back enhancement of TADF needs second collision and is the second kinetic order process. We hope that it is of minor importance.

Thus, the long-lived component of the TADF emission is essentially reduced in the presence of dioxygen, which supports the importance of the process described by Eq. (1). Efficiency of this mechanism depends on the overlap between $^3O_2$ and $^3M_1{}^*$ orbitals, their polarizability and the role of the charge-transfer interactions. The main contribution here belongs to CT of the type $O_2^- \ldots M^+$. Thus, the donor properties of the phenothiazine and phenoxazine moieties become very important in the oxygen sensing effect by the synthesized organic dyes.

The point is that the singlet excited S_1 state responsible for PL is the low-lying CT state of the HOMO-LUMO type (Fig. 3). However, the triplet T_1 state responsible for energy transfer to the singlet oxygen $O_2(^1\Delta_g)$ and for the TADF mechanism is more distorted and more localized on the benzanthrone (acceptor) moiety. Thus, both D and A components of the studied dyes are important in their PL quenching by oxygen.

All DFT calculations in this work are performed with the Gaussian 09 code [36].

3. Conclusions

Benzanthrone, as a highly rigid, planar moiety with strong electron-accepting ability, was applied for the development new TADF emitters with emission in NIR region. Four new compounds with donor-acceptor and donor-acceptor-donor structures exhibiting NIR TADF were obtained by single-step synthesis and characterized as promising candidates for application in OLEDs and optical sensors. Phenoxazine-based compound doped in 3,3′-di(9H-carbazol-9-yl)-1,1′-biphenyl was also used for the fabrication of doped TADF OLEDs with green electroluminescence and external quantum efficiency of 6.6%. Phenothiazine- and phenoxazine-based compounds with donor-acceptor structure were used as emitters for fabrication non-doped TADF OLEDs showing NIR electroluminescence. The film of molecular dispersion of phenoxazine containing compound in inert polymer ZEONEX® was used for estimation of oxygen sensing ability. The ratio of intensity of TADF taken in vacuum and of prompt fluorescence taken under oxygen purge was found to be ca. 15.2. The oxygen sensitivity of the film estimated by Stern-Volmer constant was found to be of 1.6×10^{-4} ppm^{-1}.

Author contribution statement

Uliana Tsiko designed and synthesized the materials, wrote draft of the manuscript.

Oleksandr Bezvikonnyi performed photoluminescence and oxygen sensing measurements and interpretation.

Dmytro Volyniuk investigated hole-transporting properties of the compounds, performed ionization potential measurements, contributed to writing and revising of the manuscript.

Boris F. Minaev performed DFT calculations.

Jonas Keruckas carried out electroluminescent device fabrication and characterization.

Monika Cekaviciute investigated glass forming/thermal properties of new compounds and contributed to their interpretation.

Egle Jatautiene discussed the results and reviewed the manuscript.

Viktorija Andruleviciene assisted and analyzed of DFT calculation data.

Asta Dabuliene advised and assisted with synthesis and identifications of materials.

Juozas Vidas Grazulevicius the team leader of the project, discussed the results obtained and reviewed the manuscript.

Declaration of competing interest

None.

Acknowledgment

This project has received funding from European Regional Development Fund (project No 01.2.2-LMT-K-718-01-0015) under grant agreement with the Research Council of Lithuania (LMTLT).

Appendix A. Supplementary data

Supplementary data to this article can be found online at https://doi.org/10.1016/j.dyepig.2021.109952.

References

[1] Li C, Duan R, Liang B, Han G, Wang S, Ye K, Liu Y, Yi Y, Wang Y. Deep-red to near-infrared thermally activated delayed fluorescence in organic solid films and electroluminescent devices. Angew Chem Int Ed 2017;56:11525–9. https://doi.org/10.1002/anie.201706464.

[2] Zampetti A, Minotto A, Cacialli F. Near-infrared (NIR) organic light-emitting diodes (OLEDs): challenges and opportunities. Adv Funct Mater 2019;29:1807623. https://doi.org/10.1002/adfm.201807623.

[3] Kim J, Kwon JH, Jang J, Lee H, Kim S, Hahn YK, Kim SK, Lee KH, Lee S, Pyo H, Song CS, Lee J. Rapid and background-free detection of avian influenza virus in opaque sample using NIR-to-NIR upconversion nanoparticle-based lateral flow immunoassay platform. Biosens Bioelectron 2018;112:209–15. https://doi.org/10.1016/j.bios.2018.04.047.

[4] Yu YJ, Wang XQ, Liu JF, Jiang ZQ, Liao LS. Harvesting triplet excitons for near-infrared electroluminescence via thermally activated delayed fluorescence channel. IScience 2021;24:102123. https://doi.org/10.1016/j.isci.2021.102123.

[5] Ye H, Kim DH, Chen X, Sandanayaka ASD, Kim JU, Zaborova E, Canard G, Tsuchiya Y, Choi EY, Wu JW, Fages F, Bredas JL, D'Aléo A, Ribierre JC, Adachi C. Near-infrared electroluminescence and low threshold amplified spontaneous emission above 800 nm from a thermally activated delayed fluorescent emitter. Chem Mater 2018;30:6702–10. https://doi.org/10.1021/acs.chemmater.8b02247.

[6] Shi L, Sordillo LA, Rodríguez-Contreras A, Alfano R. Transmission in near-infrared optical windows for deep brain imaging. J Biophot 2016;9:38–43. https://doi.org/10.1002/jbio.201500192.

[7] Sun L, Choi JJ, Stachnik D, Bartnik AC, Hyun BR, Malliaras GG, Hanrath T, Wise FW. Bright infrared quantum-dot light-emitting diodes through inter-dot spacing control. Nat Nanotechnol 2012;7:369–73. https://doi.org/10.1038/nnano.2012.63.

[8] Shafikov MZ, Pander P, Zaytsev AV, Daniels R, Martinscroft R, Dias FB, Williams JAG, Kozhevnikov VN. Extended ligand conjugation and dinuclearity as a route to efficient platinum-based near-infrared (NIR) triplet emitters and solution-processed NIR-OLEDs. J Mater Chem C 2021;9:127–35. https://doi.org/10.1039/d0tc04881j.

[9] Tuong Ly K, Chen-Cheng RW, Lin HW, Shiau YJ, Liu SH, Chou PT, Tsao CS, Huang YC, Chi Y. Near-infrared organic light-emitting diodes with very high external quantum efficiency and radiance. Nat Photonics 2017;11:63–8. https://doi.org/10.1038/nphoton.2016.230.

[10] Minotto A, Haigh PA, Łukasiewicz ŁG, Lunedei E, Gryko DT, Darwazeh I, Cacialli F. Visible light communication with efficient far-red/near-infrared polymer light-emitting diodes. Light Sci Appl 2020;9:2047–7538. https://doi.org/10.1038/s41377-020-0314-z.

[11] Li W, Wang B, Miao T, Liu J, Fu G, Lü X, Feng W, Wong WY. High-performance near-infrared (NIR) polymer light-emitting diodes (PLEDs) based on bipolar Ir(iii)-complex-grafted polymers. J Mater Chem C 2021;9:173–80. https://doi.org/10.1039/d0tc04377j.

[12] Uoyama H, Goushi K, Shizu K, Nomura H, Adachi C. Highly efficient organic light-emitting diodes from delayed fluorescence. Nature 2012;492:234–8. https://doi.org/10.1038/nature11687.

[13] Kaji H, Suzuki H, Fukushima T, Shizu K, Suzuki K, Kubo S, Komino T, Oiwa H, Suzuki F, Wakamiya A, Murata Y, Adachi C. Purely organic electroluminescent material realizing 100% conversion from electricity to light. Nat Commun 2015;6:1–8. https://doi.org/10.1038/ncomms9476.
[14] Li W, Li B, Cai X, Gan L, Xu Z, Li W, Liu K, Chen D, Su SJ. Tri-spiral donor for high efficiency and versatile blue thermally activated delayed fluorescence materials. Angew Chem Int Ed 2019;58:11301–5. https://doi.org/10.1002/anie.201904272.
[15] Lee DR, Kim BS, Lee CW, Im Y, Yook KS, Hwang SH, Lee JY. Above 30% external quantum efficiency in green delayed fluorescent organic light-emitting diodes. ACS Appl Mater Interfaces 2015;7:9625–9. https://doi.org/10.1021/acsami.5b01220.
[16] Karthik D, Jung YH, Lee H, Hwang S, Seo BM, Kim JY, Han CW, Kwon JH. Acceptor–donor–acceptor-type orange-red thermally activated delayed fluorescence materials realizing external quantum efficiency over 30% with low efficiency roll-off. Adv. Mater. 2021;33:2007724. https://doi.org/10.1002/adma.202007724.
[17] Leng C, You S, Si Y, Qin HM, Liu J, Huang WQ, Li K. Unraveling the mechanism of near-infrared thermally activated delayed fluorescence of TPA-based molecules: effect of hydrogen bond steric hindrance. J Phys Chem 2021;125:2905–12. https://doi.org/10.1021/acs.jpca.1c00739.
[18] Kim DH, D'Aléo A, Chen XK, Sandanayaka ADS, Yao D, Zhao L, Komino T, Zaborova E, Canard G, Tsuchiya Y, Choi E, Wu JW, Fages F, Brédas JL, Ribierre JC, Adachi C. High-efficiency electroluminescence and amplified spontaneous emission from a thermally activated delayed fluorescent near-infrared emitter. Nat Photonics 2018;12:98–104. https://doi.org/10.1038/s41566-017-0087-y.
[19] Quaranta M, Borisov SM, Klimant I. Indicators for optical oxygen sensors. Bioanal. Rev. 2012;4:115–57. https://doi.org/10.1007/s12566-012-0032-y.
[20] Steinegger A, Klimant I, Borisov SM. Purely organic dyes with thermally activated delayed fluorescence—a versatile class of indicators for optical temperature sensing. Adv. Opt. Mater. 2017;5:1700372. https://doi.org/10.1002/adom.201700372.
[21] Paisley NR, Tonge CM, Hudson ZM. Stimuli-responsive thermally activated delayed fluorescence in polymer nanoparticles and thin films: applications in chemical sensing and imaging. Front. Chem. 2020;8:229. https://doi.org/10.3389/fchem.2020.00229.
[22] Ni F, Li N, Zhan L, Yang C. Organic thermally activated delayed fluorescence materials for time-resolved luminescence imaging and sensing. Adv. Opt. Mater. 2020;8:1902187. https://doi.org/10.1002/adom.201902187.
[23] Nguyen VN, Kumar A, Lee MH, Yoon J. Recent advances in biomedical applications of organic fluorescence materials with reduced singlet-triplet energy gaps. Coord Chem Rev 2020;425:213545. https://doi.org/10.1016/j.ccr.2020.213545.
[24] Kochmann S, Baleizão C, Berberan-Santos MN, Wolfbeis OS. Sensing and imaging of oxygen with parts per Billion limits of detection and based on the quenching of the delayed fluorescence of 13C 70 fullerene in polymer hosts. Anal Chem 2013;85:1300–4. https://doi.org/10.1021/ac303486f.
[25] Zieger SE, Steinegger A, Klimant I, Borisov SM. TADF-emitting Zn(II)-Benzoporphyrin: an indicator for simultaneous sensing of oxygen and temperature. ACS Sens 2020;5:1020–7. https://doi.org/10.1021/acssensors.9b02512.
[26] Steinegger A, Borisov SM. Zn(II) schiff bases: bright TADF emitters for self-referenced decay time-based optical temperature sensing. ACS Omega 2020;5:7729–37. https://doi.org/10.1021/acsomega.0c01062.
[27] Borisov SM, Zenkl G, Klimant I. Phosphorescent platinum(II) and palladium(II) complexes with azatetrabenzoporphyrinss new-red laser diode-compatible indicators for optical oxygen sensing. ACS Appl Mater Interfaces 2010;2:366–74. https://doi.org/10.1021/am900932e.
[28] Carlini FM, Paffoni C, Boffa G. New daylight fluorescent pigments. Dyes Pigments 1982;3:59–69. https://doi.org/10.1016/0143-7208(82)80013-2.
[29] Gonta S, Utinans M, Kirilov G, Belyakov S, Ivanova I, Fleisher M, Savenkov V, Kirilova E. Fluorescent substituted amidines of benzanthrone: synthesis, spectroscopy and quantum chemical calculations. Spectrochim Acta - Part A Mol Biomol Spectrosc 2013;101:325–34. https://doi.org/10.1016/j.saa.2012.09.104.
[30] Minaev BF, Ågren H. Collision-induced b $^1\Sigma_g^+$-a $^1\Delta_g$, b $^1\Sigma_g^+$-X $^3\Sigma_g^-$ and a $^1\Delta_g$-X $^3\Sigma_g^-$ transition probabilities in molecular oxygen. J. Chem. Soc. - Faraday Trans. 1997;93:2231–9. https://doi.org/10.1039/a607263a.
[31] Wang J, Li W. Adjusting white OLEDs with yellow light emission phosphor dye and ultrathin NPB layer structure. Int J Photoenergy 2013:1–6. https://doi.org/10.1155/2013/639843. 2013.
[32] Tonge CM, Paisley NR, Polgar AM, Lix K, Algar WR, Hudson ZM. Color-tunable thermally activated delayed fluorescence in oxadiazole-based acrylic copolymers: photophysical properties and applications in ratiometric oxygen sensing. ACS Appl Mater Interfaces 2020;12:6525–35. https://doi.org/10.1021/acsami.9b22464.
[33] Minaev BF, Lunell S, Kobzev GI. Collision-induced intensity of the b1Σg+−a1Δg transition in molecular oxygen: model calculations for the collision complex O2 + H2. Int J Quant Chem 1994;50:279–92. https://doi.org/10.1002/QUA.560500405.
[34] Minaev BF. Ab initio study of the ground state properties of molecular oxygen. Spectrochim Acta - Part A Mol Biomol Spectrosc 2004;60:1027–41. https://doi.org/10.1016/S1386-1425(03)00334-2.
[35] Minaev BF, Kukueva VV, Ågren H. Configuration interaction study of the O2–C2H4 exciplex: collision-induced probabilities of spin-forbidden radiative and non-radiative transitions. J Chem Soc Faraday Trans 1994;90:1479–86.
[36] Frisch MJ, Trucks GW, Schlegel HB, Scuseria GE, Robb MB, Cheeseman JR, Scalmani G, Barone V, Menycci B, Petersson GA, Makatsuji H, Caricato M, Li X, Hratchian HP, Izmaylov AF, et al. Gaussian 09, rev. A.1. Wallingford, CT: Gaussian Inc.; 2009. https://doi.org/10.1039/FT9949001479.

Journal of Advanced Research 33 (2021) 41–51

Contents lists available at ScienceDirect

Journal of Advanced Research

journal homepage: www.elsevier.com/locate/jare

Multifunctional derivatives of pyrimidine-5-carbonitrile and differently substituted carbazoles for doping-free sky-blue OLEDs and luminescent sensors of oxygen

Uliana Tsiko [a], Oleksandr Bezvikonnyi [a], Galyna Sych [a], Rasa Keruckiene [a], Dmytro Volyniuk [a], Jurate Simokaitiene [a], Iryna Danyliv [b], Yan Danyliv [b], Audrius Bucinskas [a], Xiaofeng Tan [a], Juozas Vidas Grazulevicius [a,*]

[a] Department of Polymer Chemistry and Technology, Kaunas University of Technology, Radvilenu pl. 19, LT-50254 Kaunas, Lithuania
[b] Department of Electronic Devices, Lviv Polytechnic National University, S. Bandera 12, 79013 Lviv, Ukraine

HIGHLIGHTS

- Pyrimidine-5-carbonitrile-based compounds with efficient TADF exceeding reverse intersystem crossing rates of 10^6 s^{-1}.
- AIEE properties for the designed compounds allowing to reach PLQYs up to 50% in solid state.
- Bipolar charge-transporting properties showing hole mobility of 1.6×10^{-4} $cm^2/V \cdot s$ and electron mobility of 1.37×10^{-5} $cm^2/V \cdot s$.
- Non-doped sky-blue OLED with external quantum efficiency of 12.8%.
- Oxygen probes with fast response, high sensitivity and good stability.

GRAPHICAL ABSTRACT

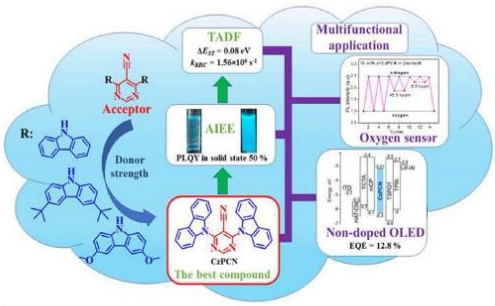

ARTICLE INFO

Article history:
Received 15 October 2020
Revised 6 January 2021
Accepted 23 January 2021
Available online 4 February 2021

Keywords:
Organic light-emitting diode
Optical sensor
Pyrimidine-5-carbonitrile
Carbazole, Thermally activated delayed fluorescence
Aggregation-induced emission enhancement

ABSTRACT

Introduction: Evolution of organic light-emitting diodes (OLEDs) reached the point, which allows to obtain maximum internal quantum efficiency of 100% partly using heavy-metal-free emitters exhibiting thermally activated delayed fluorescence (TADF). Such emitters are also predictively perfect candidates for new generation of optical sensors since triplet harvesting can be sensitive to different analytes (at least to oxygen). Although many organic TADF emitters have been reported so far as OLED emitters, the investigation of materials suitable for both OLEDs and optical sensors remains extremely rare.

Objectives: Aiming to achieve high photoluminescence quantum yields in solid-state and triplet harvesting abilities of organic semiconductors with efficient bipolar charge transport required for application in both blue OLEDs and optical sensors, symmetrical donor–acceptor-donor organic emitters containing pyrimidine-5-carbonitrile electron-withdrawing scaffold and carbazole, *tert*-butylcarbazole and methoxy carbazole donor moieties were designed, synthesized and investigated as the main objectives of this study.

Methods: New compounds were tested by many experimental methods including optical and photoelectron spectroscopy, time of flight technique, electrochemistry and thermal analyses.

Peer review under responsibility of Cairo University.
* Corresponding author.
E-mail address: juozas.grazulevicius@ktu.lt (J.V. Grazulevicius).

https://doi.org/10.1016/j.jare.2021.01.014

Results: Demonstrating advantages of the molecular design, the synthesized emitters exhibited sky-blue efficient TADF with reverse intersystem crossing rates exceeding 10^6 s^{-1}, aggregation-induced emission enhancement with photoluminescence quantum yields in solid state exceeding 50%, hole and electron transporting properties with charge mobilities exceeding 10^{-4} $cm^2/V.s$, glass-forming properties with glass transition temperatures reaching 177 °C. Sky-blue OLEDs with non-doped light-emitting layers of the synthesized emitter showed maximum external efficiency of 12.8% while the doped device with the same emitter exhibited maximum external efficiency of 14%. The synthesized emitters were also used as oxygen probes for optical sensors with oxygen sensitivity estimated by the Stern-Volmer constant of $3.24 \cdot 10^{-5}$ ppm^{-1}.

Conclusion: The developed bipolar TADF emitters with pyrimidine-5-carbonitrile and carbazole moieties showed effective applicability in both blue OLEDs and optical sensors.

Introduction

The technology of organic light emitting diodes (OLED) became one of the most expanding in the markets of displays and lighting devices [1,2]. The pressure-sensitive paint technique for luminescent sensors of oxygen is a widespread tool in various areas such as microelectronics and aerospace engineering [3–6]. Both luminescent sensor and OLED technologies require efficient metal-free emitters as an alternative of transition metals containing phosphorescent emitters which suffer from price-growing and ecological problems [7,8]. The attractive approach to solve this problems is usage of metal-free emitters exhibiting thermally activated delayed fluorescence (TADF) [9,10]. Employment of triplet excitons into luminescence of TADF emitters can break the limit of internal quantum efficiency of fluorescent OLEDs of 25% [11]. On the other hand, it is possible to use TADF emitters for fabrication of the sensors for oxygen due to the high sensitivity of excited triplet state of TADF molecules to the presence of oxygen in atmosphere [12–14]. For example, fullerene C_{70} was studied for the employment of TADF in oxygen sensing [15,16]. Potentially, TADF emitters can replace phosphorescent emissive species of electroluminescent oxygen pressure sensors. Electroluminescent pressure sensor based on oxygen quenching of electroluminescence was reported as an alternative to the conventional photoluminescent pressure-sensitive paint [17]. Taking into account that the biggest challenge of OLED technology is increase of efficiency of blue-emitting devices [18], the aim of this study was development of efficient multifunctional blue TADF emitters for OLEDs and optical sensors of oxygen.

To design efficient blue TADF emitters with appropriate charge-transporting properties required for OLEDs and with high photoluminescent quantum yields in solid-state required for both OLEDs and optical sensors, the following information was taken into account.

TADF occurs due to up-conversion of triplet excitons to the first singlet excited states through the mechanism of reverse intersystem crossing (RISC) [11]. It is facilitated by a thermal motion of atoms [19]. The small difference of energy levels between the first excited singlet (E_{S1}) and triplet (E_{T1}) excited states (ΔE_{ST}) is required for efficient RISC [20]. This condition is realized when overlap of the wavefunctions of HOMO and LUMO is minimized [21–23]. The optimal strategy for design of TADF emitters is a development of donor–acceptor or donor–acceptor-donor compounds in which HOMO is localized on an electron donating unit and LUMO is situated on an acceptor for the formation of charge transfer (CT) states [24–26].

From the investigations of Stokes reported in 1853 [27] till the introduction of the concept of aggregation-induced emission in 2001, compounds which exhibited more efficient emission in solid state than in solutions were known but they were not extensively studied [28,29]. The phenomenon of aggregation-induced emission enhancement (AIEE) is characterized by a significantly higher photoluminescence (PL) quantum yields (Φ) of the solid samples in which intramolecular vibrational and rotational motions are suppressed than of dilute solutions of compounds. Utilization of AIEE in OLEDs can help to overcome quenching of electroluminescence (EL) caused by π-π stacking in an emissive layer (EML). The promising recent area of research is development of TADF emitters exhibiting AIEE [30,31]. They are considered as promising candidates for non-doped EML of efficient OLEDs [32].

Emissive and charge-transporting properties of TADF compounds can be purposively modified by careful selection of donating and accepting moieties and the linking topology of them. Carbazole is one of the most widely used donor moieties in the design of TADF emitters [33]. Derivatives of carbazole exhibit high triplet energy, good thermal stability and hole transporting properties [11,34]. Attachment of *tert*-butyl or methoxy groups to carbazole moieties present in the molecules of emitters can lead to the suppression of the non-radiative paths of deactivation of excited states and an enhancement of TADF [26]. The increase of efficiency of TADF of the molecular mixture of cabazolyl disubstituted pyrimidine and bis[2-(diphenylphosphino)phenyl] ether oxide (DPEPO) was reached by attachment of *tert*-butyl and methyl groups to carbazole moieties [35]. The maximum value of external quantum efficiency (EQE) of the deep-blue OLED based on this molecular mixture was 8.4%. Pyrimidine-5-carbonitrile was utilized as an acceptor in TADF emitters providing uniform electron density distribution on the accepting moiety [36]. Green OLEDs based on pyrimidine-5-carbonitrile derivatives doped into 9-(30-(4,6-diphenyl-1,3,5-triazin-2-yl)-[1,10-biphenyl]-3-yl)-9H-carbazole host matrix showed EQE up to 19.8% [36]. However, blue TADF OLEDs with the emitters containing pyrimidine-5-carbonitrile acceptor moiety were not yet reported.

After analysis of the previously published approaches for efficient TADF emitters, we report on single-step synthesis and properties of new pyrimidine-5-carbonitrile and carbazole derivatives with donor–acceptor-donor structures aiming to develop efficient multifunctional blue emitters for OLEDs and optical sensors of oxygen. The obtained compounds demonstrated blue TADF and AIEE as well as high thermal and electrochemical stability and good charge-transporting properties that allowed to use them for fabrication of efficient doped and non-doped sky-blue OLEDs. In addition, the synthesized compounds were successfully utilized in highly sensitive and stable oxygen sensors. This is the first demonstration of oxygen sensing ability of pyrimidine-5-carbonitrile derivatives exhibiting TADF/AIEE.

Material and methods

General procedure of nucleophilic substitution reactions

Potassium hydroxide (2.5 eq.) was added to a solution of 9*H*-carbazole (2.5 eq.) or 3,6-di-*tert*-butyl-9H-carbazole (2.5 eq.) or

3,6-dimethoxy-9*H*-carbazole (2.5 eq.) in DMSO (25 ml). The mixture was stirred for 20 min at room temperature and then 4,6-dichloropyrimidine-5-carbonitrile (1 eq.) was added. The reaction mixture was heated to 175 °C and stirred for 1 h. After completion of the reaction, the obtained mixture was cooled down to room temperature, poured into water and filtered. The crude product was purified by column chromatography on silica gel using the eluent mixture of hexane and DCM with the volume ratio of 3:2 and recrystallized from isopropanol/DMF mixture.

4,6-Di(9*H*-carbazol-9-yl)pyrimidine-5-carbonitrile (CzPCN) was prepared from KOH (2.5 mmol, 0.28 g), 9*H*-carbazole (5 mmol, 0.84 g) and 4,6-dichloropyrimidine-5-carbonitrile (2 mmol, 0.35 g) using general procedure and yellow needle crystals were isolated in 49% yield (0.41 g). M.P.: 260–262 °C.

^{1}H NMR (400 MHz, $CDCl_3$) δ 9.34 (s, 1H), 8.06 (d, J = 7.7 Hz, 4H), 7.86 (d, J = 8.3 Hz, 4H), 7.58 – 7.48 (m, 4H), 7.39 (t, J = 7.4 Hz, 4H) ppm. ^{13}C NMR (101 MHz, $CDCl_3$) δ 161.86, 161.11, 138.46, 126.74, 125.91, 123.52, 120.71, 112.53, 112.36, 96.79 ppm. Elemental analysis: calculated for $C_{29}H_{17}N_5$, %: C, 79.98; H, 3.93; N, 16.08. Found, %: C 80.75; H 3.78; N 15.47. ESI-MS *(m/z)*: calculated for $C_{29}H_{17}N_5$, 435.48 $[M]^+$; found 457.99 $[M + Na]^+$.

4,6-bis(3,6-di-*tert*-butyl-9*H*-carbazol-9-yl)pyrimidine-5-carbonitrile (*t*CzPCN) was obtained according to general procedure from KOH (2.5 mmol, 0.28 g), 3,6-di-*tert*-butyl-9H-carbazole (5 mmol, 1.40 g) and 4,6-dichloropyrimidine-5-carbonitrile (2 mmol, 0.35 g) and yellow crystals was isolated in 36% yield (0.5 g). M.P.: 258–260 °C.

^{1}H NMR (400 MHz, $CDCl_3$) δ 9.23 (s, 1H), 8.04 (d, J = 1.5 Hz, 4H), 7.80 (d, J = 8.7 Hz, 4H), 7.57 (dd, J = 8.7, 1.8 Hz, 4H), 1.42 (s, 36H) ppm. ^{13}C NMR (101 MHz, $CDCl_3$) δ 161.81, 160.88, 146.63, 136.84, 126.10, 124.31, 116.75, 112.74, 112.33, 95.15, 34.96, 31.86 ppm. Elemental analysis: calculated for $C_{45}H_{49}N_5$, %: C, 81.90; H, 7.48; N, 10.6. Found, %: C 82.61; H 7.20; N 10.19. ESI-MS *(m/z)*: calculated for $C_{45}H_{49}N_5$, 659.90 $[M]^+$; found 682.51 $[M + Na]^+$.

4,6-bis(3,6-dimethoxy-9*H*-carbazol-9-yl)pyrimidine-5-carbonitrile (MeOCzPCN) was synthesized from KOH (2.5 mmol, 0.28 g), 3,6-dimethoxy-9*H*-carbazole (5 mmol, 1.14 g) and 4,6-dichloropyrimidine-5-carbonitrile (2 mmol, 0.35 g) by using general procedure and yellow crystals was isolated in yield 63% (0.7 g). M.P.: 286–288 °C.

^{1}H NMR (400 MHz, $(CD_3)_2SO$) δ 9.46 (s, 1H), 7.94 (d, J = 9.0 Hz, 4H), 7.88 (d, J = 2.3 Hz, 4H), 7.22 (dd, J = 9.0, 2.4 Hz, 4H), 3.94 (s, 12H) ppm. ^{13}C NMR (101 MHz, $(CD_3)_2SO$) δ 161.50, 156.21, 134.18, 133.48, 126.30, 115.56, 114.77, 104.15, 104.09, 101.50, 56.20. Elemental analysis: calculated for $C_{33}H_{25}N_5O_4$, %: C, 71.34; H, 4.54; N, 12.61; O, 11.52. Found, %: C, 72.42; H, 4.37; N, 12.13; O, 11.08. ESI-MS *(m/z)*: calculated for $C_{33}H_{25}N_5O_4$, 555.58 $[M]^+$; found 555.50 $[M + H]^+$.

Additional information on methods can be found in the supplementary information.

Results and discussion

Synthesis

4,6-Di(9*H*-carbazol-9-yl)pyrimidine-5-carbonitrile (**CzPCN**), 4,6-bis(3,6-di-*tert*-butyl-9*H*-carbazol-9-yl)pyrimidine-5-carbonitrile (***t*CzPCN**) and 4,6-bis(3,6-dimethoxy-9*H*-carbazol-9-yl)pyrimidine-5-carbonitrile (**MeOCzPCN**) were obtained by simple and inexpensive synthesis in one step *via* nucleophilic substitution reactions between 4,6-dichloropyrimidine-5-carbonitrile and carbazole derivatives. The synthetic route for the target compounds is outlined in Scheme 1. The chemical structures of the compounds were confirmed by ^{1}H and ^{13}C NMR spectroscopies, mass spectrometry and elemental analysis (SI).

Thermal, electrochemical, photoelectrical and charge-transporting properties

Thermal transitions of the synthesized compounds were investigated by thermogravimetric analysis (TGA) and differential scanning calorimetry (DSC). The results of measurements are collected in Table 1 and showed in Fig. 1*a,b*, S1. All the compounds demonstrated high thermal stability. Their values of 5% weight loss temperatures (T_d) significantly exceeded 300 °C (Fig. 1*a*). In comparison to compound **CzPCN** with T_d of 338 °C, compounds ***t*CzPCN** and **MeOCzPCN** exhibited higher T_d values of 396 °C and of 383 °C respectively. Apparently, the presence of heavy *tert*-butyl and methoxy groups in molecular structures of compounds ***t*CzPCN** and **MeOCzPCN** lead to enhancement of intermolecular interaction in the solid state. Complete weigh loss of **CzPCN** in TGA shows that the compound experienced sublimation.

All the compounds were obtained as crystalline substances after synthesis and showed two melting points in the first DSC scans (Fig. 1*b*, S1, Table 1). It can be assumed that two crystal forms of the synthesized compounds were obtained [37,38]. In the second heating scan of compound **CzPCN** (Fig. 1b) glass transition was observed at 112 °C. The further heating revealed crystallization (the temperature of crystallization (T_{cr}) was of 163 °C) and melting of only one type of polymorph at 273 °C. T_g of 177 °C was observed for compound ***t*CzPCN** in the repeated heating scan (Fig. S1b) while compound **MeOCzPCN** (Fig. S1c) did not show any capability of glass formation.

Cyclic voltammetry measurements (CV) were performed for dichloromethane (DCM) solutions of **CzPCN**, ***t*CzPCN** and **MeOCzPCN** with tetra-*n*-butylammonium hexafluorophosphate ($TBAPF_6$) as supporting electrolyte (Fig. 1c). Potentials of oxidation (E_{ox}^{onset}) and reduction (E_{red}^{onset}) half-waves and with respect to ferrocene are collected in Table 1. Using E_{ox}^{onset} and E_{red}^{onset}, the values of ionization potential (IP_{CV}) and electron affinity (EA_{CV}) were determined for the solutions of **CzPCN**, ***t*CzPCN** and **MeOCzPCN** (Table 1). The close values of IP_{CV} and EA_{CV} were observed for **CzPCN** and ***t*CzPCN** (5.82, 5.87/2.9, 2.8 eV respectively) for **CzPCN** and ***t*CzPCN** due to the similar electron-donating/electron-accepting abilities of the building moieties. Lower IP_{CV} value of **MeOCzPN** is attributed to the stronger electron-donating ability of methoxy-substituted carbazole.

Since IP_{CV} and EA_{CV} energies can not be referred to HOMO and LUMO of the studied materials [39], UV photoelectron spectrometry was further used for getting ionization potential (IP_{UPS}) and electron affinity (EA_{UPS}) for their solid-state samples (Fig. 1*d*). The values of EA_{UPS} were calculated by formula $EA_{UPS} = IP_{UPS} - E_{transport} = IP_{UPS} - E_{opt}$ assuming that the optical gaps (E_{opt}) of solid layers is approximately equal to their transport gaps ($E_{transport}$). The E_{opt} values were taken from low-energy set-on of absorption spectra of the films of **CzPCN**, ***t*CzPCN** and **MeOCzPCN** (Fig. S2). Thus, IP_{UPS} and EA_{UPS} values can be referred to the HOMO and LUMO energies of compounds **CzPCN**, ***t*CzPCN** and **MeOCzPCN** which are required for the design of appropriate structures of optoelectronic devices, OLEDs in particularly (Table 1). Higher IP_{UPS} values of **CzPCN**, ***t*CzPCN** and **MeOCzPCN** were realtive to the corresponding IP_{CV} values were observed. However, the trends of IP_{UPS} and IP_{CV} were practically the same mainly referring to the different donor substitutions. The extension on the donating carbazoles resulted in raising HOMO/LUMO energy levels.

Two representative compounds **CzPCN** and **MeOCzPCN** were selected for investigation of charge-transporting properties at room temperature. Photocurrent transients for their vacuum deposited films were recorded under positive (for holes) and negative (for electrons) polarities in time of flight (TOF) regime (Fig. 2*a*, S3). Despite of strong dispersity observed for the film of **CzPCN**, clear transit times (t_{tr}) under different electric fields could

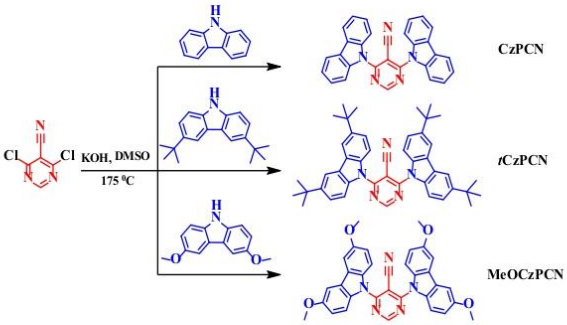

Scheme 1. Synthetic pathway to compounds **CzPCN**, ***t*CzPCN** and **MeOCzPCN**.

Table 1
Thermal, electrochemical and photoelectrical characteristics of **CzPCN**, ***t*CzPCN** and **MeOCzPCN**.

Compounds	T_d,[a] °C	T_g, °C	T_m, °C	T_{cr}, °C	E_{ox}^{onset}, V	E_{red}^{onset}, V	IP_{CV}, eV	EA_{CV}, eV	IP_{UPS}, eV	E_{opt}, eV	EA_{UPS}, eV
CzPCN	338	112[d]	273[b,d]/287[b]	277[b]/163[d]	1.02	– 1.90	5.82	2.90	6.30	2.39	3.91
***t*CzPCN**	396	177[d]	297[b]/326[b]	308[b]	1.07	– 2.00	5.87	2.80	6.10	2.47	3.63
MeOCzPN	383	–	281[b,d]/298[b,d]	283[b]/202[c]	0.76	– 1.20	5.56	3.60	5.86	2.43	3.43

[a] estimated from TGA; DSC: [b] first heating scan, [c] first cooling scan, [d] second heating scan; T_d – the temperature of 5% weight loss; T_g is glass transition temperature; T_m – melting point; T_{cr} – the temperature of crystallization; E_{ox}^{onset} and E_{red}^{onset} are onset oxidation and reduction potentials determined from CV scans of dilute DCM solutions of pyrimidine derivatives; IP_{CV}, IP_{UPS} – ionization potential and EA_{CV}, EA_{UPS} – electron affinity determined from CV and UV photoelectron spectroscopy, respectivly; E_{opt} – optical gap

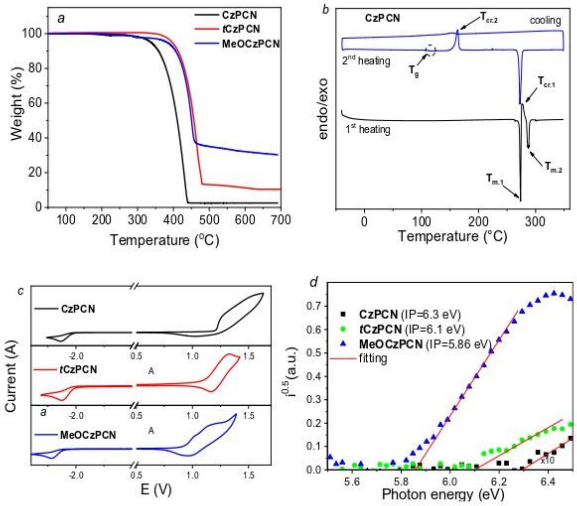

Fig. 1. TGA (*a*) and DSC (*b*) curves, cyclic voltammograms (*c*), and photoelectron emission spectra (*d*) of compounds **CzPCN**, ***t*CzPCN** and **MeOCzPCN**.

be determined for both holes and electrons from the corresponding current transients plotted in log–log scales. Similarly, t_{tr} was detected for electrons for the film of **MeOCzPCN**, while t_{tr} for holes was not detectable. Charge mobilities were calculated for **CzPCN** (for holes and electrons) and for **MeOCzPCN** (for electrons) (Fig. 2*b*). Hole mobility (μ_h) of 1.6 × 10^{-4} $cm^2/V{\cdot}s$ was observed

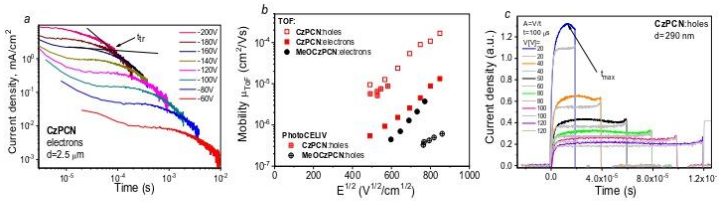

Fig. 2. Photocurrent transients for electrons for the film of compound **CzPCN** (*a*), hole/electron drift mobilities versus electric field (*E*) for the layers of the compounds **CzPCN** and **MeOCzPCN** (*b*), CELIV current transients for holes for the film of **CzPCN** (*c*).

for **CzPCN** at electric field (E) of 7.2 × 10^5 V/cm, which is close to that of many other typical carbazole-containing emitters [33], (Fig. 2*b*). Electron mobility (μ_e) of 1.37 × 10^{-5} cm^2/V·s at the same electric field. It is by ca. one magnitude lower than hole mobility. The relationship $\mu_h > \mu_e$ can be attributed to the donor–acceptor-donor molecular structure of compound **CzPCN** apparently resulting in higher HOMO-HOMO overlapping between neighbouring molecules than LUMO-LUMO overlapping.

Since it was impossible to obtain complete charge-transporting data for the studied compounds by the TOF method, charge extraction by linearly increasing voltage (CELIV) technique was applied using the thinner layers (<300 nm) [40]. The dark-CELIV (grey curves) and photo-CELIV (colour curves) current transients for holes recorded for the film **CzPCN** are plotted in Fig. 2*c*. Taking time t_{max} at the maximum of the photo-CELIV, hole mobilities were obtained for **CzPCN** at different electric fields (Fig. 2*b*). CELIV hole mobility of **CzPCN** was in good agreement with the corresponding TOF hole mobility. CELIV hole mobility was also estimated for the layer of **MeOCzPCN** (Fig. 2*b*).

Photophysical properties

UV absorption and PL spectra of the dilute solutions and of solid films of the **CzPCN**, ***t*CzPCN** and **MeOCzPCN** are presented in Fig. 3*a*, S2. The major photophysical data are summarized in Table 2. The absorption of neat films and dilute toluene solutions of the compounds in the spectral region below 330 nm corresponds to the great extent to π–π* transition of carbazole [41] (Fig. 3*a*). The positions of the lowest energy bands (LEB, Fig. S2) of the dilute solutions observed at ca. 360 nm do not fully correlate with the polarity of solvents. Nevertheless, the significant blue shifts observed for the PL spectra of the solutions in polar solvents such as acetonitrile (MeCN) and acetone relative to the spectra of the solutions in less polar dichloromethane (DCM) and tetrahydrofuran (THF) are attributed to the state of intramolecular CT from carbazole-based donors to the acceptor. Attachment of *tert*-butyl groups to carbazole units in ***t*CzPCN** resulted in the redshift of LEB compared to that of **CzPCN**. Even bigger bathochromic shift was caused by the presence methoxy groups in **MeOCzPCN**. These observations can be explained by prolonged π-conjugation of *tert*-butyl or methoxy substituted carbazole moieties [36]. Intermolecular interactions enhanced in the solid state caused redshifted and broadened LEB of neat films relative to those of the solutions. The E_g values were estimated from the plot presented in Fig. 3*b*. They were found to be of 3.09, 3.08 and 2.9 eV for **CzPCN, *t*CzPCN** and **MeOCzPCN**, respectively. The Kubelka-Munk plot is used for organic semiconductors in solid amorphous layers of OLEDs as they are commonly characterized by a near flat energy bands and direct allowed transitions [42]. The $F(R)\cdot E_{ph}$ plot is based on equation $F(R) = \frac{(1-0.1^A)^2}{2A\cdot 0.1^A}$, $F(R) = \frac{(1-0.1^A)^2}{2A\cdot 0.1^A}$. *A* and E_{ph} stand for absorbance of neat films in our case and photon energy, respectively. *F(R)* is the so-called remission, Kubelka-Munk function.

In order to examine the benefits of tuning emissive properties by electronic excitation energy transfer from host to guest, solid mixtures of the compounds and 1,3-bis(N-carbazolyl)benzene (mCP) with a doping concentration of 10% were investigated. The results are presented in Fig. S2. PL spectra of solutions, doped and non-doped films of the studied compounds contain a single narrow peak in sky-blue/green region with no signs of subvibronic distribution (Fig. 3*a*, S2). Due to guest:host interactions with the weakly polar mCP [43], the difference in energy levels of ground and first excited states of compounds is changed [44] leading to the pronounced blue shifts by 15–40 nm of PL spectra of the films of 10 wt% solid solutions of the compounds in mCP films in comparison with those neat films.

Photoluminescence quantum yields (*Φ*) of toluene solution of **CzPCN** is lower that of THF solution highlighting the intrinsic polarity of the compound and the consequent apparent hypsochromic shift of PL spectrum of the film of the molecular mixture **CzPCN**:mCP compared to that of the film of **CzPCN**. The *Φ* values of the films are higher than those of the solutions which is a mastifestation of AIEE effect. The only exclusion is the *Φ* values observed **MeOCzPCN** which were found to be similar (of ca. 2%) for the solid samples and dilute solutions. The bathochromic shift of PL spectral peak with the increase of polarity of solvents (Fig. S2) is a clear evidence of intramolecular CT state of emission. The solvatochromic effect of absorption and emission of solutions was studied in more in detail for examination of polarity of the compounds. Based on the Onsager interpretation of non-specific interactions between particles and solvent [45], the Lippert-Mataga correlation [46,47] of a Stokes shift $\Delta\nu$ and an orientation polarizability Δf $\Delta\nu = \frac{2\Delta f}{4\pi\varepsilon_0 hca^3}(\mu_e - \mu_g)^2 + \Delta\nu^0$is plotted in Fig. S5 (adjusted R^2 of 0.92–0.97): $\Delta\nu = \frac{2\Delta f}{4\pi\varepsilon_0 hca^3}(\mu_e - \mu_g)^2 + \Delta\nu^0$. The Stokes shift in the condition of absence of solvent is denoted as $\Delta\nu^0$. *a* is an Onsager cavity radius. The obtained slopes are related to the change of dipole moment of compounds in ground μ_g and excited μ_e state revealing a significant intrinsic polarity of the compounds owing to the donor–acceptor-donor structure. The slopes of ca. 9.4·10^3 cm^{-1} observed for **CzPCN** and ***t*CzPCN** are larger than that recorded for **MeOCzPCN** (7.5·10^3 cm^{-1}). Based on these data, **CzPCN** and ***t*CzPCN** can be characterized by stronger intramolecular CT than **MeOCzPCN** showing that for the designed donor–acceptor-donor structures based on the pyrimidine-5-carbonitrile accepting unit attachment of the methoxy groups to carbazoles resulted in suppressing of intramolecular CT and quantum yields.

Thermally activated delayed fluorescence

The intensity of PL of toluene solutions and neat films of the compounds was found to be considerably higher in the absence

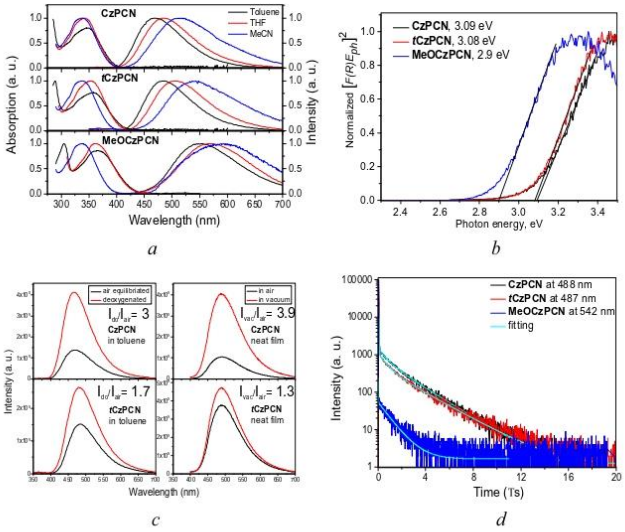

Fig. 3. *a*) Absorption spectra and normalized PL spectra of dilute 10^{-5} M toluene, THF and MeCN solutions of **CzPCN**, ***t*CzPCN** and **MeOCzPCN**; *b*) Kubelka-Munk plot for neat films; *c*) PL spectra of air equilibrated and deoxygenated dilute 10^{-5} M toluene solutions and of neat films recorded in air and in vacuum; *d*) PL decay curves of neat films.

Table 2
Photophysical characteristics of **CzPCN**, ***t*CzPCN**, **MeOCzPCN**.

Compounds/ Parameters	CzPCN	*t*CzPCN	MeOCzPCN
$\Phi^{toluene}$ (%)	2 (6*)	12 (21*)	3
Φ^{THF} (%)	15	12	1
$\Phi^{\#}$ (%)	33 (53*)	20 (25*)	2
$\Phi^{\#}_{PF}$ (%)	14	7	~0.2
$\Phi^{\#}_{DF}$ (%)	39	19*	~1.8
$\tau_{PF}{}^{\#}$ (ns)	12.9	12.2	11.4
$\tau_{DF}{}^{\#}$ (μs)	2.1	2.3	1
$\chi^{2\,\#}$	1.111	1.109	1.016
k_{RISC} (10^6 s^{-1}) #	1.56	1.32	–
k_{ISC} (10^7 s^{-1}) #	5.73	6.06	–
$E_{S1,\ THF}$ (eV)	3.17	3.02	2.89
$E_{T1,\ THF}$ (eV)	3.03	2.93	2.88
$\Delta E_{ST,\ THF}$ (eV)	0.14	0.09	0.01
$E_{S1,\ mCP}$ (eV)	2.99	2.93	2.74
$E_{T1,\ mCP}$ (eV)	2.91	2.86	2.71
$\Delta E_{ST,\ mCP}$ (eV)	0.08	0.07	0.03

Estimated by the measurements: #of neat films; *upon removing oxygen; χ^2 is a weighted sum of squares of deviations of calculated points of multiexponential fitting of a PL decay curve. The empirical formula E_{ph} [eV] = 1239.84/ λ [nm] was used to estimate energy levels of E_{S1} and E_{T1}, where λ is a wavelengths of onset of fluorescence and phosphorescence spectral bands.

of oxygen compared to that of air equilibrated samples (Fig. 3*c*). For **CzPCN** the increase was substantially higher reaching the factor of 3–3.85. The increase of emission intensity after deoxygenation is ascribed to delayed fluorescence (DF) [10]. After removal of oxygen, the spectral shape remained the same. This observation shows, that the excitons utilized in DF are recombined radiatively from the same energy levels as for prompt fluorescence (PF) pointing to the triplet up-conversion via RISC. Supressing interactions between molecules of the studied compounds and oxygen quenches non-radiative pathes of deactivation of excitation via energy thus stimulating RISC.

Multiexponential fitting of PL decay curves (Fig. 3*d*) of neat films of the compounds revealed PF with the lifetime (τ_{PF}) of ca12 ns and DF with the lifetime (τ_{DF}) in a μs range (Table 2). Rate constants of RISC and intersystem crossing (ISC), k_{RISC} and k_{ISC} respectively, can be estimated using formulas $k_{RISC} = \frac{(\Phi_{PF}+\Phi_{DF})\Phi_{ISC}}{\tau_{DF}\Phi_{PF}}$, $k_{ISC} = \frac{\Phi_{DF}}{\tau_{PF}(\Phi_{PF}+\Phi_{DF})}$, where Φ_{PF}, Φ_{DF} and Φ_{RISC} stand for yields of PF, DF and RISC respectively [23]. Knowing $\Phi = \Phi_{PF} + \Phi_{DF} = \frac{\Phi_{PF}}{1-\Phi_{ISC}\Phi_{RISC}}$ and that the maximum value of ISC yield Φ_{ISC} is limited by a quantity of electronic excitation energy not utilized in PF, the equation for estimation of k_{RISC} is simplified to $k_{RISC} = \frac{\Phi_{DF}}{\tau_{DF}\Phi_{PF}(1-\Phi_{PF})}$. Φ_{DF} values are recalculated according to the increase of PL intensity of neat films after degazation (Fig. 3*c*) [48]. The obtained values of k_{RISC} of 1.3–1.6·10^6 s^{-1} and k_{ISC} of ~ 0.6·10^8 s^{-1} for **CzPCN** and ***t*CzPCN** were found to be competitive with the characteristics of TADF emitters such as 1,2,3,5-tetrakis(carbazol-9-yl)-4,6-dicyanoben zene (4CzIPN) [25] or derivatives of pyrimidine-5-carbonitrile and carbazole [36] (Table 2, S1). The fast RISC and ISC are due to satisfactory values of ΔE_{ST} which did not exceed 140 meV. The values of ΔE_{ST} were obtained from the fluorescence and phosphorescence spectra of the solutions of the compounds recorded at liquid nitrogen temperature (Fig. S6, Table 2). The Φ_{DF}/Φ_{PF} of 10.41 was estimated for the film of **MeOCzPCN** in air. This observation explains the failure of the measurement of increase of PL intensity in a vacuum condition, since TADF appeared even in presence of oxygen. Taking into account negative effect of methoxy substitution of carbazoles on overall CT performance and corresponding low Φ values for **MeOCzPCN** it can be presumed, that most of excitons are deactivated through non-radiative ways making the proper estimation of rate constants problematic. The obtained value of k_{RISC} of ~ 10^7 s^{-1}

is an approximated exaggerated to a great extent value. The lowest ΔE_{ST} of 10 meV observed in the series of investigated emitters is suitable for efficient triplet up-conversion partially explaining the obtained high value of k_{RISC} [23].

The solid molecular mixtures of the studied compounds and mCP were studied. Phosphorescence and PL spectra of the doped films correspond to the respective spectra of neat films with the slight redshifts (Fig. S2) caused by dipolar interactions of guest and host. Doping of **CzPCN** and ***t*CzPCN** into mCP matrix resulted in the reduction of ΔE_{ST} as it is linked to the spin-vibronic coupling of local excited and CT states which are strongly affected to the polarity and rigidity of the host [23,49]. Experimental results of the measurements at 77 K are collected in (Table 2).

PL spectra and decay curves of the films of the molecular mixtures were recorded at different temperatures. They are presented in Fig. 4, S7-9. PL spectra the films remained steady over heating when the samples were degassed (Fig. 3*c*). Due to low ΔE_{ST} (up to 80 meV, Table 2), deactivation of excitons occurred via phosphorescence, PF and DF at different temperatures from excited states having similar energy levels, which is typical for compounds exhibiting TADF. As it is evident from PL decay curves, the intensity of phosphorescent component was quenched over heating due to rapidly enhanced interactions with oxygen. Simultaneously, thermal activation of DF resulted in the essential increase of TADF intensity at the temperatures exceeding 180 K.

To exclude triplet–triplet annihilation utilizing higher triplet excited states T_2, T_3 etc., investigation of power dependence of DF was performed (Fig. S10). The linear plot (fitting slope of 0.98–1.04) of the DF integrated intensity versus excitation dose of laser beam in the logarithmic scale in the whole range of intensity of excitation points to TADF.

Aggregation induced emission enhancement

The dispersions of **CzPCN** and ***t*CzPCN** in THF/water mixtures were prepared for investigation of AIEE characteristics of the compounds. The dependencies of PL intensities on water fraction are shown in Fig. 4*c,d*. The PL spectra and the relative correlation of the peak wavelengths and emission intensities are presented in Fig. S11. As it may be seen from the graphs and photos (Fig. 4*c*, *d*), at low water fractions (f_w) the dispersions of both the compounds are poorly emissive. Decrease of PL intensity in the range f_w below 40% is ascribed to the emission quenching due to an exhaustion of electronic excitation energy by intramolecular rotations. The bathochromic shift by nearly 50 nm with the increase of water fraction from 0 to 40% is caused by the increase of concentration of highly polar water influencing strong intramolecular CT processes in the emitters which is an additional reason of PL quenching. At high f_w both compounds emit blue light with the intensity maxima at ca.480 nm as the molecules being insoluble in water form aggregates. Consequently, there is a rapid increase of intensity at f_w > 70% for the dispersions of **CzPCN** and for ***t*CzPCN** in the range of f_w from 40 to 60% due to AIEE since the rotation motions of moieties of the compounds are restricted in solid state. The following decrease of PL intensity at f_w exceeding 70% observed for the dispersion of ***t*CzPCN** is explained by the formation of precipitates of a significant size. It is important to note that obtained results do not necessarily mean the decrease of Φ upon aggregation for the dispersions of ***t*CzPCN** in THF/water mixtures at high f_w.

Performance in OLEDs

Taking into account TADF and AIEE capabilities as well as bipolar charge transport and appropriate HOMO/LUMO levels for charge injections from electrodes, the synthesized compounds can be regarded as promising for doping free devices. The series of OLEDs N1-N3 with the structure of ITO / HAT-CN (10 nm) / TCTA (30 nm) / mCP (7 nm) / EML (25 nm) / TSPO1 (3 nm) / TPBi (30 nm) / LiF (0.4 nm) / Al were fabricated in order to test the layers of **CzPCN**, ***t*CzPCN** and **MeOCzPCN** as non-doped light-emitting layers, respectively. Major electroluminescent data are collected in

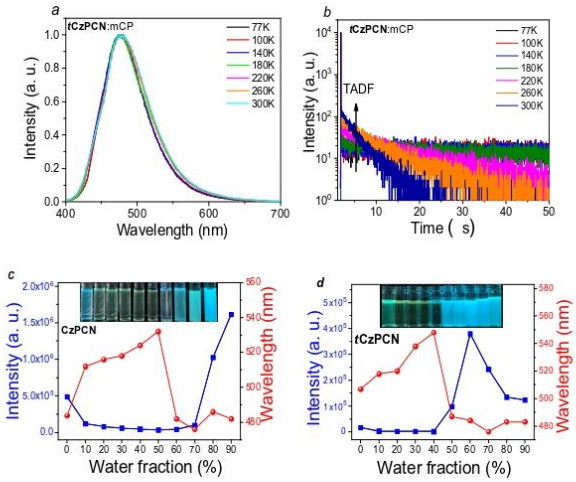

Fig. 4. Normalized PL spectra (*a*) and PL decay curves (*b*) recorded at the different temperatures under N_2 atmosphere for 10 wt% solid solution of ***t*CzPCN** in mCP. Plots of PL intensities and peak wavelengths versus f_w of the dispersions of **CzPCN** (*c*) and ***t*CzPCN** (*d*) in THF/water mixtures.

Table 3, Fig. 5, S12. Dipyrazino[2,3-f:2′,3′-h]quinoxaline-2,3,6,7,10,11-hexacarbonitrile (HAT-CN) and LiF were employed for the injection of charge carriers. The layers of tris(4-carbazoyl-9-ylphenyl)amine (TCTA) and 2,2′,2″-(1,3,5-benzinetriyl)-tris(1-phenyl-1-H-benzimidazole) (TPBi) were utilized as the hole and electron transporting layers, respectively. 1,3-bis(N-carbazolyl)benzene (mCP) and diphenyl[4-(triphenylsilyl)phenyl]phosphine oxide (TSPO1) were employed for the blocking electrons and holes, respectively. The electrodes were indium-tin oxide (ITO) and aluminium. For the studied derivatives negative values of IP_{UPS} were taken as a HOMO value and LUMO energy levels were estimated by an addition of E_g calculated from Kubelka-Munk plot to HOMO values (Fig. 5*a*).

The EL spectral characteristics of the compounds are in an accordance with the PL properties (Fig. 3*a*, 5*b*). As it can be seen from EL spectra and corresponding CIE coordinates (Fig. 5*b*, S12), OLEDs containing emitting layers of **CzPCN**, ***t*CzPCN** emit near sky-blue range while **MeOCzPCN** is a totally green emitter.

Taking into account the out-coupling factor, it is evident that the obtained maximum values of EQE of the devices (Table 3) correlate with the values of Φ of the neat films of the compounds (Table 2). This observation is an indication of the excellent charge balance in EML. Device N1 exhibited maximum EQE of 12.8% of which is practically the same as for the corresponding doped device D1 which will be discussed below. Much lower maximum EQE of 5.1% was obtained for the non-doped ***t*CzPCN**-based device **N2** (Table 3).

Aiming to obtain better hole-electron balance within the light-emitting layers, the structure of OLEDs was additionally modified by insertion of guest:host system instead of neat EML. The characteristics of OLEDs based on **CzPCN**, ***t*CzPCN** and **MeOCzPCN** 10 wt% doped into mCP were investigated in detail. The series of devices D1-D3 respectively were fabricated. As it was mentioned above, device D1 showed a slight improvement of efficiency compared device N1. Meanwhile, efficiency of OLED D2 was significantly higher than that of N2 (EQE of 5.1 and 13.7%). This observation can apparently be attributed to better hole-electron balance in doped light-emitting layer of device D2 compared to that of non-doped device N2.

Unlike OLEDs with neat films of **CzPCN** and ***t*CzPCN**, devices with doped EML of these emitters exhibited practically close to identical efficiencies and EL spectra. High efficiency OLED based on EML of ***t*CzPCN** doped in mCP can be additionally explained by suppression of non-radiative ways of relaxation of excited states. Analogous improvement was not achieved for device based on the emitter with methoxy groups since this derivative exhibited low photoluminescence quantum yield (Table 2). Efficiency roll-off evident form the rapid decline of efficiency at 100 cd/m^2 of L is bigger for device D3 than for N3 despite the exhibition of the same maximum EQE of 1.4%. This observation can apparently be explained by the non-ideal host–guest interaction. The incomplete energy transfer from host to **MeOCzPCN** is manifested by the presence of EL spectral band of D3 at ca.380 nm, typical for mCP [50]. It also caused a substantial shift of CIE coordinates to those of blue color.

Oxygen sensitivity

Interactions with oxygen are mostly responsible for the non-radiative deactivation of excitations through the energy losses. Taking pronounced AIEE properties into account, and high values of photoluminescence quantum yield in solid-state, **CzPCN** and ***t*CzPCN** were selected for the investigation of the optical oxygen sensitivity. The 10 wt% solid solutions of the compounds in rigid matrix were prepared to detect collisional quenching of a luminophore. Zeonex® was selected as a matrix because of its well-studied ability of supressing intermolecular interactions [51–53]. The samples were put into an inert atmosphere of nitrogen. Upon increasing of oxygen concentration the PL intensity continuously dropped (Fig. 6*a*,*b*, S14). No any significant difference in intensity in the same conditions over time was detected showing a great immediate response to the molecules of oxygen and a great stability of the emission.

PL decay curves of the solid solutions of **CzPCN** and ***t*CzPCN** in Zeonex® were recorded under nitrogen and oxygen conditions to study the impact of collisional quenching on emissive characteristics of the systems (Fig. 6*c*, S13). The long-lived component of the emission was drastically reduced in the presence of oxygen, espe-

Table 3
Summary of OLED parameters.

OLED	EML	L_{max}, 10^{3}cd/m^2	η_c, cd/A	η_p, lm/W	λ_{EL}, nm	EQE, %	CIE 1931
N1	**CzPCN**	13.1	32.4 (17.5)	18.8 (9.2)	494	12.8 (6.9)	(0.20, 0.36)
D1	**CzPCN**:mCP	23.1	33.3 (17.6)	20.2 (9.1)	489	14 (7.4)	(0.18, 0.33)
N2	***t*CzPCN**	13.2	12.3 (9.9)	4.6 (3.6)	490	5.1 (4.1)	(0.19, 0.35)
D2	***t*CzPCN**:mCP	14.8	33.7 (19.4)	18 (8.7)	490	13.7 (7.9)	(0.18, 0.35)
N3	**MeOCzPCN**	9.3	4.0 (3.4)	2.1 (1.6)	524	1.4 (1.2)	(0.30, 0.49)
D3	**MeOCzPCN**:mCP	13.7	3.8 (0.6)	1.2 (0.3)	500	1.4 (0.2)	(0.21, 0.43)

L_{max} – maximum brightness. η_c and η_p – maximum current and power efficiency, respectively. λ_{EL} – wavelength of EL spectral peak at 8 V. Efficiency values at L of 100 cd/m^2 are showed in parentheses.

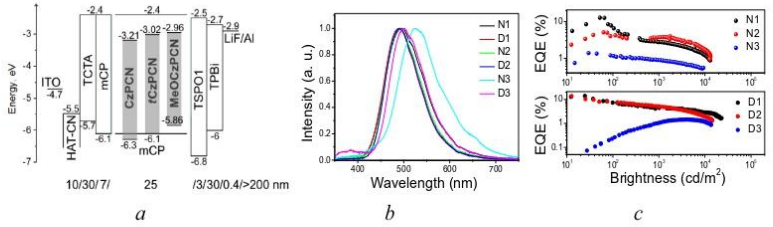

Fig. 5. OLEDs N1-N3 and D1-D3: *a*) Equilibrium energy diagram and structure; *b*) normalized EL spectra recorded at 8 V; *c*) EQE.

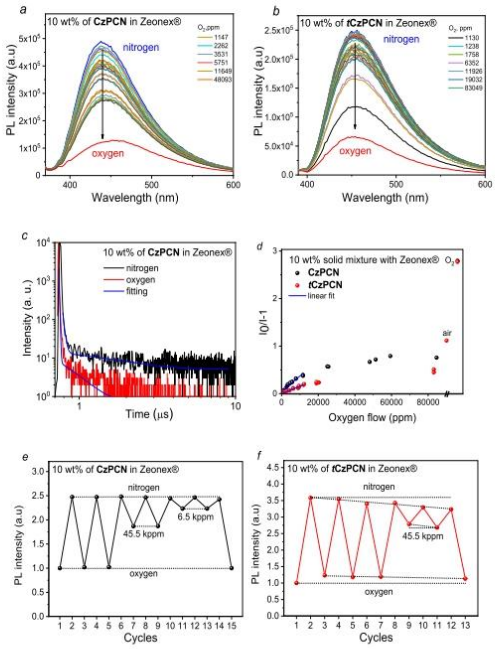

Fig. 6. PL spectra (*a, b*) and PL decays (*c*) of 10 wt% solid solutions of **CzPCN** (*a, c*) or **tCzPCN** (*b*) in Zeonex® recorded in different atmosphere at room temperature; *d*) Stern-Volmer plots and oxygen response (*e, f*) of the films of 10 wt% solid solutions of **CzPCN** (*e*) and **tCzPCN** (*f*) in Zeonex®.

cially for the solid solutions of **CzPCN**. In PL decay curve of the solid solution of this compound DF is almost absent. Stern-Volmer relation of $\frac{I_0}{I} - 1$ and oxygen flow (Fig. 6*d*) demonstrated the oxygen sensitivity in the wide range of the oxygen flow corresponding to the oxygen partial pressure [54]. Since the fluorophore quenching by oxygen is a dynamic process, the correlation is linear. However, as expected for dye:matrix systems, downward curvature [48] takes place at the oxygen flow exceeding 20000 ppm. According to the Stern-Volmer equation, the well-known characteristic of optical sensors Stern-Volmer constant $K_{SV} = \frac{I_0}{I} - 1$ was estimated from the slope of the linear fit as it is shown in Fig. 6*d* (adjusted R^2 are 0.94 and 0.97 for the samples containing **CzPCN** and **tCzPCN**, respectively) [48]. K_{SV} was calculated to be $3.24 \cdot 10^{-5}$ and $1.49 \cdot 10^{-5}$ ppm^{-1} for the solid dispersions of **CzPCN** and **tCzPCN** in Zeonex®, respectively. These values are comparable with that of TADF oxygen probes [55]. They are slightly lower than K_{SV} values earlier observed for phosphorescent oxygen probes with long-lived emission (>1 ms) [56,57]. Taking into account that the oxygen sensing properties correlate with TADF, thermal motions of molecules activate RISC at elevated temperatures and consequently the oxygen sensitivity is expected to be enhanced [19]. The synthesized compounds have a great potential for the application as optical oxygen sensors reaching necessary requirements: a) fast response to the oxygen postulated from the stability of PL quenching over time; b) sustainable oxygen sensitivity; c) good quality of the films of solid dispersions in Zeonex®; d) appropriate thermal stability and photophysical properties described above [48].

Conclusions

Exploiting donor–acceptor-donor molecular structure, simple cost-effective synthesis of new sky-blue luminophores containing pyrimidine-5-carbonitrile electron-withdrawing scaffold and electron-donating carbazole, *tert*-butylcarbazole or methoxy carbazole moieties were developed. Using the synthesized compounds as blue emitters, maximum external quantum efficiencies of 12.8 and 14% of were achieved for non-doped and doped electroluminescent devices respectively. Such performances were observed due to bipolar charge transport, thermal stability, and high photoluminescent quantum efficiency in solid state of the newly developed emitters. The different donor substitution of pyrimidine-5-carbonitrile unit affects the thermally activated delayed fluorescence and aggregation-induced emission enhancement properties of the compounds giving a path for oxygen sensor application. The developed oxygen sensor showed good sensitivity characterized by Stern-Volmer constant of $3.24 \cdot 10^{-5}$ ppm^{-1}. They were characterized by high stability and repeatability of the sensitivity.

Declaration of Competing Interest

The authors declare that they have no known competing financial interests or personal relationships that could have appeared to influence the work reported in this paper.

Acknowledgements

This project has received funding from European Regional Development Fund (project No 01.2.2-LMT-K-718-01-0015) under grant agreement with the Research Council of Lithuania (LMTLT).

Appendix A. Supplementary data

Supplementary data to this article can be found online at https://doi.org/10.1016/j.jare.2021.01.014.

References

[1] Savage N. Tomorrow's industries: from OLEDs to nanomaterials. Nature 2019;576:S20–2. doi: https://doi.org/10.1038/d41586-019-03764-1.
[2] Leo K. Organic light-emitting diodes: Efficient and flexible solution. Nat Photonics 2011;5:716–8. doi: https://doi.org/10.1038/nphoton.2011.288.
[3] Gregory JW, Asai K, Kameda M, Liu T, Sullivan JP. A review of pressure-sensitive paint for high-speed and unsteady aerodynamics. Proc Inst Mech Eng Part G J Aerosp Eng 2008;222:249–90. doi: https://doi.org/10.1243/09544100JAERO243.
[4] Gregory JW, Sakaue H, Liu T, Sullivan JP. Fast pressure-sensitive paint for flow and acoustic diagnostics. Annu Rev Fluid Mech 2014;46:303–30. doi: https://doi.org/10.1146/annurev-fluid-010313-141304.
[5] Huang CY, Matsuda Y, Gregory JW, Nagai H, Asai K. The applications of pressure-sensitive paint in microfluidic systems. Microfluid Nanofluidics 2015;18:739–53. doi: https://doi.org/10.1007/s10404-014-1510-z.
[6] Matsuda Y, Uchida T, Suzuki S, Misaki R, Yamaguchi H, Niimi T. Pressure-sensitive molecular film for investigation of micro gas flows. Microfluid Nanofluidics 2011;10:165–71. doi: https://doi.org/10.1007/s10404-010-0664-6.
[7] Yersin H. Highly Efficient OLEDs with Phosphorescent Materials 2008. doi: https://doi.org/10.1002/9783527621309.
[8] Minaev B, Baryshnikov G, Agren H. Principles of phosphorescent organic light emitting devices. PCCP 2014;16:1719–58. doi: https://doi.org/10.1039/c3cp53806k.
[9] Tao Y, Yuan K, Chen T, Xu P, Li H, Chen R, et al. Thermally activated delayed fluorescence materials towards the breakthrough of organoelectronics. Adv Mater 2014;26:7931–58. doi: https://doi.org/10.1002/adma.201402532.
[10] Adachi C. Third-generation organic electroluminescence materials. Jpn J Appl Phys 2014;53. doi: https://doi.org/10.7567/JJAP.53.060101.
[11] Uoyama H, Goushi K, Shizu K, Nomura H, Adachi C. Highly efficient organic light-emitting diodes from delayed fluorescence. Nature 2012;492:234–8. doi: https://doi.org/10.1038/nature11687.
[12] Minaev B. Photochemistry and spectroscopy of singlet oxygen in solvents. Recent advances which support the old theory. Chem Chem Technol 2016;10:519–30.
[13] Paisley NR, Tonge CM, Hudson ZM. Stimuli-Responsive Thermally Activated Delayed Fluorescence in Polymer Nanoparticles and Thin Films: Applications in Chemical Sensing and Imaging. Front Chem 2020;8. doi: https://doi.org/10.3389/fchem.2020.00229.
[14] Méhes G, Nomura H, Zhang Q, Nakagawa T, Adachi C. Enhanced electroluminescence efficiency in a spiro-acridine derivative through thermally activated delayed fluorescence. Angew Chemie - Int Ed 2012;51:11311–5. doi: https://doi.org/10.1002/anie.201206289.
[15] Kochmann S, Baleizão C, Berberan-Santos MN, Wolfbeis OS. Sensing and imaging of oxygen with parts per Billion limits of detection and based on the quenching of the delayed fluorescence of 13C 70 fullerene in polymer hosts. Anal Chem 2013;85:1300–4. doi: https://doi.org/10.1021/ac303486f.
[16] Berberan-Santos MN, Garcia JMM. Unusually strong delayed fluorescence of C70. J Am Chem Soc 1996;118:9391–4. doi: https://doi.org/10.1021/ja961782s.
[17] Matsuda Y, Ueno K, Yamaguchi H, Egami Y, Niimi T. Organic electroluminescent sensor for pressure measurement. Sensors (Switzerland) 2012;12:13899–906. doi: https://doi.org/10.3390/s121013899.
[18] Giebink NC, D'Andrade BW, Weaver MS, MacKenzie PB, Brown JJ, Thompson ME, et al. Intrinsic luminance loss in phosphorescent small-molecule organic light emitting devices due to bimolecular annihilation reactions. J Appl Phys 2008;103. doi: https://doi.org/10.1063/1.2884530.
[19] Ogiwara T, Wakikawa Y, Ikoma T. Mechanism of intersystem crossing of thermally activated delayed fluorescence molecules. J Phys Chem A 2015;119:3415–8. doi: https://doi.org/10.1021/acs.jpca.5b02253.
[20] Zhang Q, Li B, Huang S, Nomura H, Tanaka H, Adachi C. Efficient blue organic light-emitting diodes employing thermally activated delayed fluorescence. Nat Photonics 2014;8:326–32. doi: https://doi.org/10.1038/nphoton.2014.12.
[21] Wong MY, Zysman-Colman E. Purely Organic Thermally Activated Delayed Fluorescence Materials for Organic Light-Emitting Diodes. Adv Mater 2017;29. doi: https://doi.org/10.1002/adma.201605444.
[22] Dias FB, Bourdakos KN, Jankus V, Moss KC, Kamtekar KT, Bhalla V, et al. Triplet harvesting with 100% efficiency by way of thermally activated delayed fluorescence in charge transfer OLED emitters. Adv Mater 2013;25:3707–14. doi: https://doi.org/10.1002/adma.201300753.
[23] Dias FB, Penfold TJ, Monkman AP. Photophysics of thermally activated delayed fluorescence molecules. Methods Appl Fluoresc 2017;5. doi: https://doi.org/10.1088/2050-6120/aa537e.
[24] Liu Y, Li C, Ren Z, Yan S, Bryce MR. All-organic thermally activated delayed fluorescence materials for organic light-emitting diodes. Nat Rev Mater 2018;3. doi: https://doi.org/10.1038/natrevmats.2018.20.
[25] Hosokai T, Matsuzaki H, Nakanotani H, Tokumaru K, Tsutsui T, Furube A, et al. Evidence and mechanism of efficient thermally activated delayed fluorescence promoted by delocalized excited states. Sci Adv 2017;3. doi: https://doi.org/10.1126/sciadv.1603282.
[26] Chan CY, Cui LS, Kim JU, Nakanotani H, Adachi C. Rational Molecular Design for Deep-Blue Thermally Activated Delayed Fluorescence Emitters. Adv Funct Mater 2018;28. doi: https://doi.org/10.1002/adfm.201706023.
[27] Stokes GG. LXI. On the metallic reflexion exhibited by certain non-metallic substances . London, Edinburgh, Dublin Philos Mag J Sci 1853;6:393–403. https://doi.org/10.1080/14786445308647395.
[28] Luo J, Xie Z, Xie Z, Lam JWY, Cheng L, Chen H, et al. Aggregation-induced emission of 1-methyl-1,2,3,4,5-pentaphenylsilole. Chem Commun 2001;18:1740–1. doi: https://doi.org/10.1039/b105159h.
[29] Chen Y, Lam JWY, Kwok RTK, Liu B, Tang BZ. Aggregation-induced emission: Fundamental understanding and future developments. Mater Horizons 2019;6:428–33. doi: https://doi.org/10.1039/c8mh01331d.
[30] Guo J, Zhao Z, Tang BZ. Purely Organic Materials with Aggregation-Induced Delayed Fluorescence for Efficient Nondoped OLEDs. Adv Opt Mater 2018;6. doi: https://doi.org/10.1002/adom.201800264.
[31] Danyliv Y, Lytvyn R, Volyniuk D, Bezvikonnyi O, Hladka I, Grazulevicius JV. Derivatives of carbazole and chloropyridine exhibiting aggregation induced emission enhancement and deep-blue delayed fluorescence. Dye Pigment 2018;149:588–96. doi: https://doi.org/10.1016/j.dyepig.2017.11.027.
[32] Rizzo F, Cucinotta F. Recent Developments in AIEgens for Non-doped and TADF OLEDs. Isr J Chem 2018;58:874–88. doi: https://doi.org/10.1002/ijch.201800049.
[33] Wex B, Kaafarani BR. Perspective on carbazole-based organic compounds as emitters and hosts in TADF applications. J Mater Chem C 2017;5:8622–53. doi: https://doi.org/10.1039/c7tc02156a.
[34] Kimoto A, Cho JS, Higuchi M, Yamamoto K. Synthesis of asymmetrically arranged dendrimers with a carbazole dendron and a phenylazomethine dendron. Macromolecules 2004;37:5531–7. doi: https://doi.org/10.1021/ma0499674.
[35] Serevičius T, Skaisgiris R, Fiodorova I, Steckis V, Dodonova J, Banevičius D, et al. Achieving efficient deep-blue TADF in carbazole-pyrimidine compounds. Org Electron 2020;82. doi: https://doi.org/10.1016/j.orgel.2020.105723.
[36] Jang JS, Lee HL, Lee KH, Lee JY. Electrostatic potential dispersing pyrimidine-5-carbonitrile acceptor for high efficiency and long lifetime thermally activated delayed fluorescence organic light-emitting diodes. J Mater Chem C 2019;7:12695–703. doi: https://doi.org/10.1039/c9tc04304g.
[37] Hladka I, Volyniuk D, Bezvikonnyi O, Kinzhybalo V, Bednarchuk TJ, Danyliv Y, et al. Polymorphism of derivatives of tert -butyl substituted acridan and perfluorobiphenyl as sky-blue OLED emitters exhibiting aggregation induced thermally activated delayed fluorescence. J Mater Chem C 2018;6:13179–89. doi: https://doi.org/10.1039/c8tc04867c.
[38] Galer P, Korošec RC, Vidmar M, Šket B. Crystal structures and emission properties of the BF2 complex 1-phenyl-3-(3,5-dimethoxyphenyl)-propane-1,3-dione: Multiple chromisms, aggregation- or crystallization-induced emission, and the self-assembly effect. J Am Chem Soc 2014;136:7383–94. doi: https://doi.org/10.1021/ja501977a.
[39] Bredas JL. Mind the gap!. Mater Horizons 2014;1:17–9. doi: https://doi.org/10.1039/c3mh00098b.
[40] Pivrikas A, Sariciftci NS, Juška G, Österbacka R. A review of charge transport and recombination in polymer/fullerene organic solar cells. Prog Photovoltaics Res Appl 2007;15:677–96. doi: https://doi.org/10.1002/pip.791.
[41] Siraj N, Das S, Hasan F, Lu C, Kiruri LW, Steege Gall KE, et al. Enhanced S2 emission in carbazole-based ionic liquids. RSC Adv 2015;5:9939–45. doi: https://doi.org/10.1039/c4ra12362j.
[42] Liu J. Deep-blue efficient OLED based on NPB with little efficiency roll-off under high current density. Appl Phys A Mater Sci Process 2017;123. doi: https://doi.org/10.1007/s00339-017-0840-6.
[43] Zhang Y, Li Z, Li C, Wang Y. Suppressing efficiency roll-off of TADF based OLEDs by constructing emitting layer with dual delayed fluorescence. Front Chem 2019;7. doi: https://doi.org/10.3389/fchem.2019.00302.
[44] Jeon SK, Park HJ, Lee JY. Blue-shifted emission color and high quantum efficiency in solution-processed blue thermally activated delayed fluorescence organic light-emitting diodes using an intermolecular interaction suppressing host decorated with blocking groups. J Mater Chem C 2018;6:6778–83. doi: https://doi.org/10.1039/c8tc02050g.
[45] Onsagbr L. Electric Moments of Molecules in Liquids. J Am Chem Soc 1936;58:1486–93. doi: https://doi.org/10.1021/ja01299a050.
[46] Mataga N, Kaifu Y, Koizumi M. Solvent Effects upon Fluorescence Spectra and the Dipolemoments of Excited Molecules. Bull Chem Soc Jpn 1956;29:465–70. doi: https://doi.org/10.1246/bcsj.29.465.
[47] Sumalekshmy S, Gopidas KR. Photoinduced Intramolecular Charge Transfer in Donor-Acceptor Substituted Tetrahydropyrenes. J Phys Chem B 2004;108:3705–12. doi: https://doi.org/10.1021/jp022549l.
[48] Santos PL, Ward JS, Data P, Batsanov AS, Bryce MR, Dias FB, et al. Engineering the singlet-triplet energy splitting in a TADF molecule. J Mater Chem C 2016;4:3815–24. doi: https://doi.org/10.1039/c5tc03849a.

[49] Etherington MK, Gibson J, Higginbotham HF, Penfold TJ, Monkman AP. Revealing the spin-vibronic coupling mechanism of thermally activated delayed fluorescence. Nat Commun 2016;7. doi: https://doi.org/10.1038/ncomms13680.
[50] Wu Q, Zhang S, Yue S, Zhang Z, Xie G, Zhao Y, et al. Enhanced efficiency in single-host white organic light-emitting diode by triplet exciton conversion. J Lumin 2013;143:108–12. doi: https://doi.org/10.1016/j.jlumin.2013.04.037.
[51] Hayduk M, Riebe S, Voskuhl J. Phosphorescence Through Hindered Motion of Pure Organic Emitters. Chem - A Eur J 2018;24:12221–30. doi: https://doi.org/10.1002/chem.201800521.
[52] Ward JS, Nobuyasu RS, Batsanov AS, Data P, Monkman AP, Dias FB, et al. The interplay of thermally activated delayed fluorescence (TADF) and room temperature organic phosphorescence in sterically-constrained donor-acceptor charge-transfer molecules. Chem Commun 2016;52:2612–5. doi: https://doi.org/10.1039/c5cc09645f.
[53] Kabe R, Adachi C. Organic long persistent luminescence. Nature 2017;550. doi: https://doi.org/10.1038/nature24010.
[54] Narayanaswamy R, Wolfbeis OS. Optical Sensors: Industrial Environmental and Diagnostic Applications. vol. 1. 2004. https://doi.org/10.1007/978-3-662-09111-1.
[55] Steinegger A, Klimant I, Borisov SM. Purely Organic Dyes with Thermally Activated Delayed Fluorescence–A Versatile Class of Indicators for Optical Temperature Sensing. Adv Opt Mater 2017;5. doi: https://doi.org/10.1002/adom.201700372.
[56] Yoshihara T, Yamaguchi Y, Hosaka M, Takeuchi T, Tobita S. Ratiometric molecular sensor for monitoring oxygen levels in living cells. Angew Chemie - Int Ed 2012;51:4148–51. doi: https://doi.org/10.1002/anie.201107557.
[57] Zach PW, Freunberger SA, Klimant I, Borisov SM. Electron-Deficient Near-Infrared Pt(II) and Pd(II) Benzoporphyrins with Dual Phosphorescence and Unusually Efficient Thermally Activated Delayed Fluorescence: First Demonstration of Simultaneous Oxygen and Temperature Sensing with a Single Emitter. ACS Appl Mater Interfaces 2017;9:38008–23. doi: https://doi.org/10.1021/acsami.7b10669.

Materials Today Chemistry 25 (2022) 100955

Contents lists available at ScienceDirect

Materials Today Chemistry

journal homepage: www.journals.elsevier.com/materials-today-chemistry/

Triphenylamino or 9-phenyl carbazolyl-substituted pyrimidine-5-carbonitriles as bipolar emitters and hosts with triplet harvesting abilities

U. Tsiko [a], D. Volyniuk [a], V. Andruleviciene [a], K. Leitonas [a], G. Sych [b], O. Bezvikonnyi [a], V. Jasinskas [c], V. Gulbinas [c], P. Stakhira [d], J.V. Grazulevicius [a, *]

[a] Department of Polymer Chemistry and Technology, Kaunas University of Technology, Radvilenu Pl. 19, LT-50254, Kaunas, Lithuania
[b] Univ. Grenoble Alpes, Univ. Savoie Mont Blanc, CNRS, Grenoble INP, LEPMI, 38000 Grenoble, France
[c] Center for Physical Sciences and Technology, LT-10257, Vilnius, Lithuania
[d] Lviv Polytechnic National University, S. Bandera 12, 79013, Lviv, Ukraine

ARTICLE INFO

Article history:
Received 8 March 2022
Received in revised form
15 April 2022
Accepted 17 April 2022
Available online xxx

Keywords:
Hot-exciton
Bipolar charge-transport
Operation time
Organic light-emitting diode
pyrimidine-5-carbonitrile

ABSTRACT

To obtain highly efficient organic semiconductors exhibiting fast emission decays, triplet-harvesting abilities and good bipolar charge-transporting properties for optoelectronic applications, compounds containing triphenylamine or 9-phenylcarbazole as donor moieties and pyrimidine-5-carbonitrile as electron-withdrawing unit were synthesised. Toluene solutions of the compounds demonstrated high photoluminescence quantum yields reaching 98%. As required for electroluminescent device applications, compound containing triphenylamino moiety showed high mobilities of both electrons and holes, which reached 4.4×10^{-4} $cm^2/V \times s$ and 7.3×10^{-3} $cm^2/V \times s$, respectively at electric field of 3.6×10^5 V/cm. This triplet-harvesting mechanism was confirmed by the theoretical and experimental studies including a femtosecond transient absorption pump–probe technique and time-resolved electroluminescence spectroscopy. Pure-blue and greenish-blue fluorescent organic light-emitting diodes (OLEDs) with external quantum efficiency (EQE) reaching 7% and 6%, corresposndingly, were obtained using the newly synthesised compounds as emitters. The operation time (T50) of ca. 650 h were observed for blue OLED and of ca. 3800 h for greenish-blue OLED until reaching the half initial brightness (100 cd/m^2). EQE of more than 20% and T50 exceeding 20,000 h were observed for electroluminescent devices based on emitter characterised by triplet–triplet annihilation and thermally activated delayed fluorescence which was utilised to test hosting properties of the differently donor-substituted pyrimidine-5-carbonitriles.

1. Introduction

One of the most significant fields of application of organic semiconductors is the fabrication of organic light-emitting diodes (OLEDs), which are widely used in displays and lighting devices [1]. The main challenge in the development of OLEDs is the design and synthesis of materials suitable for blue OLEDs due to the problems related to lifetime, purity of colour, and efficiency [2]. A combination of donor and acceptor moieties in a single molecule allows to obtain efficient light-emitting materials exhibiting useful phenomena such as intramolecular and intermolecular (exciplex-based) thermally activated delayed fluorescence (TADF) [3,4], room temperature phosphorescence [5,6], triplet–triplet annihilation (TTA) [7,8], that allow to harvest triplet excitons formed under electrical pumping and convert them into light breaking the theoretical limits of internal and external quantum efficiencies of 25% and 5%, respectively for OLEDs based on conventional fluorescent emitters [9].

Blue TTA-based OLEDs usually exhibit low EQE while the problems related to TADF-based blue OLEDs are efficiency roll-off and durability [10]. Both TTA and TADF as well as phosphorescent (Phos) emitters are characterised by the microsecond-lived emission in contrast to nanosecond-lived emission of conventional fluorescent emitters. Meanwhile, long lived excited triplet states can participate in the formation of hot excitons [11]. Additionally, because of the long life time of triplets, hot polarons can be formed due to the exciton–polaron annihilation in light-emitting layers of

* Corresponding author.
E-mail address: juozas.grazulevicius@ktu.lt (J.V. Grazulevicius).

https://doi.org/10.1016/j.mtchem.2022.100955
2468-5194/

OLEDs based on Phos., TTA or TADF emitters. In contrast to red or green emitters, the energy of hot excitons and polarons in PhOLEDs, and blue TADF-OLEDs is higher (~6.0 eV) than the energy of the chemical bonds in blue OLED materials (ca. 3.5–5 eV). This leads to chemical bond dissociation and formation of defects in light-emitting layers [12]. Since blue Phos, TTA or TADF emitters cannot survive for a long time under electrical excitation due to the exciton-exciton and exciton-polaron annihilations, there is a fundamental limitation in the usage of such emitters in long-living blue OLEDs. Since the lifetimes of high efficiency blue PhOLEDs and TADF-OLEDs are insufficient for practical applications, blue fluorescent OLEDs with significantly lower efficiency are used in commercial displays and lighting devices. For these reasons, it is still important to develop highly efficient fluorescent materials exhibiting additional phenomena such a hybridised local and charge transfer (HLCT) excited-state or hot-exciton mechanism that do not affect fluorescence lifetimes. Utilisation of the mentioned above phenomena would allow to get nanosecond-lived emission, thus the ultrashort time response (ultrahigh switching frequency) of display pixels based on them. These phenomena provide the significant increase of maximum EQE of blue fluorescent devices, that to accordance with spin statistics and light extraction efficiency can be only up to 5%. Recently reported blue OLEDs based on HLCT emitter showed EQE as high as 11.47% [13]. Another mechanism, which allows to increase the efficiency of fluorescent materials is based on upper level triplet–singlet intersystem crossing [14]. Due to the possibility of conversion of excitons from triplet high-lying excited states into singlet excitons allows to obtain non-doped blue fluorescent devices with EQE exceeding 10% [10,14,15]. Upper level triplet–singlet intersystem crossing was exploited in the devices containing anthracene and phenanthroimidazole-based emitters, which are obtained by multi-step synthetic routes [10,14]. Therefore, the development of new readily obtainable fluorescent materials with extra phenomena is an important way for the improvement of efficiency of blue OLEDs.

To develop highly efficient and cost-effective OLEDs is still a challenge despite of the significant research efforts devoted to obtain easily synthesisable and efficient organic emitters and hosts [16,17]. Triphenylamine and carbazole moieties are broadly used for the design of bipolar hosts materials for application in OLEDs. Derivatives of both carbazole and triphenylamine demonstrated high-hole mobilities and high value of triplet energy of ca. 3 eV [18]. In combination with electron-transporting moieties such as triazine [19], pyridine [20,21], benzimidazole [22,23], oxadiazole [24,25], etc., they were used for synthesis of highly efficient bipolar host materials. Derivatives of pyrimidine were also reported as promising bipolar hosts for blue and green OLEDs [26–28]. Recently, we reported on the usage of the modified pyrimidine electron-withdrawing unit, that is, pyrimidine-5-carbonitrile in the design of electronically active compounds [29]. The previously reported pyrimidine-5-carbonitrile derivatives showed good electroluminescent and oxygen sensitivity properties due to the microsecond-lived TADF. However, those compounds due to the highly twisted molecular structures were characterised by relatively inefficient charge-transport with hole and electron mobilities slightly exceeding 10^{-4} $cm^2/V \times s$ at electric field of ca. 5×10^5 V/cm [29]. That limited their applicability as OLED hosts. As it was reported previously, the similar compound 4,6-bis [4-(9-carbazolyl)phenyl] pyrimidine containing pyrimidine as acceptor moiety and carbazole as donor unit in which phenyl ring was also used as the linker between acceptor and donor units did not show TADF properties [30]. This compound was characterised by the large singlet–triplet gap but showed efficient prompt fluorescence. Introduction of the linker between donor and acceptor moieties can have an impact on the dihedral angle between them, different vibronic processes including radiative and non-radiative transitions, the values of kinetic constants [31]. In this study, we aimed to achieve both efficient nanosecond-lived emission and highly efficient bipolar charge-transport for new derivatives of pyrimidine-5-carbonitrile restricting TADF by introduction of the phenyl spacer between donor and acceptor units. As a result, charge mobility reaching 10^{-3} $cm^2/V \times s$ at electric field of 3.6×10^5 V/cm and absence of TADF were obtained for the new derivatives of pyrimidine-5-carbonitrile.

In this work, we report on the synthesis and properties of new derivatives pyrimidine-5-carbonitrile and 9-phenylcarbazole or triphenylamine as efficient OLED emitters with nanosecond-lived emission and as bipolar OLED hosts. The hot exciton triplet-to-singlet intersystem crossing was observed for the developed materials. The participation of high-lying triplet excitons in emission process was studied and confirmed by the theoretical calculations and experimental evidences, for example, EQE values higher than theoretical limit of simple fluorescence (5%) and long-lived electroluminescence. Due to the highly efficient emission the synthesised compounds were used as emitters for fabrication of blue and greenish-blue fluorescent OLEDs. The derivatives were used as bipolar hosts for orange-red TADF/TTA based OLEDs showed operation time of 20,000 h (until reaching half initial brightness of 100 cd/m^2) and maximum EQE exceeding 20%.

2. Results and discussion

2.1. Synthesis

The target compounds 4,6-bis(4-(diphenylamino)phenyl)pyrimidine-5-carbonitrile (**TPAPm**) and 4,6-bis(4-(9H-carbazol-9-yl) phenyl)pyrimidine-5-carbonitrile (**CzPm**) were obtained by Suzuki–Miyaura cross-coupling reactions as it is demonstrated in Scheme 1. The chemical structures of the compounds were confirmed by ^1H and ^{13}C NMR analysis, mass spectrometry and elemental analysis (SI).

For compound **TPAPm** the crystal was obtained from methanol additionally proving the molecular structure. The crystal structure of compound **TPAPm** is presented in Fig. 1a. As a result, many parameters of its X-ray structure (including the parameters of molecular packing of **TPAPm** which is shown in Fig. S1a) can be obtained using the crystallographic data. The crystal structure of **TPAPm** was deposited in Cambridge Crystallographic Data Centre with the corresponding CCDC deposition number 2165986. Fig. S1a, shows that there are many short distances between **TPAPm** molecules (some of the short distances were measured as they are marked). The X-ray and theoretical geometries of **TPAPm** exhibit a similar global shape (Table S1). The differences between experimental and theoretical dihedral angels are due to the crystal-packing forces, which are not taken into account during the theoretical geometry optimisations of isolated molecules. Unfortunately, we did not manage to obtain the crystals of compound

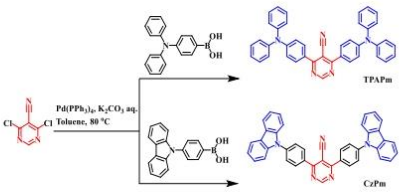

Scheme 1. Synthesis of **TPAPm** and **CzPm**.

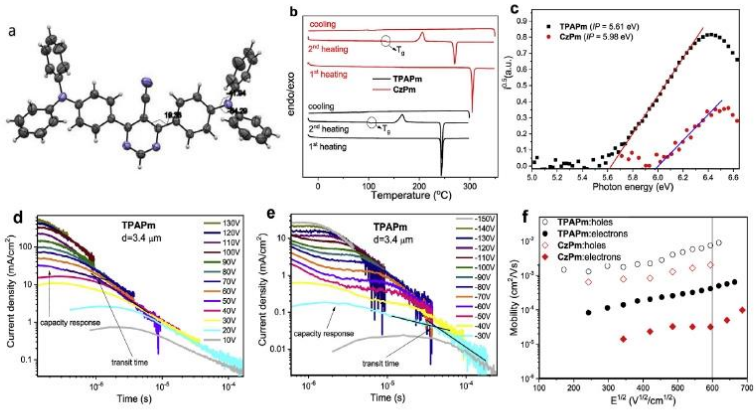

Fig. 1. The crystal structure of compound **TPAPm** (a), DSC (b) curves, photoelectron emission spectra (c), TOF current transients for holes (d) and electrons (e) for the solid sample of **TPAPm** and hole/electron drift mobilities (f) for the films of **TPAPm** and **CzPm.**

CzPm although the different solvents with the different polarities were used for the growing of the crystals.

2.2. Thermal properties

The thermal properties of **TPAPm** and **CzPm** were studied by thermogravimetric analysis (TGA) and differential scanning calorimetry (DSC). Both the compounds exhibited high thermal stability. Their temperatures of 5% of wight loss (T_d) were found to be of 375 °C and 423 °C, respectively (Table 1, Fig. S1b). The complete weigh loss in the single-stage processes shows that the samples of the compounds were subjected to sublimation during TGA experiments. **TPAPm** and **CzPm** were found to be capable of glass formation. They showed glass transitions in the second heating scans. The value of temperatures of glass transition (T_g) were collected from DSC curves (Fig. 1b) in the second heating scans. Carbazolyl-containing compound demonstrated higher value of T_g of 135 °C (Table 1) relative to the compound containing triphenylamino groups (102 °C). This observation can be explained by the enhanced rigidity of carbazole unit. According to these T_g values, both compounds are expected demonstrate a stable work in OLEDs under Joule heating in a wide temperature range.

In the first and second heating scans compound **TPAPm** demonstrated the same value of melting point (T_m) of 243 °C. In contrast, carbazole-based derivative **CzPm** showed two different melting points. In the first heating scan T_m of 305 C° was observed while in the second heating scan T_m of 270 °C was recorded (Fig. 1b, Table 1). Such observation is typically attributed to the existence of two different polymorphs [32].

2.3. Ultraviolet photoelectron spectroscopy and time-of-flight measurements

The transport levels of **TPAPm** and **CzPm**, thus the ionisation potentials (IP_{UPS}) and electron affinities (EA_{UPS}) of the solid films of the compounds, were investigated by combination of ultraviolet photoelectron spectroscopy (UPS) in air and absorption spectroscopy (Fig. 2a). Electron affinities were estimated by the formula $EA_{UPS} = IP_{UPS}$-E_{opt}, where E_{opt} is the optical gap taken from the absorption spectra. The UPS method is required for the estimation of the fundamental energy gaps of organic semiconductors [33]. The ability to transport charges under external voltage in the solid-state, that is, the hole and electron mobilities of the solid vacuum-deposited films, was studied by time of flight (TOF) method. The selection of the TOF method was grounded on the possibility to obtain dependences of charge mobility versus wide electric fields with lower errors in comparison to other methods such as the steady-state current density or field-effect transistor methods, which is sensitive to charge injecting electrodes [34]. The accurate selection electrodes is not needed in the case of TOF (charges are generated by optical excitation) [34].

The lower IP_{UPS} value of 5.61 eV was obtained for compound **TPAPm** in comparison to 5.98 eV observed for **CzPm** (Fig. 1c, Table 1). This observation can be attributed to the presence of triphenylamino substituents with stronger electron-donating abilities in **TPAPm**. The slightly different E_{opt} values of 2.75 and 2.94 eV, respectively were obtained for compounds **TPAPm** and **CzPm** because of the different formation of charge transfer (CT) states. The close EA_{UPS} values of 2.86 and 2.92 eV were estimated for **TPAPm** and **CzPm**, respectively.

Table 1
Thermal, photoelectrical, and charge-transporting characteristics of compounds **TPAPm** and **CzPm**.

Compounds	T_d, °C	T_g,°C	T_m,°C	T_{cr},°C	IP_{UPS}, eV	E_{opt},eV	EA_{UPS}, eV	μ_h, $cm^2/V \times s$	μ_e, $cm^2/V \times s$
TPAPm	375	102[c]	243[a,b]	167[b]	5.61	2.75	2.86	7.3×10^{-3}	4.4×10^{-4}
CzPm	423	135[c]	305[a]/270[b]	206[b]	5.98	2.94	2.92	2.1×10^{-3}	0.4×10^{-4}

Determined from TGA: T_d – the temperature of 5% weight loss; determined from DSC: *a* – first heating, *b* – second heating, T_g – the temperature of glass transition, T_m – melting point, T_{cr} – crystallisation temperature, IP_{UPS} – ionisation potential determined from photoelectron emission curves. EA_{UPS} – electron affinity determined by using ultraviolet photoelectron spectroscopy. E_{opt} – the optical gap. μ_h and μ_e – hole and electron mobilities. * – values taken at 3.6×10^5 V/cm.

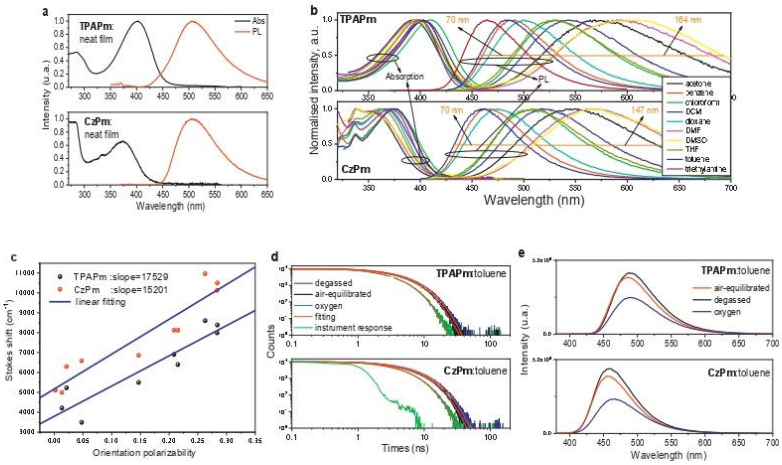

Fig. 2. Absorption and PL spectra of neat films (a) and different solutions (b) as well as corresponding Lippert–Mataga plots (c) of compounds **TPAPm** and **CzPm**. PL spectra (d) and PL decay curves (e) of toluene solutions of **TPAPm** and **CzPm** under different conditions (air-equilibrated, degassed, oxygen).

To estimate charge carrier mobilities of **TPAPm** and **CzPm**, the transit times (t_{tr}) for holes or electrons were taken from the TOF current transients at the corresponding positive or negative external voltages (V), that is, at different electric fields, which are estimated by the formula $E = V/d$, where d is a thicknesses of the tested vacuum deposited films (Fig. 1d,**e**, **S2**). The TOF current transients were recorded under condition that a time range of capacity response is much smaller than a time range of free carrier signals (marked by arrows in (Fig. 1d,**e**)). Since the recorded TOF current transients contained the well visible plateaus and a relatively short tails for both hole and electrons, it can be concluded that compounds **TPAPm** and **CzPm** are characterised by charge carrier transport with comparatively low dispersity. Using t_{tr} values for holes or electrons taken at different voltages, hole (μ_h) and electron (μ_e) mobilities were calculated using formula $\mu_{h/e} = d^2/V \times t_{tr}$ for the compounds. Charge mobilities versus electric field are plotted in Fig. 1e. In contrast to organic semiconductors typically used in OLEDs [35], both the compounds showed high-hole mobilities reaching 10^{-3} $cm^2/V \times s$ and by ca. One order of magnitude lower electron mobilities reaching 10^{-4} $cm^2/V \times s$ at high electric fields (Fig. 1f). Compound **TPAPm** showed higher both hole and electron mobilities at the same electric fields than compound **CzPm**. This observation can be attributed to the flexible structure of triphenylamino group in contrast to the rigid structure of carbazole moiety leading to more compact molecular packing in the films **TPAPm**. As a result, more appropriate HOMO/HOMO and LUMO/LUMO overlapping is realised for hoping of free holes or electrons between neighbouring molecules of **TPAPm**. Nevertheless, according to the results of charge transport measurements, both **TPAPm** and **CzPm** have a big potential for application in OLEDs at least as the host materials.

2.4. Photophysical properties of the compounds

The absorption bands observed in high-energy region (286, 298 nm for the films of **TPAPm** and 283, 318, 334 nm for the solid samples of **CzPm**) are attributed to the localised aromatic π-π* or n−π* transitions of triphenylamino or 9-phenylcarbazolyl groups (Fig. 2a) [36]. The absorption spectra of dilute solutions of compounds **TPAPm** and **CzPm** in different solvents show high intensity low-energy absorption bands (Fig. 2a and b). Based on the theoretical results presented in Fig. S3, these bands can be attributed to the electronic transition $S_0 \rightarrow S_1$ which is dominated by the intramolecular charge transfer (ICT) between electron-donating phenylcarbazolyl group in **CzPm** or triphenylamino group in **TPAPm** and electron-accepting pyrimidine-5-carbonitrile moieties with some contribution from the local excitations (LE) in phenyl linker. The smaller oscillator strength of the $S_0 \rightarrow S_1$ transition of 0.549 was calculated for **CzPm** compared to 0.998 estimated for **TPAPm**. This observation indicates weaker LE as well as stronger ICT in **CzPm**. (Fig. S3). Slightly different positions of the low-energy bands were observed in absorption spectra of the solutions of **TPAPm** and **CzPm** due to the solvatochromic effect caused by ICT (Fig. 2a and b). Previously, the similar nature of low-energy band was observed for 4,6-bis [4-(9-carbazolyl)phenyl]pyrimidine containing slightly weaker acceptor pyrimidine than pyrimidine-5-carbonitrile. Nevertheless, as it will be shown below, TADF was not detected neither for **CzPm** and **TPAPm** nor for the previously studied 4,6-bis [4-(9-carbazolyl)phenyl]pyrimidine [30].

The toluene solutions of compounds **TPAPm** and **CzPm** demonstrated blue emission with maximum intensities at 486 nm and 458 nm, correspondingly (Table 2). The neat films of both the derivatives showed green emission with maximum centred at 506 nm demonstrating that the intrinsic polarities of the solid samples of **TPAPm** and **CzPm** are higher than that of toluene (Fig. 2a). The fluorescence of toluene solutions of the synthesised compounds is highly efficient. The values of photoluminescence quantum yield (Φ_{PL}) reached 90% for the solution of **TPAPm** and 98% for the solution of **CzPm**. The values of Φ_{PL} of the neat films of **TPAPm** and **CzPm** were found to be lower and exceeded 45% and 30%, respectively.

Table 2
Photophysical parameters of toluene solutions and neat films of compounds **TPAPm** and **CzPm** and guest–host solid solutions.

Compounds	λ_{PL} (in nm)	Φ_{PL} (in %)	τ_1/τ_2 (in ns)	Rel_1/Rel_2 (in %)	χ^2
$TPAPm^{tol}$	486	90*	3.75/-	100	1.084
$CzPm^{tol}$	458	98*	5.17/-	100	1.027
$TPAPm^{film}$	506	45	2.86/8.49	62.64/37.56	1.222
$CzPm^{film}$	508	30	3.88/9.63	37.65/62.35	1.228
TPAPm in mCBP	506	21	2.02/4.87	67.36/32.64	1.224
CzPm in mCBP	476	18	2.44/7.04	49.71/50.29	1.218

Guest–host solid solutions: 20 wt% of emitters in hosts; λ_{PL} – the wavelength at the maximum intensity of photoluminescence; Φ_{PL} – the photoluminescence quantum yield, * – degassed conditions; τ_1/τ_2 – the lifetimes of prompt and delayed fluorescence; Rel_1/Rel_2 – contribution ratio of τ_1/τ_2; χ^2 – the weighted sum of squares of deviations of calculated points of multiexponential fitting of a PL decay curve.

For the analysis of the excited state properties of **TPAPm** and **CzPm** in more details, their solvatochromic effects were investigated using the Lippert–Mataga solvatochromic model (Fig. 2c). For this purpose, the absorption and PL spectra of ten dilute solutions of **TPAPm** and **CzPm** were recorded. They are presented in Fig. 2b. The positions of the PL spectral peaks are mostly predetermined by the polarity of solvents. The Lippert–Mataga dependences [37–39] of the Stokes shifts $\Delta\tilde{\nu}$ versus orientation polarisability of a solvent Δf are plotted in Fig. 2c. The approach is based on the Onsager interpretation of the non-specific electrostatic interactions between molecules of material and solvent in a solution [40]. The relation, which the plot is based on, is $\Delta\tilde{\nu} = \frac{2\Delta f}{4\pi\varepsilon_0 hca^3}(\mu_e - \mu_g)^2 + \Delta\tilde{\nu}^0$. Here, is the Stokes shift in a condition of the absence of impact of solvation while a is denoted as an Onsager cavity radius. The slope of Lippert–Mataga plot corresponds directly to the difference of the dipole moments of a molecule in excited and ground states. The values of slopes for **TPAPm** and **CzPm** were found to be of 15,201 and 17,529 cm^{-1}, respectively.

PL decay curves of toluene solutions and of neat films of **TPAPm** and **CzPm** were found in the nanosecond range confirming the prompt fluorescence nature of emission without any sign of delayed fluorescence, for example, TADF or TTA (Fig. 2d, S4, Table 2). This observation is not expected taking into account the results of investigation of PL intensity of toluene solutions of **TPAPm** and **CzPm** under the different conditions (air equilibrated, degassed, and oxygen equilibrated) (Fig. 2e). After deoxygenation, the PL intensity of toluene solutions of both the compounds slightly increased but after purging with oxygen their PL intensity significantly dropped down. This observation may confirm that triplet excitons participate in emission processes of derivatives **TPAPm** and **CzPm**. It is known, that triplet excitons are very sensitive to the presence of oxygen [41,42]. PL decay curves of toluene solutions of **TPAPm** and **CzPm** were recorded under different conditions (Fig. 2d). Lifetimes of excited states in oxygen atmosphere were found to be considerably shorter than in air that additionally confirms the participation of triplet excitons in emission what is not usual for purely fluorescent materials. Several mechanisms could be responsible for the emissive triplet harvesting of **TPAPm** and **CzPm** [10,14,43–45].

- One of them is ***room-temperature phosphorescence*** [5,45,50]. Since additional bands or shoulders were not observed after deoxygenation, room-temperature phosphorescence is highly unlikely (Fig. 2e, S5).
- Another possible mechanism might be ***thermally activated delayed fluorescence.*** However, it is not the case for **TPAPm** and **CzPm** since no delayed fluorescence was observed due to relatively high singlet–triplet splitting (Fig. 2d).
- ***Triplet–triplet annihilation*** is also unlikely for **TPAPm** and **CzPm** since the linear fits of their integrated PL intensities versus excitation intensities revealed the slopes lower than unity displaying no contribution of TTA emission under optical excitation (Fig. S6a) [46,47]. In addition, the linear fits of their electroluminescence (EL) intensities versus current densities revealed the slopes lower than unity displaying no contribution of TTA emission under electrical excitation as it will be discussed below (Fig. S6b).
- ***Emission of hybridised local and charge transfer states,*** **ca**n partly be the case for **TPAPm** and **CzPm** due to the closely situated several excited states predicted by theoretical calculations (see discussion below, Fig. 3a).
- We suppose that the mechanism of ***emissive triplet harvesting is upper level triplet–singlet intersystem crossing*** [10,14]. This mechanism may be partly in combination with contribution of TADF and/or TTA despite their evidence is very limited/non-observed.

2.5. Time-resolved measurements

To provide more study on emission behaviour of **TPAPm** and **CzPm**, time-resolved measurements were performed for toluene solutions and the films of the doped compounds **TPAPm** and **CzPm**. Their PL decay curves were recorded in visible spectral region (400–700 ns) with the step of 3 nm at constant time (3 min) (Fig. S4c). Photoluminescence spectra recorded at the different times after excitation are plotted in Fig. 3c, S4d,e and Fig. 4a in 3D and 2D coordinates. Initially, taking into account just time-taking processes of upper level triplet–singlet intersystem crossing and consequent internal conversion, we expected to obtain similar spectra of prompt and delayed fluorescence resulted from relaxation of singlet excitons from S_1. In contract to the steady-state fluorescence spectra which contain single bands, two bands with the different intensities at the different times after excitation are well observed in time resolved fluorescence spectra of non-oxygenated toluene solutions of **TPAPm** and **CzPm** (Fig. 3c and Fig. S4d). Presence of those two bands is not consistent with one band of steady-state fluorescence of their non-oxygenated toluene solutions (Fig. 2e). Moreover, if the upper level triplet crossing mechanism is operative in solution, the steady-state spectra in oxygen saturated solutions should show only the high energy single band. In contrast, the steady-state spectra in degassed solutions must show two emission bands. Despite there are no clear observation of two bands for the steady-state spectra in degassed solutions, there are seen shift of maxima between PL spectra of degassed and oxygen saturated solutions. This observation apparently attributed to the triplet harvesting (caused by overlapping of two bands). Thus, degassed solutions do not show two emission bands because the most of intensity of observed emission is related to simple fluorescence from ultrafast relaxation of S_1 states (Fig. S11). By the other words, the intensity of 'delayed' fluorescence (which attributed to triplet harvesting) is much lower than intensity of ultrafast fluorescence. Meanwhile, the time-resolved

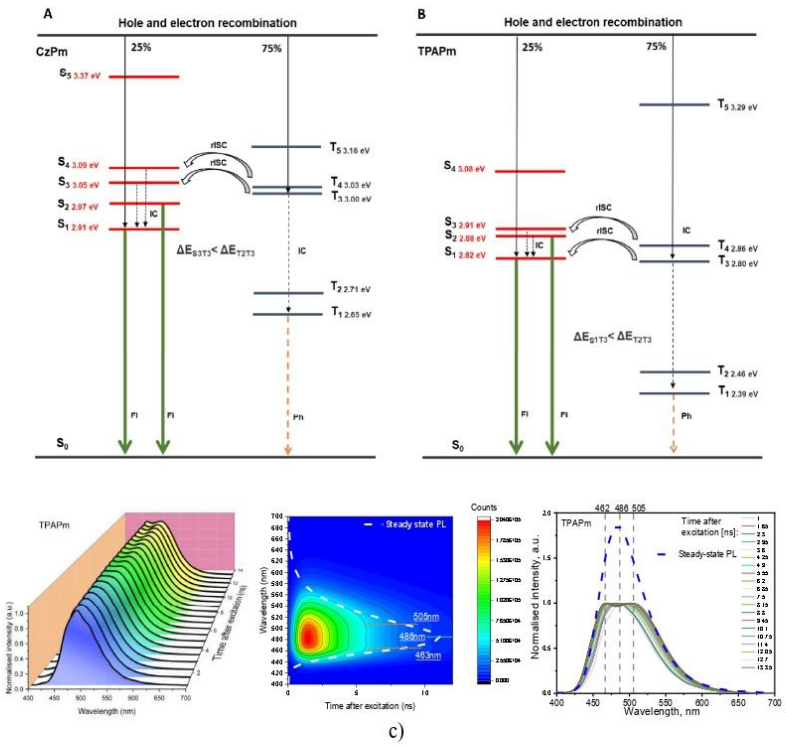

Fig. 3. Energy diagram of the singlet and triplet excited states of **CzPm** (a) and **TPAPm** (b) calculated using TD-B3LYP 6-31G (d,p):CPCM (DMSO). Time-resolved spectra (c) of the toluene solutions of **TPAPm** recorded at the different times after excitation.

spectra are not attributed to intensity of ultrafast fluorescence since the delay was used when corresponding PL decay curves were recorded (Fig. S4b). As a result, the time-resolved spectra with two bands were recorded (one band is attributed to simple fluorescence, and second one is attributed to triplet harvesting ability as it discussed below).

Theoretical calculation discussed below revealed existence of closely situated S_1 and S_2 states of both the compounds. Therefore, this observation is clear evidence of relaxation of singlet excitons from S_1 and S_2 both contributing to the total emission. Thus, the steady-state fluorescence spectra of **TPAPm** and **CzPm** are caused by overlapping of fluorescence both from S_1 and S_2. Apparently, S_2 of **TPAPm** and **CzPm** become emissive due to overloading of S_2 by upper level triplet–singlet intersystem crossing, as shown in Fig. 3c. Stronger separation of S_1 and S_2 emission bands was observed for the films of **TPAPm** (20 wt%):mCBP and **CzPm** (20 wt%):mCBP (Fig. 4a and Fig. S4e) apparently due to either intermolecular interactions or polarity effects.

Keeping this in mind, we studied the theoretical vertical singlet and triplet excitation energies (Fig. 3a).

The theoretical study revealed a relatively large singlet−triplet energy splitting (ΔE_{ST}) between S_1 and T_1 of 0.26 eV and 0.52 eV for **CzPm** and **TPAPm**, respectively. It complicates transfer of triplet excitons from T_1 to S_1 through reverse internal system crossing (rISC) typical for TADF materials. However, very small ΔE_{ST} between high energy levels ($\Delta E_{S3T3} = 0.05$ eV, $\Delta E_{S3T4} = 0.02$ eV for **CzPm** and $\Delta E_{S1T3} = 0.02$ eV, $\Delta E_{S2T4} = 0.02$ eV for **TPAPm**) suggests that rISC along the high-lying triplet states and singlet states can compete with the internal conversion (IC) process between triplet excited states ($\Delta E_{T2T3} = 0.29$ eV for **CzPm** and $\Delta E_{T2T3} = 0.34$ eV for **TPAPm**). This kind of rISC channels results in the triplet-harvesting via upper triplet levels in **CzPm** and **TPAPm**. Theoretically, 100% exciton utilisation can be reached in OLEDs containing such materials, thus enhancing efficiency of OLEDs [15].

PL and phosphorescence (PH) spectra of frozen THF solutions of the compounds were recorded at 77 K (Fig. 4b). The wavelengths of PL and PH spectra at maximum intensities of the emission were used for estimation of the values of the first singlet (S_1) and triplet (T_1) energy levels of **TPAPm** and **CzPm**. Compound **TPAPm** demonstrated low triplet energy of 2.31 eV, while **CzPm** showed

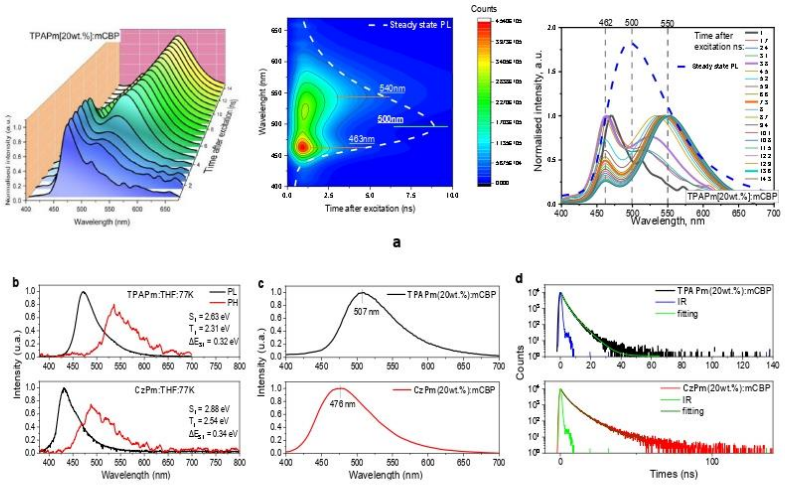

Fig. 4. Time-resolved photoluminescence spectra (a) of the 20 wt%. solid solution of **TPAPm** in mCBP recorded at the different times after excitation. PL and PH spectra of frozen THF solutions of **TPAPm** and **CzPm** (b), PL spectra, (c) and PL decay curves (d) of guest–host systems.

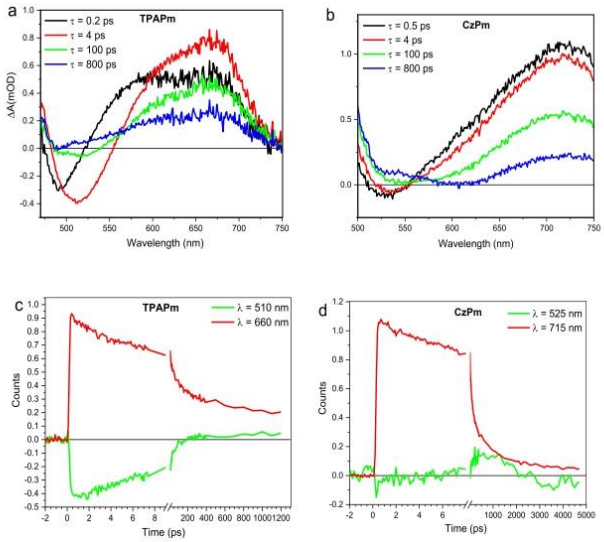

Fig. 5. Time-resolved TA of 1 wt% of molecular dispersions of **TPAPm** (a) and **CzPm** (b) in Zeonex matrix and the corresponding TA kinetics curves (c, d) recorded at the different probe wavelengths.

significantly higher triplet energy of 2.54 eV. The ΔE_{ST} values of the compounds were found to be comparable. **TPAPm** showed ΔE_{ST} of 0.32 eV while **CzPm** exhibited ΔE_{ST} of 0.34 eV. As a result, TADF properties were not detected for **TPAPm** and **CzPm** as it was mentioned above. In addition, we measured the values of ΔE_{ST} for 20 wt% solid solutions of **TPAPm** and of **CzPm** in mCBP. They were found to be of 0.27 eV and 0.26 eV, respectively (Fig. S7). We note that slightly different values of S_1 and T_1 of compounds obtained for THF solutions and the layers of the solid solutions in mCBP observed at 77 K may be attributed to deformations of dihedral angles between the moities in the solid samples. To support this assumption, we also evaluated the energies of the excited states for the rotation of the D–A bonds (Fig. S8).

2.6. Transient differential absorption

To support claims on triplet harvesting processes of **TPAPm** and **CzPm** which appeared via upper level rISC, the presence of these energy states has to be confirmed. A femtosecond transient absorption pump–probe technique allows experimentally to do that. Transient absorption (TA) spectra and decay kinetics were recorded for 1 wt% and 20 wt% molecular dispersions of **TPAPm** and **CzPm** in Zeonex under excitation to high-excited states by 400 nm light (Fig. 5, **S9**, **S10**). To minimize effect of hosts and intermolecular interactions, the inert polymer Zeonex with relatively low polarity was selected as the matrix [48]. The TA measurements showed more complex dynamics than that observed for simple fluorescent emitters [49]. The TA spectra of the films of the molecular dispersions of **TPAPm** and **CzPm** in Zeonex showed spectral evolutions taking place on several and hundreds of ps time scales. Since molecules were dispersed in solid Zeonex matrix, conformational changes, formation of dimers or aggregates are unlikely. Taking the case of the film of 1 wt% solid solution of **TPAPm** in Zeonex as an example of a semi-quantitative analysis, TA spectra are characterised by one negative (at ca. 490 nm) and two positive (at ca. 550 and 670 nm) induced absorption bands. Since **TPAPm** exhibits no absorption, and thus, absorption bleaching is not possible in the 500 nm region, the negative band should be attributed to the stimulated emission, while the two positive bands can be assigned to the excited state absorption. We can distinguish three characteristic spectral shapes represented by the TA spectra at 0.2 ps, 4 ps, and 800 ps (Fig. 5a). According to the theoretical energy diagram, absorption of the excitation light at 400 nm used for the sample excitation creates high singlet excited states S_4 or S_5. The first spectrum with the stimulated emission band at ca. 490 nm can be attributed to the vibrationally 'hot', conformationally nonequilibrated combination of closely energetically situated S_4–S_2 excited states. Cooling and equilibration create a relaxed S_2 excited state during the initial several ps and cause a red-shift of the luminescence band towards 515 nm. The subsequent excited state dynamics during several hundreds of ps cause weakening of the stimulated emission, which is finally overwhelmed by the excited state absorption. This process can be attributed to the S_2 to S_1 relaxation, which was also observed as the evolution of the time-resolved PL spectra of the films of 20 wt% solid solution of**TPAPm in** mCBP (Fig. 4a). In the case of the 1 wt% solid solution of **TPAPm** in Zeonex, the weakening of the stimulated emission band indicates that the S_1 state possesses a lower transition dipole moment to S_0 state than the higher singlet excited states. This weakening is less clear in Fig. 4a because of insufficient time resolution for the films of 20 wt% solid solutions of **TPAPm** in CBP. Meanwhile, PL measurements were performed for the 1 wt% solid solution of **TPAPm** in Zeonex with a streak camera with 3 ps time resolution on a 120 ps time range reveals only the S_2 state luminescence and its decay confirming that the time-resolved luminescence of the S_1 state is much weaker (Fig. S11c in SI).

The high time resolution of the transient absorption and streak camera measurements reveals the dynamics of the S_2 to S_1 relaxation. This process is highly nonexponential. The initial relaxation phase takes place on a time scale of tens of picoseconds, and continues during hundreds of ps. Moreover, according to the PL dynamics presented in Fig. 4a, the PL spectra modifications last for several nanoseconds. This nonexponential behaviour suggests a strong inhomogeneity of the system. We speculate that the formation of the S_1 state may strongly depend on the conformational states of the molecules, which may be significantly different for the molecules embedded in a solid matrix causing different S_2 to S_1 transition rates. Consequently, the evolution of the spectra is in agreement with the presence of closely situated several excited states predicted by the theoretical calculations and supports the prediction of relatively slow cascade relaxation of these states (Fig. 3a and b).

The TA data, which indicate the formation of the additional states, well support the presented above energy diagram of the singlet and triplet excited states of **TPAPm** and **CzPm** (Fig. 3a and b). As demonstrated below, the electroluminescence spectra of the **TPAPm** and **CzPm** based devices correspond to the sum of both S_2 and S_1 luminescence bands, which shows that the S_2 state is mainly populated in operating devices, apparently by the rISC process as suggested in Fig. 3a and b.

2.7. Photophysical properties of OLED guest-host systems

To develop guest–host systems for light-emitting layers of efficient OLEDs, both charge-transporting and photophysical properties of hosts and guests must be considered. To prevent reabsorption, the emission spectrum of a guest has to be red-shifted in comparison to the absorption spectrum of a host. Considering low-energy edges of absorption spectra at 450 and 422 nm of **TPAPm** and **CzPm,** respectively, it can be concluded that the compounds can be used as the hosts for green-red emitters (Fig. 2a). To avoid energy leakages through triplet levels of a host, a T_1 value of a host has to be higher than S_1/T_1 values of an emitter. Taking into account the first triplet levels of 2.31 eV observed for **TPAPm** and 2.54 eV recorded for **CzPm,** it can be concluded these compounds can be used as hosts for orange-red emitters (Fig. 4b). Following the above requirements, 2,7-bis(9,9-dimethylacridin-10(9H)-yl)dibenzo [a,c]phenazine (AcDbp) was selected as the possible advanced TADF/TTA emitter [51]. It was recently used for the fabrication highly efficient OLEDs [51]. Briefly introducing AcDbp, it should be mentioned that this compound additionally to combination of TADF/TTA triplet-harvesting properties is characterised by bipolar charge transport with mobilities exceeding 10^{-3} $cm^2/V \cdot s$ at high electric fields, singlet energy of 2.55 eV and triplet energy of 2.35 eV, ionisation potential of 5.5eV and electron affinity of 2.77 eV. It shows good performance in OLED as the emitter (maximum EQE of 19.4%) [51].

Hosting properties of **TPAPm** and **CzPm** were investigated under optical and electrical excitations using guest–host systems AcDbp(20 wt%):**TPAPm** and AcDbp(20 wt%):**CzPm**. Light-emitting properties of **TPAPm** and **CzPm** were additionally studied using solid mixtures of **TPAPm** (20 wt%):mCBP and **CzPm** (20 wt%):mCBP. The photophysical parameters of the solid guest–host mixtures are collected in Table 2.

PL spectra of the studied guest–host systems are mainly related to the emissions of the guests (Fig. 4c). The low-intensity emissions observed in high-energy spectral region that could be related to the emission of hosts. This host emission is apparently not related to the pure host–guest Förster resonance energy transfer but to small area located (focused) optical excitation. These conclusions are supported by the total absence of host emissions in

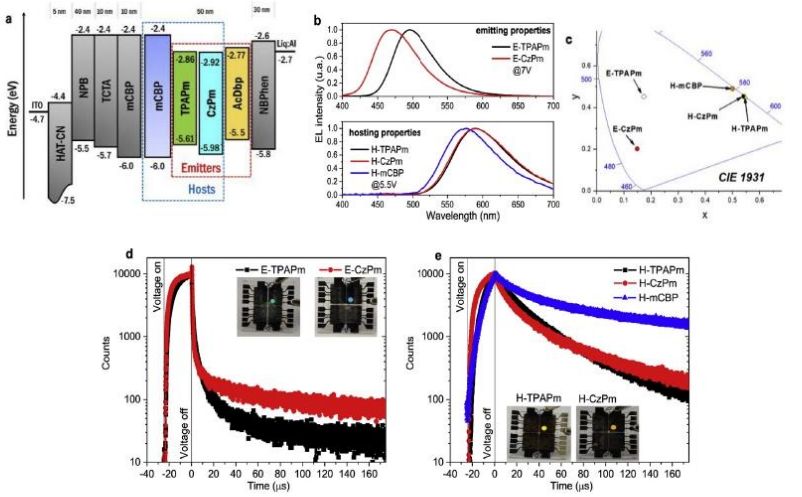

Fig. 6. Equilibrium energy diagram (a), EL spectra at constant voltage (b), and corresponding CIE colour coordinates (c) of OLEDs. TREL curves of devices **E-TPAPm** and **E-CzPm** (d) and devices **H-TPAPm**, **H-CzPm** and **H**-mCBP (e). Insets show photos of OLEDs.

electroluminescence (EL) spectra of OLEDs based on these systems as light-emitting materials (Fig. 6b). PL spectra of the solid layers of **TPAPm** and **CzPm** doped in mCBP host are very similar to PL spectra for their toluene solutions because of the similar dielectric constant of toluene and mCBP (Fig. 2c). In contrast to the TADF/TTA emitter AcDbp, PL decays of the systems **TPAPm**:mCBP and **CzPm**:mCBP were found in the nanosecond range (Fig. 4d, S4) [51]. However, the shapes of PL decay curves of the molecular mixtures **TPAPm**:mCBP and **CzPm**:mCBP were very similar to PL decays of previously published emitters exhibiting triplet harvesting phenomenon via upper level triplet−singlet intersystem crossing [14]. Because of the same mechanism of triplet harvesting of **TPAPm** and **CzPm**, high-efficient OLEDs were obtained using them as emitters. Emitter AcDbp doped in both hosts **TPAPm** and **CzPm** exhibited orange emission (Fig. S4a) with delayed fluorescence similar that previously observed for AcDbp (Fig. S4b) [51].

2.8. Electroluminescent devices

Aiming to study emitting and hosting properties of compounds **CzPm** and **TPAPm**, the layers of above described guest-host systems **TPAPm**:mCBP/**CzPm**:mCBP and AcDbp:**TPAPm**/AcDbp:**CzPm** were used as light-emitting layers in OLEDs with the structure ITO/HAT-CN [5]/NPB [40 nm]/TCTA [10 nm]/mCBP [10 nm]/light-emitting layer [50 nm]/NBPhen [30 nm]/LiF [2 nm]/Al. In devices **E-TPAPm** and **E-CzPm** devices, compounds **CzPm** and **TPAPm** were used as the emitters while in devices **H-TPAPm** and **H-CzPm** they were used as hosts (Fig. 6a, Table 3). The reference device **H**-mCBP was also fabricated for the comparison of hosting properties of **CzPm** and **TPAPm** with those of the commercial host mCBP. TADF/TTA emitter AcDbp [51] was used in the reference device **H**-mCBP.

The multi-layer device structure contained the layers of commercial materials such as hole-injecting layer of hexaazatriphenylenehexacabonitrile (HAT-CN), hole-transporting layers of di (1-naphthyl)-N,N′-diphenyl (NPB), tris(4-carbazoyl-9-ylphenyl) amine (TCTA), and 3,3-di (9H-carbazol-9-yl)biphenyl (mCBP), electron-transporting layer of 2,9-bis(naphthalen-2-yl)-4,7-diphenyl-1,10-phenanthroline (NBPhen) and electron-injecting layer of fluorolithium (LiF) (Fig. S12). Such device structure ensures the recombination of charges and generation of excitons within the light-emitting layers. As a result, the same EL spectra were recorded at different external voltages (Fig. S13). Devices **E-TPAPm** and **E-CzPm** were characterised by bluish green and blue EL with CIE colour coordinates of (0.174, 0.454) and (0.149, 0.203),

Table 3
Device out-put parameters

Motif of EL test	Emitting property test		Hosting property test		
Device structure	ITO/HAT-CN/NPB/TCTA/mCBP/emitting layer/nBPhen/Liq/Al				
Device name	**E-TPAPm**	**E-CzPm**	**H-TPAPm**	**H-CzPm**	**H**-mCBP
Emitting layer	**TPAPm**:mCBP	**CzPm**:mCBP	AcDbp:**TPAPm**	AcDbp:**CzPm**	AcDbp:mCBP
V_{ON} (V) @ 10 cd/m^2	4.3	4.4	3.0	4.5	3.85
EQE_{max}, EQE_{100}, EQE_{1000} (%)	**6.0, 4.7, 4.2**	**7.0, 4.7, 3.9**	**20.7, 12.0, 7.9**	**13.7, 6.1, 4.7**	**20.2, 12.4, 5.3**
CIE (x,y) @ 1000 cd/m^2	(0.174, 0.454)	(0.149, 0.203)	(0.546, 0.449)	(0.54, 0.455)	(0.5, 0.49)
LT50,* hour @ 100 cd/m^2	3896	648	2063	6481	22,336

* device lifetimes calculated by formula $LT(L_1) = LT(L_0) \times (L_0/L_1)^n$ using experimental data from Fig. 7e and f and assuming n = 1.75, where L_1 is luminescence at 100 cd/m^2.

respectively. The EL spectra of devices **E-TPAPm** and **E-CzPm** were very similar to PL spectra of the corresponding films of host-guest mixtures **TPAPm**:mCBP and **CzPm**:mCBP used as light-emitting layers (Fig. 4c). When compounds **TPAPm** and **CzPm** were used as hosts for the orange emitter AcDbp, orange EL were observed for devices **H-TPAPm** and **H-CzPm** without any evidences of emissions of hosts in their EL spectra (Fig. 6b). EL spectra of devices **H-TPAPm** and **H-CzPm** were found to be slightly red-shifted in comparison to EL spectra of the reference device **H**-mCBP and previously published EL spectra of AcDbp-based devices [51]. This observation can be explained by strong sensitivity of TADF/TTA emission of emitter AcDbp to the dipole moments of surrounding molecules, which are higher of bipolar compounds **TPAPm** and **CzPm** than that of mCBP. Since compounds **TPAPm** and **CzPm** are characterised by prompt fluorescence, narrower full width at half maxima (FWHM), thus purer emission colours, were observed for devices **E-TPAPm** and **E-CzPm** than for TADF OLEDs **H-TPAPm**, **H-CzPm** and **H**-mCBP (Table 3, S2).

Transient electroluminescence (TREL) signals help to prove the considerable participation of triplet excitons in electroluminescence of the devices (Fig. 6 d,e). In contrast to PL decay curves of emitters **TPAPm** and **CzPm** (Fig. S4b), TREL signals of devices **E-TPAPm** and **E-CzPm** demonstrated hundreds of microseconds lived emission definitely related to triplet harvesting abilities of **TPAPm** and **CzPm**. Since intensity of long-lived EL of device E-**CzPm** is stronger than that of device **E-TPAPm**, emitter **CzPm** is characterised by more efficient triplet harvesting than **TPAPm.** When compound AcDbp was used as an emitter, the shapes of TREL signals of OLEDs **H-TPAPm**, **H-CzPm** and **H**-mCBP were very similar to the previously published TREL signals of devices based on a TADF/TTA emitter [52]. Considerably faster EL kinetics were observed for devices **H-TPAPm** and **H-CzPm** than for **H**-mCBP. This observation could be related to process of upper level triplet singlet intersystem crossing of **TPAPm** and **CzPm** hosts which is not observed for the conventional host mCBP. Thus, the faster triplet harvesting was observed for AcDbp-based devices when hosts **TPAPm** and **CzPm** were used. Taking into account the big differences of the shapes of TREL signals of devices **E-TPAPm**/**E-CzPm** and AcDbp-based devices (Fig. 6 d,e), triplet harvesting of emitters **TPAPm** and **CzPm** is attributed rather to upper level rISC but not to TADF or TTA as it was in the case of emitter AcDbp [51]. This observation additionally confirms the above considerations.

The similar turn-on (voltage at 10 cd/m^2) and driving (voltage at 10 mA/cm^2) voltages were observed for devices **E-TPAPm** and **E-CzPm** due to the same device structure with the same host mCBP used (Fig. 7a, Table 3). Only small differences in turn-on and driving voltages of these devices can be attributed to the direct charge injection and charge transport through HOMO/LUMO of emitters **TPAPm** and **CzPm**. Thus, charge-transporting properties of emitters **TPAPm** and **CzPm** did not affect much the dependencies of current density versus voltage of devices **E-TPAPm** and **E-CzPm**. In contrast, very different turn-on and driving voltages were observed for devices **H-TPAPm**, **H-CzPm** and **H**-mCBP in which the different hosts **TPAPm, CzPm** and mCBP were used (Fig. 7b, Table 3, S2). The lowest turn-on and driving voltages of 3.0 and 5.0 V were obtained for device **H-TPAPm** based on the host **TPAPm** with either higher hole/electron mobilities or with more appropriate for charge injection HOMO/LUMO in comparison to those of host **CzPm** and reference host mCBP (Fig. 1e, **6a**, Table 3, S2). As a result, high maximum power efficiency (PE) of 28.6 lm/W was achieved for device **H-TPAPm** in contrast to that of device **H-CzPm** with the same emitter and device structure. This result directly demonstrates the relationship between high charge mobility of the host **TPAPm** and PE of the device.

When compounds **TPAPm** and **CzPm** were used as OLED emitters, the high maximum EQEs of the devices of 6 and 7% were obtained (Fig. 7c). Since the theoretical limit of EQE for prompt fluorescence based OLEDs is of 5%, this result additionally confirms the ability of triplet harvesting by compounds **TPAPm** and **CzPm** as it was discussed above. In addition, this observation shows the considerable participation of triplet excitons in electroluminescence.

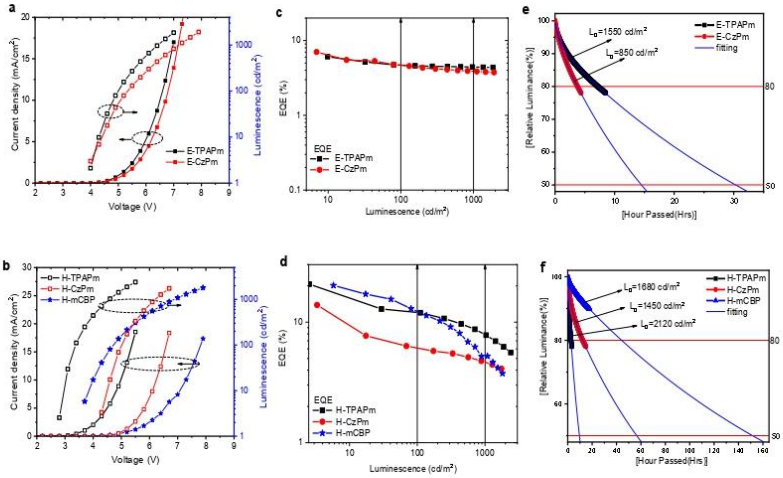

Fig. 7. Current density and luminescence versus voltage (a, b), EQE versus luminescence (c, d) and device lifetimes (e, f) for the fabricated devices.

When compounds **TPAPm** and **CzPm** were used as OLED hosts, the high maximum EQEs of 20.7% and 13.7% were obtained for devices **H-TPAPm** and **H-CzPm**. EQE of **H-TPAPm** slightly exceeded EQE of the reference device **H**-mCBP which was found to be of 20.2% (Fig. 7d, **S13**, Table 3, S2). The EQE differences of devices **H-TPAPm** and **H-CzPm** can be explained by the different charge mobilities of hosts **TPAPm** and **CzPm** (Fig. 1e). The highest roll-off efficiency, thus the highest EQE at 1000 cd/m^2 was observed for device **H-TPAPm**. This observation can be also attributed to high charge mobility of compound **TPAPm** leading to good charge balance at wide range of the applied voltages (Fig. 7d).

EL intensities versus applied voltages are plotted in Fig. 7e,**f**. Since the different initial luminance (marked by the arrows) was selected for the devices, the direct comparison of device life-times is not possible. Therefore, the formula LT (L_1) = LT (L_0) × (L_0/L_1)^n was used for the prediction of device life times (LT80 and LT50) at 80 and 50% EL intensity, initial luminance of 100 and 1000 cd/m^2 assuming the escalation factor n = 1.75. The experimental values of escalation factor for OLEDs are typically in the range of 1.65−1.95 (Table 3, S2) [53,54]. In this formula, LT (L_0) is the experimental value of LT80 at EL intensity of 80% of chosen luminance L_0, LT (L_1) is predicted lifetime at luminance L_1. To get LT50, experimental data were analysed using the formula L/L0 = a × exp$^{-\alpha t}$ + b × exp$^{-\beta t}$, where the first-exponential term is related to the rapid initial decay, the second-one is related to the long-term degradation, a, b, α, β are fitting parameters, which are related to functional materials used and device processing [55].

Approximately five times higher device lifetimes were obtained for OLEDs **E-TPAPm** in comparison to those of device **E-CzPm** (Table 3). These results can be mainly attributed to the different triplet energies (2.31 eV for **TPAPm** and 2.54 eV for **CzPm**) of the emitters (Fig. 4c). It is known that hot exactions with double energy can be formed leading to chemical bond dissociation and formation of defects in light-emitting layers when two triplets meet one another [12]. Due to the higher energy of hot exciton of 5.08 eV estimated for emitter **CzPm** compared to that of 4.62 eV observed for emitter **TPAPm**, the higher stability was achieved for device **E-TPAPm** (Table 3, S2).

When compounds **TPAPm** and **CzPm** were used as hosts for the same emitter AcDbp, the opposite device lifetimes were observed. Device **H-CzPm** was characterised by higher stability in comparison to the stability of device **H-TPAPm**. Thus, high triplet excitons of **CzPm** practically did not affect the device stability. Apparently, the molecular stability plays the main role in this case. In particular, the fused carbazole unit provided higher device stability that flexible triphenylamine moieties. The reference device (**H**-mCBP) showed the highest stability with predicted LT50 of 22,336 h at initial luminance of 100 cd/m^2 (Table 3). The stability of the reference device **H**-mCBP shows potential of recently developed emitter AcDbp. Summarizing, the device investigations demonstrate not only potential of developed compounds **TPAPm** and **CzPm** as emitters and hosts with rare triplet-harvesting ability but also provide additional stability results for TADF/TTA emitter AcDbp which were not discussed in the previous work [51].

3. Conclusions

Two new derivatives triphenylamine and 9-phenylcarbazole as donor moieties and pyrimidine-5-carbonitrile as electron-withdrawing unit with ability to harvest high-lying triplets were developed and characterised. The obtained materials were used as emitters for the fabrication high-efficiency doped blue and greenish-blue fluorescent OLEDs with EQE$_{max}$ of 7% and 6%. High efficiency of the fluorescent devices exceeding theoretically possible 5% is attributed to upper level triplet singlet intersystem crossing. In accordance with the theoretical calculations, reverse internal system crossing can appear between T_3 and S_1 for triphenylamine-based compound and between T_3 and S_2 for carbazolyl-containing compound. In our case, the slight increase of efficiency of OLEDs shows that not all high-energy triplet excitons were converted into singlet excitons. Using the synthesised compounds as host materials orange TADF/TTA based OLEDs were fabricated. They showed EQE$_{max}$ of 20.7% and 13.7% as well as LT50 (100 cd/m^2) of 2063 and 6481 h. A higher efficiency was achieved for the device based on host with triphenylamino groups. This host demonstrated good bipolar charge-transporting properties with charge mobilities in the range of 10^{-3} cm^2/V × s at electric field of 3.6 × 10^5 V/cm and low triplet energy of 2.31 eV. However, the device with carbazole-based host showed by ca. three times higher durability in comparison to the device with the host containing triphenylamine groups.

Credit author statement

Uliana Tsiko: Conceptualization, Writing − original draft, Investigation, Dmytro Volyniuk: Conceptualization, Writing − original draft, Investigation, Validation, Visualization; Viktorija Andruleviciene: Data curation, Investigation, Writing − review & editing, Visualization, Karolis Leitonas: Data curation, Methodology, Investigation, Visualization; Galyna Sych: Supervision, Formal analysis; Oleksandr Bezvikonnyi: Investigation; Vidmantas Jasinskas: Investigation; Vidmantas Gulbinas: Validation, Writing − review & editing, Supervision; Pavlo Stakhira: Project administration, Formal analysis; Juozas Vidas Grazulevicius: Funding acquisition, Validation, Writing − review & editing, Supervision.

Declaration of competing interest

The authors declare the following financial interests/personal relationships that may be considered as potential competing interests: Juozas Vidas Grazulevicius reports financial support was provided by Research Council of Lithuania. Dmytro Volyniuk reports a relationship with Research Council of Lithuania that includes: funding grants.

Acknowledgment

This work was supported by the project of scientific co-operation program between Lithuania and Ukraine 'Development of highly efficient white light-emitting diodes utilizing organic emitters with exciplex and thermally-assisted fluorescence for lighting applications (LUW)' (grant No. S-LU-20-9) under grant agreement with the Research Council of Lithuania (LMTLT). Dr. Audrius Bucinskas is acknowledged for providing X-ray analysis for **TPAPm**.

Appendix A. Supplementary data

Supplementary data to this article can be found online at https://doi.org/10.1016/j.mtchem.2022.100955.

References

[1] H. Uoyama, K. Goushi, K. Shizu, H. Nomura, C. Adachi, Highly efficient organic light-emitting diodes from delayed fluorescence, Nature 492 (2012) 234−238, https://doi.org/10.1038/nature11687.
[2] Z. Xu, B.Z. Tang, Y. Wang, D. Ma, Recent advances in high performance blue organic light-emitting diodes based on fluorescence emitters, J. Mater. Chem. C 8 (2020) 2614−2642, https://doi.org/10.1039/c9tc06441a.
[3] T. Hosokai, H. Matsuzaki, H. Nakanotani, K. Tokumaru, T. Tsutsui, A. Furube, K. Nasu, H. Nomura, M. Yahiro, C. Adachi, Evidence and mechanism of efficient

thermally activated delayed fluorescence promoted by delocalized excited states, Sci. Adv. 3 (2017), e160328, https://doi.org/10.1126/sciadv.1603282.
[4] C. Adachi, Third-generation organic electroluminescence materials, Jpn. J. Appl. Phys. 53 (2014), 060101, https://doi.org/10.7567/JJAP.53.060101.
[5] P. Data, M. Okazaki, S. Minakata, Y. Takeda, Thermally activated delayed fluorescence: vs. room temperature phosphorescence by conformation control of organic single molecules, J. Mater. Chem. C 7 (2019) 6616–6621, https://doi.org/10.1039/c9tc00909d.
[6] G. Zhan, Z. Liu, Z. Bian, C. Huang, Recent advances in organic light-emitting diodes based on pure organic room temperature phosphorescence materials, Front. Chem. 7 (2019) 305, https://doi.org/10.3389/fchem.2019.00305.
[7] X. Wang, R. Tom, X. Liu, D.N. Congreve, N. Marom, An energetics perspective on why there are so few triplet-triplet annihilation emitters, J. Mater. Chem. C 8 (2020) 10816–10824, https://doi.org/10.1039/d0tc00044b.
[8] W. Liu, S. Ying, R. Guo, X. Qiao, P. Leng, Q. Zhang, Y. Wang, D. Ma, L. Wang, Nondoped blue fluorescent organic light-emitting diodes based on benzonitrile-anthracene derivative with 10.06% external quantum efficiency and low efficiency roll-off, J. Mater. Chem. C 7 (2019) 1014–1021, https://doi.org/10.1039/c8tc05707a.
[9] T. Tsutsui, Progress in electroluminescent devices using molecular thin films, MRS Bull. 22 (1997) 39–45, https://doi.org/10.1557/S0883769400033613.
[10] X. Lv, L. Xu, Y. Yu, W. Cui, H. Zhou, M. Cang, Q. Sun, Y. Pan, S. Xue, W. Yang, High external quantum efficiency and low efficiency roll-off achieved simultaneously in nondoped pure-blue organic light-emitting diodes based on a hot-exciton fluorescent material, Chem. Eng. J. 408 (2021) 127333, https://doi.org/10.1016/j.cej.2020.127333.
[11] N.C. Giebink, B.W. D'Andrade, M.S. Weaver, P.B. MacKenzie, J.J. Brown, M.E. Thompson, S.R. Forrest, Intrinsic luminance loss in phosphorescent small-molecule organic light emitting devices due to bimolecular annihilation reactions, J. Appl. Phys. 103 (2008), 044509, https://doi.org/10.1063/1.2884530.
[12] J. Lee, C. Jeong, T. Batagoda, C. Coburn, M.E. Thompson, S.R. Forrest, Hot excited state management for long-lived blue phosphorescent organic light-emitting diodes, Nat. Commun. 8 (2017) 15566, https://doi.org/10.1038/ncomms15566.
[13] X. Lv, M. Sun, L. Xu, R. Wang, H. Zhou, Y. Pan, S. Zhang, Q. Sun, S. Xue, W. Yang, Highly efficient non-doped blue fluorescent OLEDs with low efficiency roll-off based on hybridized local and charge transfer excited state emitters, Chem. Sci. 11 (2020) 5058–5065, https://doi.org/10.1039/d0sc01341b.
[14] Y. Xu, X. Liang, X. Zhou, P. Yuan, J. Zhou, C. Wang, B. Li, D. Hu, X. Qiao, X. Jiang, L. Liu, S.J. Su, D. Ma, Y. Ma, Highly efficient blue fluorescent OLEDs based on upper level triplet–singlet intersystem crossing, Adv. Mater. 31 (2019) 1807388, https://doi.org/10.1002/adma.201807388.
[15] Y. Xu, P. Xu, D. Hu, Y. Ma, Recent progress in hot exciton materials for organic light-emitting diodes, Chem. Soc. Rev. 50 (2021) 1030–1069, https://doi.org/10.1039/d0cs00391c.
[16] Q. Zhang, B. Li, S. Huang, H. Nomura, H. Tanaka, C. Adachi, Efficient blue organic light-emitting diodes employing thermally activated delayed fluorescence, Nat. Photonics 8 (2014) 326–332, https://doi.org/10.1038/nphoton.2014.12.
[17] D.R. Lee, J.M. Choi, C.W. Lee, J.Y. Lee, Ideal molecular design of blue thermally activated delayed fluorescent emitter for high efficiency, small singlet-triplet energy splitting, low efficiency roll-off, and long lifetime, ACS Appl. Mater. Interfaces 8 (2016) 23190–23196, https://doi.org/10.1021/acsami.6b05877.
[18] T. Chatterjee, W.Y. Hung, W.F. Tang, H.F. Chen, K.T. Wong, Carbazole-bridged triphenylamine-bipyridine bipolar hosts for high-efficiency low roll-off multicolor PhOLEDs, Org. Electron 50 (2017) 204–212, https://doi.org/10.1016/j.orgel.2017.07.036.
[19] L. Bao, J. Zhu, W. Song, H. Zhou, J. Huang, H. Mu, J. Su, New carbazole-based bipolar hosts for efficient green phosphorescent organic light-emitting diodes, Org. Electron. 83 (2020) 105672, https://doi.org/10.1016/j.orgel.2020.105672.
[20] S.H. Ye, L. Li, M. Zhang, Z. Zhou, M.H. Quan, L.F. Guo, Y. Wang, M. Yang, W.Y. Lai, W. Huang, Pyridine linked fluorene hybrid bipolar host for blue, green, and orange phosphorescent organic light-emitting diodes toward solution processing, J. Mater. Chem. C 5 (2017) 11937–11946, https://doi.org/10.1039/c7tc04339b.
[21] W. Song, L. Shi, L. Gao, P. Hu, H. Mu, Z. Xia, J. Huang, J. Su, Triazolo[1,5-a] pyridine as building blocks for universal host materials for high-performance red, green, blue and white phosphorescent organic light-emitting devices, ACS Appl. Mater. Interfaces 10 (2018) 5714–5722, https://doi.org/10.1021/acsami.7b18202.
[22] Z.J. Gao, T.H. Yeh, J.J. Xu, C.C. Lee, A. Chowdhury, B.C. Wang, S.W. Liu, C.H. Chen, Carbazole/benzimidazole-based bipolar molecules as the hosts for phosphorescent and thermally activated delayed fluorescence emitters for efficient OLEDs, ACS Omega 5 (2020) 10553–10561, https://doi.org/10.1021/acsomega.0c00967.
[23] Y. Zhao, C. Wu, P. Qiu, X. Li, Q. Wang, J. Chen, D. Ma, New benzimidazole-based bipolar hosts: highly efficient phosphorescent and thermally activated delayed fluorescent organic light-emitting diodes employing the same device structure, ACS Appl. Mater. Interfaces 8 (2016) 2635–2643, https://doi.org/10.1021/acsami.5b10464.
[24] Y. Tao, Q. Wang, Y. Shang, C. Yang, L. Ao, J. Qin, D. Ma, Z. Shuai, Multifunctional bipolar triphenylamine/oxadiazole derivatives: highly efficient blue fluorescence, red phosphorescence host and two-color based white OLEDs, Chem, Commun. Now. (2009) 77–79, https://doi.org/10.1039/b816264f.
[25] Y. Zheng, A.S. Batsanov, V. Jankus, F.B. Dias, M.R. Bryce, A.P. Monkman, Bipolar molecules with high triplet energies: synthesis, photophysical, and structural properties, J. Org. Chem. 76 (2011) 8300–8310, https://doi.org/10.1021/jo201488v.
[26] S.W. Li, C.H. Yu, C.L. Ko, T. Chatterjee, W.Y. Hung, K.T. Wong, Cyanopyrimidine-carbazole hybrid host materials for high-efficiency and low-efficiency roll-off TADF OLEDs, ACS Appl. Mater. Interfaces 10 (2018) 12930–12936, https://doi.org/10.1021/acsami.8b02766.
[27] G.H. Kim, R. Lampande, M.J. Park, H.W. Bae, J.H. Kong, J.H. Kwon, J.H. Park, Y.W. Park, C.E. Song, Highly efficient bipolar host materials with indenocarbazole and pyrimidine moieties for phosphorescent green light-emitting diodes, J. Phys. Chem. C 118 (2014) 28757–28763, https://doi.org/10.1021/jp507036h.
[28] J. Yoon, C. Lee, S.H. Park, D.W. Kang, H. Kim, J.E. Jeong, H.Y. Woo, C.S. Hong, S. Park, M.J. Cho, D.H. Choi, Pyrimidine-based bipolar host materials for high efficiency solution processed green thermally activated delayed fluorescence OLEDs, J. Mater. Chem. C 8 (2020) 2196–2204, https://doi.org/10.1039/c9tc05727g.
[29] U. Tsiko, O. Bezvikonnyi, G. Sych, R. Keruckiene, D. Volyniuk, J. Simokaitiene, I. Danyliv, Y. Danyliv, A. Bucinskas, X. Tan, J.V. Grazulevicius, Multifunctional derivatives of pyrimidine-5-carbonitrile and differently substituted carbazoles for doping-free sky-blue OLEDs and luminescent sensors of oxygen, J. Adv. Res. 33 (2021) 41–51, https://doi.org/10.1016/j.jare.2021.01.014.
[30] T. Serevičius, J. Dodonova, R. Skaisgiris, D. Banevičius, K. Kazlauskas, S. Juršėnas, S. Tumkevičius, Optimization of the carbazole-pyrimidine linking pattern for achieving efficient TADF, J. Mater. Chem. C 8 (2020) 11192–11200, https://doi.org/10.1039/d0tc02194f.
[31] X.K. Chen, S.F. Zhang, J.X. Fan, A.M. Ren, Nature of highly efficient thermally activated delayed fluorescence in organic light-emitting diode emitters: nonadiabatic effect between excited states, J. Phys. Chem. C 119 (2015) 9728–9733, https://doi.org/10.1021/acs.jpcc.5b00276.
[32] P. Galer, R.C. Korošec, M. Vidmar, B. Šket, Crystal structures and emission properties of the BF2 complex 1-phenyl-3-(3,5-dimethoxyphenyl)-propane-1,3-dione: multiple chromisms, aggregation- or crystallization-induced emission, and the self-assembly effect, J. Am. Chem. Soc. 136 (2014) 7383–7394, https://doi.org/10.1021/ja501977a.
[33] J.L. Bredas, Mind the gap!, Mater. Horizons 1 (2014) 17–19, https://doi.org/10.1039/c3mh00098b.
[34] A. Kokil, K. Yang, J. Kumar, Techniques for characterization of charge carrier mobility in organic semiconductors, J. Polym. Sci., Part B: Polym. Phys. 50 (2012) 1130–1144, https://doi.org/10.1002/polb.23103.
[35] P. Chulkin, O. Vybornyi, M. Lapkowski, P.J. Skabara, P. Data, Impedance spectroscopy of OLEDs as a tool for estimating mobility and the concentration of charge carriers in transport layers, J. Mater. Chem. C 6 (2018) 1008–1014, https://doi.org/10.1039/c7tc04599a.
[36] S.A. Bagnich, S. Athanasopoulos, A. Rudnick, P. Schroegel, I. Bauer, N.C. Greenham, P. Strohriegl, A. Köhler, Excimer formation by steric twisting in carbazole and triphenylamine-based host materials, J. Phys. Chem. C 119 (2015) 2380–2387, https://doi.org/10.1021/jp512772j.
[37] N. Mataga, Y. Kaifu, M. Koizumi, Solvent effects upon fluorescence spectra and the dipolemoments of excited molecules, Bull. Chem. Soc. Jpn. 29 (1956) 465–470, https://doi.org/10.1246/bcsj.29.465.
[38] S. Sumalekshmy, K.R. Gopidas, Photoinduced intramolecular charge transfer in donor-acceptor substituted tetrahydropyrenes, J. Phys. Chem. B 108 (2004) 3705–3712, https://doi.org/10.1021/jp022549l.
[39] E. Lippert, Dipolmoment und Elektronenstruktur von angeregten Molekülen, Z. Naturforsch. A. 10 (1955) 541–545, https://doi.org/10.1515/zna-1955-0707.
[40] L. Onsagbr, Electric moments of molecules in liquids, J. Am. Chem. Soc. 58 (1936) 1486–1493, https://doi.org/10.1021/ja01299a050.
[41] B.F. Minaev, Ab initio study of the ground state properties of molecular oxygen, Spectrochim. Acta Part A Mol. Biomol. Spectrosc 60 (2004) 1027–1041, https://doi.org/10.1016/S1386-1425(03)00334-2.
[42] M. Bregnhøj, M. Westberg, B.F. Minaev, P.R. Ogilby, Singlet oxygen photophysics in liquid solvents: converging on a unified picture, Acc. Chem. Res. 50 (2017) 1920–1927, https://doi.org/10.1021/acs.accounts.7b00169.
[43] C. Zhou, S. Xiao, M. Wang, W. Jiang, H. Liu, S. Zhang, B. Yang, Modulation of excited state property based on benzo[a, c]phenazine acceptor: three typical excited states and electroluminescence performance, Front. Chem. 7 (2019) 141, https://doi.org/10.3389/fchem.2019.00141.
[44] H. Usta, D. Alimli, R. Ozdemir, E. Tekin, F. Alkan, R. Kacar, A.G. Altas, S. Dabak, A.G. Gürek, E. Mutlugun, A.F. Yazici, A. Can, A hybridized local and charge transfer excited state for solution-processed non-doped green electroluminescence based on oligo(: p -phenyleneethynylene), J. Mater. Chem. C 8 (2020) 8047–8060, https://doi.org/10.1039/d0tc01266a.
[45] Q. Wei, N. Fei, A. Islam, T. Lei, L. Hong, R. Peng, X. Fan, L. Chen, P. Gao, Z. Ge, Small-molecule emitters with high quantum efficiency: mechanisms, structures, and applications in OLED, Devices, Adv. Opt. Mater. 6 (2018) 1800512, https://doi.org/10.1002/adom.201800512.
[46] H. Wu, G.V. Baryshnikov, A. Kuklin, B.F. Minaev, B. Wu, L. Gu, L. Zhu, H. Ågren, Y. Zhao, Multidimensional structure conformation of persulfurated benzene for highly efficient phosphorescence, ACS Appl. Mater. Interfaces 13 (2021) 1314–1322, https://doi.org/10.1021/acsami.0c16338.

[47] X. Qiao, D. Ma, Nonlinear optoelectronic processes in organic optoelectronic devices: triplet-triplet annihilation and singlet fission, Mater. Sci. Eng. R Reports 139 (2020) 100519, https://doi.org/10.1016/j.mser.2019.100519.
[48] M. Yamazaki, Industrialization and application development of cyclo-olefin polymer, J. Mol. Catal. Chem. 213 (2004) 81–87, https://doi.org/10.1016/J.MOLCATA.2003.10.058.
[49] S. Nad, H. Pal, Electron transfer from aromatic amines to excited coumarin Dyes: fluorescence quenching and picosecond transient absorption studies, J. Phys. Chem. 104 (1999) 673–680, https://doi.org/10.1021/JP9932062.
[50] K. Leitonas, A. Tomkeviciene, G. Baratte, A. Dabuliene, S.M. Punniyakoti, D. Volyniuk, J.V. Grazulevicius, Oxygen sensing properties of thianthrene and phenothiazine derivatives exhibiting room temperature phosphorescence: effect of substitution of phenothiazine moieties, Sensors Actuators B Chem. 345 (2021) 130369, https://doi.org/10.1016/J.SNB.2021.130369.
[51] V. Andruleviciene, K. Leitonas, D. Volyniuk, G. Sini, J.V. Grazulevicius, V. Getautis, TADF versus TTA emission mechanisms in acridan and carbazole-substituted dibenzo[a,c]phenazines: towards triplet harvesting emitters and hosts, Chem. Eng. J. 417 (2021) 127902, https://doi.org/10.1016/j.cej.2020.127902.
[52] J. Grüne, N. Bunzmann, M. Meinecke, V. Dyakonov, A. Sperlich, Kinetic modeling of transient electroluminescence reveals TTA as an efficiency-limiting process in exciplex-based TADF OLEDs, J. Phys. Chem. C 124 (2020) 25667–25674, https://doi.org/10.1021/ACS.JPCC.0C06528.
[53] L.S. Cui, A.J. Gillett, S.F. Zhang, H. Ye, Y. Liu, X.K. Chen, Z. Sen Lin, E.W. Evans, W.K. Myers, T.K. Ronson, H. Nakanotani, S. Reineke, J.L. Bredas, C. Adachi, R.H. Friend, Fast spin-flip enables efficient and stable organic electroluminescence from charge-transfer states, Nat. Photonics 14 (2020) 636–642, https://doi.org/10.1038/s41566-020-0668-z.
[54] Z.Q. Zhu, K. Klimes, S. Holloway, J. Li, Efficient cyclometalated platinum(II) complex with superior operational stability, Adv. Mater. 29 (2017) 1605002, https://doi.org/10.1002/adma.201605002.
[55] C. Féry, B. Racine, D. Vaufrey, H. Doyeux, S. Cinà, Physical mechanism responsible for the stretched exponential decay behavior of aging organic light-emitting diodes, Appl. Phys. Lett. 87 (2005) 1–3, https://doi.org/10.1063/1.2133922.

UDK 547.759+621.383.52](043.3)

SL 344. 2022-*-*, * leidyb. apsk. l. Tiražas 14 egz. Užsakymas * .

Išleido Kauno technologijos universitetas, K. Donelaičio g. 73, 44249 Kaunas
Spausdino leidyklos „Technologija“ spaustuvė, Studentų g. 54, 51424 Kaunas